2022

Synthetic Methods for Improved Scope and Efficiency of Copper-Catalyzed Regioselective Alkene Boracarboxylation

Steven William Knowlden
West Virginia University, swk0005@mix.wvu.edu

Synthetic Methods for Improved Scope and Efficiency of Copper-Catalyzed Regioselective Alkene Boracarboxylation

Steven W. Knowlden

Dissertation submitted to the
Eberly College of Arts and Sciences
at West Virginia University

in partial fulfillment of the requirements for the degree
of

Doctor of Philosophy in Chemistry

Committee:

Brian Popp, Ph.D., Committee Chair
Jessica Hoover, Ph.D.
Björn Söderberg, Ph.D.
Kung Wang, Ph.D.
Mark McLaughlin, Ph.D.

Department of Chemistry

Morgantown, West Virginia 2022

Keywords: boracarboxylation, Xantphos, reductive carboxylation, alkene, boron, copper

Abstract

Synthetic Methods for Improved Scope and Efficiency of Copper-Catalyzed Regioselective Alkene Boracarboxylation

Steven Knowlden

The synthesis of carboxylic acids is important to the chemistry community, owing to the broad applicability of these compounds as fine chemicals and pharmaceuticals. Method development over the last decade has focused on the preparation of carboxylic acids through transition metal catalysis utilizing CO_2 as a C1 synthon. Copper-catalyzed heteroelement(bora and sila)-carboxylation protocols provide functional group rich carboxylic acid products, yet remain underdeveloped and thus underutilized. Consequently, catalytic reductive difunctionalization methodologies in which CO_2 and B(pin) (pin = pinacolate: 2,3-dimethyl-2,3-butanediolate) are installed across the double bond of a vinyl arene were recently developed. These boracarboxylation protocols provided novel, pharmaceutically relevant, α-aryl propionic acids bearing a β-boryl functionality in good to excellent yields; however, the alkene scope was limited. Here, solutions to substrate scope limitations and methods to improve reaction efficiency will be presented. Reactivity studies of sterically challenging α-substituted vinyl arene substrates revealed a complex kinetic interplay between catalytic reduction of CO_2 and alkene migratory insertion reaction pathways. These results have impacted the ways in which the catalytic boracarboxylation system is altered to allow for transformation of challenging alkene substrates. The method in which the α-substituted vinyl arenes were boracarboxylated led to a glovebox-free benchtop synthesis of borylated Ibuprofen. Moreover, the benchtop method circumvents the need to use a prefunctionalized copper(I)-precatalyst through *in-situ* generation of the active catalytic species from readily available and easily synthesized starting materials. Guided by previous experimental studies, a catalytic phosphine additive, Xantphos, led to expansion of the boracarboxylation scope to unactivated alkenes. Insights from these studies are expected to contribute to increased use of Xantphos as a catalytic additive in copper(I)-boryl catalysis.

.

Dedicated to my wife Elizabeth Knowlden

My parents William Knowlden and Katherine Ryerson

and my grandmother Suzanne Knowlden

Acknowledgements

I would like to begin by thanking my friends and family for always supporting me during my journey at West Virginia University, the encouragement you provided me was deeply appreciated. A special thanks to my father William, grandmother Suzanne, mother Katherine, stepmother Linda, aunt Roxanne, uncle John, sisters Lauren and Madison, and cousins Brittany and Matthew, for always being there for me when times were tough. Also, thank you to my in-laws Robert, Debbie, and Tom Burgio. Knowing that they were all just a phone call or text away gave me peace of mind during the most difficult times in this journey. I could always count on them for good times and great laughs, something we all need in graduate school. The hard work ethic that my father has had his entire life (even now as he gets older, sorry dad), has always inspired me to do better and work harder even in the most trying of times, no excuses!

Next, I would like to thank my advisor, Dr. Brian Popp, for making me the scientist that I am today. The mentoring, guidance, encouragement, and constant support he provided me through this difficult journey is the reason why I was even able to make it this far. Brian taught me to never stop questioning, while also showing me how to conduct my research, presentations, and scientific writing with meticulous precision. Brian is also an extraordinarily kind person and has always treated me and other graduate students respectfully. This is shown through the research group when everyone does not hesitate to stop what they are doing and help each other out, much like Brian himself. Thank you again Brian, I cannot say it enough.

Which leads me to the fantastic group of people that I was fortunate to spend my time working with day in and day out, my groupmates. All the senior graduate students had a key role in my education. Thank you to Dr. Trina Perrone for teaching me how to do synthetic chemistry, she is an amazing mentor. Next, I would like to thank Dr. Brian Nichols for always there to talk to about potential ideas, guiding me even though it was taking time away from him trying to finish his Ph. D. He was always willing to discuss chemistry with me and help me out. Furthermore, I would like to thank Dr. Notashia Baughman for showing me the importance of doing things with extreme attention to detail. By doing so, many aspects of my research proceeded much smoother. Also thank you to Dr, Jessica Rogers for always providing me feedback on any of the questions I asked her. Thank you to the current group members, Randika Abeysinghe, Alexa Martin, Stephen Long, Carly Gordon, Mason Hamilton, and Randall Koziel, all of whom have always been willing to talk through ideas with me and provide suggestions to help me along the way. I wish them all the best in their personal and professional endeavors. I was also fortunate to work with a great many talented undergraduates. Thank you to Natalie Ziemer, Maxwell Reese, Owen Hamilton, Amanda Swistok, Tiffany Taylor, Anala Schultz, and Kenny Zheng.

Additionally, I would like to thank my committee members, Dr. Jessica Hoover, Dr. Björn Söderberg, Dr. Kung Wang, and Dr. Mark McLaughlin for taking the time to serve on my committee. I appreciate the time that they took to attend all my oral presentations and provide valuable feedback on my research. Thank you to Dr. Novruz Akhmedov, the NMR Facility director here at WVU, for all his guidance in analysis of complex mixtures via NMR spectroscopy. His expertise in NMR spectroscopy provided valuable insight into many of the synthetic problems that I faced through my journey. Next, I want to thank the staff here at WVU, as they have always been extremely helpful,

and were instrumental in keeping the lab operational. Thank you to Randy and Chad. The number of pumps, condensers, hotplates, and miscellaneous things that they fixed for us was no small feat. A special thanks to Allen Burns, because without him I would not have been able to do any of the research in my second chapter, as he was crucial in building and designing the pressure apparatus.

Finally, I would like to give a special thank you to my wife Elizabeth. She always supported me during this journey, and always made sure that I was doing alright. She kept me on track, while always encouraging me and helping me with everything that I felt as if I couldn't do on certain days. I had the pleasure of getting married to her during the last few months. Even before we were married, she was always there for me regardless of what she had going on in her own life. Elizabeth is an amazing person, and if it wasn't for her, I wouldn't have made it nearly this far. I am extremely fortunate to have been able to share this journey with such an amazing person, I love you, Elizabeth.

Table of Contents

		Page
Dedication		iii
Acknowledgements		iv
Table of Contents		vi
List of Figures		viii
List of Schemes		ix
List of Tables		x
List of Abbreviations		xi

Chapter 1: *Utilization of CO_2 in Transition Metal Catalyzed Reductive Carboxylation Reactions*

1.1	Reductive Carboxylation Strategies	1
1.2	Catalytic Reductive Carboxylation of C-X Bonds with CO_2	4
1.3	Catalytic Reductive Carboxylation of Unsaturated Motifs with CO_2	6
1.4	Catalytic Carboxylative Difunctionalization of Unsaturated Motifs with CO_2	10
1.5	Boracarboxylation of Vinyl Arenes	13
1.5.1	Investigation of PPh_3 Additive	16
1.5.2	Mechanistic Studies	21
1.6	Summary	27
1.7	References	28

Chapter 2: *Regioselective Boracarboxylation of α-Substituted Vinyl Arene*

2.1	Introduction	32
2.2	Results and Discussion	33
2.2.1	Initial CO_2 pressure effects on the boracarboxylation of vinyl arenes	33
2.2.2	Boracarboxylation of α-Substituted Vinyl Arenes Reaction Optimization and Scope	36
2.3	Conclusions	42
2.4	Experimental Section	42
2.5	References	47

Chapter 3: *Synthesis of Novel Borylated Ibuprofen Derivative through Suzuki Cross-Coupling and Boracarboxylation Methodologies.*

3.1	Introduction	51
3.2	Reaction Protocols	53
3.3	Representative Results	56
3.4	Discussion and Concluding remarks	59
3.5	Experimental Methods	60
3.6	References	61

Chapter 4: *Regioselective Boracarboxylation of Unactivated Alkenes Enabled by Catalytic Xantphos Additive*

4.1	Introduction	63
4.2	Reaction Optimization	66
4.3	Boracarboxylation of Unactivated Akenes Reaction Scope	74
4.4	Conclusions	77
4.5	Experimental Section	77
4.6	References	80

Appendix I: NMR Characterization Data 83

List of Figures

Figure 1.1	Reductive carboxylation reactions and copper-boryl catalyzed difunctionalizations	1
Figure 1.2	General mechanism of copper(I) boryl catalyzed difunctionalization of alkenes	2
Figure 1.3	Popp's Boracarboxylation of Vinyl Arenes	3
Figure 1.4	Popp's boracarboxylation of vinyl arenes mechanism (left) Sadighi previous mechanistic work (right).	13
Figure 1.5	Adapted from Baughman N. N and Popp, B. V., **2020**. *Comments on Inorganic Chemistry*, 40:4, 159-175. Computed structure of ICyCu(β-borylbenzyl) carboxylation transition state (top left A) NBO orbitals (top left B). Transition states of carboxylation $\Delta H^{\ddagger}$ values (bottom left). Natural charge on boron, and the effect of boron valence deficiency (top right). Relationship between stabilization energies from NBO analysis (black) and B-O interaction distances (red).	22
Figure 1.6	Isolated carboxylated IPrCu(β-borylbenzyl) complexes (top left). Experimental and calculated VT ^{1}H NMR spectra (right). DFT modeling of [Cu] binding to each oxygen in the pinacol ring (bottom left).	23
Figure 1.7	Potential carboxylation pathways (top left). $\Delta\Delta G^{\ddagger}$ energies comparison between experimental and computational systems (right). Depiction of the HOMO of the IMeCu(β-borylbenzyl) and the direct CO_2 insertion transition state, and model of the key stereoelectronic interactions in the transition state (right). Adapted from Baughman, N. N.; Akhmedov, N. G.; Petersen, J. L.; Popp, B. V. *Organometallics* **2021**, *40* (1), 23–37	24
Figure 1.8	Phosphine additive effects	25
Figure 1.9	Reaction coordinates for carboxylation	26
Figure 2.1	Apparatus used for high-pressure reaction	33
Figure 2.2	Catalytic cycle for copper-catalyzed boracarboxylation with competitive CO_2 reduction and hydro/protoboration pathways.	35
Figure 2.3	^{11}B NMR spectra of selected crude boracarboxylation reactions in $CDCl_3$.	36
Figure 3.1	Medicinal relevance of boracarboxylation	52
Figure 3.2	^{1}H NMR spectrum of *p*-Isobutyl Styrene	56
Figure 3.3	^{1}H NMR spectrum of *bora*-Ibuprofen	57
Figure 3.4	^{13}C NMR spectrum of *bora*-Ibuprofen	58
Figure 3.5	^{11}B NMR spectrum of *bora*-Ibuprofen	58
Figure 4.1	Pyrridoisoindolinone characterization data and mechanism	76

List of Schemes

Scheme 1.1	Carboxylation of C-X bonds	4
Scheme 1.2	Copper catalyzed carboxylation of C_{sp2}-X and direct carboxylation of activated C-H bonds	5
Scheme 1.3	Hydrocarboxylation of Alkynes	7
Scheme 1.4	Hydrocarboxylation of Alkenes	8
Scheme 1.5	Tandem hydroboration-carboxylation strategies and Martin's hydrocarboxylation of olefins with CO_2 and H_2O	9
Scheme 1.6	Carbocarboxylation of alkynes	10
Scheme 1.7	Intramolecular aminocarboxylation of alkynes	11
Scheme 1.8	Bora- and sila- carboxylative difunctionalization of alkynes	12
Scheme 1.9	Preliminary mechanistic investigations	20
Scheme 2.1	Transition-metal-catalyzed strategies to access synthetically useful a-quaternary carboxylic acids and derivatives.	32
Scheme 3.1	Synthesis of *bora*-Ibuprofen precursor	53
Scheme 3.2	Synthesis of *bora*-Ibuprofen	54
Scheme 4.1	Previous carboxylative and carbonylative difunctionalization work	63

List of Tables

Table 1.1	Boracarboxylation of vinyl arenes reaction optimization	14
Table 1.2	Boracarboxylation of vinyl arenes substrate scope and synthetic utility	15
Table 1.3	Boracarboxylation of vinyl arenes secondary ligand optimization	17
Table 1.4	Boracarboxylation of electron-deficient vinyl arene optimization	18
Table 1.5	Scope of new catalytic conditions vs. previous catalytic conditions	19
Table 2.1	Effect of CO_2 Pressure on Boracarboxylation of Vinyl Arenes 1a and 4	35
Table 2.2	Effect of CO_2 pressure and base on boracarboxylation of electron deficient 1b	37
Table 2.3	Effect of Catalyst on Boracarboxylation of Electron Neutral 1a[a]	38
Table 2.4	Boracarboxylation Reaction Optimization with Electron Neutral 1a	39
Table 2.5	Boracarboxylation Reaction Scope	41
Table 4.1	Wu's borocarbonylation selected reaction optimization examples highlighting Xantphos effect	64
Table 4.2	Wu's cyclopropanation selected reaction optimization examples highlighting Xantphos effect	65
Table 4.3	Reaction stoichiometry optimization	66
Table 4.4	ICyCuCl and Xantphos loading optimization	67
Table 4.5	Solvent and temperature optimization	69
Table 4.6	Copper precatalyst optimization	70
Table 4.7	Phosphine additive optimization	71
Table 4.8	Base optimization	72
Table 4.9	Reaction optimization of other parameters	73
Table 4.10	Substrate scope of unactivated alkenes	75

List of Abbreviations

atm	atmosphere
B_2pin_2	bis(pinacolato)diboron
BBN	9-borabicyclo[3.3.1]nonane
Bn	benzyl
Bz	Benzoyl
BOC	tert-butyloxycarbonyl
Bpin	Boronic acid pinacol ester
DCM	dichloromethane
DFT	Density functional theory
DMA	N,N-dimethylacetamide
DMF	N,N-dimethylformamide
DMSO	Dimethyl sulfoxide
DPEPhos	bis[(2-diphenylphosphino)phenyl] ether
Cy-DPEPhos	bis[(2-cyclohexylphosphino)phenyl] ether
DPPF	1-1'-bis(diphenylphosphino)ferrocene
DTBM-SEGPHOS	5,5'-bis[di(3,5-di-tert-butyl-4-methoxyphenyl)phosphino]-4,4'-bi-1,3- benzodioxole
ICy	1,3-dicyclohexyl-imidazol-2-ylidene
SICy	1,3-dicyclohexyl-4,5-dihydroimidazol-2-ylidene
IPr	1,3-bis(2,6-diisopropylphenyl)-imidazol-2-ylidene
SIPr	1,3-bis(2,6-diisopropylphenyl)-4,5-dihydroimidazol-2-ylidene
IMes	1,3-bis(2,4,6-trimethylphenyl)-imidazol-2-ylidene
SIMes	1,3-bis(2,4,6-trimethylphenyl)-4,5-dihydroimidazol-2-ylidene
NHC	N-heterocyclic carbene
NSAID	Non-steroidal anti-inflammatory drug
THF	Tetrahydrofuan
TMEDA	N,N,N',N'-tetramethylethylenediamine

CHAPTER 1: *Utilization of CO_2 in Transition Metal Catalyzed Reductive Carboxylation Reactions*

1.1 Reductive Carboxylation Strategies

Catalytic carboxylation reactions in which CO_2 is utilized are highly desirable transformations in synthetic organometallic chemistry. To date, many types of methodologies have been developed with CO_2 as the linchpin, despite its thermodynamic stability and kinetic inertness. These transformations have enabled the conversion of a highly abundant, sustainable carbon feedstock into value-added products such as carboxylic acids, amino acids, esters, and ethers.[1] Carboxylic acids are instrumental building blocks for the manufacturing of agrochemicals and pharmaceuticals, with over 450 widely used carboxylic acid containing drugs marketed worldwide.[2]

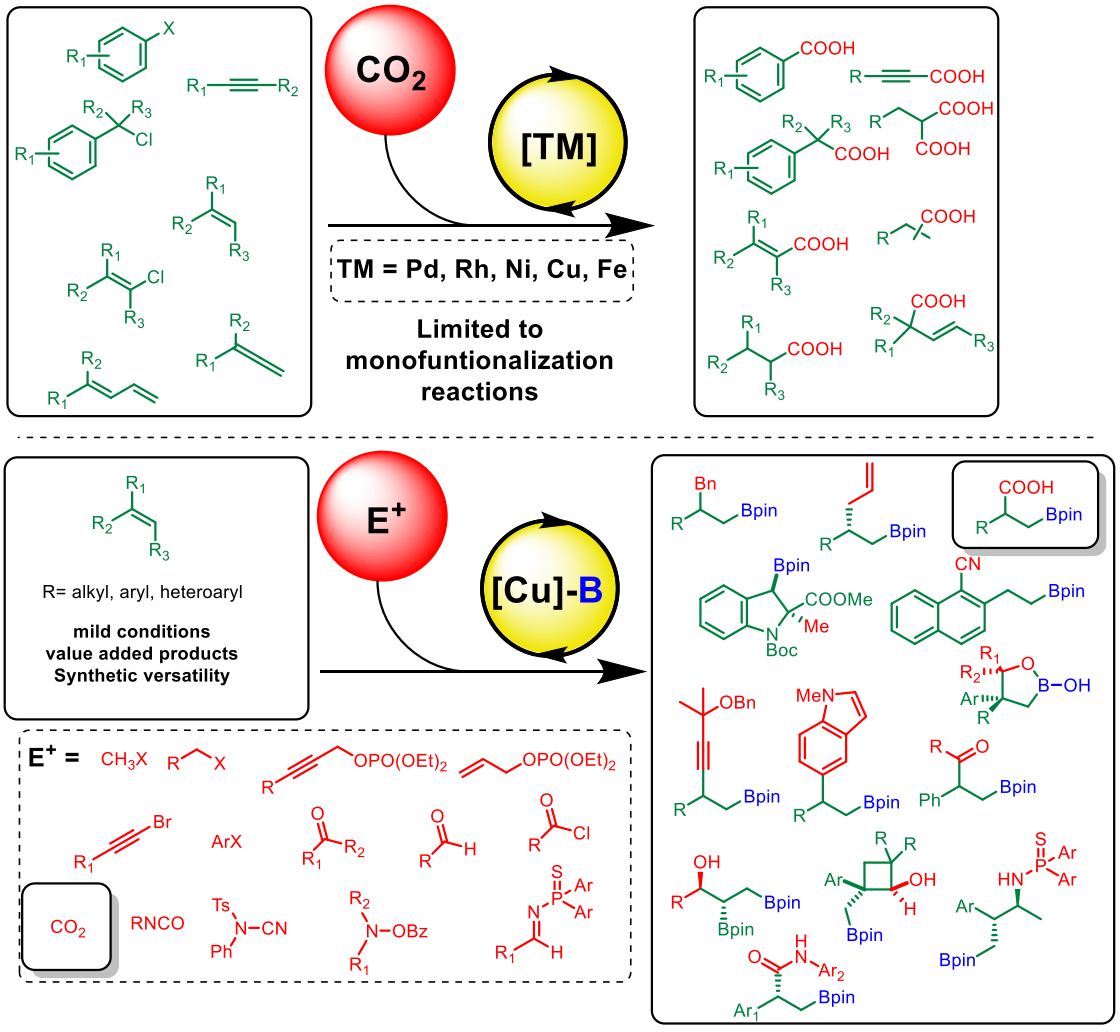

Figure 1.1 Reductive carboxylation reactions and copper-boryl catalyzed difunctionalizations

Direct carboxylation of organometallic reagents (Grignards, C-Li, C-Zn, etc.) with CO_2 is a traditional and reliable method and has demonstrated wide scope and functional group tolerance.[3] However, the major pitfall of

these transformations is the requirement of a stoichiometric amount of sensitive organometallic reagents. An alternate approach is the catalytic reductive carboxylation of C-X (Br, Cl, H, etc.) bonds[4] (Figure 1.1). Typically, these transformations occur under mild conditions and avoid the use of large amounts of sensitive organometallic reagents. Another strategy is the reductive carboxylation of unsaturated compounds with CO_2 (Figure 1.1). Starting materials such as alkynes, allenes, alkenes, and dienes have been employed in these transformations.[1] However, in the case of alkenes, these transformations can only be achieved with highly reactive reagents, harsh conditions, and precious metal catalysts, due to their less reactive nature. Moreover, these methodologies are monofunctionalization reactions.[1] Consequently, carboxylation while introducing other synthetically or medicinally relevant functional groups is highly sought after. Based on these catalytic systems, borylative and silylative carboxylation reactions were developed using alkynes, allenes, and imines as substrates; however, utilization of alkene substrates remained elusive in these systems.

Copper-boryl catalysis is a powerful synthetic tool for the difunctionalization of alkenes, spanning an variety of unsaturated substratesand electrophiles, leading to a extensive amount of a value-added transformations of alkenes[5] (Figure 1.1). A general mechanism through which these reactions proceed is displayed in Figure 1.2.

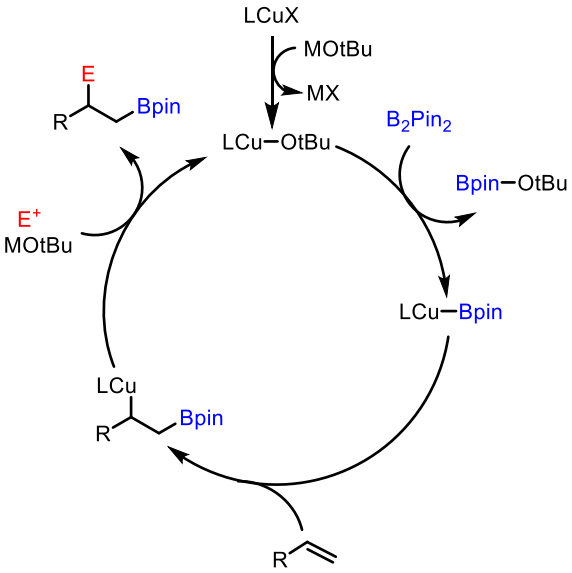

Figure 1.2 General mechanism of copper(I) boryl catalyzed difunctionalization of alkenes

Initially, a copper(I) alkoxide is generated followed by transmetallation with a boron reagent to afford the active copper(I)-boryl catalyst. Upon alkene insertion, the nucleophilic copper(I) alkyl species captures an electrophile, leading to the generation of product.[5] In 2016, the Popp group reported the first methodology in which CO_2 is the electrophile in this transformation with alkenes.[6] This novel difunctionalization reaction employs CO_2 and stable reagent bispinacolato diboron. with readily available styrene substrates and converts them to highly functionalized carboxylic acid derivatives under mild conditions with minimal side product formation. However, this methodology was largely limited to electron neutral and rich vinyl arenes, with electron deficient substrates proceeding poorly.

Another drawback in this transformation was the high catalyst loading (12 mol%) required for the reaction to proceed smoothly.

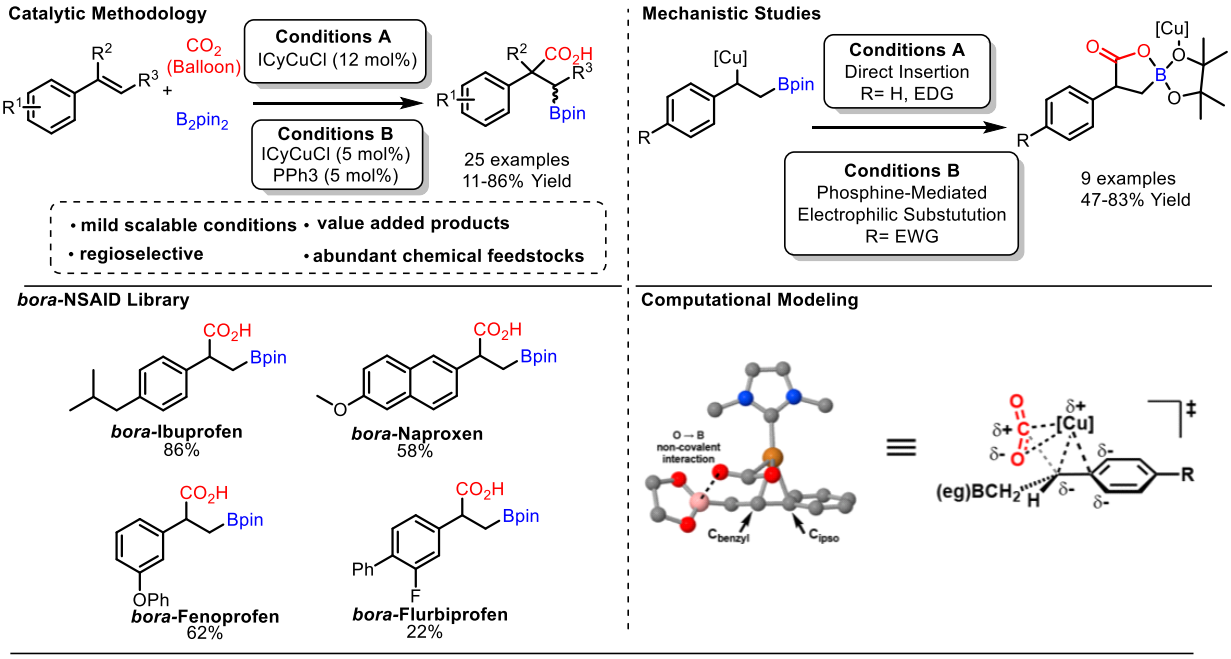

Figure 1.3 Popp's Boracarboxylation of Vinyl Arenes

To address these issues, triphenylphosphine was employed as a secondary ligand, along with increase of styrene concentration, allowing for facile access to electron deficient vinyl arenes at lower catalyst loadings.[7] To better understand the limitations of the original reaction as well as the role of exogenous phosphine (Figure 1.3), we investigated the carboxylation step of the boracarboxylation mechanism experimentally through kinetic experiments with the complementary density functional theory (DFT) experiments.[8,9] In this study, it was demonstrated that multiple pathways are operative in the carboxylation step of the boracarboxylation mechanism depending on the electronic nature of the vinyl arene. Kinetic observations demonstrated that electronically deficient vinyl arenes carboxylate slower than their electron rich counterparts. The reaction rate was accelerated through use of exogenous triphenylphosphine additive.

In this chapter, a summarization of recent methodological and mechanistic work toward optimization and expansion of the boracarboxylation methodology is presented. Information will be presented within the context of catalytic reductive carboxylation chemistry used to synthesize carboxylic acids, where CO_2 is utilized as a C1 synthon.

1.2 Catalytic Reductive Carboxylation of C-X Bonds with CO_2

Transition metal catalyzed strategies for reductive carboxylation of C-X bonds with CO_2 are useful synthetic protocols that provide access to a variety of carboxylic acid derivatives (Scheme 1.2). In 2009, the Martin group reported the direct carboxylation of aryl bromides to afford benzoic acids using a Pd^{II} catalyst supported by the biphenyl monophosphine ligand ^{t}Bu-Xphos with diethylzinc as a reductant under 10 atm of CO_2.[10] The advantage of this methodology was the ability to carboxylate aryl halides without the need to prepare stoichiometric amounts of organometallic intermediates. However, the scope was limited, and the reaction required a high CO_2 pressure, a strong reductant, and a precious metal catalyst. Catalytic transformations under milder conditions using earth abundant metal catalysts have also been developed. In 2012, Tsuji et. al reported a Ni^{II}-catalyzed carboxylation of challenging aryl- and vinyl chloride substrates with a Manganese reductant and Et_4NI additive under the mild conditions of 1 atm of CO_2 at room temperature (Scheme 1.2).[11] This methodology provided direct access to both benzoic acids and acrylic acids. However, specific conditions are required for many substrates, thus limiting its generality. Consequently, the Hazari group reported a mechanistically guided strategy to generalize the Tsuji methodology (Scheme 1.2).[12]

Scheme 1.1 Carboxylation of C-X bonds

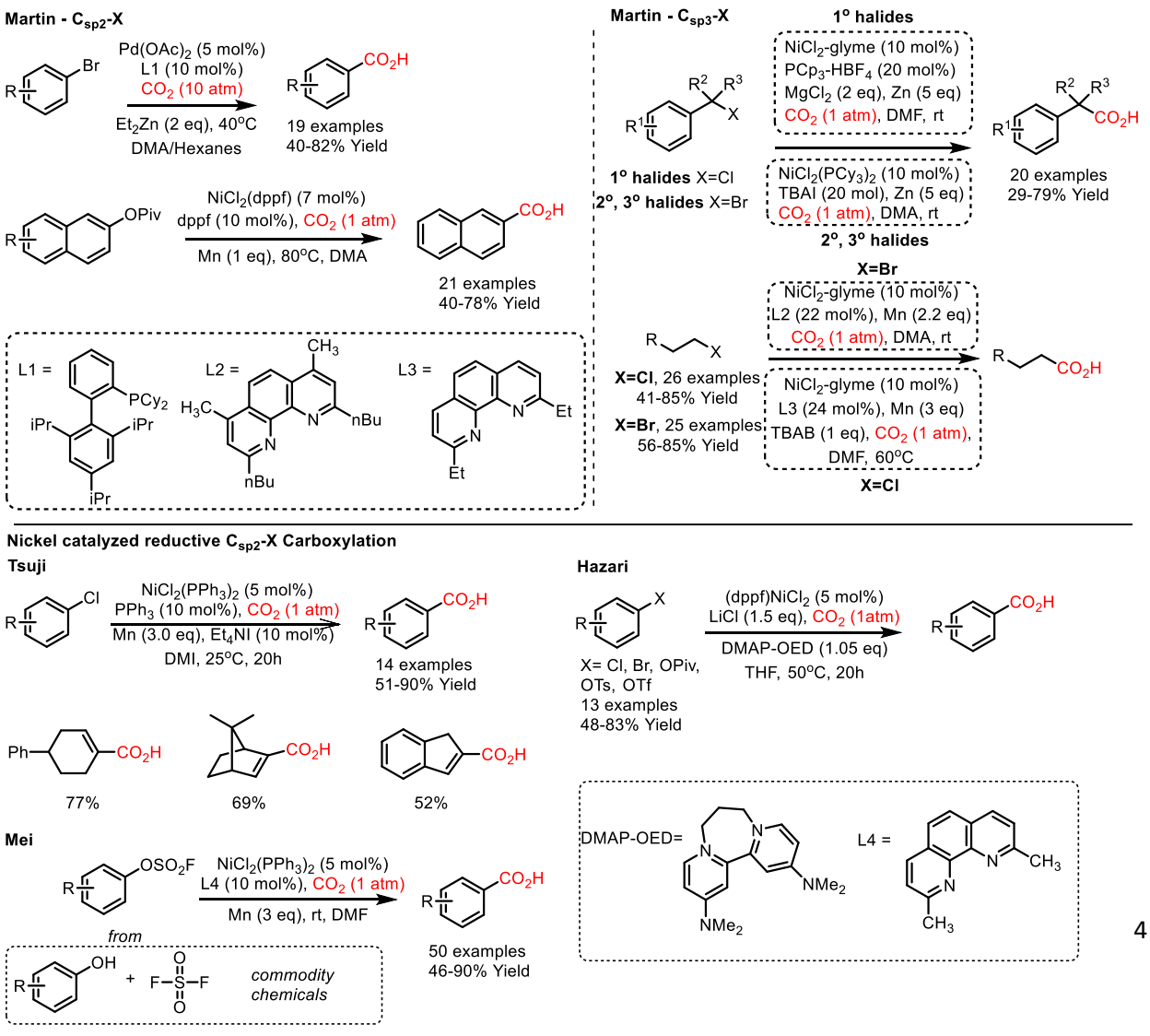

They demonstrated that the Manganese and Zinc reductants are non-innocent in this transformation, and the MnX_2 (X= Br or Cl) obtained is proposed to act as both a catalytically beneficial Lewis acid and halide source. Subsequently, through use of a LiCl additive and DMAP-OED as a homogenous organic reductant, the new methodology tolerates a variety of halides and pseudohalides. Additionally, C-O pseudohalide electrophiles are viable alternatives for traditional organic halides, as they can be easily synthesized from large libraries of widely available phenol and alcohol substrates. The Mei group employed these C-O pseudohalides in their Ni^{II}-catalyzed carboxylation of phenol derivatives, replacing commonly employed organic halides with organic fluorosulfates synthesized from abundant and inexpensive commodity chemicals (Scheme 1.2).[13] Despite this, this process still relies on activated sulfonate electrophiles. In 2014, the Martin group successfully carboxylated robust benzylic- and aryl ester motifs chemoselectively.[14] Utilizing a dppf-ligated nickel(II) complex and 1 atm of CO_2. As a result, aryl and benzylic carboxylic acids were afforded in moderate to high yields, expanding reductive carboxylation to less activated ester pseudohalide derivatives.

Previously, the Martin group was responsible for expanding the field of Ni-catalyzed reductive carboxylation reactions from sp_2 to sp_3 electrophiles through use of primary, secondary, and tertiary benzyl halides.[15] They demonstrated that the use of highly electron-rich phosphines in combination with either a $MgCl_2$ or Bu_4NI additive and a Zinc reductant was crucial in this transformation.

Scheme 1.2 Copper catalyzed carboxylation of C_{sp2}-X and direct carboxylation of activated C-H bonds

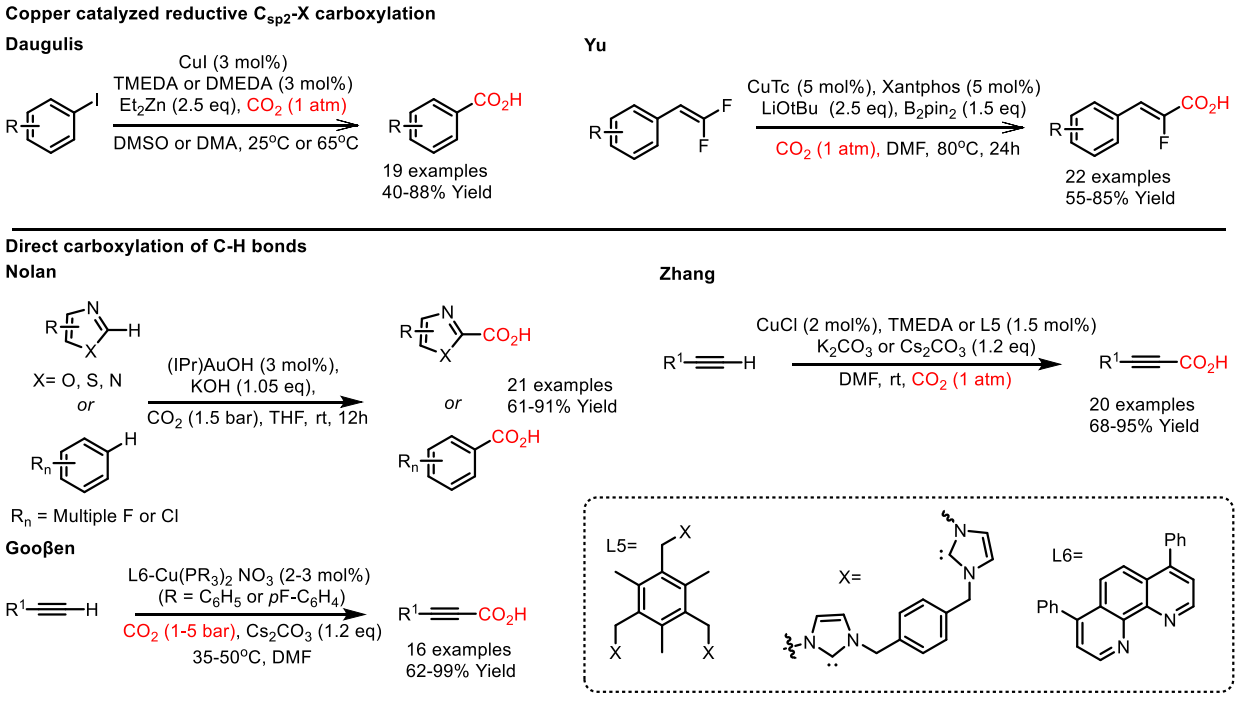

The Martin group also expanded their carboxylation methodology to unactivated alkyl bromides,[16] sulfonates,[16] and chlorides[17] through use of a phenanthroline-ligated Ni^{II} complex (Scheme 1.2 top right). The ligand scaffold had a

significant influence on reactivity in these systems, with the rigidity of the phenanthroline backbone providing access to less reactive alkyl chlorides.

In addition to the Pd- and Ni-catalyzed C_{sp2}-X carboxylation methodologies with CO_2, the Dauglis group reported the copper-catalyzed carboxylation of aryl iodides (Scheme 1.3, top left).[18] However, the scope was limited to aryl iodides, and the reaction required superstochiometric amounts of pyrophoric, highly reactive Et_2Zn as a reducing agent. Also, this protocol was not very robust, as multiple ligands, solvents, and temperature combinations were necessary depending on the substrate. More recently, the Cu-catalyzed carboxylation of gem-difluorodienes and α-trifluoromethyl alkenes has been reported (Scheme 1.3, top right).[19] This scalable protocol utilizes an inexpensive copper catalyst to obtain a variety of valuable α-fluoroacrylic acids and α,α-difluorocarboxylates with high chemoselectivity, which are present in many pharmaceuticals.

Direct carboxylation strategies of C-H bonds with CO_2 are desirable transformations because they often avoid the use of prefunctionalized starting materials (Scheme 1.3, bottom). As a result, these protocols are favorable from an atom economy standpoint. In 2010, the Nolan group reported the carboxylation of electron-deficient heterocycles catalyzed by Au^I and Cu^I NHC (N-Heterocyclic Carbene) complexes,[20] wherein carboxylation occurs regioselectively at the most acidic C-H bond. The transformation occurs by protonolysis of the acidic heteroaromatic C-H, followed by CO_2 insertion into the [M]-C bond to afford the [M] carboxylate species, which can then undergo metathesis with potassium hydroxide to afford the carboxylate salt. The mechanism demonstrates the need for a highly electron deficient heteroaromatic substrate, thus limiting generality. Base metal catalyzed carboxylation of terminal alkynes with CO_2 is an effective strategy utilized to deliver propiolic acids in a single step. In 2010, the Gooβen group reported the catalytic carboxylation of both aliphatic and aromatic terminal alkynes.[21] Aliphatic alkynes were carboxylated under 1 bar of CO_2 and required a more electron rich phosphine ligated copper(I) precatalyst species than their aryl counterparts, which required 5 bars of CO_2 and slightly lower temperature and catalyst loading. The Zhang group reported a similar methodology wherein terminal alkynes were carboxylated using a Cu-TMEDA system, or in the case of less reactive substrates, a Cu-polyNHC system.[22] They propose that this Cu-polyNHC system can activate CO_2 for insertion into the Cu-alkynyl species. However, this transformation was limited in scope, and required a variety of base, time, and ligand combinations depending on the substrates employed.

1.3 Catalytic Reductive Carboxylation of Unsaturated Motifs with CO_2

These methodologies set the foundation for modern catalytic carboxylation chemistry as they provide highly valuable carboxylic acid moieties through utilization of CO_2, a powerful and renewable C1 synthon, in moderate to high yields. However, C-X functionalization reactions are limited to prefunctionalized organic halide and pseudohalide substrates, thus limiting their atom economy. In the case of C-H functionalization reactions, they are limited to activated substrates and often require complex catalysts. Alternatively, catalytic reductive carboxylation strategies wherein unsaturated substrates are employed provide the desired carboxylic acid products directly in a single step from readily available starting materials. Among these strategies is the hydrocarboxylation

of alkynes and alkenes, which can also provide carboxylic acids with greater synthetic utility and medicinal value if non-hydride coupling partners are employed in these transformations.

Scheme 1.3 Hydrocarboxylation of alkynes

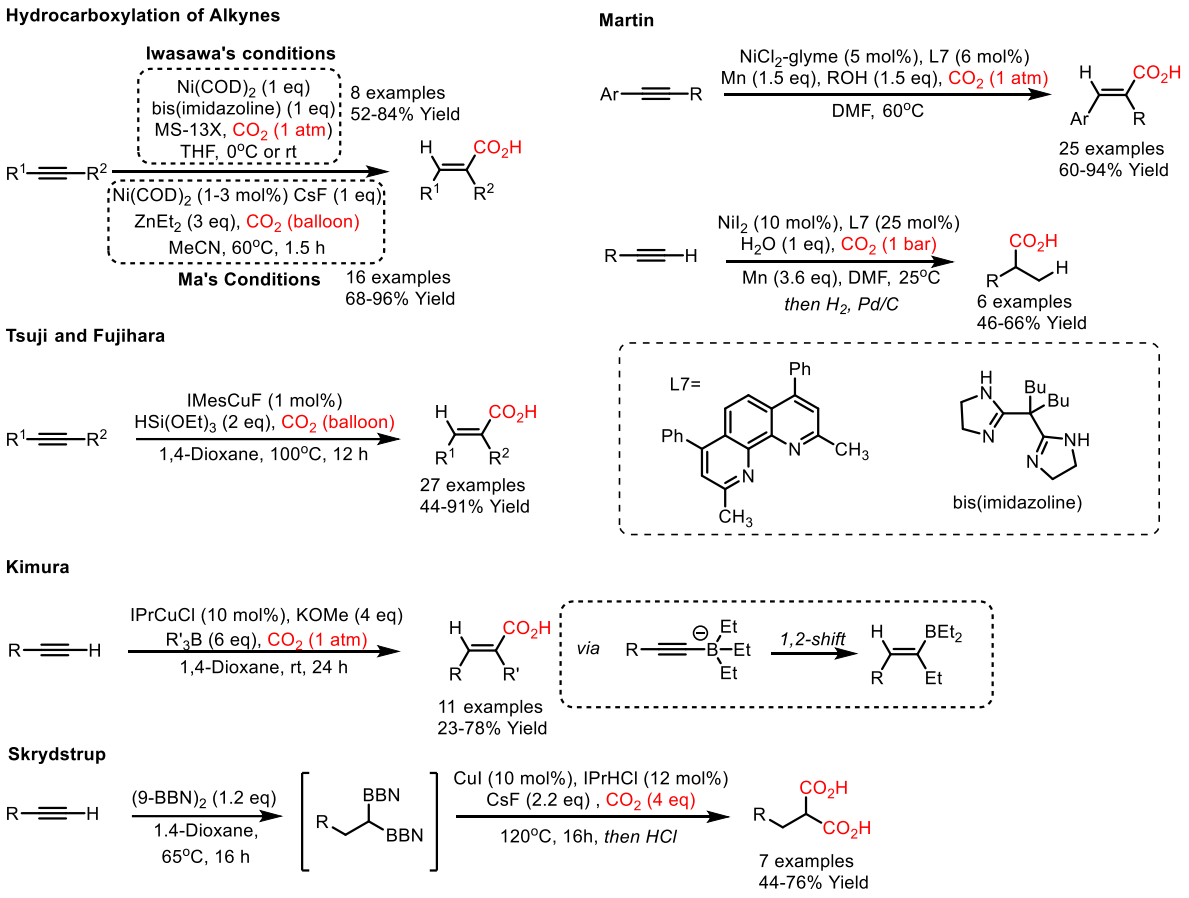

Hydrocarboxylation of alkynes with CO_2 provides industrially relevant acrylic acids (Scheme 1.4). In 2004, the Iwasawa group reported the regiodivergent coupling of alkynes with CO_2.[23] By altering the steric profile of the bidentate bis(amidine) ligand employed in this transformation, both linear and branched acrylic acid derivatives can be obtained. However, stochiometric amounts of Ni are employed, and the yield of the branched product is low. In 2011, the Ma group demonstrated that catalytic reductive carboxylation of symmetric and asymmetric alkynes with diethyl zinc as a reductant can be achieved with a Ni catalyst, using CsF as an additive and a balloon of CO_2.[24] When asymmetric alkynes were employed, the α-aryl acrylic acid isomer was obtained, which is consistent with the regiochemistry of the hydrozincation step of the mechanism. Around the same time, Fujihara and Tsuji published an analogous Cu-catalyzed protocol using a hydrosilane reductant and IMesCuF precatalyst.[25] The reaction proceeds through insertion of alkyne into a Cu-H, followed by CO_2 fixation by the Cu-C intermediate to afford symmetric and asymmetric acrylic acid products in moderate to high yields. A significant drawback in these methodologies is that stoichiometric amounts of reductant are necessary, leading to harsher reaction conditions and an unfavorable atom

economy. A methodology published by the Martin group, however, utilizes simple alcohols as the proton source in their transformation.[26] This regioselective protocol employs a phenanthroline-ligated Ni catalyst with a single atmosphere of CO_2, Manganese reductant, and a simple alcohol proton source isopropanol. In the case of the asymmetric alkynes, β-aryl acrylic acids are obtained exclusively, with little to no formation of the opposite regioisomer. This regioselectivity arises from selective protonation of an oxanickelacyclopentene intermediate. The Martin group used this mechanistic insight to synthesize branched aliphatic carboxylic acid motifs from terminal alkynes. This method uses water as the proton source and relies on reduction of the acrylic acid to the branched aliphatic acid product.[27] The Kimura group offers a multicomponent approach to polysubstituted acrylic acids, using terminal alkynes as coupling partners.[28] The authors proposed that an alkynyl boronate complex undergoes a 1,2-alkyl migration, thus triggering a CO_2 insertion. In 2017, The Skrydstrup group published a tandem hydroboration-carboxylation of alkyne substrates to access malonic acid derivatives. This was achieved by the double hydroboration of terminal alkynes, followed by carboxylation of the diborylated species.[29]

Catalytic carboxylation reactions with alkyne substrates are important strategies for the synthesis of acrylic acid derivatives, however synthesis of aliphatic acids from these alkyne derivatives is limited. These aliphatic acids are prominent in a large variety of vital drugs and natural products.[2] These products can be directly accessed through hydrocarboxylation of the less enthalpically favorable alkene substrates (Scheme 1.5). In 2008, Rovis set the foundation for these methodologies through the regioselective hydrocarboxylation of styrene derivatives wherein the Markovnikov carboxylic acid product is obtained.[30] This protocol employs a Ni^{II} catalyst with a diethylzinc reductant, under 1 atm of CO_2 at room temperature. The mechanism is proposed to proceed through alkene insertion into a Ni-H bond, generated upon transmetallation/β-hydride elimination with diethylzinc, followed by carboxylation of the Ni-alkyl intermediate. Thomas reported a different approach toward α-aryl propionic acid pharmacophores from electron rich and neutral styrenes using an inexpensive iron precatalyst, in tandem with a Grignard reagent as the hydride source to undergo a hydrometallation pathway which traps CO_2.[31] Inspired by this work, the Xi group reported a similar catalytic transformation using a Ti^{IV} precatalyst with a Grignard reagent as the hydride source[32]. A LiBr additive was key in their method, leading to significantly higher yields and regioselectivities. The Xi group was able to expand their methodology to unactivated alkenes as well.

Scheme 1.4 Hydrocarboxylation of alkenes

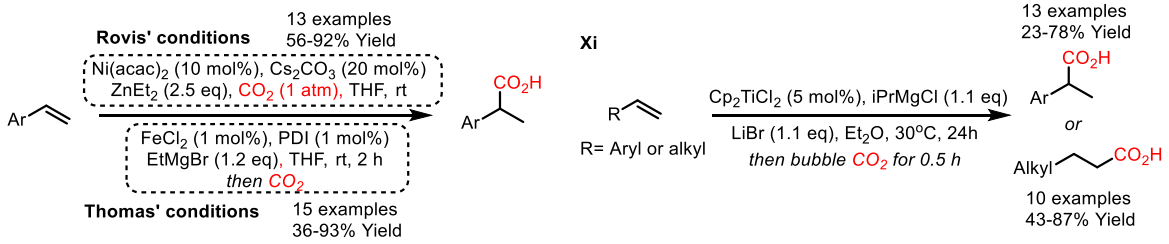

The key limitation of these protocols is the reliance on stoichiometric amounts of highly reactive and poorly chemoselective organozinc and Grignard reagents. Consequently, protocols wherein these reagents are absent will allow for higher chemoselectivity, leading to more robust methodologies (Scheme 1.6). In 2011, the Hou and Sawamura groups independently reported their hydroboration-carboxylation strategies employing terminal alkynes to afford the anti-markovnikov aliphatic carboxylic acid products.[33,34] The Hou system relied on an NHC-copper(I) complex, while the Sawamura system relied on a phenanthroline-ligated copper(I) complex. Both methodologies avoided the use of harsh reagents, resulting in broad functional group compatibility using base metal catalysts, and primary carboxylic acid products were obtained in moderate to high yields. While these methods proved to be robust, they were limited to primary carboxylic acid derivatives. The Skrydstrup methodology described previously allowed access to secondary acids by way of substituted alkene precursors.[29]

Scheme 1.5 Tandem hydroboration-carboxylation strategies and Martin's hydrocarboxylation of olefins with CO_2 and H_2O

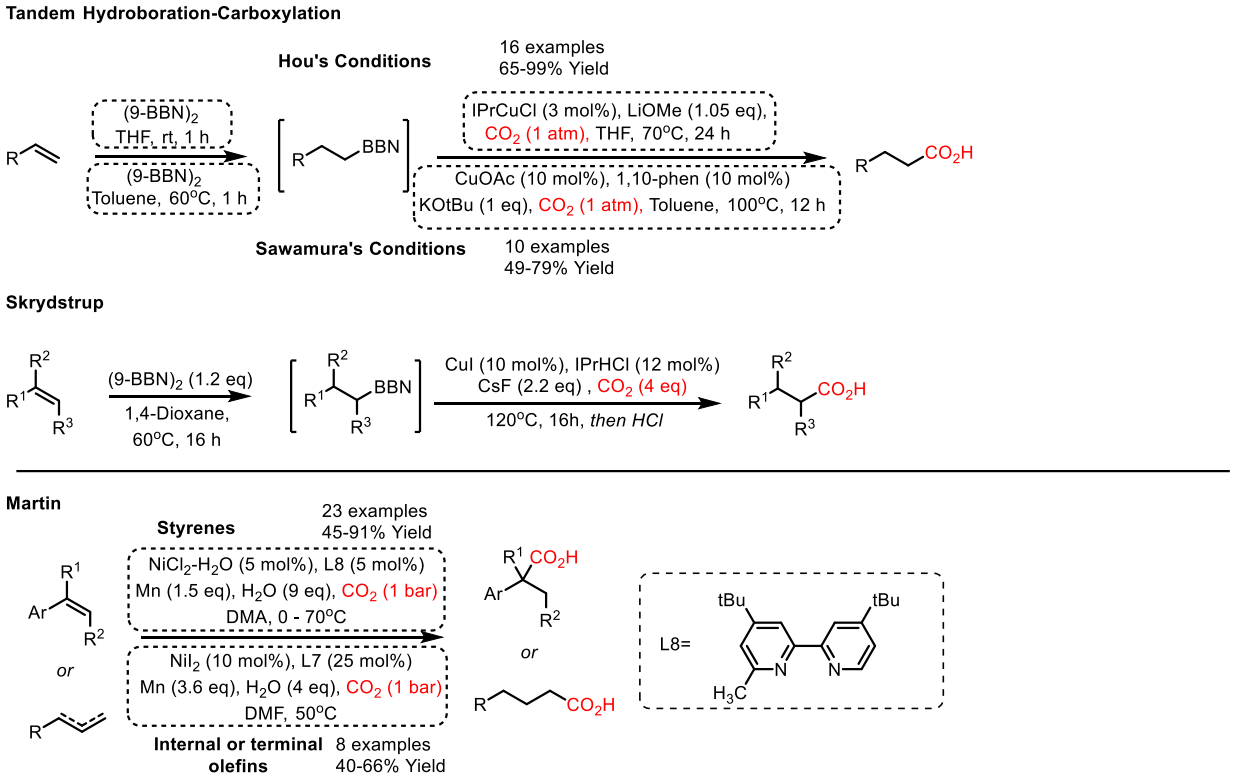

While these methods avoid the use of highly reactive organometallic reactants, they are still limited in that they require prefunctionalization of the alkene through in situ hydroboration, resulting in a diminished atom economy. Subsequently, the Martin group reported a Ni^{II}-catalyzed hydrocarboxylation methodology using alkenes, H_2O, and CO_2, three highly abundant, inexpensive chemical feedstocks (Scheme 1.6, bottom).[27] This methodology employed styrene derivatives and terminal olefin substrates and converted them into value-added carboxylic acid derivatives. By altering the ligand and reaction stoichiometry and substrate employed, both branched and linear

regioisomers can be obtained. To date, this protocol is one of the greenest strategies used to synthesize aliphatic carboxylic acids, with H_2O as a hydride source, as opposed to other organometallic reagents.

1.4 Catalytic Carboxylative Difunctionalization of Unsaturated Motifs with CO_2

Hydrocarboxylation of unsaturated compounds are powerful methodologies that deliver value-added carboxylic acid products from ubiquitous starting materials. However, the value of this transformation could be increased through incorporation of a non-hydride coupling partner, thereby allowing direct access to more structurally diverse compounds. Prior to the Popp group's publication in November of 2016, very few carboxylative difunctionalization reactions employing unsaturated compounds existed in the literature.

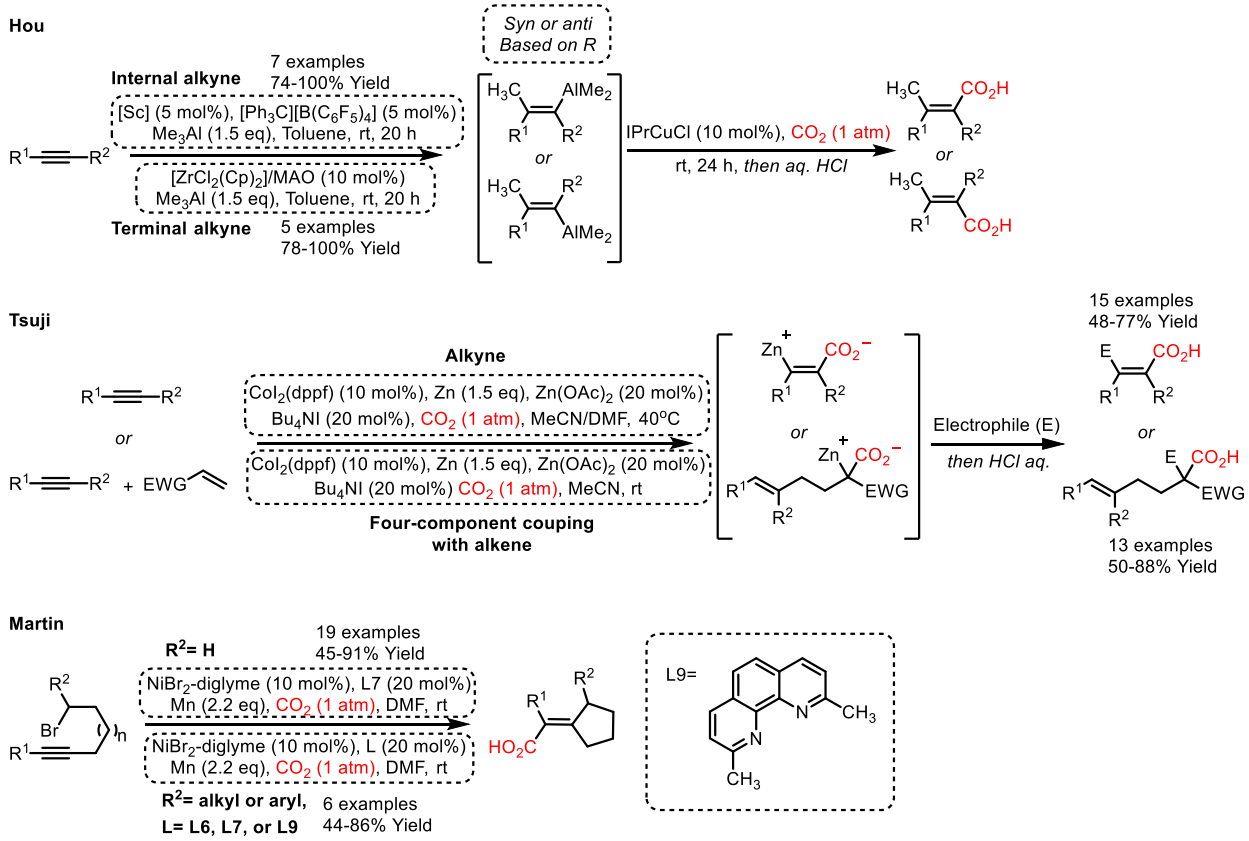

Scheme 1.6 Carbocarboxylation of alkynes

In the area of carbocarboxylation reactions (Scheme 1.7), the Hou group published the methylative carboxylation of terminal alkynes in 2013.[35] This method proceeds by the Zr^{IV}-catalyzed methylative alumination of the terminal alkyne, followed by transmetallation with a copper catalyst then CO_2 insertion into the resulting vinyl copper species. The myriad of conditions needed for this transformation and strong trimethyl aluminum reductant led to poor chemoselectivity and a limited substrate scope. In 2016, the Tsuji group reported the cobalt-catalyzed carboxyzincation of alkynes[36], wherein the resulting stereodefined Z-carboxyzincated alkene products were trapped by a variety of electrophiles, providing access to multisubstituted acrylic acids without erosion of stereochemistry.

They were also able to develop conditions wherein a four-component coupling reaction can be achieved with an alkyne, acrylate or acrylamide substrate, CO_2, and Zn powder. The Martin group published an intramolecular carbocarboxylation reaction through a Ni-catalyzed cascade pathway under mild conditions wherein the selectivity is dictated by the ligand selection.[37] Alteration of the backbone of the ligand was crucial to selectively synthesize the *anti* regioisomer when secondary alkyl bromides were employed.

Although carbocarboxylation reactions provide more structurally diverse carboxylic acids, further functionalization of these substrates is limited to mainly carboxylic acid transformations. However, when a heteroelement is introduced into the substrate, a larger library of chemical transformations can be accessed due to the synthetic versatility and medicinal relevance of those heteroatoms (Scheme 1.8). In 2012, the Kondo and Ma groups reported their respective strategies for the synthesis of 3-carboxylated indole derivatives through a tandem cyclization/CO2 fixation from 2-ethynylanilines.[38,39] The Ma group conditions relied on an inexpensive copper precatalyst, dimethyl zinc reductant, and cesium fluoride base. They proposed an aminometallation of the alkyne, followed by fluoride activated CO_2 capture leading to the carboxylated indoles. The practicality of their method was demonstrated through three-step synthesis of a cytotoxic indoloquinolinone in gram quantities. The Kondo protocol is a transition metal free process which relies on high base loading and high CO_2 pressure. This method tolerates a wide variety of functional groups and can also be applied to 2-ethynyl phenol, resulting the formation of a 3-carboxylated benzofuran.

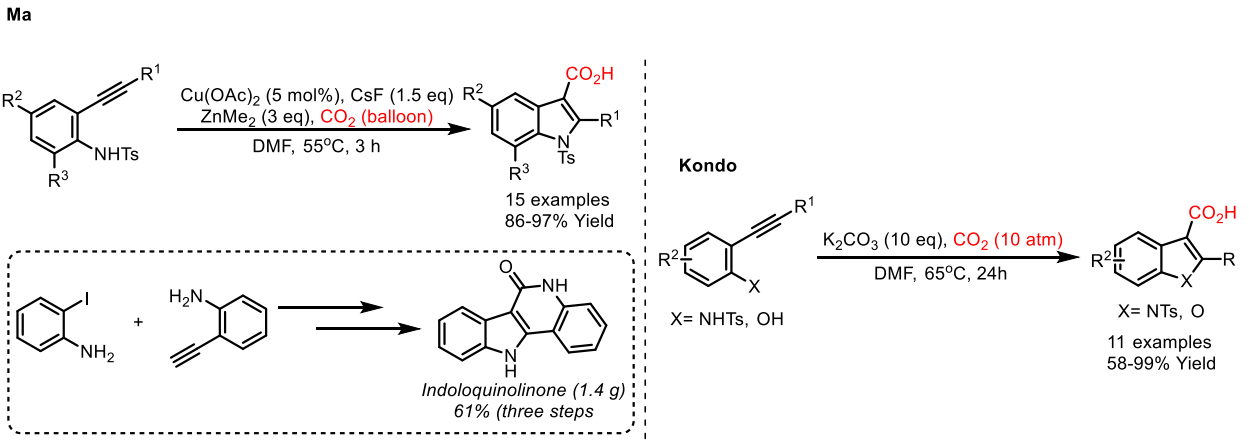

Scheme 1.7 Intramolecular aminocarboxylation of alkynes

Bora- and sila- carboxylative difunctionalization reactions were also developed in the early 2010s (Scheme 1.9). The Tsuji group reported the copper-catalyzed silacarboxylation of alkynes[40] and allenes[41] in 2012 and 2014, respectively. In their methodology with alkynes, low catalyst loading of a tricyclohexylphosphine-ligated copper complex with one atmosphere of CO_2, using a heteroleptic B-Si reductant provides silalactonate products in high yields. These products were able to undergo Hiyama cross-coupling reactions to afford tetrasubstituted alkene substrates. Allenes were able to be regiodivergently silacarboxylated to afford both vinyl and allyl silane derivatives.

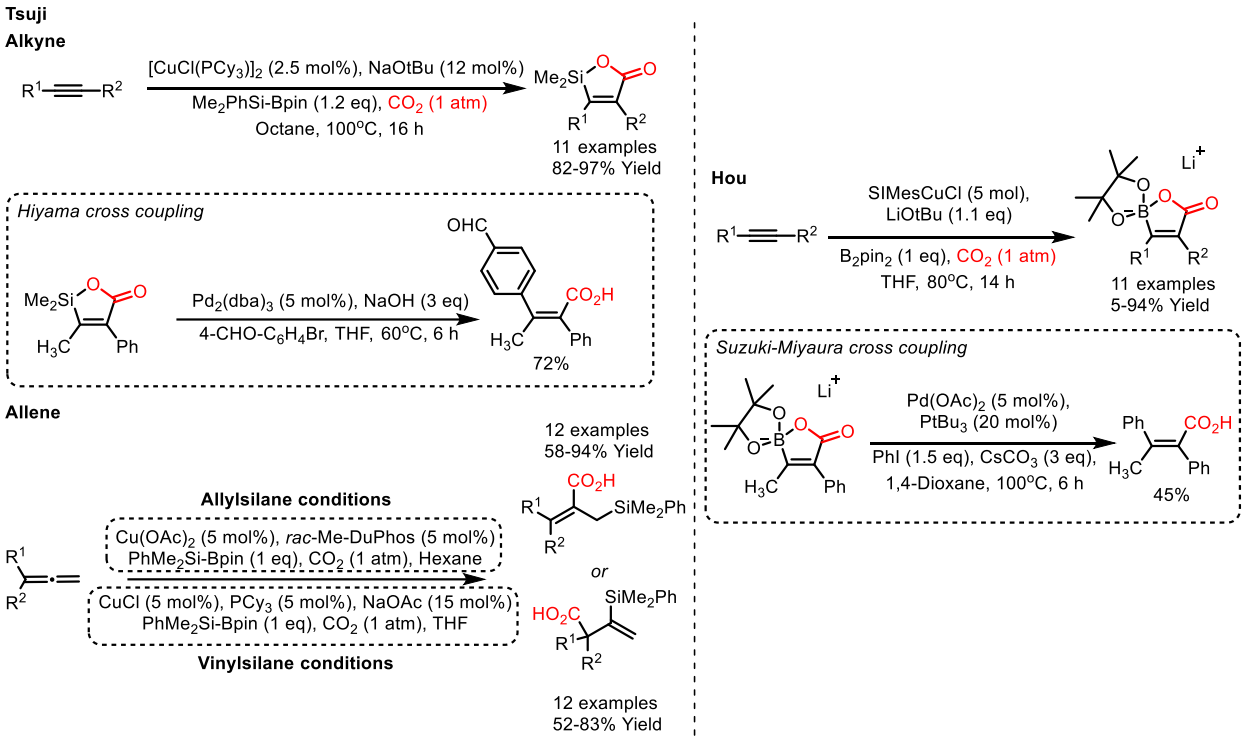

Scheme 1.8 Bora- and sila- carboxylative difunctionalization of alkynes

The regioselectivity arose from the silylcupration of allenes, wherein a bulkier bidentate *rac*-Me-DuPhos ligated copper complex led to the vinyl silanes, and a more electron rich tricyclohexylphosphine ligated copper species led to carboxylated allyl silanes. In 2012, Hou reported the regioselective catalytic boracarboxylation of alkynes with diboron and CO_2.[42] The proposed mechanism for this transformation proceeds through *syn* borylcupration of an alkyne from an NHC-copper(I) boryl complex. Subsequent nucleophilic addition of the alkenyl copper species to CO_2, followed by salt metathesis with LiO^tBu affords the boralactonate product. The boralactonate is amenable to Suzuki-cross coupling, leading to tetrasubstituted alkenes.

1.5 Boracarboxylation of Vinyl Arenes

These hetero(element)carboxylative difunctionalization reactions set the basis for a multitude of impactful chemical transformations. However, these methodologies are limited to alkyne or allene substrates, owing to the stronger enthalpic driving force of the reductive coupling reactions with these substrates. Moreover, the commercial availability of alkynes and allenes is limited, thus requiring extra synthetic steps in their transformations, leading to a diminished atom economy. Consequently, protocols in which hetero(element)carboxylative difunctionalization of more readily available olefin substrates are highly desirable. Specifically, borylative carboxylation of olefins is an especially powerful transformation, owing to the plethora of synthetic transformations and medicinal relevance provided by the resulting borylated aliphatic carboxylic acids.

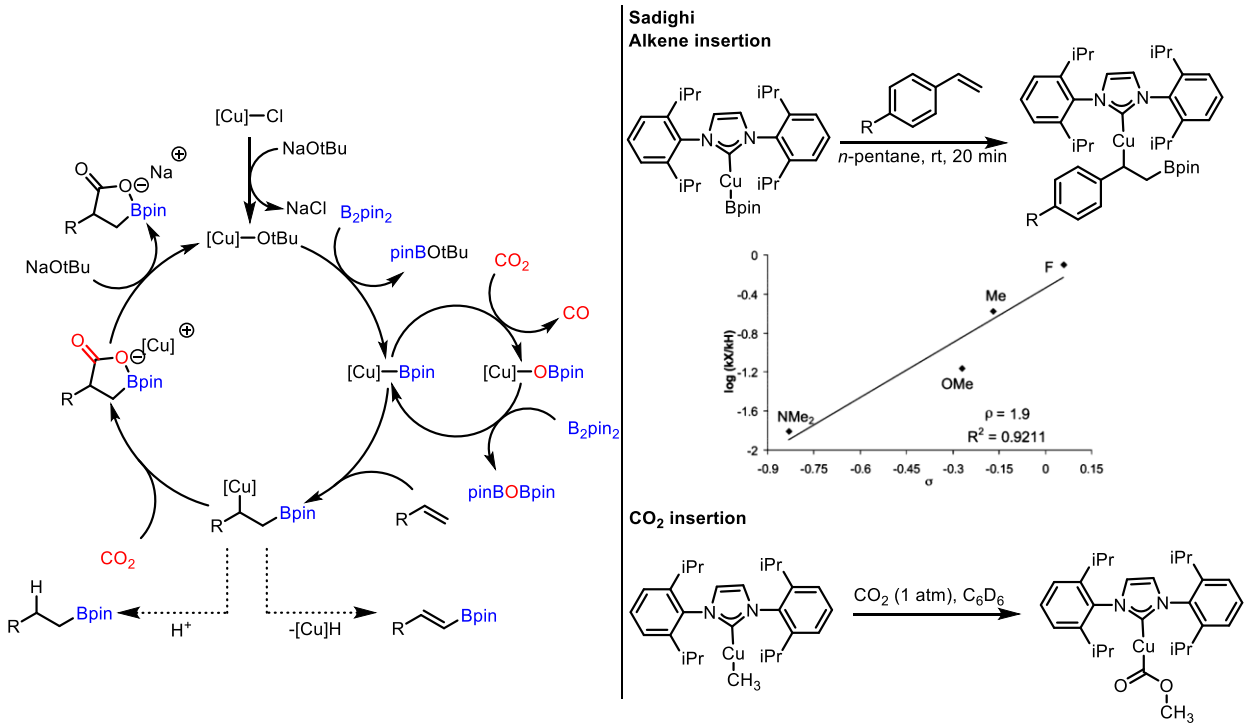

Figure 1.4 Popp's boracarboxylation of vinyl arenes mechanism (left) Sadighi previous mechanistic work (right).

Inspired by the copper(I)-boryl catalyzed boracarboxylation of alkynes, the Popp group developed a methodology in which alkenes underwent a similar transformation.[6] In 2006, Sadighi demonstrated that regioselective migratory insertion of styrene into an NHC-ligated copper(I)-boryl complex was a facile process.[43] Previously, he demonstrated that CO_2 can readily insert into copper(I)-methyl bonds to form a copper(I) acetate complex.[44] Based on these literature precedents, the Popp group wanted to use mechanistic insights to rationally design a methodology in which olefins can be boracarboxylated, thus a mechanism for this transformation was proposed (Figure 1.3). Beginning with a Cu-O^{t}Bu species, transmetallation with a diboron reagent will provide the active copper(I) boryl species wherein olefin insertion should occur readily. The resulting copper-alkyl can capture CO2, and upon salt metathesis with base the boracarboxylation product is produced, turning over the catalytic cycle. However, this strategy is not without significant challenges to overcome. The first of which being the competitive

CO_2/alkene insertion into a copper boryl species.[45] Sadighi and coworkers demonstrated that copper(I) boryl complexes can readily reduce CO_2 to CO. Moreover, if alkene insertion occurs selectively over CO_2 reduction, another challenge to overcome would be the competitive protodemetallation pathway of the copper alkyl intermediate, affording the formal anit-Markovnikov hydroboration product.

Table 1.1 Boracarboxylation of vinyl arenes reaction optimization

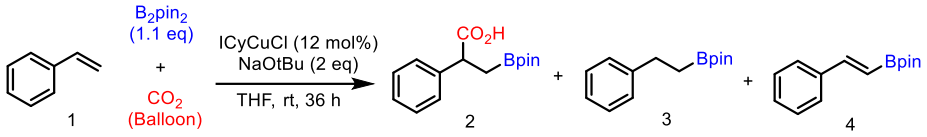

Entry	Deviation from conditions above	2 (%)	3 (%)	4 (%)	conv (%)
1	**none**	**91**	**6**	**<1**	**98**
2	IPrCuCl (12 mol%) instead of ICyCuCl	17	<1	<1	99
3	IMesCuCl (12 mol%) instead of ICyCuCl	85	<1	8	100
4	SIMesCuCl (12 mol%) instead of ICyCuCl	70	4	<1	100
5	PPh_3 (13 mol%) and CuCl (12 mol%) instead of ICyCuCl	1	13	22	99
6	$PMePh_2$ (13 mol%) and CuCl (12 mol%) instead of ICyCuCl	21	11	17	98
7	PEt_3 (13 mol%) and CuCl (12 mol%) instead of ICyCuCl	58	11	14	100
8	PCy_3 (13 mol%) and CuCl (12 mol%) instead of ICyCuCl	79	14	5	99
9	SEGPHOS (13 mol%) and CuCl (12 mol%) instead of ICyCuCl	0	2	6	94
10	Me-BPE (13 mol%) and CuCl (12 mol%) instead of ICyCuCl	11	12	41	100
11	Xantphos (13 mol%) and CuCl (12 mol%) instead of ICyCuCl	20	17	8	98
12	CuCl (12 mol%) instead of ICyCuCl	0	2	1	92

Due to the reactive nature of the copper alkyl intermediate, β-hydride elimination to afford a vinyl boronate species is another potential side reaction. Given the proposed mechanism and the propensity of vinyl arenes to insert into NHC-copper(I)-boryl complexes, the Popp group reasoned styrene would be an ideal alkene target for boracarboxylation (Table 1.1). Gratifyingly, when an inexpensive ICyCu^{t}Cl precatalyst was employed with a CO_2 balloon, NaO^{t}Bu, and a low loading of B_2pin_2 diboron reductant, 91% of the boracarboxylated product was obtained with minimal side product formation. Unsurprisingly, a strong σ-donating ICyCu^{t}Cl precatalyst was best for this transformation, and other NHC copper precatalysts lead to a diminishment in yield. Electron rich monodentate phosphines were able to provide the desired product in high yield, and in fact, as the electron rich nature of the phosphine increases, so does the yield. However, when bidentate phosphines are employed in this transformation the product yield decreases significantly, and larger quantities of side products 2 and 3 are observed. A control experiment with a CuCl precatalyst in the absence of ligand results in no product, thus confirming the electron rich NHC ligand is necessary for this transformation.

Table 1.2 Boracarboxylation of vinyl arenes substrate scope and synthetic utility

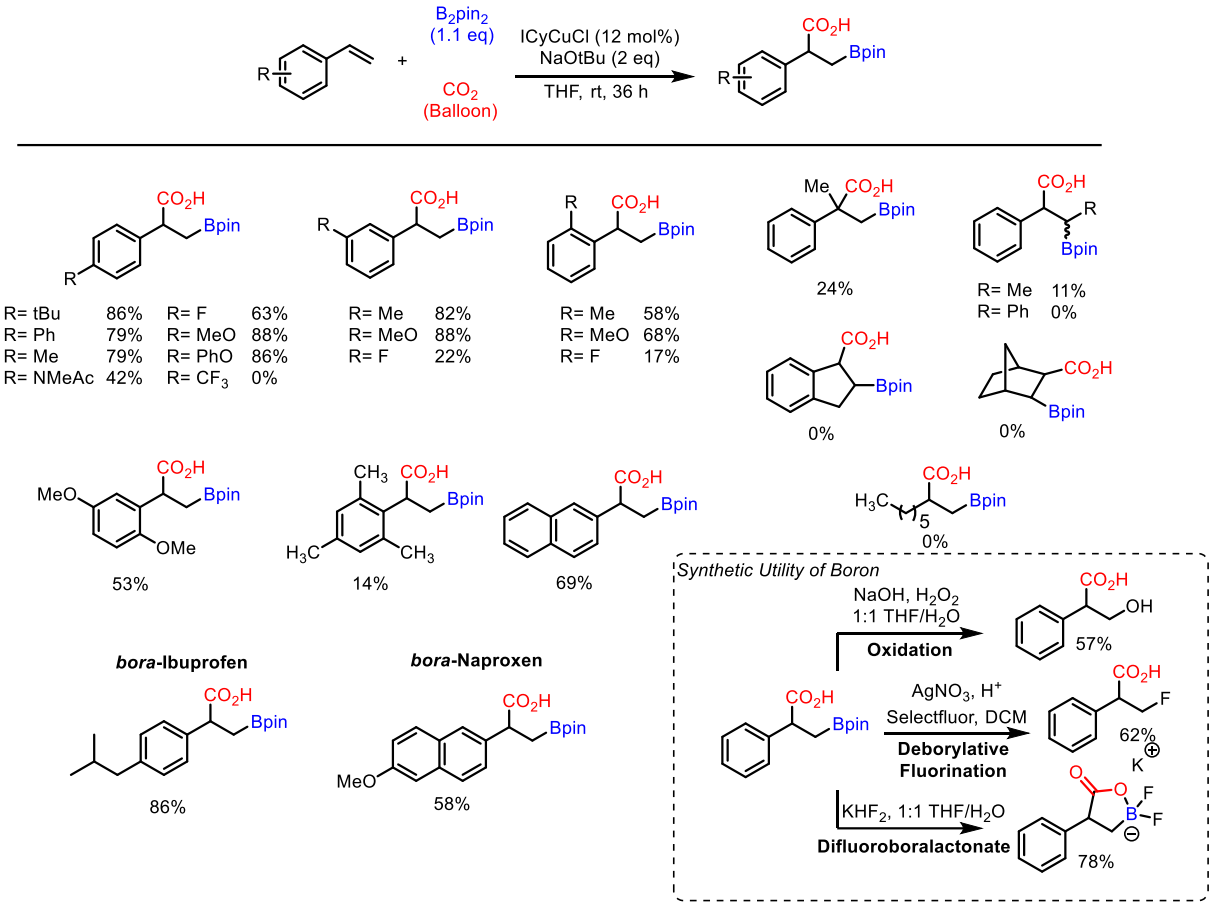

The low loading of B_2pin_2 (1.1 equiv.) likely suggests that the copper(I)-boryl-catalyzed CO_2 reduction pathway is not operative, as it consumes B_2pin_2, and as a result higher loading would be necessary.

With the optimized conditions in hand, the Popp group investigated the scope of vinyl arenes (Scheme 1.10). The reaction proceeded excellently with electron-neutral and electron-rich p-substituted vinyl arenes, with functional groups such as -tertbutyl, -methyl, -methoxy, -phenoxy -N-methylamide and -fluoro and proved to be completely regioselective for the branched aliphatic carboxylic acid product. Ortho- and meta-substituted methyl- and methoxy-substituted vinyl arenes were tolerated in modest to high yields; however, when the more electron deficient ortho- and meta-substituted fluoro derivatives were employed, a diminished yield was obtained, and the reactions required elevated temperatures. Styrene substrates bearing multiple substitutions such as 2,5-dimethoxy, and 2,4,6-trimethyl were boracarboxylated regioselectively, albeit at moderate (53%) and poor (14%) yields, respectively, suggesting that steric bulk on the arene did not influence the regioselectivity of the reaction. The extended π-system substrate 2-vinylnaphthelene delivered a 69% yield of desired boracarboxylated product.

Substantially electron deficient substrates such as p-trifluoromethylstyrene and p-cyanostyrene were not tolerated under these reaction conditions, even at elevated temperatures (Scheme 1.10). Sadighi and coworkers demonstrated that electron deficient vinyl arenes inserted into Cu-boryl species more readily than their electron rich

counterparts.[43] This suggests that the carboxylation step is the more kinetically challenging mechanistic step. Further screening of activated and unactivated olefin substrates such as 1-octene, norbornene, trans-stilbene, and indene did not afford any product, even at elevated temperature. However, when α- and β-methyl styrene were employed, low yield of the boracarboxylated product was obtained in both cases. Both substrates retained the same regiochemistry as their monosubstituted styrene counterparts, and the β-methyl styrene was obtained as an inseparable mixture of diastereomeric products.

The boracarboxylation strategy could prove useful in drug development, as the α-aryl propionic acid pharmacophore is present in many nonsteroidal anti-inflammatory drugs, and boron containing compounds have been demonstrated to be potent therapeutics.[46,47] The Popp group demonstrated that synthesis of two novel borylated NSAIDs was possible using their protocol (Scheme 1.10), delivering racemic bora-Ibuprofen and bora-Naproxen in good yields. When the synthetic utility of the boracarboxylated products was being explored, a silver-catalyzed fluorination with selectfluor afforded the formal fluorocarboxylated product, which can have potential medicinal chemistry applications. Also, treatment of boracarboxylated styrene with KHF_2 provided a novel difluoroboralactonate salt in high yield, and oxidation of the boron affords tropic acid derivatives, both of which have potential for further synthetic elaborations.

The novel boracarboxylation of vinyl arenes was achieved regioselectively with many substrates, affording moderate to excellent yields and minimal side product formation. Under mild conditions, highly abundant cheap styrene substrates were converted to highly valuable borylated carboxylic acid derivatives, using a CO_2 as a sustainable C1 synthon and stable B_2pin_2 as a reductant. As a result of this transformation, three new classes of compounds were accessed, demonstrating the practicality of the method. Nevertheless, this protocol experienced limitations, such as poor scope of electron deficient substrates and high catalyst loadings (12 mol%). In our literature search for potential solutions, we found that PPh_3 has demonstrated beneficial effects as a secondary ligand in other reductive copper-catalyzed processes through capture of copper decomposition species.[48,49,50,51] Consequently, we began reaction optimization with PPh_3 as a secondary ligand using p-terbutylstyrene as a model substrate.[7]

1.5.1 Investigation of PPh_3 Additive

Under the standard boracarboxylation conditions, excellent yield of the desired boracarboxylated product was obtained, with trace yield of unfavorable protoboration and dehydrogenative borylation side products[6]. Under nearly identical conditions, we obtained NMR yields within error of our the previously reported method, with only 5% NHC copper precatalyst loading, relying on PPh_3 as a secondary ligand (Table 1.2, entry 1). Initially, when the catalyst loading was lowered from 12 mol% to 5 mol%, we saw a significant decrease in yield. Originally, we demonstrated that a PPh_3-ligated copper species was catalytically active; however, the yields were low, and significant amounts of side products were observed relative to the yield obtained. Since electron rich phosphines led to higher yields under our original conditions, we hypothesized that when paired with ICyCuCl, a more competent boracarboxylation catalyst could be realized.

Table 1.3 Boracarboxylation of vinyl arenes secondary ligand optimization

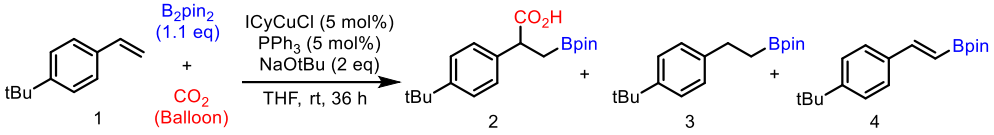

Entry	Deviation from conditions above	2 (%)	3 (%)	4 (%)	conv (%)
1	**none**	**89**	**<1**	**<1**	**>99**
2	ICyCuCl (12 mol%) and no PPh_3	92	<1	<1	>99
3	No PPh_3	60	<1	<1	95
4	CuCl (12 mol%) and PPh_3 (13 mol%)	18	8	16	65
5	PCy_3 (5 mol%) instead of PPh_3	82	<1	<1	>99
6	$P(OPh)_3$ (5 mol%) instead of PPh_3	44	28	<1	>99
7	Pyridine (5 mol%) instead of PPh_3	60	<1	<1	>99
8	ICyCuCl (2.5 mol%) and PPh_3 (3 mol%) at 40°C	78	15	<1	>99
9	ICyCuCl (2.5 mol%) and PCy_3 (3 mol%) instead of PPh_3 at 40°C	69	8	<1	85

However, slightly diminished yields were obtained from when PPh_3 was employed as the secondary ligand. Utilizing $P(OPh)_3$ as an additive proved to have a detrimental effect, as the yield is decreased from when only ICyCuCl is employed at 5 mol%. Unsurprisingly, pyridine had no effect as an additive, as in our previous study when it was used as a primary ligand, no reaction occurred. When we altered the catalyst and secondary ligand loading further, the reaction proceeded excellently with 78% yield obtained with catalyst loading as low as 2.5 mol% and PPh_3 loadings of 3 mol%. However, low catalyst loading led to formation of protoboration product compared to trace yield observed at higher loadings. Once again when PCy_3 was employed at these lower loadings, yields decreased significantly.

After developing a more efficient catalytic system through use of PPh_3 as a secondary ligand, we applied this protocol to electron deficient vinyl arenes to determine if these originally unreactive substrates would afford boracarboxylated product (Table 1.3). Reaction with para-trifluoromethyl styrene resulted in poor yield under the original boracarboxylation conditions, with a high yield of the undesired protoborylated product. However, when the new optimized conditions were employed, the yield of boracarboxylated product increased and doubled that of the undesired protoborylated product. When the catalyst, secondary ligand, and styrene concentration was increased further, moderate yield of the desired product was obtained in nearly threefold amount respective to the protoborylated product. Moreover, when higher styrene loading is employed in the absence of a PPh_3 secondary ligand, nearly equimolar amounts of both products are obtained at moderate yields. Undoubtedly, the suppression of undesired protoborylated product when PPh_3 is employed, along with the observed increase in boracarboxylated product yield, demonstrates its competency as a secondary ligand in this catalytic system.

Table 1.4 Boracarboxylation of electron-deficient vinyl arene optimization

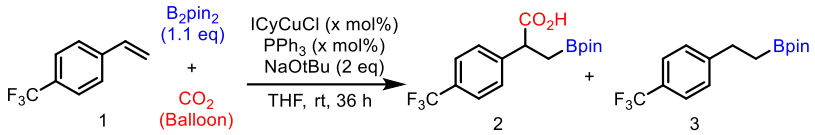

Entry	ICyCuCl (mol%)	PPh_3 (mol %)	1 (equiv)	2 (% Yield)	3 (% Yield)
1	12	0	1	9	18
2	12	0	5	40	44
3	5	5	5	22	51
4	5 at 40°C	5	5	31	33
5	5	5	2	27	63
6	5 at 40°C	5	2	36	35
7	5	5	1	28	13
8	12	12	2	53	20

When the catalyst and secondary ligand concentrations are lowered, nearly identical yields are obtained at varying styrene concentrations, and protoborylation becomes favored. Mild heating at these conditions results in diminishment of protoborylation, (Entry 4 and 5, Table 1.4) but both products are present in equimolar amounts. These latter results further exemplify that the optimized conditions from Table 1.2 provide a system in which boracarboxylation is favored over protoborylation significantly. Therefore, with these conditions in hand we decided to compare the vinyl arene scope of the two systems to better understand the catalytic efficiency.

Condition A in Table 1.5 consisted of the catalyst system in which 5 mol% of ICyCuCl and 5 mol% of PPh_3 is employed, whereas condition B represents the 12 mol% loading. It is worth nothing that isolation and purification of these products is difficult due to their decomposition when exposed to silica gel column chromatography. As a result, the removal of PPh_3 from the reaction mixture exacerbated isolation issues, leading to lower yields. Despite this complication, at lower catalyst loading, electron rich and neutral substrates still proceeded well, with crude yields comparable to the higher catalyst loading method. The N-methyl amide substrate was obtained in higher yields. These new conditions also enabled the synthesis of a previously unobtainable acetoxy-substituted substrate in moderate yield. As a result of lower catalyst loading, significant scale up to afford gram quantities of these boracarboxylated products is more attainable. In fact, when the p-^{t}Bu substrate is employed on a 40-mmol scale, 8 grams (60% yield) of boracarboxylated product is obtained. The borylated Ibuprofen derivative is also amenable to scalable conditions, resulting in acquisition of single crystals suitable for X-ray crystallographic characterization. Along with bora-Naproxen, comparative yields are obtained between both catalytic conditions for the two originally reported bora-NSAIDs in this method. Two more borylated NSAID derivatives were also prepared in good to excellent yields with both catalytic systems, further demonstrating the practicality of both sets of reaction conditions.

Table 1.5 Scope of new catalytic conditions vs. previous catalytic conditions

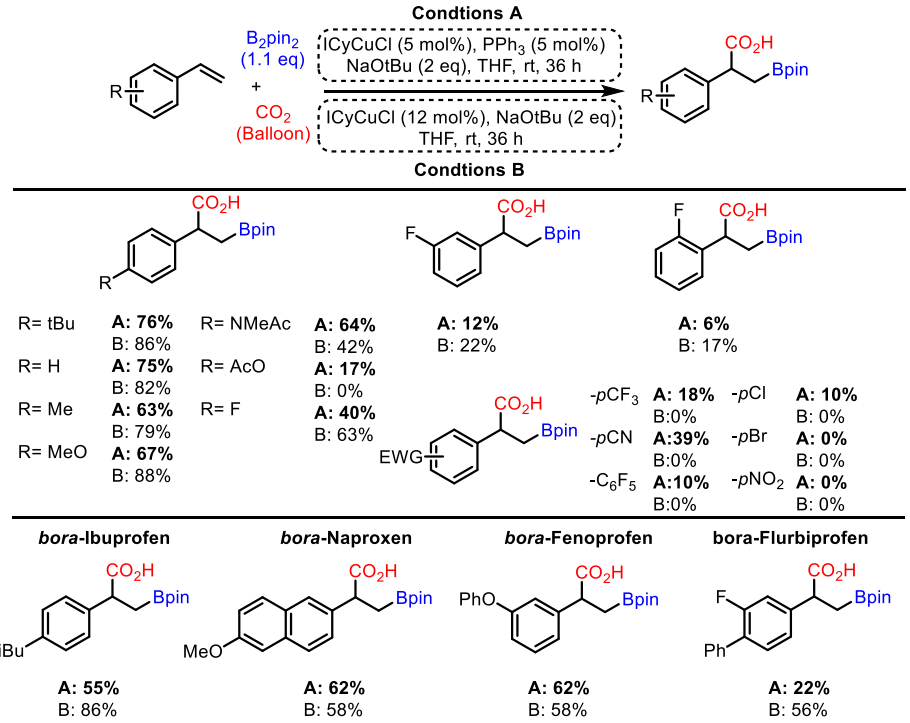

When a larger scope of electron deficient vinyl arenes was revisited, mild heating was required to obtain yields of these unfavorable substrates. However, even with these problematic substrates, the system with lower catalyst loading delivered the boracarboxylated fluoro-substituted arene products in comparable yields to the original method. Notably, previously unobtainable electron deficient vinyl arenes such as p-CF_3 styrene and p-CN styrene are successfully boracarboxylated in moderate crude yields. However, when halogenated bromo- and chloro-arene substrates are employed, along with highly electron deficient substrates such as pentafluoroaryl- and p-NO_2 styrene, no isolable products were obtained.

After addressing the initial high catalyst loading and the limited scope, the Popp group sought to elucidate the role of PPh_3 in catalysis. Experimental studies by Sadighi[44,45] and computational studies by Lin[52] demonstrated that copper(I)-boryl insertion of alkenes occurs in a *syn* fashion. The resulting copper(I)-alkyl species is carboxylated through either a direct insertion pathway, or an S_E-type pathway. Initially when we employed trans β-methylstyrene as a mechanistic probe the diastereomeric ratio of products obtained (7:1 *syn* to

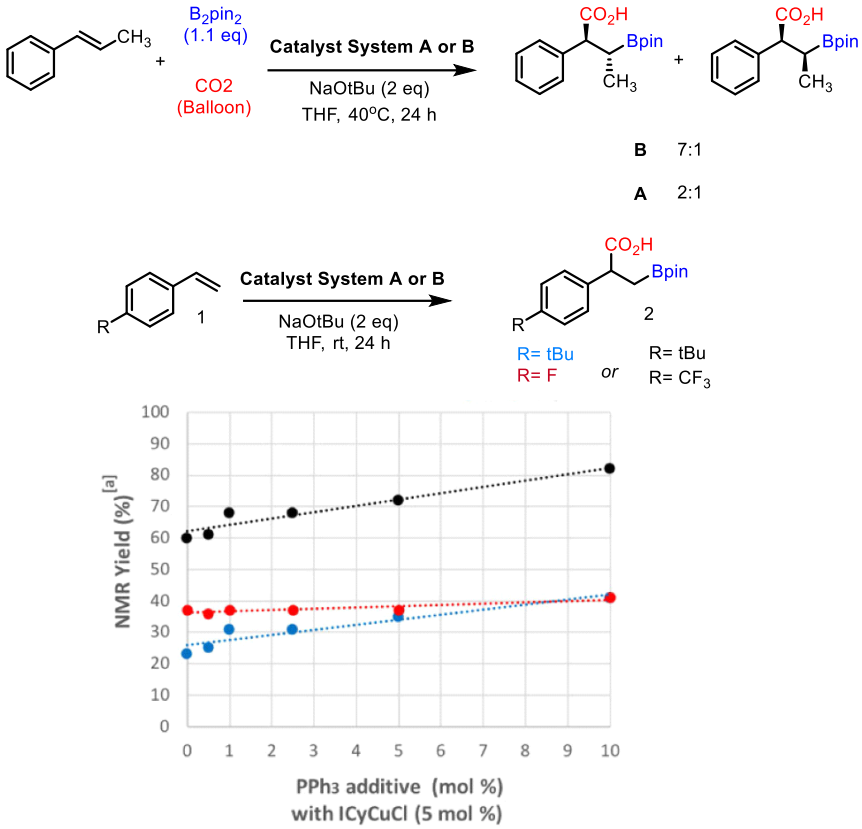

Entry	Catalyst System	1 (equiv)	2-*p*tBu	2-*p*CF_3
1	B	1	0	41
2	A	1	0	23
3	B	0.1	0	18
4	B	0.1 (1.1 eq *p*CF_3)	0	9

Scheme 1.9 Preliminary mechanistic investigations

anti) supported a direct insertion pathway.[6] However, when the catalytic system with PPh_3 was employed for this transformation, nearly complete erasure of the diastereoselectivity (2:1) was observed (Scheme 1.12), with *syn* insertion product slightly favored. When the diastereo-enriched product was subjected to the same PPh_3 reaction conditions, erosion in diastereomer ratio did not occur. These experiments suggest that PPh_3 plays a role in the carboxylation step of the mechanism, with a potential S_E-type carboxylation pathway becomes operative under these conditions. Furthermore, when an electron deficient and electron rich substrate were employed simultaneously under both sets of catalytic conditions, the electron deficient substrate was boracarboxylated exclusively. Interestingly, when equimolar amounts of both substrates were employed, the original condition's reaction yield nearly doubled that of the PPh_3 conditions, suggesting that an electron rich styrene additive could allow for higher yields of electron deficient substrates. This is further exemplified when catalytic amounts of an electron rich substrate is employed as an additive under the original reaction conditions. The yield obtained of the electron deficient substrate is doubled,

and none of the electron rich substrate is boracarboxylated. These results suggest that the electron deficient substrate selectively inserts into the copper-boryl species, and the PPh_3 additive enhances the reactivity of the copper alkyl species with CO_2 (Scheme 1.12).

The experimental studies conducted wherein PPh_3 was employed as a secondary ligand, in combination with alteration of reaction stoichiometry, led to lower catalyst loading and expansion of boracarboxylation reaction scope to various electron deficient vinyl arene substrates, thereby addressing two major reaction limitations. Additionally, two novel borylated NSAIDs (Flurbiprofen and Fenoprofen) were synthesized, further demonstrating the viability of this new method. Preliminary mechanistic experiments suggest that PPh_3 potentially affects carboxylation, leading to an S_E carboxylation pathway. Even so, the complete role of PPh_3 had not yet been realized, and these methodologies are still limited to activated vinyl arene substrates. Therefore, generalization of the boracarboxylation of alkenes would require in-depth mechanistic studies. Although there are sufficient literature precedents to support the proposed mechanism[40,41,42], direct evidence supported through either computations or experiments is lacking. Furthermore, in previous studies, the rate determining step in the proposed mechanism was identified as the carboxylation of the copper(I)-benzyl species.[6,7,52,53] Subsequently, in 2020 the Popp group began their mechanistic studies through density functional theory with a specific focus on the carboxylation step of the mechanism. Particularly, using boron valence deficiency calculations, they sought to determine whether or not boron activated CO_2 for insertion through Lewis acid/base interactions between the proximal oxygen of CO_2 and boron. Moreover, in 2021 they reported a multistep approach wherein they performed experimental studies of the key carboxylation step in the copper(I)-catalyzed boracarboxylation of vinyl arenes, complemented by density functional theory, with an emphasis on reaction kinetics.

1.5.2 Mechanistic Studies

Initial computational analysis revealed an interaction between boron and the proximal oxygen of metal-bound CO_2, a process which hadn't been realized in the previous studies. Computations performed by the Lu group in 2017[53] demonstrated that the sterics of the ancillary ligands employed in the catalytic reaction directly affected the CO_2 insertion energy barrier; however, the role of boron was not explored. As a result, the Popp group decided to explore the the electronic effect of the boron on the CO_2 insertion barrier in the boracarboxylation of styrene[8].

The study began by first identifying the carboxylation transition state wherein the ideal ICy-ligated copper-benzyl species with a reduced ethyleneglycato boron ester is employed. Immediately, a potential non-covalent interaction between the boron and the proximal oxygen of CO_2 was evident (Figure 1.4). To better understand this interaction, natural bond orbital 2nd order perturbation analysis was utilized. This analysis revealed a stabilization energy of 8.7 kcal/mol calculated from the interaction of lone pair of the CO_2 oxygen and the vacant p orbital of boron. Since the enthalpic barrier of CO_2 insertion between IMe and

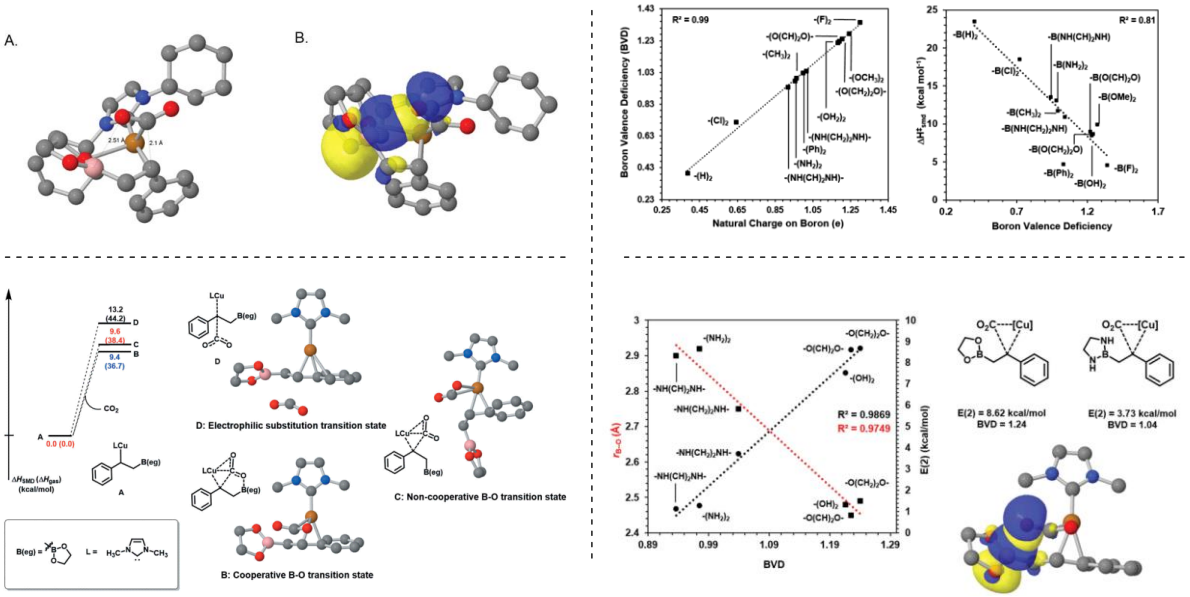

Figure 1.5 Adapted from Baughman N. N and Popp, B. V., **2020**. *Comments on Inorganic Chemistry*, 40:4, 159-175. Computed structure of ICyCu(β-borylbenzyl) carboxylation transition state (top left A) NBO orbitals (top left B). Transition states of carboxylation $\Delta H^{\ddagger}$ values (bottom left). Natural charge on boron, and the effect of boron valence deficiency (top right). Relationship between stabilization energies from NBO analysis (black) and B-O interaction distances (red).

ICy are comparable, the Popp group decided that truncated IMe ligand would remove the steric contributions that the ligand had on the energy barrier of CO_2 insertion. Thus, this is the ligand employed for the remainder of this study.

Three potential carboxylation pathways were envisioned: 1) A pathway in which boron interacts with the proximal oxygen of CO_2; 2) a noncooperative pathway wherein boron is directed away from the metal center; and 3) an S_E pathway like the one proposed previously, wherein copper doesn't participate directly in C-C bond formation. The latter S_E pathway was the least energetically favored pathway, which agrees with the initial experimental data with β-methyl styrene back in 2016. The cooperative CO_2/boron interaction transition state (pathway 1) is nearly identical in energy with the noncooperative pathway with THF solvation. However, in the gas phase path 1 is energetically favored. To better understand this difference in energy barrier, a variety of electronic different boron moieties were evaluated computationally.

Each boron center was evaluated through both natural charge (NC) and boron valence deficiency (BVD) (Figure 1.4). BVD is a measurement of the Lewis acidity of boron by way of the propensity of the respective boron moiety to accept electrons. This value is determined by subtracting the NBO-computed natural valency of boron from its formal valence. When the natural charge on boron was calculated and compared against the BVD, a positive linear relationship was observed wherein the values were nearly identical, thus confirming their direct relationship. Next, for each of the boron species, the enthalpic barrier of insertion was calculated. As the electronegativity of the groups bound to boron increased, the energy barrier decreased, thereby further supporting a carboxylation pathway in which boron can activate CO_2.

Strong computational evidence shows that boron can assist in CO_2 insertion via an activation pathway. However, preliminary mechanistic experiments demonstrated that multiple carboxylation pathways are possible depending on the catalytic system employed. These experiments also alluded to two potential carboxylation pathways: a direct CO_2 insertion pathway and a phosphine-mediated S_E pathway. Thus, the Popp group decided to approach this complex problem through experimental studies corroborated computationally.

The Popp group began their studies with the isolation of highly reactive active catalytic species ICyCuO^{t}Bu, ICyCuBpin, and the ICyCu(β-borylbenzyl) based off of their catalytic system[6]. However, only ICyCuO^{t}Bu was able to be successfully synthesized a previous report[43] and upon attempting to synthesize other species rapid decomposition occurred, similar to observations in previous reports. As a result, they decided to go forward with the more stable IPr NHC-ligated copper precatalyst. Following the methodology reported by Sadighi,[43] a variety of IPrCu(β-borylbenzyl) complexes were afforded in moderate yields, including novel para- substituted acetoxy-, methoxycarbonyl-, and trifluoromethyl- derivatives (Figure 1.5). With these complexes in hand, we proceeded with the carboxylation of these reactive intermediates.

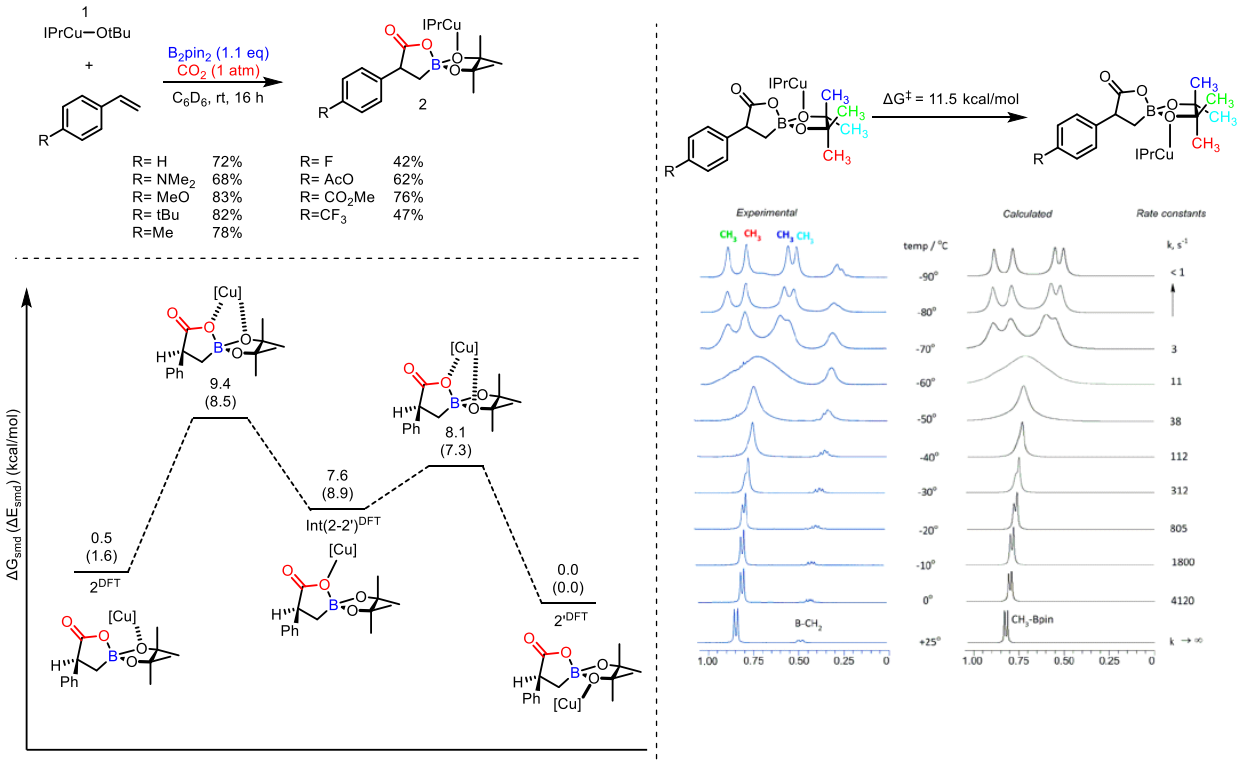

Figure 1.6 Isolated carboxylated IPrCu(β-borylbenzyl) complexes (top left). Experimental and calculated VT ^{1}H NMR spectra (right). DFT modeling of [Cu] binding to each oxygen in the pinacol ring (bottom left).

Moderate to excellent yields of the resulting spiroboralactonate species were obtained, ranging from electron rich (para-methoxy) to electron poor (para-trifluoromethyl) derivatives. In the case of the electron deficient substrates, a

longer reaction time and PPh_3 additive was necessary for carboxylation to occur. X-ray crystallographic data of 2 confirmed the solid state spiroboralactonate structure, with copper bound to one of the pinacolate oxygens.

Variable temperature ^1H NMR studies were conducted to determine whether this copper-oxygen binding mode would be observed in solution (Figure 1.5). As the temperature decreased from room temperature (25°C) to -90°C, the two diastereotopic methyl resonances on the pinacol ring split into four unique resonances, implying dynamic behavior in solution. This dynamic behavior was further studied computationally, wherein the oxygens present in the 5-membered borapinacolate ring can each individually bind to copper. The barrier for this dynamic behavior is low (~2kcal/mol), implying rapid exchange at room temperature (Figure 1.5). The proposed mechanism was then further studies through kinetic analysis. Previously, it was demonstrated that the electronic rich alkenes proceeded well in this transformation, and electron deficient alkenes proceeded poorly.[6]

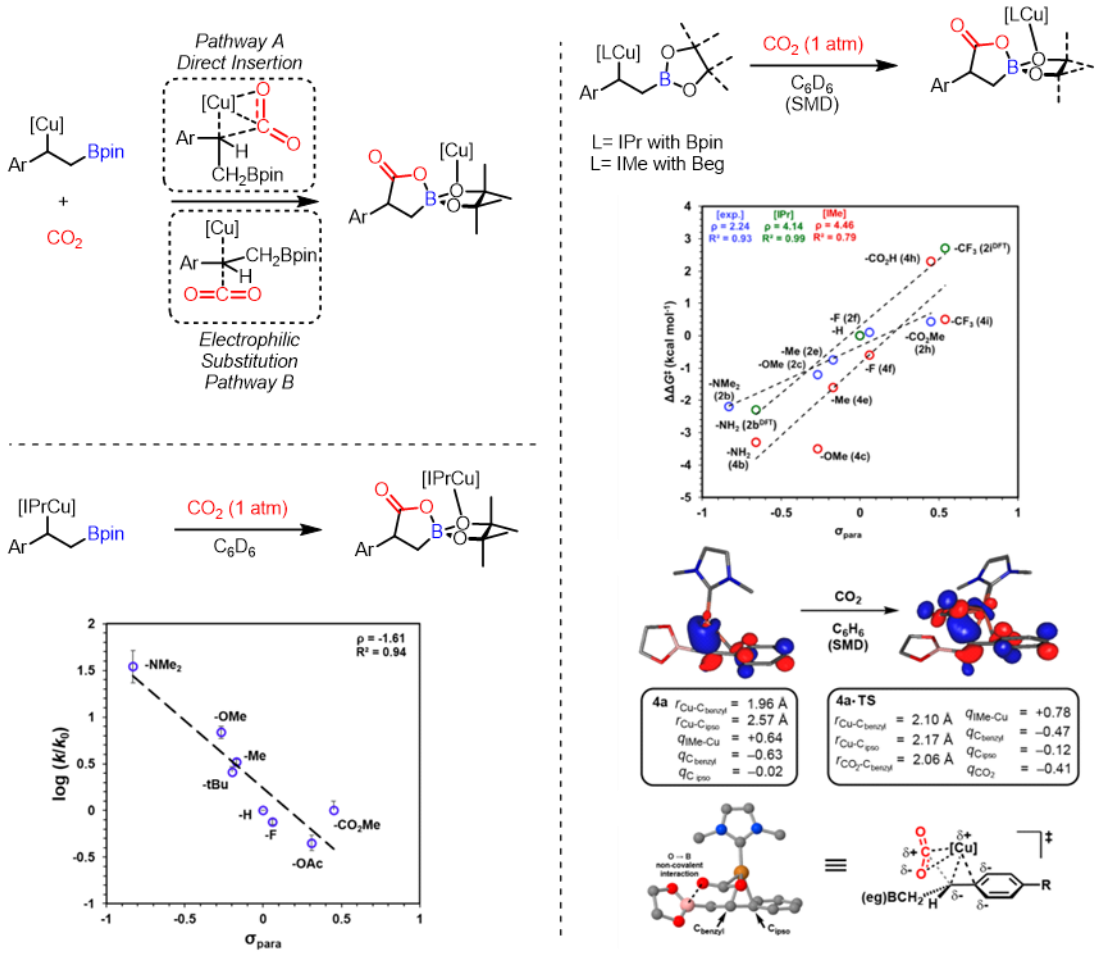

Figure 1.7 Potential carboxylation pathways (top left). $\Delta\Delta G^{\ddagger}$ energies comparison between experimental and computational systems (right). Depiction of the HOMO of the IMeCu(β-borylbenzyl) and the direct CO_2 insertion transition state, and model of the key stereoelectronic interactions in the transition state (right). Adapted from Baughman, N. N.; Akhmedov, N. G.; Petersen, J. L.; Popp, B. V. *Organometallics* **2021**, *40* (1), 23–37

Thus, the carboxylation studies began with varying the electronic nature of the inserted alkene in the IPrCu(β-borylbenzyl) complexes. Unsurprisingly, Hammett analysis revealed that carboxylation rates decreased as the electron deficient nature of the complex increased, and in the case of the electron deficient para-CF_3 substrate, the yield of the carboxylation was poor (<5% via NMR).

As mentioned previously, two potential carboxylation pathways are possible (Figure 1.6): direct carboxylation and an S_E pathway proceeding through a carbanion masked by copper. In the case of the S_E pathway, an S_E1 pathway would need a large negative charge buildup to stabilize the benzylic carbanion intermediate. The Hammett analysis revealed a large negative ρ value (-1.61) indicating positive charge buildup, which is inconsistent with an S_E1 mechanism. However, Hammett analysis alone cannot differentiate between a direct insertion and a S_E2 pathway. Therefore, the Popp group turned to density functional theory to provide insight into the potential active pathway. To cut down on computational expense, the IPrCu(β-borylbenzyl) complex was replaced with a IMeCu(β-borylbenzyl) complex, with an ethyleneglycato boronate ester as the boryl group. The calculated free energy changes between the IMe system and the experimental data were in reasonable agreement. Electron-rich arenes exhibited lower barriers for insertion then their electron-poor counterparts. When the energy barriers of carboxylation were calculated for choice IPr-ligated β-borylbenzyl copper complexes, similar electronic dependence was observed. Interestingly, the visualization of the carboxylation transition state shows a weak noncovalent interaction of the copper center with the neighboring ipso carbon of the arene. A lengthening of Cu-C_{benzyl} bond is observed along with a shortening of Cu-C_{ipso} bond (Figure 1.6). Potential delocalization of electron density from copper to the arene unit results in destabilization of the benzylic anion, leading to a poorer nucleophile. Thus, a higher barrier for CO_2 insertion in the case of electron poor arenes is observed. All these computational results strongly suggest that the direct insertion pathway is the kinetically favored pathway for insertion in NHC-ligated copper complexes.

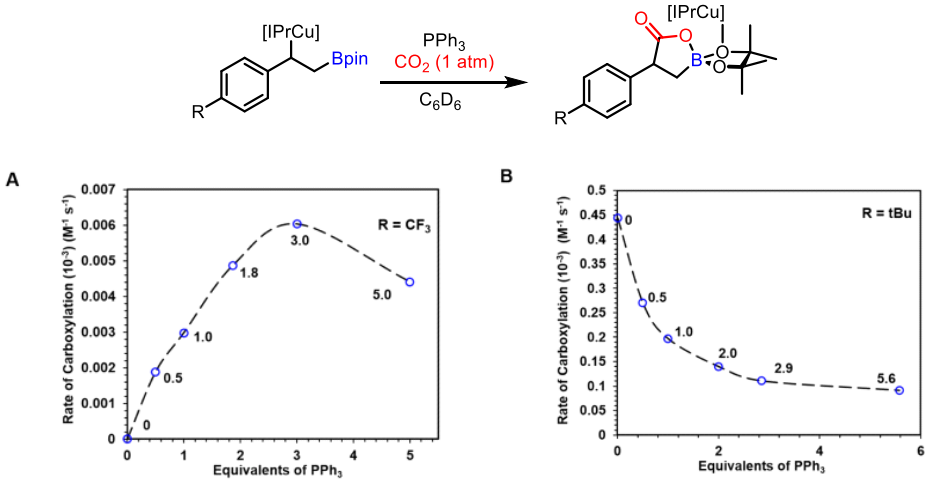

Figure 1.8 Phosphine additive effects

When a PPh_3 additive is added to catalytic reactions, enhanced reactivity of electron deficient arenes is observed. The Popp group surmised that utilization of a PPh_3 additive could potentially allow for carboxylation of the electron deficient IPrCu(β-borylbenzyl) complexes[7]. When stoichiometric PPh_3 is introduced, carboxylation of an electron deficient pCF_3 IPrCu(β-borylbenzyl) complex was observed via ^1H NMR spectroscopy. In situ monitoring using ^{31}P NMR spectroscopy showed no new resonances, thus the Popp group decided to examine the kinetic impact of PPh_3 at various concentrations (Figure 1.7). In the case of the electron deficient complex, the reaction rate increased as the PPh_3 concentration increased, with saturation dependance observed at concentrations higher than 3 equivalents. This rate increase implies that a different mechanistic pathway for carboxylation is now operative under phosphine-mediated conditions, as in the absence of phosphine no product yield is observed over the course of multiple days. Notably, when an electron rich p-tBu IPrCu(β-borylbenzyl) complex was employed for carboxylation under phosphine mediated conditions, inhibition of carboxylation is observed. These results demonstrate that in the case of an electron rich IPrCu(β-borylbenzyl) complex, a phosphine mediated pathway is disfavored over the traditional direct CO_2 insertion pathway, whereas the opposite is true for an electron deficient IPrCu(β-borylbenzyl) complex.

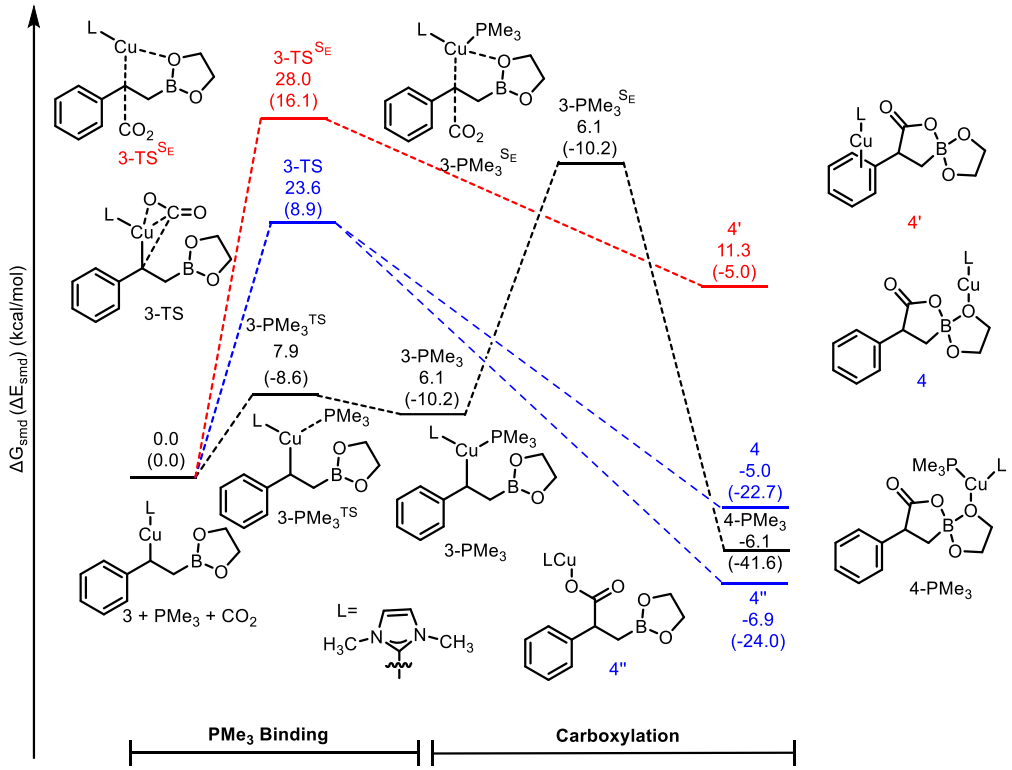

Figure 1.9 Reaction coordinates for carboxylation

The Popp group decided to proceed with computational studies to understand the nature of the interaction between phosphine and the truncated IMeCu(β-borylbenzyl) complex used previously. PMe_3 was used as a model phosphine ligand, and a transition state wherein PMe_3 was coordinated to the IMeCu(β-borylbenzyl) complex was identified and attempts to determine a direct CO_2 insertion transition state of this complex was unsuccessful. Therefore, both a phosphine- assisted and unassisted alternative S_E2 pathway were considered and compared against

the phosphine-free direct insertion pathway (Figure 1.8). The PMe_3-assisted S_E2 pathway was over 2 kcal/mol more favorable than the unassisted pathway, yet the direct insertion pathway was the lowest energy pathway overall. Furthermore, NBO analysis shows that PMe_3 stabilizes the cationic copper center. Subsequently, this leads to greater anionic character of the benzyl anion, allowing for a more facile carboxylation to occur.

1.6 Summary

Chapter 1 has examined the Popp group's boracarboxylation methodology in the context of other catalytic reductive carboxylation chemistry, exemplifying the advantages of a difunctionalization protocol wherein value-added aliphatic carboxylic acid products are provided directly from readily available, abundant chemical feedstocks using base metal catalysis. The initial issues with high catalyst loading and poor tolerance of electron deficient substrates were addressed by using a secondary ligand, and key mechanistic details were revealed with concomitant experimental studies and density functional theory analysis of potential reaction intermediates. However, the scope of the reaction remains limited to mostly mono-functionalized activated alkenes, and the reaction can only be performed under extremely strict oxygen- and moisture-free conditions. Therefore, the following chapters will describe synthetic methods for improved scope and catalytic efficiency in the boracarboxylation of alkenes, addressing these issues. Chapter 2 examines reactivity of α-substituted vinyl-arene substrates by way of reaction optimization in a system that contains multiple competitive pathways arising from unfavorable alkene insertion. Chapter 3 provides an approach to synthesize a novel borylated ibuprofen derivative through Suzuki cross-coupling and boracarboxylation methodologies. This chapter also provides a benchtop method where boracarboxylation of two substrates can be achieved in moderate to high yields without the need for a glovebox or prefunctionalized copper(I) precatalyst. Chapter 4 explores Xantphos as a catalytic additive that allows for boracarboxylation of unactivated alkene substrates in moderate yields, improving the reaction scope greatly and leading to discovery of a synthetic route to access pyrroloisoindolinones in high yields from phthalimides.

1.7 References

[1] (a) Sable, D. A.; Vadagaonkar, K. S.; Kapdi, A. R.; Bhanage, B. M. Carbon Dioxide Based Methodologies for the Synthesis of Fine Chemicals. *Org. Biomol. Chem.* **2021**, *19* (26), 5725–5757. (b)Fujihara, T.; Tsuji, Y. Carboxylation Reactions Using Carbon Dioxide as the C1 Source via Catalytically Generated Allyl Metal Intermediates. *Front. Chem.* **2019**, *7*, 430. (c) Shi, Y.; Pan, B.-W.; Zhou, Y.; Zhou, J.; Liu, Y.-L.; Zhou, F. Catalytic Enantioselective Synthesis Using Carbon Dioxide as a C1 Synthon. *Org. Biomol. Chem.* **2020**, *18* (42), 8597–8619. (d) Lluna-Galán, C.; Izquierdo-Aranda, L.; Adam, R.; Cabrero-Antonino, J. R. Catalytic Reductive Alcohol Etherifications with Carbonyl-Based Compounds or CO2 and Related Transformations for the Synthesis of Ether Derivatives. *ChemSusChem* **2021**, *14* (18), 3744–3784. (e)Cabrero-Antonino, J. R.; Adam, R.; Beller, M. Catalytic Reductive N-Alkylations Using CO2 and Carboxylic Acid Derivatives: Recent Progress and Developments. *Angew. Chem. Int. Ed.* **2019**, *58* (37), 12820–12838. (f) Yuan, L.; Qi, M.-Y.; Tang, Z.-R.; Xu, Y.-J. Coupling Strategy for CO2 Valorization Integrated with Organic Synthesis by Heterogeneous Photocatalysis. *Angew. Chem. Int. Ed.* **2021**, *60* (39), 21150–21172. (g) Wang, L.; Que, S.; Ding, Z.; Vessally, E. Oxidative Carboxylation of Olefins with CO2: Environmentally Benign Access to Five-Membered Cyclic Carbonates. *RSC Adv.* **2020**, *10* (15), 9103–9115. (h) Pimparkar, S.; Dalvi, A. K.; Koodan, A.; Maiti, S.; Al-Thabaiti, S. A.; Mokhtar, M.; Dutta, A.; Lee, Y. R.; Maiti, D. Recent Advances in the Incorporation of CO2 for C–H and C–C Bond Functionalization. *Green Chem.* **2021**, *23* (23), 9283–9317. (i) Claver, C.; Yeamin, M. B.; Reguero, M.; Masdeu-Bultó, A. M. Recent Advances in the Use of Catalysts Based on Natural Products for the Conversion of CO2 into Cyclic Carbonates. *Green Chem.* **2020**, *22* (22), 7665–7706. (j) Saini, S.; Prajapati, P. K.; Jain, S. L. Transition Metal-Catalyzed Carboxylation of Olefins with Carbon Dioxide: A Comprehensive Review. *Catal. Rev.* **2020**, 1–47. (k) Liu, X.-F.; Li, X.-Y.; He, L.-N. Transition Metal-Catalyzed Reductive Functionalization of CO2. *Eur. J. Org. Chem.* **2019**, *2019* (14), 2437–2447. (l) Pradhan, S.; Roy, S.; Sahoo, B.; Chatterjee, I. Utilization of CO2 Feedstock for Organic Synthesis by Visible-Light Photoredox Catalysis. *Chem. – Eur. J.* **2021**, *27* (7), 2254–2269.

[2] (a) Lassila, T.; Hokkanen, J.; Aatsinki, S.-M.; Mattila, S.; Turpeinen, M.; Tolonen, A. Toxicity of Carboxylic Acid-Containing Drugs: The Role of Acyl Migration and CoA Conjugation Investigated. *Chem. Res. Toxicol.* **2015**, *28* (12), 2292–2303. (b) Ballatore, C.; Huryn, D. M.; Smith III, A. B. Carboxylic Acid (Bio)Isosteres in Drug Design. *ChemMedChem* **2013**, *8* (3), 385–395.

[3] Tortajada, A.; Juliá-Hernández, F.; Börjesson, M.; Moragas, T.; Martin, R. Transition-Metal-Catalyzed Carboxylation Reactions with Carbon Dioxide. *Angew. Chem. Int. Ed.* **2018**, *57* (49), 15948–15982.

[4] Tortajada, A.; Börjesson, M.; Martin, R. Nickel-Catalyzed Reductive Carboxylation and Amidation Reactions. *Acc. Chem. Res.* **2021**, *54* (20), 3941–3952.

[5] Whyte, A.; Torelli, A.; Mirabi, B.; Zhang, A.; Lautens, M. Copper-Catalyzed Borylative Difunctionalization of π-Systems. *ACS Catal.* **2020**, *10* (19), 11578–11622.

[6] Butcher, T. W.; McClain, E. J.; Hamilton, T. G.; Perrone, T. M.; Kroner, K. M.; Donohoe, G. C.; Akhmedov, N. G.; Petersen, J. L.; Popp, B. V. Regioselective Copper-Catalyzed Boracarboxylation of Vinyl Arenes. *Org. Lett.* **2016**, *18* (24), 6428–6431.

[7] Perrone, T. M.; Gregory, A. S.; Knowlden, S. W.; Ziemer, N. R.; Alsulami, R. N.; Petersen, J. L.; Popp, B. V. Beneficial Effect of a Secondary Ligand on the Catalytic Difunctionalization of Vinyl Arenes with Boron and CO2. *ChemCatChem* **2019**, *11* (23), 5814–5820.

[8] Baughman, N. N.; Popp, B. V. Evidence of Boron Assistance for CO2 Activation during Copper-Catalyzed Boracarboxylation of Vinyl Arenes: A Synthetic Model for Cooperative Fixation of CO2. *Comments Inorg. Chem.* **2020**, *40* (4), 159–175.

[9] Baughman, N. N.; Akhmedov, N. G.; Petersen, J. L.; Popp, B. V. Experimental and Computational Analysis of CO2 Addition Reactions Relevant to Copper-Catalyzed Boracarboxylation of Vinyl Arenes: Evidence for a Phosphine-Promoted Mechanism. *Organometallics* **2021**, *40* (1), 23–37.

[10] Correa, A.; Martín, R. Palladium-Catalyzed Direct Carboxylation of Aryl Bromides with Carbon Dioxide. *J. Am. Chem. Soc.* **2009**, *131* (44), 15974–15975.

[11] Fujihara, T.; Nogi, K.; Xu, T.; Terao, J.; Tsuji, Y. Nickel-Catalyzed Carboxylation of Aryl and Vinyl Chlorides Employing Carbon Dioxide. *J. Am. Chem. Soc.* **2012**, *134* (22), 9106–9109.

[12] Charboneau, D. J.; Brudvig, G. W.; Hazari, N.; Lant, H. M. C.; Saydjari, A. K. Development of an Improved System for the Carboxylation of Aryl Halides through Mechanistic Studies. *ACS Catal.* **2019**, *9* (4), 3228–3241.

[13] Ma, C.; Zhao, C.-Q.; Xu, X.-T.; Li, Z.-M.; Wang, X.-Y.; Zhang, K.; Mei, T.-S. Nickel-Catalyzed Carboxylation of Aryl and Heteroaryl Fluorosulfates Using Carbon Dioxide. *Org. Lett.* **2019**, *21* (7), 2464–2467.

[14] Correa, A.; León, T.; Martin, R. Ni-Catalyzed Carboxylation of C(Sp2)– and C(Sp3)–O Bonds with CO2. *J. Am. Chem. Soc.* **2014**, *136* (3)

[15] León, T.; Correa, A.; Martin, R. Ni-Catalyzed Direct Carboxylation of Benzyl Halides with CO2. *J. Am. Chem. Soc.* **2013**, *135* (4), 1221–1224.

[16] Liu, Y.; Cornella, J.; Martin, R. Ni-Catalyzed Carboxylation of Unactivated Primary Alkyl Bromides and Sulfonates with CO2. *J. Am. Chem. Soc.* **2014**, *136* (32), 11212–11215.

[17] Börjesson, M.; Moragas, T.; Martin, R. Ni-Catalyzed Carboxylation of Unactivated Alkyl Chlorides with CO2. *J. Am. Chem. Soc.* **2016**, *138* (24), 7504–7507.

[18] Tran-Vu, H.; Daugulis, O. Copper-Catalyzed Carboxylation of Aryl Iodides with Carbon Dioxide. *ACS Catal.* **2013**, *3* (10), 2417–2420.

[19] Yan, S.-S.; Wu, D.-S.; Ye, J.-H.; Gong, L.; Zeng, X.; Ran, C.-K.; Gui, Y.-Y.; Li, J.; Yu, D.-G. Copper-Catalyzed Carboxylation of C–F Bonds with CO2. *ACS Catal.* **2019**, *9* (8), 6987–6992.

[20] Boogaerts, I. I. F.; Nolan, S. P. Carboxylation of C−H Bonds Using N-Heterocyclic Carbene Gold(I) Complexes. *J. Am. Chem. Soc.* **2010**, *132* (26), 8858–8859.

[21] Gooßen, L. J.; Rodríguez, N.; Manjolinho, F.; Lange, P. P. Synthesis of Propiolic Acids via Copper-Catalyzed Insertion of Carbon Dioxide into the C□H Bond of Terminal Alkynes. *Adv. Synth. Catal.* **2010**, *352* (17), 2913–2917.

[22] Yu, D.; Zhang, Y. Copper- and Copper–N-Heterocyclic Carbene-Catalyzed C─H Activating Carboxylation of Terminal Alkynes with CO2 at Ambient Conditions. *Proc. Natl. Acad. Sci.* **2010**, *107* (47), 20184–20189.

[23] Aoki, M.; Kaneko, M.; Izumi, S.; Ukai, K.; Iwasawa, N. Bidentate Amidine Ligands for Nickel(0)-Mediated Coupling of Carbon Dioxide with Unsaturated Hydrocarbons. *Chem. Commun.* **2004**, No. 22, 2568–2569

[24] Li, S.; Yuan, W.; Ma, S. Highly Regio- and Stereoselective Three-Component Nickel-Catalyzed Syn-Hydrocarboxylation of Alkynes with Diethyl Zinc and Carbon Dioxide. *Angew. Chem. Int. Ed.* **2011**, *50* (11), 2578–2582.

[25] Fujihara, T.; Xu, T.; Semba, K.; Terao, J.; Tsuji, Y. Copper-Catalyzed Hydrocarboxylation of Alkynes Using Carbon Dioxide and Hydrosilanes. *Angew. Chem. Int. Ed.* **2011**, *50* (2), 523–527.

[26] Wang, X.; Nakajima, M.; Martin, R. Ni-Catalyzed Regioselective Hydrocarboxylation of Alkynes with CO2 by Using Simple Alcohols as Proton Sources. *J. Am. Chem. Soc.* **2015**, *137* (28), 8924–8927.

[27] Gaydou, M.; Moragas, T.; Juliá-Hernández, F.; Martin, R. Site-Selective Catalytic Carboxylation of Unsaturated Hydrocarbons with CO2 and Water. *J. Am. Chem. Soc.* **2017**, *139* (35), 12161–12164.

[28] Kuge, K.; Luo, Y.; Fujita, Y.; Mori, Y.; Onodera, G.; Kimura, M. Copper-Catalyzed Stereodefined Construction of Acrylic Acid Derivatives from Terminal Alkynes via CO2 Insertion. *Org. Lett.* **2017**, *19* (4), 854–857.

[29] Juhl, M.; Laursen, S. L. R.; Huang, Y.; Nielsen, D. U.; Daasbjerg, K.; Skrydstrup, T. Copper-Catalyzed Carboxylation of Hydroborated Disubstituted Alkenes and Terminal Alkynes with Cesium Fluoride. *ACS Catal.* **2017**, *7* (2), 1392–1396.

[30] Williams, C. M.; Johnson, J. B.; Rovis, T. Nickel-Catalyzed Reductive Carboxylation of Styrenes Using CO2. *J. Am. Chem. Soc.* **2008**, *130* (45), 14936–14937.

[31] Greenhalgh, M. D.; Thomas, S. P. Iron-Catalyzed, Highly Regioselective Synthesis of α-Aryl Carboxylic Acids from Styrene Derivatives and CO2. *J. Am. Chem. Soc.* **2012**, *134* (29), 11900–11903.

[32] Shao, P.; Wang, S.; Chen, C.; Xi, C. Cp2TiCl2-Catalyzed Regioselective Hydrocarboxylation of Alkenes with CO2. *Org. Lett.* **2016**, *18* (9), 2050–2053

[33] Ohishi, T.; Zhang, L.; Nishiura, M.; Hou, Z. Carboxylation of Alkylboranes by N-Heterocyclic Carbene Copper Catalysts: Synthesis of Carboxylic Acids from Terminal Alkenes and Carbon Dioxide. *Angew. Chem. Int. Ed.* **2011**, *50* (35), 8114–8117.

[34] Ohmiya, H.; Tanabe, M.; Sawamura, M. Copper-Catalyzed Carboxylation of Alkylboranes with Carbon Dioxide: Formal Reductive Carboxylation of Terminal Alkenes. *Org. Lett.* **2011**, *13* (5), 1086–1088.

[35] Takimoto, M.; Hou, Z. Cu-Catalyzed Formal Methylative and Hydrogenative Carboxylation of Alkynes with Carbon Dioxide: Efficient Synthesis of α,β-Unsaturated Carboxylic Acids. *Chem. – Eur. J.* **2013**, *19* (34), 11439–11445.

[36] Nogi, K.; Fujihara, T.; Terao, J.; Tsuji, Y. Carboxyzincation Employing Carbon Dioxide and Zinc Powder: Cobalt-Catalyzed Multicomponent Coupling Reactions with Alkynes. *J. Am. Chem. Soc.* **2016**, *138* (17), 5547–5550

[37] Wang, X.; Liu, Y.; Martin, R. Ni-Catalyzed Divergent Cyclization/Carboxylation of Unactivated Primary and Secondary Alkyl Halides with CO2. *J. Am. Chem. Soc.* **2015**, *137* (20), 6476–6479.

[38] Li, S.; Ma, S. Quadri-Synergetic Effect for Highly Effective Carbon Dioxide Fixation and Its Application to Indoloquinolinone. *Adv. Synth. Catal.* **2012**, *354* (13), 2387–2394.

[39] Inamoto, K.; Asano, N.; Nakamura, Y.; Yonemoto, M.; Kondo, Y. Synthesis of 3-Carboxylated Indoles through a Tandem Process Involving Cyclization of 2-Ethynylanilines Followed by CO2 Fixation in the Absence of Transition Metal Catalysts. *Org. Lett.* **2012**, *14* (10), 2622–2625.

[40] Fujihara, T.; Tani, Y.; Semba, K.; Terao, J.; Tsuji, Y. Copper-Catalyzed Silacarboxylation of Internal Alkynes by Employing Carbon Dioxide and Silylboranes. *Angew. Chem. Int. Ed.* **2012**, *51* (46), 11487–11490.

[41] Tani, Y.; Fujihara, T.; Terao, J.; Tsuji, Y. Copper-Catalyzed Regiodivergent Silacarboxylation of Allenes with Carbon Dioxide and a Silylborane. *J. Am. Chem. Soc.* **2014**, *136* (51), 17706–17709.

[42] Zhang, L.; Cheng, J.; Carry, B.; Hou, Z. Catalytic Boracarboxylation of Alkynes with Diborane and Carbon Dioxide by an N-Heterocyclic Carbene Copper Catalyst. *J. Am. Chem. Soc.* **2012**, *134* (35), 14314–14317.

[43] Laitar, D. S.; Tsui, E. Y.; Sadighi, J. P. Copper(I) β-Boroalkyls from Alkene Insertion: Isolation and Rearrangement. *Organometallics* **2006**, *25* (10), 2405–2408.

[44] Mankad, N. P.; Gray, T. G.; Laitar, D. S.; Sadighi, J. P. Synthesis, Structure, and CO2 Reactivity of a Two-Coordinate (Carbene)Copper(I) Methyl Complex. *Organometallics* **2004**, *23* (6), 1191–1193.

[45] Laitar, D. S.; Müller, P.; Sadighi, J. P. Efficient Homogeneous Catalysis in the Reduction of CO2 to CO. *J. Am. Chem. Soc.* **2005**, *127* (49), 17196–17197.

[46] Baker, S. J.; Ding, C. Z.; Akama, T.; Zhang, Y.-K.; Hernandez, V.; Xia, Y. Therapeutic Potential of Boron-Containing Compounds. *Future Med. Chem.* **2009**, *1* (7), 1275–1288.

[47] Thareja, S.; Zhu, M.; Ji, X.; Wang, B. Boron-Based Small Molecules in Disease Detection and Treatment (2013–2016). *Heterocycl. Commun.* **2017**, *23* (3), 137–153.

[48]Zhu, S.; Buchwald, S. L. Enantioselective CuH-Catalyzed Anti-Markovnikov Hydroamination of 1,1-Disubstituted Alkenes. *J. Am. Chem. Soc.* **2014**, *136* (45), 15913–15916.

[49] Ascic, E.; Buchwald, S. L. Highly Diastereo- and Enantioselective CuH-Catalyzed Synthesis of 2,3-Disubstituted Indolines. *J. Am. Chem. Soc.* **2015**, *137* (14), 4666–4669.

[50] Bandar, J. S.; Ascic, E.; Buchwald, S. L. Enantioselective CuH-Catalyzed Reductive Coupling of Aryl Alkenes and Activated Carboxylic Acids. *J. Am. Chem. Soc.* **2016**, *138* (18), 5821–5824.

[51] Lipshutz, B. H.; Noson, K.; Chrisman, W.; Lower, A. Asymmetric Hydrosilylation of Aryl Ketones Catalyzed by Copper Hydride Complexed by Nonracemic Biphenyl Bis-Phosphine Ligands. *J. Am. Chem. Soc.* **2003**, *125* (29), 8779–8789.

[52] Lin, S.; Lin, Z. DFT Studies on the Mechanism of Copper-Catalyzed Boracarboxylation of Alkene with CO2 and Diboron. *Organometallics* **2019**.

[53] Lv, X.; Wu, Y.; Lu, G. Computational Exploration of Ligand Effects in Copper-catalyzed Boracarboxylation of Styrene with CO2. *Catal. Sci. Technol*. **2017**, 7, 5049–5054

CHAPTER 2: *Regioselective Boracarboxylation of α-Substituted Vinyl Arenes – adapted from* Steven W. Knowlden and Brian V. Popp, *Organometallics* **Article ASAP**

DOI: https://doi.org/10.1021/acs.organomet.2c00184

2.1 Introduction

Carbon dioxide is a useful C1 synthon that is utilized in a variety of organometallic transformations such as C-H functionalization, carboxylation, esterification, alcohol etherification, and N-alkylation.[1,2] Synthesis of quaternary centers via carboxylation,[3] to provide synthetically and medicinally important carboxylic acids,[4] is particularly difficult due to the sterically congested nature of the organometallic intermediate. Classic synthetic methods to access such centers using CO_2, such as Grignard carboxylation, require harsh conditions that limit functional group tolerance and reaction efficiency. Consequently, methods to deliver such α-quaternary carboxylic acids utilizing transition metal catalysis have been identified as highly desirable.[5]

Method development over the last decade has focused on preparation of α-quaternary carboxylic acids using late transition metal catalysis. Tan reported a robust rhodium-catalyzed asymmetric hydroformylation/oxidation of simple 2-substituted allylic alcohols,[6] while Stoltz reported an elegant iridium-catalyzed asymmetric allylic functionalization using a C1 source (Figure 2.1A).[7] Palladium, nickel and copper-catalyzed carboborylative alkene difunctionalization,[8] for example boracyanation and boraarylation of 2-substituted dienes (Figure 2.1B),[9] provides attractive products that feature a synthetically valuable organoboron functional group as well as a new functionalized quaternary carbon center. Copper-catalyzed heteroelement-(bora and sila)-carboxylation offers similarly attractive functional group rich products while using CO_2 as the electrophilic reaction partner; however, such transformations with alkyne,[10] imine,[11] allene,[12] and vinyl arene lacking vinylic substitution[13] remain underdeveloped and consequently

Scheme 2.1 Transition-metal-catalyzed strategies to access synthetically useful α-quaternary carboxylic acids and derivatives.

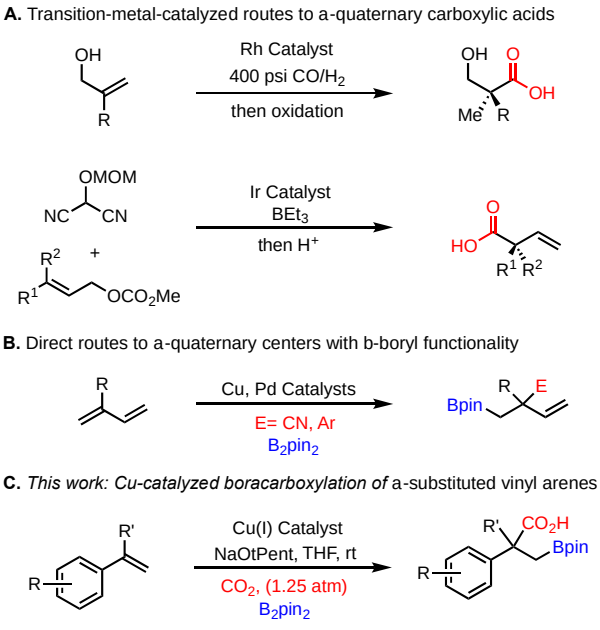

underutilized. In 2016, we presented a single example of α-methyl-styrene boracarboxylation, albeit in low yield, which provided motivation to improve and broaden the reaction to access useful α-quaternary carboxylic acids bearing a β-boronic ester functional group (Figure 2.1C).[13a]

We published experimental and computational studies of well-defined copper complex reactivity with CO_2 associated with boracarboxylation in 2021.[14,15] The studies confirmed that the carboxylation step was the turnover limiting step and provided evidence for divergent carboxylation pathways based on vinyl arene electronic structure. While stoichiometric carboxylation of α-methyl-styrene was not studied, we reasoned that the efficiency of catalytic boracarboxylation of sterically hindered vinyl arenes would benefit from increased CO_2 pressure. Here, we present CO_2 pressure effects on catalytic boracarboxylation that provide the needed insights to realize new boracarboxylation methods for α-substituted vinyl arenes.

2.2 Results and Discussion

2.2.1 Initial CO_2 pressure effects on the boracarboxylation of vinyl arenes

We commenced our CO_2 pressure studies by first building a medium pressure (~12 atm) gas manifold with four separate reaction ports (Figure S-1). Our original boracarboxylation conditions using 12 mol% ICyCuCl, 1.1 equiv B_2pin_2, and a balloon of CO_2 for 36 hours at room temperature in THF led to 24 % yield of boracarboxylated product **2a** (Table 1, Entry 1), as well as trace amounts of formal hydroboration product (**3a**) from α-methyl-styrene (**1a**).[13a] Increased CO_2 pressure (3 atm) led to no boracarboxylated product **2a** with nearly full conversion of substrate **1a** (Entry 2). Even a super-stoichiometric amount of B_2pin_2 (2.0 equiv) led to inferior results relative to our original conditions (Entry 3-4).

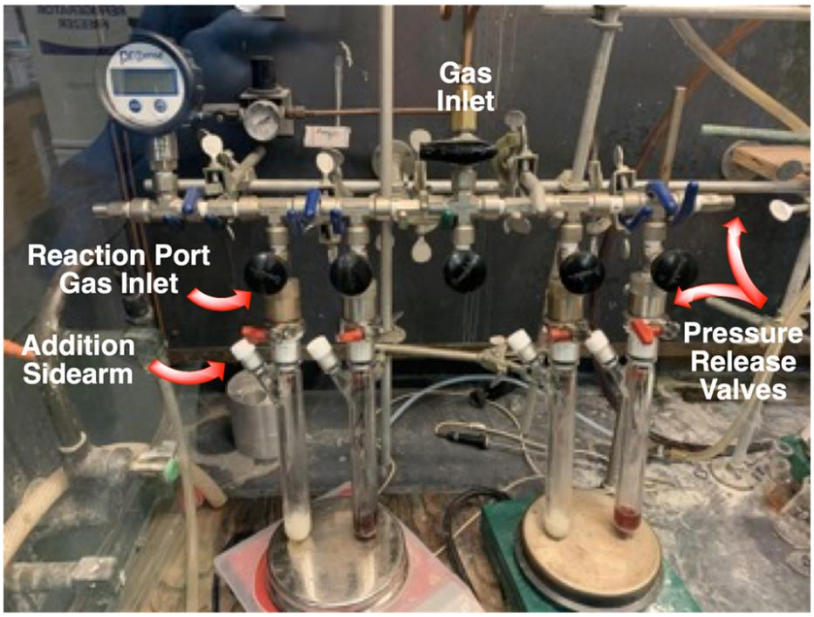

Figure 2.1. Apparatus used for high-pressure reaction

These results contradicted our expectations, prompting the evaluation of increased CO_2 pressure on an unsubstituted vinyl arene (*p*-tert-butylstyrene, **4**) boracarboxylation reaction. Our original catalytic conditions with a CO_2 balloon afforded 86% yield of boracarboxylated product **5** (Table 1, Entry 5). Higher CO_2 pressure (3 atm) led

to a significant reduction in boracarboxylation yield and conversion, which could be recovered by doubling B_2pin_2 loading (Table 1, Entry 6-7). Using 3 atm CO_2 pressure and 2.0 equiv B_2pin_2, comparable yields to those obtained at 1 atm CO_2 were obtained after only 30 min, which is consistent with a turnover-limiting step that is dependent on CO_2 concentration (Entry 8).

The differing reactivity of **1a** and **4** could not be readily explained initially. We noted incomplete conversion of sterically hindered **1a** at higher CO_2 pressures, which suggested that B_2pin_2 was consumed via an alternate pathway that did not involve **1a**. The accepted boracarboxylation catalytic mechanism (Figure 2.3) suggests that such a side reaction could result from competitive CO_2 reduction and alkene insertion at a copper-boryl intermediate (ie., [Cu]Bpin).[16] A consequence of this competition would be the CO_2 reduction byproduct, pinB-O-Bpin, which has a characteristic ^{11}B chemical shift around 22 ppm in $CDCl_3$. Indeed, the crude ^{11}B NMR spectrum for boracarboxylation of **1a** (Table 1, Entry 3-4) showed only minimal amounts of product **2a** (33 ppm), unreacted B_2pin_2 (30.6 ppm), and large amounts of pinB-O-Bpin (Figure 2.4A-B). Conversely, ^{11}B NMR analysis of boracarboxylation of vinyl arene **4** (Table 1, Entry 6) showed predominately product **5**, also observed at 33 ppm, and comparatively less pinB-O-Bpin (Figure 2.4C).

Table 2.1. Effect of CO_2 Pressure on Boracarboxylation of Vinyl Arenes 1a and 4[a]

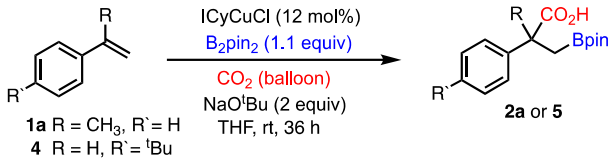

Entry	Substrate	Variation from std. cond.	Yield (%)[b]	2a|5	Convn (%)[b]
1	**1a**	None	24		89
2	**1a**	CO_2 (3 atm)	0		94
3	**1a**	CO_2 (3 atm), B_2pin_2 (2 equiv)	15		66
4	**1a**	CO_2 (1 atm), B_2pin_2 (2 equiv)	21		76
5	**4**	none	86		>99
6	**4**	CO_2 (3 atm)	52		66
7	**4**	CO_2 (3 atm), B_2pin_2 (2 equiv)	78		86
8	**4**	CO_2 (3 atm), B_2pin_2 (2 equiv), 30 min	81		89

[a] Reactions performed on 0.25 mmol scale with respect to vinyl arene. [b] Yield determined by ^1H NMR integration using 20 mol% mesitylene as an internal standard.

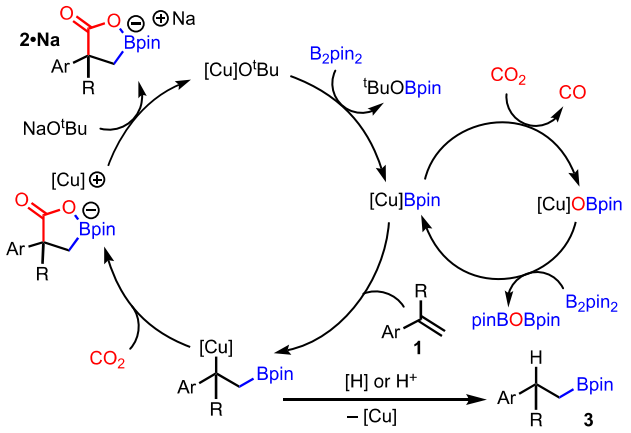

Figure 2.2 Catalytic cycle for copper-catalyzed boracarboxylation with competitive CO_2 reduction and hydro/protoboration pathways.

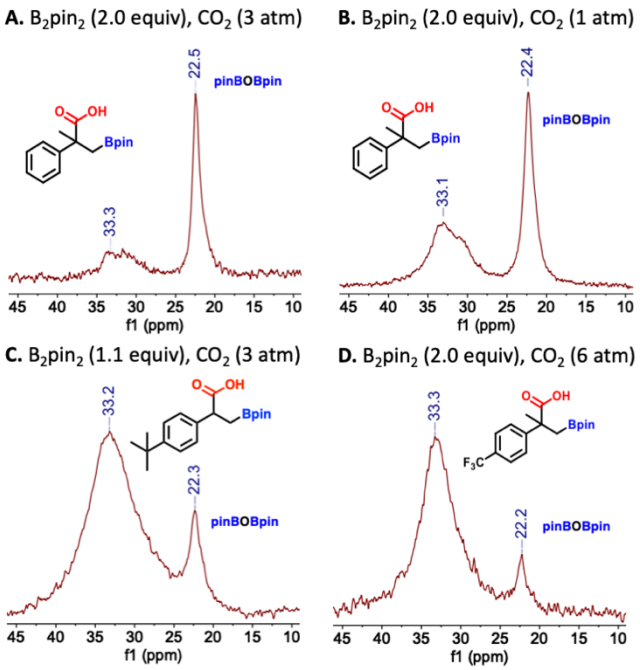

Figure 2.3. ^{11}B NMR spectra of selected crude boracarboxylation reactions in $CDCl_3$. (Note: Unreacted B_2pin_2 at 30.6 ppm)

2.2.2 Boracarboxylation of α-Substituted Vinyl Arenes Reaction Optimization and Scope

The combined observations of boracarboxylation product yield, substrate conversion, and CO_2 reduction byproduct pinB-O-Bpin under different pressures of CO_2 suggested that modest change in the steric profile from **4** to **1a** impacts the relative rates of CO_2 and alkene insertion at [Cu]Bpin (cf., Table 2.1). Unsubstituted vinyl arene **4** appears to insert faster than CO_2, so subsequent turnover limiting carboxylation can be accelerated by increased CO_2 pressure. α-Methylstyrene **1a** appears to insert slower than CO_2, so increased CO_2 pressure leads to faster catalytic CO_2 reduction and consumption of reductant B_2pin_2, but not faster, more productive boracarboxylation. The emerging qualitative picture indicates that for an alkene to be a suitable substrate it must, at a minimum, outcompete CO_2 for insertion into the [Cu]Bpin intermediate.

Sadighi demonstrated experimentally, and Marder later confirmed computationally, that electron deficient alkenes insert faster into NHCCu-boryl complexes.[17] Consequently, we prepared a-methyl-*p*-trifluoromethylstyrene (**1b**) and subjected it to boracarboxylation for 2 hours at both 3 and 6 atm CO_2. Gratifyingly, only small amounts of pinB-O-Bpin were evident from crude ^{11}B NMR spectra (cf., Figure 3D), and excellent NMR yields (>80%) with quantitative substrate conversion were obtained (Table 2.2, Entry 1-2). Quantifiable amounts of formal hydroboration product **3b**, generally 5-10%, were also observed. This suggested that while alkene insertion outcompetes CO_2 reduction, the more sterically hindered, electron deficient Cu-benzyl intermediate does not carboxylate efficiently, as expected by our recent experimental/computational studies,[14b] allowing hydro/proto-decupration or other

decomposition pathway to compete kinetically. This is further emphasized by the steep decline in the yield of **2b** when CO_2 pressure is reduced to 1.25 atm (Entry 3).

Bases were next screened for boracarboxylation of electron-deficient **1b** at high CO_2 pressure (6 atm). For MO^{t}Bu bases, potassium and lithium were inferior cations relative to sodium (Table 2.2, Entry 4-5). All other sodium alkoxide bases, both sterically small and large, gave yields of **2b** between 32-90% while NaOTMS gave predominately formal hydroboration product **3b**. Yields of **2b** with NaOEt (90% after 2 hr, Entry 7) and NaO^{t}Pent (85% after 3 hr, Entry 13) were comparable, so each was also screened at lower pressures.

Table 2.2 Effect of CO_2 pressure and base on boracarboxylation of electron deficient 1b[a]

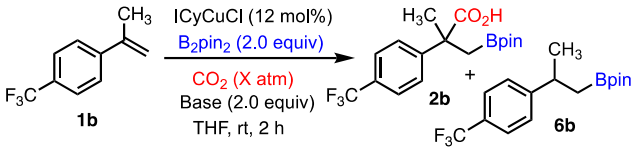

Entry	Base	*p*CO_2 (atm)	Yield (%)[b] 2b	6b	Convn (%)[b]
1	NaO^{t}Bu	6	80	10	>99
2		3	84	8	>99
3		1.25	24	8	>99
4	KO^{t}Bu	6	57	14	>99
5	LiO^{t}Bu	6	<5	<5	>99
6	NaOMe	6	65	<5	>99
7	NaOEt	6	90	9	>99
8		3	82	9	>99
9		1.25	58	14	>99
10	NaO^{i}Pr	6	32	26	>99
11	NaOTMS	6	0	83	>99
12	NaO^{t}Pent	6	71	6	>99
13[c]		6	85	12	>99
14		3	71	20	>99
15		1.25	67	24	>99

[a] Reactions performed on 0.25 mmol scale with respect to vinyl arene. [b] Yield and conversion determined by ^{1}H NMR integration using 20 mol% mesitylene as an internal standard. [c] 3 hr.

The small ethoxide base leads to 32% reduction in yield from 6-to-1.25 atm CO_2 (Entry 7-9). The large tert-pentoxide base leads to a more modest drop in yield and significant amounts (>20%) of side product **3b** at lower CO_2 pressures.

Next, boracarboxylation reactions were carried out for 24 hours with competent alkoxide bases at low CO_2 pressure (1.25 atm), due to the competitive CO_2 reduction illustrated earlier, using weakly electron-deficient α-methyl-*p*-fluorostyene (**1g**) and electron-neutral **1a**. Yields around 30% or less were obtained even with 5.0 equiv of B_2pin_2 (cf., Table 2.3, Entry 1). Unfortunately, ICyCuCl catalyst with the reaction condition variations discussed above appear to allow efficient reactivity with only strongly electron-deficient **1b**. This setback prompted us to screen a selection of isolated and in situ-generated NHC-copper catalysts at high B_2pin_2 loading (5.0 equiv) to compensate for catalytic inefficiency due to competitive CO_2 reduction. Less sterically bulky IMesCuCl precatalyst gave 50% yield of **2a** but inefficient conversion. Further modification to the more donating SIMesCuCl precatalyst, gave **2a** in 83% yield. In situ preparation of both IMesCuCl and SIMesCuCl from the imidazolium salt, base, and CuCl, provided **2a** in <5% and 95% yield respectively, while the bulky SIPrCuCl precatalyst, also prepared in situ, did not give identifiable product (Entry 4-6).

Table 2.3. Effect of Catalyst on Boracarboxylation of Electron Neutral 1a[a]

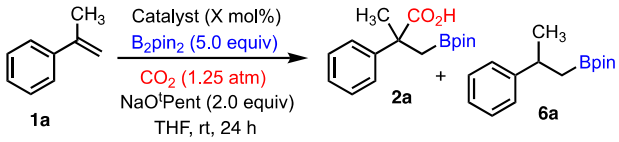

Entry	Catalyst	Yield (%)[b]		Convn (%)[b]
		2a	6a	
1	ICyCuCl (13 mol%)	31	<5	>99
2	IMesCuCl (13 mol%)	50	0	72
3	SIMesCuCl	83	0	90
4	IMesH•Cl (13 mol%) CuCl (12 mol%)	<5	0	>99
5[c]	SIMesH•Cl (13 mol%) CuCl (12 mol%)	0	0	97
6	SIPrH•Cl (13 mol%) CuCl (12 mol%)	0	37	36

[a] Reactions performed on 0.25 mmol scale with respect to vinyl arene. [b] Yield and conversion determined by ^{1}H NMR integration using 20 mol% mesitylene as an internal standard. [c] No NaO^{t}Pent added.

A final round of **1a** boracarboxylation optimization, using in situ generated SIMesCuCl precatalyst, was carried out (Table 4). Replacement of NaO^{t}Pent with NaOEt and NaO^{t}Bu led to diminished yields although minimally so in the latter case (Entry 2-3), while removal of base led to no characterizable products (Entry 4). Increased loading of B_2pin_2 (3 equiv) or reduced B_2pin_2 loading with increased loading of **1a** led to almost exclusive formal hydroboration product **3a** (Entry 5-6). The catalytic reaction was unaffected by increased base loading (3 equiv) and temperature (45 °C) (Entry 7-8). Variation of CO_2 pressure from 1.25 atm led to lower yields and incomplete conversion collectively (Entry 9-11). Addition of PPh_3 as a secondary ligand, which was previously used by us to improve catalyst efficiency and substrate scope,[13b] led to a modest reduction of yield (Entry 11). A control reaction showed that ancillary ligand precursor SIMesH•Cl is necessary for catalytic turnover (Entry 13).

Table 2.4. Boracarboxylation Reaction Optimization with Electron Neutral 1a [a]

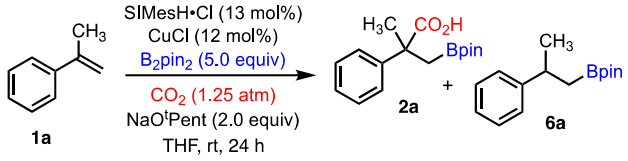

Entry	Variation from Standard Conditions	Yield (%)[b] 2a	6a	Convn (%)[b]
1	None	95	0	>99
2	NaOEt instead of NaOtPent	59	6	93
3	NaOtBu instead of NaOtPent	85	<5	>99
4	No NaOtPent	0	0	97
5	3.0 equiv B_2pin_2	<5	15	>99
6	1.0 equiv B_2pin_2, 3.0 equiv 1a	0	20	ND
7	3.0 equiv NaOtPent	85	<5	>99
8	45 °C	87	<5	>99
9	CO_2 (balloon)	60	7	93
10	CO_2 (3 atm)	36	0	68
11	CO_2 (6 atm)	55	0	72
12	PPh_3 additive (5 mol%)	68	13	92
13	No SIMesH•Cl	0	<5	80

[a] Reactions performed on 0.25 mmol scale with respect to vinyl arene. [b] Yield and conversion determined by ^{1}H NMR integration using 20 mol% mesitylene as an internal standard.

The optimized catalyst system featuring in situ generated SIMesCuCl, CO_2 (1.25 atm), B_2pin_2 (5.0 equiv), NaOtPent (2.0 equiv) in THF at room temperature was used to evaluate the substrate scope as related to steric/electronic modification of the arene ring and α-position (Table 2.5). Boracarboxylation of α-methyl styrene provided 71% isolated yield (95% by ^{1}H NMR analysis) as opposed to 24% crude yield under our originally published reaction conditions. A good isolated yield (72%) of electron-deficient *p*-trifluoromethyl-substituted **2b** and a moderate isolated yield (44%) of electron-rich *p*-methoxy-substituted **2c** was obtained. Other electron neutral substrates (**1d-f**) were similarly reactive, affording moderate to good yields of boracarboxylated products. Weakly (*p*- and *m*-F; **2g-h**), moderately (3,4-difluoro; **2j**), and strongly (m-CF_3; **2k**) electron deficient products were also isolated in moderate-to-good yields. Not surprisingly given the apparent sensitivity of insertion and carboxylation rates to the steric characteristics of both the alkene substrate and the subsequent organocopper intermediate, the reaction was quite sensitive to *o*-F (**2i**) and *o*-CF_3 (**2l**) substitution affording crude products in less than 10% yield. Electron rich heteroarene products, with benzothiophene (**2m**) and indole (**2n**) moieties, were obtained in isolated yields of 65% and 50%, respectively.

Substitution at the α-position was also generally tolerated if the substituting group was not too bulky. Ethyl and n-propyl substitution afforded products **2o-p** in good yields (55-71%), but a significant drop in yield (35%) was obtained for n-butyl substituted product **2q**. Larger groups, such as iso-propyl, were not tolerated, affording no isolable boracarboxylation product. The exocyclic alkene of 1-methyleneindane was boracarboxylated to give **2s** in 51% isolated yield. Finally, we assessed 1,1-diarylethylene substrates (**2t-y**). Unsurprisingly, these substrates proceeded poorly under the optimized catalytic conditions presumably due to the additional steric bulk of the second aryl ring and/or radical decomposition of the organocopper intermediate.[18] The products were also exceedingly difficult to isolate cleanly with significant product decomposition observed for **2t-2w**. Continued method development work will be necessary to identify a suitable steric and electronic environment at the copper center to allow better access to these 1,1-diarylethane boracarboxylated products.

Table 2.5. Boracarboxylation Reaction Scope[a]

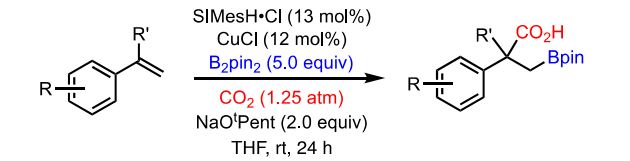

aryl substitution

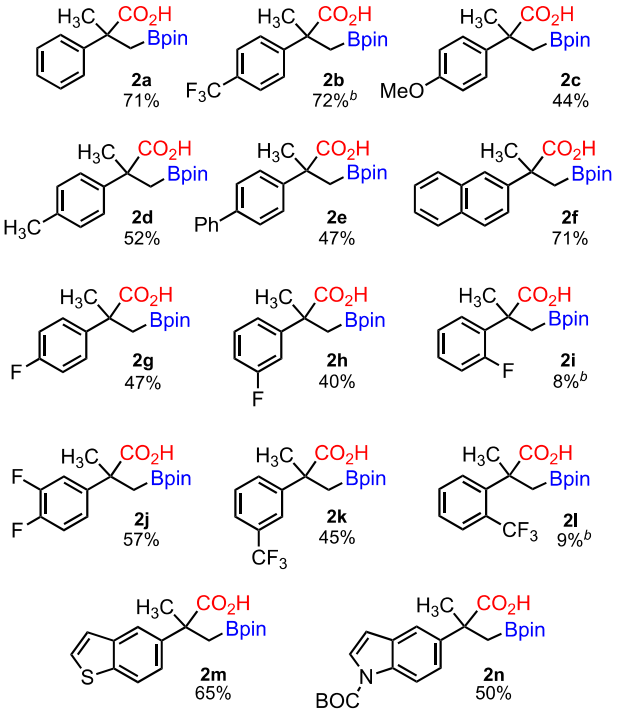

α-alkyl substitution

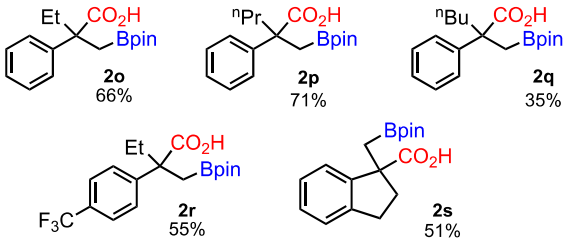

α-aryl substitution[b]

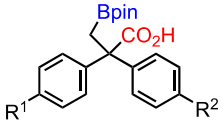

2t	R^1=R^2= H	8%
2u	R^1= H R^2 = OMe	14%
2v	R^1= OMe R^2= OMe	5%
2w	R^1= OMe R^2= CF_3	11%
2x	R^1= H R^2= CF_3	20 %
2y	R^1= CF_3 R^2= CF_3	0%

[a] Reactions performed on 0.25 mmol scale with respect to vinyl arene, all yields are isolated unless otherwise specified.

[b] Crude yield due to remaining impurities

2.3 Conclusions

We have presented here the impacts of increased CO_2 pressure on copper-catalyzed boracarboxylation of vinyl arene and α-methylstyrene. The results revealed a complex interplay between kinetically competitive insertion reactions during which the pressure of CO_2 can have both positive and negative impacts on catalytic turnover. These studies led us to the unexpected realization that low CO_2 concentration was critical to achieve relatively efficient boracarboxylation on more sterically demanding substrates such as α-methylstyrene. A diverse substrate scope that includes synthetically useful heteroarenes highlights the potential utility of this mild catalytic method to provide functional group rich, α-quaternary carboxylic acids. Future in-depth kinetics studies are planned to better understand the interplay of CO_2 reduction and alkene boracarboxylation pathways under different catalytic regimes and realize continued systematic alkene boracarboxylation substrate scope expansion.

2.4 Experimental Section

General Considerations: All air and moisture sensitive experiments were set up in a nitrogen-filled MBraun 200B dual-port glovebox, and before each experiment the glovebox atmosphere was tested using diethyl zinc. The boracarboxylation reactions were performed in Ace Glass 35ml double-walled two-neck pressure tubes. The pressure tubes, miscellaneous glassware, and unused magnetic stir bars were dried in an oven at 180 °C for at least 24 hours. All glassware used in the glovebox was dried for at least 24h in the 180 ˚C oven. An in-house built multi-reaction-port gas manifold (Figure S-1) was used to perform reactions at modest CO_2 pressures (less than 6 atm). *All reactions carried out with CO_2 pressure above atmospheric were performed behind a blast shield.* All solvent were dried on a Glass Contour solvent purification system, and further stored over activated 4Å mol sieves. All liquids were degassed via freeze/pump/thaw cycles prior to use. Substrates **1a**, **1g** and **1t** were obtained from commercial sources and used as received. Substrates **1b-f, 1h-l, 1o-s, 1u-v** were prepared through Wittig reactions from the respective ketone; **1b** and **1h** were distilled prior to use.[19] Substrates **1m** and **1n** were prepared through Suzuki cross-coupling reactions.[20] Substrates **1w-y** were prepared according to literature precedent.[21] Spectroscopic characterization of boracarboxylated products **2a-b** matched the original report.[13a] $CDCl_3$ was purchased from Cambridge Isotope Laboratories, Inc. NMR spectra were recorded on either a 400 MHz Agilent or 600 MHz Agilent NMR spectrometer. ^{1}H, ^{13}C, ^{11}B, and ^{19}F NMR experiments were acquired in $CDCl_3$ using tetramethylsilane as a reference in quartz NMR tubes. ^{11}B NMR resonances were referenced relative to an external $BF_3{\cdot}OEt_2$ standard. High-resolution mass spectra were recorded on a Thermo Fisher Scientific Q-Exactive Mass Spectrometer with samples dissolved in acetonitrile.

Synthesis of substrates 2b-2x: In a nitrogen filled glovebox, a 20 ml scintillation vial was charged with SIMesHCl (10.3 mg, 0.0275 mmol, 13 mol%), NaO^{t}Pent (55.0 mg, 0.50 mmol, 2.0 equiv) and anhydrous, degassed THF (2 ml). The vial was then capped and stirred for 15 minutes to afford a clear, colorless solution. This solution was then transferred using a 9” glass pipet to a separate 20 ml scintillation vial containing CuCl (2.7 mg, 0.025 mmol, 12 mol%) and stirred for 1 hour. To a 35 ml double-walled two neck glass pressure tube, B_2pin_2 (315.0 mg, 1.25 mmol, 5.0 eq), vinyl arene (0.25 mmol, 1.0 eq) and anhydrous, degassed THF (2 ml) were added then sealed

with a fresh rubber septum. The catalyst solution was then loaded into a 5.0 ml Hamilton gas-tight syringe, and then the needle was plugged using a rubber septum. The pressure tube and catalyst solution were then removed from the glovebox and swiftly connected to the gas manifold under a continuous flow of Ar gas. Once attached, the tube was purged with Ar gas for additional 2 minutes, at which point the catalyst solution was added via the sidearm. The tube was purged with CO_2 for 2 minutes, brought to desired CO_2 pressure, isolated from the main manifold, and stirred at room temperature for 24 hours. Upon completion, the crude mixture was added to a 60 ml separatory funnel containing 20 ml of 1M HCl, and then extracted with CH_2Cl_2 (3 x 4 ml) and collected in a 20 ml scintillation vial. The combined organic extracts were concentrated under vacuum, and mesitylene (20 mol%) was added to the crude reaction mixture. The mixture was then dissolved in 1 ml of $CDCl_3$ and analyzed by ^1H NMR spectroscopy to obtain an NMR yield. Subsequently, the crude mixture was taken up in Et_2O (10 ml) then extracted with saturated $NaHCO_3$ (4 x 3 ml). The aqueous layer was acidified by slow addition of 12M HCl (5 ml) then extracted with CH_2Cl_2 (4 x 3 ml). The organic layer was dried over Na_2SO_4 and the solvent was removed in vacuo to afford boracarboxylated product, which could be further purified by recrystallization from either heptane or heptane/toluene (1:1 v/v).

Characterization data

2b 3-((4,4,5,5-tetramethyl-1,3,2-dioxaborolan-2-yl)-2-methyl-2-(4-trifluoromethylphenyl) propionic acid. White solid, (64 mg, 72% crude yield). ^1H NMR (400 MHz, $CDCl_3$): δ 7.54 (m, 4H), 1.70 (s, 3H), 1.60 (d, J = 15.7 Hz, 1H), 1.46 (d, J = 15.7 Hz, 1H), 1.10 (s, 6H), 1.09 (s, 6H). ^{13}C NMR (151 MHz, $CDCl_3$): δ 182.1, 148.6, 129.0 (q, J = 32.5 Hz), 126.6, 125.5, 125.2, 123.9 (broad q, J=270.7 Hz), 83.3, 48.0, 25.0, 24.5, 23.1 (broad due to quadrupolar broadening from ^{11}B). ^{11}B NMR (128 MHz, $CDCl_3$: δ 33.0. ^{19}F NMR (376 MHz, $CDCl_3$) δ -62.6. HRMS (ESI): m/z calc. for $C_{17}H_{22}BF_3O_4$ $[M-H]^-$: 358.1524, found 358.1530.

2c 3-((4,4,5,5-tetramethyl-1,3,2-dioxaborolan-2-yl)-2-methyl-2-(4-methoxyphenyl) propionic acid. White solid, (35 mg isolated, 44% yield). ^1H NMR (600 MHz, $CDCl_3$): δ 7.35 – 7.28 (m, 2H), 6.87 – 6.79 (m, 2H), 3.77 (s, 3H), 1.66 (s, 3H), 1.60 (d, J = 15.7 Hz, 1H), 1.42 (d, J = 15.6 Hz, 1H), 1.13 (s, 6H), 1.12 (s, 6H). ^{13}C NMR (101 MHz, $CDCl_3$): δ 182.2, 158.3, 136.8, 127.1, 113.6, 83.2, 55.2, 47.1, 25.3, 24.6, 24.6, 23.2 (broad due to quadrupolar broadening from ^{11}B). ^{11}B NMR (128 MHz, $CDCl_3$: δ 33.2. HRMS (ESI): m/z calc. for $C_{17}H_{25}BF_3O_5$ $[M-H]^-$: 320.1756, found 320.1756.

2d 3-((4,4,5,5-tetramethyl-1,3,2-dioxaborolan-2-yl)-2-methyl-2-(4-methylphenyl) propionic acid. Pale yellow solid, (38 mg isolated, 52% yield). ^1H NMR (400 MHz, $CDCl_3$): δ 7.28 (d, J = 8.3 Hz, 2H), 7.09 (d, J = 7.9 Hz, 2H), 2.29 (s, 3H), 1.66 (s, 3H), 1.61 (d, J = 15.7 Hz, 1H), 1.40 (d, J = 15.7 Hz, 1H), 1.14 (s, 6H), 1.12 (s, 6H).^{13}C NMR (151 MHz, $CDCl_3$): δ 182.7, 141.9, 136.2, 128.9, 125.8, 83.1, 47.5, 25.3, 24.6, 24.6, 23.2 (broad due to quadrupolar broadening from ^{11}B), 20.9. ^{11}B NMR (128 MHz, $CDCl_3$: δ 33.4.HRMS (ESI): m/z calc. for $C_{17}H_{25}BO_4$ $[M-H]^-$: 303.1773, found 303.1778.

2e 3-((4,4,5,5-tetramethyl-1,3,2-dioxaborolan-2-yl)-2-methyl-2-biphenyl propionic acid. White solid, (43 mg isolated, 47% yield). ^{1}H NMR (400 MHz, $CDCl_3$): δ 7.58 – 7.50 (m, 4H), 7.47 (d, *J* = 8.5 Hz, 2H), 7.41 (dd, *J* = 8.4, 6.9 Hz, 2H), 7.35 – 7.27 (m, 1H), 1.73 (s, 3H), 1.66 (d, *J* = 15.7 Hz, 1H), 1.49 (d, *J* = 15.7 Hz, 1H), 1.13 (s, 6H), 1.12 (s, 6H). ^{13}C NMR (151 MHz, $CDCl_3$): δ 181.3, 143.8, 140.7, 139.6, 128.7, 127.2, 127.0, 127.0, 126.4, 83.3, 47.7, 25.5, 24.6, 24.6, 23.1 (broad due to quadrupolar broadening from ^{11}B). ^{11}B NMR (128 MHz, $CDCl_3$): δ 32.9. HRMS (ESI): m/z calc. for $C_{22}H_{27}BO_4$ [M-H]$^-$: 366.1963, found 366.1967.

2f 3-((4,4,5,5-tetramethyl-1,3,2-dioxaborolan-2-yl)-2-methyl-2-(2-naphtyl) propionic acid. White solid, (60 mg isolated, 71% yield). ^{1}H NMR (400 MHz, $CDCl_3$): δ 7.84 – 7.74 (m, 4H), 7.52 (dd, *J* = 8.8, 2.0 Hz, 1H), 7.46 – 7.39 (m, 2H), 1.79 (s, 3H), 1.73 (d, *J* = 15.7 Hz, 1H), 1.53 (d, *J* = 15.7 Hz, 1H), 1.10 (s, 6H), 1.08 (s, 6H). ^{13}C NMR (101 MHz, $CDCl_3$): δ 182.8, 142.2, 133.2, 132.2, 128.1, 127.9, 127.4, 126.0, 125.8, 124.7, 124.3, 83.2, 48.1, 25.2, 24.6, 24.6, 23.2 (broad due to quadrupolar broadening from ^{11}B). ^{11}B NMR (128 MHz, $CDCl_3$: δ 33.0. HRMS (ESI): m/z calc. for $C_{20}H_{25}BO_4$ [M-H]$^-$: 340.1807, found 340.1809

2g 3-((4,4,5,5-tetramethyl-1,3,2-dioxaborolan-2-yl)-2-methyl-2-(4-fluorophenyl) propionic acid. White solid, (38 mg isolated, 47% yield). ^{1}H NMR (400 MHz, $CDCl_3$): δ 7.35 (dd, *J* = 8.7, 5.2 Hz, 2H), 6.95 (t, *J* = 8.6 Hz, 2H), 1.67 (s, 3H), 1.56 (d, *J* = 15.7 Hz, 1H), 1.44 (d, *J* = 15.6 Hz, 1H), 1.11 (s, 6H), 1.10 (s, 6H). ^{13}C NMR (151 MHz, $CDCl_3$): δ 182.6, 161.6 (d, *J* = 245.4 Hz), 140.4, 127.7 (d, *J* = 7.9 Hz), 114.9 (d, *J* = 21.0 Hz), 83.2, 47.5, 25.1, 24.6, 23.4 (broad due to quadrupolar broadening from ^{11}B). ^{11}B NMR (128 MHz, $CDCl_3$: δ 33.9. ^{19}F NMR (376 MHz, $CDCl_3$) δ -116.6 (p, *J* = 7.3, 6.8 Hz). HRMS (ESI): m/z calc. for $C_{16}H_{22}BFO_4$ [M-H]$^-$: 308.1556, found 308.1560

2h 3-((4,4,5,5-tetramethyl-1,3,2-dioxaborolan-2-yl)-2-methyl-2-(3-fluorophenyl) propionic acid. White solid, (30 mg isolated, 40% yield). ^{1}H NMR (400 MHz, $CDCl_3$): δ 7.28 – 7.21 (m, 1H), 7.18 – 7.08 (m, 2H), 6.90 (tdd, *J* = 8.2, 2.6, 1.0 Hz, 1H), 1.67 (s, 3H), 1.58 (d, *J* = 15.7 Hz, 1H), 1.42 (d, *J* = 15.7 Hz, 1H), 1.12 (s, 6H), 1.11 (s, 6H). ^{13}C NMR (151 MHz, $CDCl_3$): δ 182.2, 162.7 (d, *J* = 245.2 Hz), 147.4, 147.3, 129.6 (d, *J* = 8.1 Hz), 121.7, 121.7, 113.6 (d, *J* = 21.0 Hz), 113.3 (d, *J* = 22.5 Hz), 83.3, 47.8, 25.0, 24.6, 24.5, 23.1 (broad due to quadrupolar broadening from ^{11}B). ^{11}B NMR (128 MHz, $CDCl_3$: δ 28.4. ^{19}F NMR (376 MHz, $CDCl_3$) δ -117.9. HRMS (ESI): m/z calc. for $C_{16}H_{22}BFO_4$ [M-H]$^-$: 307.1522, found 307.1520.

2i 3-((4,4,5,5-tetramethyl-1,3,2-dioxaborolan-2-yl)-2-methyl-2-(2-fluorophenyl) propionic acid. Colorless oil, (6.2 mg, 8% crude yield). ^{1}H NMR (400 MHz, $CDCl_3$): δ 7.34 (td, *J* = 7.9, 1.7 Hz, 1H), 7.19 (tdd, *J* = 7.2, 5.0, 1.7 Hz, 1H), 7.07 (td, *J* = 7.5, 1.3 Hz, 1H), 7.00 – 6.90 (m, 1H), 1.71 (s, 3H), 1.53 (d, *J* = 15.1 Hz, 1H), 1.45 (d, *J* = 15.1 Hz, 1H), 1.11 (s, 6H), 1.09 (s, 6H). ^{11}B NMR (128 MHz, $CDCl_3$: δ 27.0. ^{19}F NMR (376 MHz, $CDCl_3$) δ -116.3. HRMS (ESI): m/z calc. for $C_{16}H_{22}BFO_4$ [M-H]$^-$: 307.1522, found 307.1520.

2j 3-((4,4,5,5-tetramethyl-1,3,2-dioxaborolan-2-yl)-2-methyl-2-(3,4-difluorophenyl) propionic acid. White solid, (46 mg isolated, 57% yield). ^{1}H NMR (400 MHz, $CDCl_3$): δ 7.22 (ddd, *J* = 12.3, 7.5, 2.8 Hz, 1H), 7.13 – 7.01 (m, 2H), 1.65 (s, 3H), 1.55 (d, *J* = 15.7 Hz, 1H), 1.41 (d, *J* = 15.7 Hz, 1H), 1.12 (s, 6H), 1.11 (s, 6H). ^{13}C NMR (101 MHz, $CDCl_3$): δ 182.1, 152.1 – 149.3 (m), 149.5 – 146.4 (m), 141.7, 122.1, 116.7 (d, *J* = 17.1 Hz), 115.6 (d, *J* = 18.1 Hz), 83.3, 47.4, 25.0, 24.6, 23.2 (broad due to quadrupolar broadening from ^{11}B). ^{11}B NMR (128 MH, $CDCl_3$: δ 32.5. ^{19}F NMR (376 MHz, $CDCl_3$) δ -137.7 – -137.9 (m), -140.9 (m). HRMS (ESI): m/z calc. for $C_{16}H_{21}BF_2O_4$ [M-H]$^-$: 326.1462, found 326.1466

2k 3-((4,4,5,5-tetramethyl-1,3,2-dioxaborolan-2-yl)-2-methyl-2-(3-trifluoromethylphenyl) propionic acid. White solid, (40 mg isolated, 45% yield). ^{1}H NMR (400 MHz, $CDCl_3$): δ 7.66 (d, *J* = 2.2 Hz, 1H), 7.59 (d, *J* = 7.9 Hz, 1H), 7.47 (d, *J* = 7.7 Hz, 1H), 7.40 (t, *J* = 7.8 Hz, 1H), 1.72 (s, 3H), 1.60 (d, *J* = 15.7 Hz, 1H), 1.48 (d, *J* = 15.7 Hz, 1H), 1.10 (s, 6H), 1.09 (s, 6H). ^{13}C NMR (101 MHz, $CDCl_3$): δ 182.2, 145.5, 130.5 (broad q, J=32.0), 129.7, 128.7, 124.2 (broad q, J=274.3 Hz), 123.6, 122.9, 83.3, 47.9, 25.0, 24.5, 24.5, 23.2 (broad due to quadrupolar broadening from ^{11}B). ^{11}B NMR (128 MHz, $CDCl_3$: δ 33.3. ^{19}F NMR (376 MHz, $CDCl_3$) δ -62.6. HRMS (ESI): m/z calc. for $C_{17}H_{22}BF_3O_4$ [M-H]$^-$: 358.1524, found 358.1530.

2l 3-((4,4,5,5-tetramethyl-1,3,2-dioxaborolan-2-yl)-2-methyl-2-(2-trifluoromethylphenyl) propionic acid. Yellow oil, (8.5 mg, 9% crude yield). ^{1}H NMR (400 MHz, $CDCl_3$): 7.66 – 7.60 (m, 2H), 7.48 (t, *J* = 7.2 Hz, 1H), 7.36 (t, *J* = 7.6 Hz, 1H), 1.84 (s, 3H), 1.63 – 1.56 (m, 2H), 1.07 (s, 6H), 1.05 (s, 6H). ^{11}B NMR (128 MHz, $CDCl_3$: δ 27.5 ^{19}F NMR (376 MHz, $CDCl_3$) δ -59.5 HRMS (ESI): m/z calc. for $C_{17}H_{22}BF_3O_4$ [M-H]$^-$: 358.1524, found 358.1519.

2m 3-((4,4,5,5-tetramethyl-1,3,2-dioxaborolan-2-yl)-2-methyl-2-(5-benzothiophenyl) propionic acid. White solid, (57 mg isolated, 66% yield). ^{1}H NMR (400 MHz, $CDCl_3$): 7.86 (d, *J* = 1.7 Hz, 1H), 7.79 (d, *J* = 8.5 Hz, 1H), 7.45 – 7.37 (m, 2H), 7.28 (dd, *J* = 5.4, 0.8 Hz, 1H), 1.77 (s, 3H), 1.70 (d, *J* = 15.7 Hz, 1H), 1.52 (d, *J* = 15.6 Hz, 1H), 1.11 (s, 6H), 1.09 (s, 6H). ^{13}C NMR (151 MHz, $CDCl_3$): δ 182.9, 141.1, 139.7, 138.1, 126.7, 124.0, 122.8, 122.2, 120.7, 83.2, 47.9, 25.4, 24.6, 24.6, 23.4 (broad due to quadrupolar broadening from ^{11}B). ^{11}B NMR (128 MHz, $CDCl_3$: δ 33.6. HRMS (ESI): m/z calc. for $C_{18}H_{23}BO_4S$ [M-H]$^-$: 346.1371, found 346.1377.

2n 3-((4,4,5,5-tetramethyl-1,3,2-dioxaborolan-2-yl)-2-methyl-2-((N-BOC)-5-indole) propionic acid White solid, (53 mg isolated, 50% yield). ^{1}H NMR (400 MHz, $CDCl_3$): δ 8.02 (d, *J* = 8.4 Hz, 1H), 7.57 (dd, *J* = 16.2, 2.9 Hz, 2H), 7.35 (dd, *J* = 8.8, 2.0 Hz, 1H), 7.25 (s, 1H), 6.51 (d, *J* = 3.8 Hz, 1H), 1.74 (s, 3H), 1.70 (d, *J* = 15.8 Hz, 1H), 1.65 (s, 10H), 1.50 (d, *J* = 15.7 Hz, 1H), 1.13 (s, 5H), 1.11 (s, 6H). ^{13}C NMR (151 MHz, $CDCl_3$): δ 181.3, 149.8, 139.3, 130.6, 126.2, 122.5, 122.0, 118.1, 114.9, 110.0, 107.5, 83.6, 83.3, 47.82, 28.2, 26.0, 24.6, 24.6, 23.4 (broad due to quadrupolar broadening from ^{11}B). ^{11}B NMR (128 MHz, $CDCl_3$: δ 28.6. HRMS (ESI): m/z calc. for $C_{23}H_{32}BNO_6$ [M-H]$^-$: 428.2250, found 428.2244.

2o 3-((4,4,5,5-tetramethyl-1,3,2-dioxaborolan-2-yl))-2-phenyl-2-ethyl propionic acid. White solid, (50 mg isolated, 66% yield). ^{1}H NMR (400 MHz, $CDCl_3$): δ 7.35 (d, *J* = 7.4 Hz, 2H), 7.27 (t, *J* = 7.6 Hz, 2H), 7.22 – 7.16 (m, 1H), 2.15 (q, *J* = 7.4 Hz, 2H), 1.61 (d, *J* = 15.8 Hz, 1H), 1.52 (d, *J* = 15.8 Hz, 1H), 1.11 (s, 6H), 1.09 (s, 6H), 0.75 (t, *J* = 7.4 Hz, 3H). ^{13}C NMR (151 MHz, $CDCl_3$): δ 181.4, 143.1, 128.1, 126.6, 126.6, 83.2, 52.0, 30.6, 24.6, 24.6, 17.7 (broad due to quadrupolar broadening from ^{11}B), 8.94. ^{11}B NMR (128 MHz, $CDCl_3$: δ 28.1. HRMS (ESI): m/z calc. for $C_{17}H_{25}BO_4$ [M-H]$^-$: 304.1807, found 304.1812.

2p 3-((4,4,5,5-tetramethyl-1,3,2-dioxaborolan-2-yl))-2-phenyl-2-propyl propionic acid. White solid, (57 mg isolated, 71% yield). ^{1}H NMR (400 MHz, $CDCl_3$): δ 7.39 – 7.34 (m, 2H), 7.27 (dd, *J* = 8.5, 6.8 Hz, 2H), 7.21 – 7.16 (m, 1H), 2.09 (m, 2H), 1.63 (d, *J* = 15.7 Hz, 1H), 1.55 (s, 1H), 1.14-1.05 (m, 2H), 1.12 (s, 6H), 1.09 (s, 6H), 0.86 (t, *J* = 7.2 Hz, 3H). ^{13}C NMR (101 MHz, $CDCl_3$): δ 181.9, 143.4, 128.1, 126.6, 126.5, 83.2, 51.6, 40.0, 24.6, 18.2 (broad due to quadrupolar broadening from ^{11}B), 17.79, 14.54. ^{11}B NMR (128 MHz, $CDCl_3$: δ 33.2. HRMS (ESI): m/z calc. for $C_{18}H_{27}BO_4$ [M-H]$^-$: 318.1963, found 318.1966.

2q 3-((4,4,5,5-tetramethyl-1,3,2-dioxaborolan-2-yl))-2-phenyl-2-nbutyl propionic acid. White solid, (29 mg isolated, 35% yield). ^{1}H NMR (400 MHz, $CDCl_3$): δ 7.36 (d, *J* = 7.3 Hz, 2H), 7.27 (t, *J* = 7.5 Hz, 2H), 7.19 (t, *J* = 7.2 Hz, 1H), 2.16 - 2.03 (m, 2H), 1.63 (d, *J* = 15.8 Hz, 1H), 1.53 (d, *J* = 15.8 Hz, 1H), 1.33 – 1.20 (m, 2H), 1.15 – 1.00 (m, 2H), 1.12 (s, 6H), 1.09 (s, 6H), 0.83 (t, *J* = 7.3 Hz, 3H). ^{13}C NMR (101 MHz, $CDCl_3$): δ 181.5, 143.4, 128.1, 126.6, 126.5, 83.2, 51.5, 37.5, 26.6, 24.6, 23.1, 18.2 (broad due to quadrupolar broadening from ^{11}B), 13.89. ^{11}B NMR (128 MHz, $CDCl_3$: δ 33.7. HRMS (ESI): m/z calc. for $C_{19}H_{29}BO_4$ [M-H]$^-$: 332.2120, found 332.2124.

2r 3-((4,4,5,5-tetramethyl-1,3,2-dioxaborolan-2-yl))-2-(4-trifluoromethylphenyl)-2-ethyl propionic acid. White solid, (51 mg isolated, 55% yield). ^{1}H NMR (400 MHz, $CDCl_3$): δ 7.54 (d, *J* = 8.5 Hz, 2H), 7.49 (d, *J* = 8.5 Hz, 2H), 2.18 (q, *J* = 7.4 Hz, 2H), 1.60 (d, *J* = 15.7 Hz, 1H), 1.53 (d, *J* = 15.7 Hz, 1H), 1.10 (s, 6H), 1.08 (s, 6H), 0.75 (t, *J* = 7.4 Hz, 3H). ^{13}C NMR (101 MHz, $CDCl_3$): δ 181.6, 147.1, 128.9 (q, *J* = 32.3 Hz), 127.1, 125.0, 125.0, 124.1 (broad q, J=272.7) 83.3, 52.2, 30.4, 24.5, 17.8 (broad due to quadrupolar broadening from ^{11}B), 8.85. ^{11}B NMR (128 MHz, $CDCl_3$: δ 33.1.^{19}F NMR (376 MHz, $CDCl_3$) δ -62.6. HRMS (ESI): m/z calc. for $C_{17}H_{22}BF_3O_4$ [M-H]$^-$: 372.1681, found 372.1682.

2s 3-((4,4,5,5-tetramethyl-1,3,2-dioxaborolan-2-yl))-2-(4-trifluoromethylphenyl)-2-(α-indane) propionic acid. Off-white solid, (39 mg isolated, 51% yield). ^{1}H NMR (600 MHz, $CDCl_3$): δ 7.31 (dd, *J* = 6.4, 2.1 Hz, 1H), 7.21 – 7.12 (m, 3H), 3.12 - 3.04 (m, 1H), 2.95 – 2.88 (m, 1H), 2.82 – 2.75 (m, 1H), 2.13 – 2.05 (m, 1H), 1.70 (d, *J* = 15.7 Hz, 1H), 1.22 (d, *J* = 15.7 Hz, 1H), 1.15 (s, 6H), 1.14 (s, 6H). ^{13}C NMR (151 MHz, $CDCl_3$): δ 182.3, 146.2, 143.9, 127.5, 126.4, 124.5, 124.0, 83.2, 56.0, 37.3, 31.1, 24.6, 24.6, 21.9(broad due to quadrupolar broadening from ^{11}B). ^{11}B NMR (128 MHz, $CDCl_3$: δ 33.5. HRMS (ESI): m/z calc. for $C_{17}H_{23}BO_4$ [M-H]$^-$: 302.1650, found 302.1654.

2t 3-((4,4,5,5-tetramethyl-1,3,2-dioxaborolan-2-yl)-2,2-diphenyl propionic acid. Off-white yellow solid, (7.0 mg, 8% crude yield). ^{1}H NMR (400 MHz, $CDCl_3$): δ 7.37 – 7.11 (m, 15H), 1.94 (s, 2H), 1.06 (s, 12H). HRMS (ESI): m/z calc. for $C_{21}H_{25}BO_4$ [M-H]$^-$: 351.1773, found 351.1768.

2u 3-((4,4,5,5-tetramethyl-1,3,2-dioxaborolan-2-yl)-2-phenyl-2-(4-methoxyphenyl) propionic acid. White solid, (13 mg, 14% crude yield). ^{1}H NMR (600 MHz, $CDCl_3$): δ 7.33 – 7.15 (m, 7H), 6.81 – 6.73 (m, 2H), 3.76 (s, 3H), 2.00 – 1.89 (m, 2H), 1.06 (s, 12H). HRMS (ESI): m/z calc. for $C_{22}H_{27}BO_5$ [M-H]$^-$: 381.1874, found 381.1874.

2v 3-((4,4,5,5-tetramethyl-1,3,2-dioxaborolan-2-yl)-2,2-di(4-methoxyphenyl)-propionic acid. White solid, (5.0 mg, 5% crude yield). ^{1}H NMR (400 MHz, $CDCl_3$): δ 7.22 – 7.17 (m, 4H), 6.81 – 6.73 (m, 4H), 3.76 (s, 6H), 1.92 (s, 2H), 1.07 (s, 12H). HRMS (ESI): m/z calc. for $C_{23}H_{29}BO_6$ [M-H]$^-$: 411.1984, found 411.1977.

2w 3-((4,4,5,5-tetramethyl-1,3,2-dioxaborolan-2-yl)-2-(4-methoxyphenyl)-2-(4-trifluoromethylphenyl) propionic acid. Off-white yellow solid, (12 mg, 11% crude yield). ^{1}H NMR (600 MHz, $CDCl_3$): δ 7.49 (d, *J* = 8.2 Hz, 2H), 7.40 (d, *J* = 8.3 Hz, 2H), 7.25 – 7.21 (m, 2H), 6.84 – 6.80 (m, 2H), 3.79 (s, 3H), 2.03 (d, *J* = 15.7 Hz, 1H), 1.87 (d, *J* = 15.8 Hz, 1H), 1.07 (s, 6H), 1.06 (s, 6H). ^{13}C NMR (151 MHz, $CDCl_3$): δ 178.4, 158.6, 149.0, 135.4, 129.5, 129.1, 128.7 (broad q, J=32.8 Hz), 124.5, 124.5, 124.2 (broad q, J=271.8 Hz), 123.3, 113.4, 83.6, 83.2, 77.2, 77.0, 76.8, 57.0, 55.2, 29.7, 24.8, 24.5, 24.5, 23.7 (broad due to quadrupolar broadening from ^{11}B). ^{11}B NMR (128 MHz, $CDCl_3$: δ 26.8. ^{19}F NMR (376 MHz, $CDCl_3$) δ -67.28. HRMS (ESI): m/z calc. for $C_{23}H_{26}BF_3O_5$ [M-H]$^-$: 449.1753, found 449.1741.

2x 3-((4,4,5,5-tetramethyl-1,3,2-dioxaborolan-2-yl)-2-phenyl-2-(4-trifluoromethylphenyl) propionic acid. Off-white solid, (21 mg isolated, 20% yield). ^{1}H NMR (600 MHz, $CDCl_3$): δ 7.49 (d, *J* = 8.4 Hz, 2H), 7.41 (d, *J* = 8.3 Hz, 2H), 7.32 – 7.22 (m, 5H), 2.04 (d, *J* = 15.8 Hz, 1H), 1.91 (d, *J* = 15.8 Hz, 1H), 1.06 (s, 6H), 1.04 (s, 6H). ^{13}C NMR (151 MHz, $CDCl_3$): δ 174.2, 143.8, 138.7, 124.4, 124.1 (broad q, J = 32.3), 123.6, 123.3, 122.4, 119.8 (broad q, J=3.8 Hz), 119.4 (broad q, J = 272.7 Hz), 78.8, 53.0, 19.8, 19.00. ^{11}B NMR (128 MHz, $CDCl_3$: δ 28.5. ^{19}F NMR (376 MHz, $CDCl_3$) δ -67.3. HRMS (ESI): m/z calc. for $C_{22}H_{24}BF_3O_4$ [M-H]$^-$: 419.1647, found 419.1638.

2.5 References

([1]) For general reviews on CO_2 utilization, see: (a) Artz, J.; Müller, T. E.; Thenert, K. Sustainable Conversion of Carbon Dioxide: An Integrated Review of Catalysis and Life Cycle Assessment. *Chem. Rev.* **2018**, *118*, 434-504. (b) Liu, Q.; Wu, L.; Jackstell, R.; Beller, M. Using Carbon Dioxide as a Building Block in Organic Synthesis. *Nat. Commun.* **2015**, *6*, 5933-5948. (c) Aresta, M.; Dibenedetto, A.; Angelini, A. Catalysis for the Valorization of Exhaust Carbon: from CO_2 to Chemicals, Materials, and Fuels. Technological Use of CO2. *Chem. Rev.* **2014**, *114*, 1709-1742. (d) Tsuji, Y.; Fujihara, T. Carbon Dioxide as a Carbon Source in Organic Transformations: Carbon-Carbon Bond Forming Reactions by Transition-Metal Catalysts. *Chem. Commun.* **2012**, *48*, 9956-9964. (e) Peters, M.;

Köhler, B.; Kuckshinrichs, W.; Leitner, W.; Markewitz, P.; Müller, T. E. Chemical Technologies for Exploiting and Recycling Carbon Dioxide into the Value Chain. *ChemSusChem* **2011**, *4*, 1216-1240. (f) Sakakura, T.; Choi, J.; Yasuda, H. Transformation of Carbon Dioxide. *Chem. Rev.* **2007**, *107*, 2365-2387.

([2]) (a) Sable, D. A.; Vadagaonkar, K. S.; Kapdi, A. R.; Bhanage, B. M. Carbon Dioxide Based Methodologies for the Synthesis of Fine Chemicals. *Org. Biomol. Chem.* **2021**, *19*, 5725–5757. (b)Fujihara, T.; Tsuji, Y. Carboxylation Reactions Using Carbon Dioxide as the C1 Source via Catalytically Generated Allyl Metal Intermediates. *Front. Chem.* **2019**, *7*, 430. (c) Shi, Y.; Pan, B.-W.; Zhou, Y.; Zhou, J.; Liu, Y.-L.; Zhou, F. Catalytic Enantioselective Synthesis Using Carbon Dioxide as a C1 Synthon. *Org. Biomol. Chem.* **2020**, *18*, 8597–8619. (d) Lluna-Galán, C.; Izquierdo-Aranda, L.; Adam, R.; Cabrero-Antonino, J. R. Catalytic Reductive Alcohol Etherifications with Carbonyl-Based Compounds or CO_2 and Related Transformations for the Synthesis of Ether Derivatives. *ChemSusChem* **2021**, *14*, 3744–3784. (e)Cabrero-Antonino, J. R.; Adam, R.; Beller, M. Catalytic Reductive N-Alkylations Using CO_2 and Carboxylic Acid Derivatives: Recent Progress and Developments. *Angew. Chem. Int. Ed.* **2019**, *58*, 12820–12838. (f) Yuan, L.; Qi, M.-Y.; Tang, Z.-R.; Xu, Y.-J. Coupling Strategy for CO_2 Valorization Integrated with Organic Synthesis by Heterogeneous Photocatalysis. *Angew. Chem. Int. Ed.* **2021**, *60*, 21150–21172. (g) Wang, L.; Que, S.; Ding, Z.; Vessally, E. Oxidative Carboxylation of Olefins with CO_2: Environmentally Benign Access to Five-Membered Cyclic Carbonates. *RSC Adv.* **2020**, *10*, 9103–9115. (h) Pimparkar, S.; Dalvi, A. K.; Koodan, A.; Maiti, S.; Al-Thabaiti, S. A.; Mokhtar, M.; Dutta, A.; Lee, Y. R.; Maiti, D. Recent Advances in the Incorporation of CO_2 for C–H and C–C Bond Functionalization. *Green Chem.* **2021**, *23*, 9283–9317. (i) Claver, C.; Yeamin, M. B.; Reguero, M.; Masdeu-Bultó, A. M. Recent Advances in the Use of Catalysts Based on Natural Products for the Conversion of CO_2 into Cyclic Carbonates. *Green Chem.* **2020**, *22* , 7665–7706. (j) Saini, S.; Prajapati, P. K.; Jain, S. L. Transition Metal-Catalyzed Carboxylation of Olefins with Carbon Dioxide: A Comprehensive Review. *Catal. Rev.* **2020**, 1–47. (k) Liu, X.-F.; Li, X.-Y.; He, L.-N. Transition Metal-Catalyzed Reductive Functionalization of CO_2. *Eur. J. Org. Chem.* **2019**, *2019*, 2437–2447. (l) Pradhan, S.; Roy, S.; Sahoo, B.; Chatterjee, I. Utilization of CO_2 Feedstock for Organic Synthesis by Visible-Light Photoredox Catalysis. *Chem. – Eur. J.* **2021**, *27*, 2254–2269.

([3]) (a) Xue, W.; Jia, X.; Wang, X.; Tao, X.; Yin, Z.; Gong, H. Nickel-Catalyzed Formation of Quaternary Carbon Centers Using Tertiary Alkyl Electrophiles. *Chem. Soc. Rev.* **2021**, *50*, 4162–4184. (b) Wang, Z. Construction of All-Carbon Quaternary Stereocenters by Catalytic Asymmetric Conjugate Addition to Cyclic Enones in Natural Product Synthesis. *Org. Chem. Front.* **2020**, *7*, 3815–3841. (c) Zeng, X.-P.; Cao, Z.-Y.; Wang, Y.-H.; Zhou, F.; Zhou, J. Catalytic Enantioselective Desymmetrization Reactions to All-Carbon Quaternary Stereocenters. *Chem. Rev.* **2016**, *116*, 7330–7396. (d) Long, R.; Huang, J.; Gong, J.; Yang, Z. Direct Construction of Vicinal All-Carbon Quaternary Stereocenters in Natural Product Synthesis. *Nat. Prod. Rep.* **2015**, *32*, 1584–1601.

([4]) (a) Lamberth, C.; Dinges, J. *Bioactive Carboxylic Compound Classes: Pharmaceuticals and Agrochemicals*; John Wiley & Sons, 2016. (b) Maag, H. Prodrugs of Carboxylic Acids. In *Prodrugs: Challenges and Rewards Part 1*; Stella, V. J., Borchardt, R. T., Hageman, M. J., Oliyai, R., Maag, H., Tilley, J. W., Eds.; *Biotechnology: Pharmaceutical Aspects*; Springer: New York, NY, 2007; pp 703–729.

([5]) (a) Ling, T.; Rivas, F. All-Carbon Quaternary Centers in Natural Products and Medicinal Chemistry: Recent Advances. *Tetrahedron* **2016**, *72*, 6729–6777. (b) Seephonkai, P.; Pyne, S. G.; Willis, A. C.; Lie, W. Bioactive Compounds from the Roots of Strophioblachia Fimbricalyx. *J. Nat. Prod.* **2013**, *76*, 1358–1364. (c) Dong, L.; Cheng, L.-Z.; Yan, Y.-M.; Wang, S.-M.; Cheng, Y.-X. Commiphoranes A–D, Carbon Skeletal Terpenoids from Resina Commiphora. *Org. Lett.* **2017**, *19*, 286–289. (d) Newman, D. J.; Cragg, G. M. Natural Products as Sources of New Drugs from 1981 to 2014. *J. Nat. Prod.* **2016**, *79*, 629–661.

([6]) Sun, X.; Frimpong, K.; Tan, K. L. Synthesis of Quaternary Carbon Centers via Hydroformylation. *J. Am. Chem. Soc.* **2010**, *132*, 11841–11843.

([7]) Shockley, S. E.; Hethcox, J. C.; Stoltz, B. M. Enantioselective Synthesis of Acyclic α-Quaternary Carboxylic Acid Derivatives through Iridium-Catalyzed Allylic Alkylation. *Angew. Chem. Int. Ed.* **2017**, *56*, 11545–11548.

([8]) (a) Liu, Z.; Gao, Y.; Zeng, T.; Engle, K. M. Transition-Metal-Catalyzed 1,2-Carboboration of Alkenes: Strategies, Mechanisms, and Stereocontrol. *Isr. J. Chem.* **2020**, *60*, 219–229. (b) Torelli, A.; Whyte, A.; Polishchuk, I.; Bajohr, J.; Lautens, M. Stereoselective Construction of γ-Lactams via Copper-Catalyzed Borylacylation. *Org. Lett.* **2020**, *22* (20), 7915–7919. (c) Bergmann, A. M.; Dorn, S. K.; Smith, K. B.; Logan, K. M.; Brown, M. K. Catalyst-Controlled 1,2- and 1,1-Arylboration of α-Alkyl Alkenyl Arenes. *Angew. Chem., Int. Ed.* **2019**, 58,

1719−1723. (d) Wu, N.-Y.; Xu, X.-H.; Qing, F.-L. Copper-Catalyzed Regioselective Borylfluoromethylation of Alkenes. *ACS Catal.* **2019**, 9, 5726−5731. (e) Gong, T.-J.; Yu, S.-H.; Li, K.; Su, W.; Lu, X.; Xiao, B.; Fu, Y. Copper-Catalyzed Alkynylboration of Alkenes with Diboron Reagents and Bromoalkynes. *Chem. - Asian J.* **2017**, 12, 2884−2888. (f) Kageyuki, I.; Yoshida, H.; Takaki, K. Three-Component Carboboration of Alkenes under Copper Catalysis. *Synthesis* **2014**, 46, 1924−1932.

([9]) (a) Jia, T.; He, Q.; Ruscoe, R. E.; Pulis, A. P.; Procter, D. J. Regiodivergent Copper Catalyzed Borocyanation of 1,3-Dienes. *Angew. Chem. Int. Ed.* **2018**, *57*, 11305–11309. (b) Smith, K. B.; Brown, M. K. Regioselective Arylboration of Isoprene and Its Derivatives by Pd/Cu Cooperative Catalysis. *J. Am. Chem. Soc.* **2017**, *139*, 7721–7724.

([10]) (a) Zhang, L.; Cheng, J.; Carry, B.; Hou, Z. Catalytic Boracarboxylation of Alkynes with Diborane and Carbon Dioxide by an *N*-Heterocyclic Carbene Copper Catalyst. *J. Am. Chem. Soc.* **2012**, *134*, 14314–14317. (b) Fujihara, T.; Tani, Y.; Semba, K.; Terao, J.; Tsuji, Y. Copper-Catalyzed Silacarboxylation of Internal Alkynes by Employing Carbon Dioxide and Silaboranes. *Angew. Chem. Int. Ed.* **2012**, *51*, 11487-11490.

([11]) Li, Z.; Zhang, L.; Nishiura, M.; Luo, G.; Luo, Y.; Hou, Z. CO_2 Activation by Lewis Pairs Generated Under Copper Catalysis Enables Difunctionalization of Imines. *J. Am. Chem. Soc.* **2020**, *142*, 1966–1974.

([12]) Tani, Y.; Fujihara, T.; Terao, J.; Tsuji, Y. Copper-Catalyzed Regiodivergent Silacarboxylation of Allenes with Carbon Dioxide and a Silylborane. *J. Am. Chem. Soc.* **2014**, *136*, 17706–17709.

([13]) (a) Butcher, T. W.; McClain, E. J.; Hamilton, T. G.; Perrone, T. M.; Kroner, K. M.; Donohoe, G. C.; Akhmedov, N. G.; Petersen, J. L.; Popp, B. V. Regioselective Copper-Catalyzed Boracarboxylation of Vinyl Arenes. *Org. Lett.* **2016**, *18*, 6428–6431. (b) Perrone, T. M.; Gregory, A. S.; Knowlden, S. W.; Ziemer, N. R.; Alsulami, R. N.; Petersen, J. L.; Popp, B. V. Beneficial Effect of a Secondary Ligand on the Catalytic Difunctionalization of Vinyl Arenes with Boron and CO_2. *ChemCatChem* **2019**, *11*, 5814-5820.

([14]) (a) Baughman, N. N.; Popp, B. V. Evidence of Boron Assistance for CO_2 Activation during Copper-Catalyzed Boracarboxylation of Vinyl Arenes: A Synthetic Model for Cooperative Fixation of CO2. *Comments Inorg. Chem.* **2020**, *40*, 159–175. (b) Baughman, N. N.; Akhmedov, N. G.; Petersen, J. L.; Popp, B. V. Experimental and Computational Analysis of CO_2 Addition Reactions Relevant to Copper-Catalyzed Boracarboxylation of Vinyl Arenes: Evidence for a Phosphine-Promoted Mechanism. *Organometallics* **2021**, *40*, 23–37.

([15]) For other complimentary experimental and computational studies on carboxylation reactions relevant to boracarboxylation at organocopper(I) species, see: (a) Mankad, N. P.; Gray, T. G.; Laitar, D. S.; Sadighi, J. P. Synthesis, Structure, and CO_2 Reactivity of a Two-Coordinate (Carbene)Copper(I) Methyl Complex. *Organometallics* **2004**, *23*, 1191–1193. (b) Lin, S.; Lin, Z. DFT Studies on the Mechanism of Copper-Catalyzed Boracarboxylation of Alkene with CO_2 and Diboron. *Organometallics* **2019**, *38*, 240-247. (c) García-López, D.; Pavlovix, L.; Hopmann, K. H. To Bind or Not to Bind: Mechanistic Insights into C-CO_2 Bond Formation with Late Transition Metals. *Organometallics* **2020**, *39*, 1339-1347. (d) Obst, M.; Pavlovic, L.; Hopmann, K. H. Carbon-Carbon Bonds with CO_2: Insights from Computational Studies. *J. Organomet. Chem.* **2018**, *864*, 115-127. (e) Lv, X.; Wu, Y. B.; Lu, G. Computational Exploration of Ligand Effects in Copper-Catalyzed Boracarboxylation of Styrene with CO_2. *Catal. Sci. Technol.* **2017**, *7*¸5049-5054.

([16]) (a) Laitar, D. S.; Müller, P.; Sadighi, J. P. Efficient Homogeneous Catalysis in the Reduction of CO_2 to CO. *J. Am. Chem. Soc.* **2005**, *127*, 17196–17197. (b) Zhao, H.; Lin, Z.; Marder, T. B. Density Function Theory Studies on the Mechanism of the Reduction of CO_2 to CO Catalyzed by Copper(I) Boryl Complexes. *J. Am. Chem. Soc.* **2006**, *128*, 15637-15643.

([17]) (a) Laitar, D. S.; Tsui, E. Y.; Sadighi, J. P. Copper(I) β-Boroalkyls from Alkene Insertion: Isolation and Rearrangement. *Organometallics* **2006**, *25*, 2405–2408. (c) Dang, L.; Zhao, H.; Lin, Z.; Marder, T. B. DFT Studies of Alkene Insertions into Cu-B Bonds in Copper(I) Boryl Bonds. *Organometallics* **2007**, *26*, 2824-2832.

([18]) The ^{1}H NMR spectrum of **1t** crude boracarboxylation reaction mixture revealed 30% conversion of **1t** with product **2t** (8%) and formal hydroboration product **3t** (22%). The ^{11}B NMR spectrum showed trace amounts (<5%) of pinB-O-Bpin, suggesting that competitive CO_2 reduction did not contribute significantly to inefficient boracarboxylation catalysis.

([19]) Liwosz, T. W.; Chemler, S. R. Copper-Catalyzed Oxidative Amination and Allylic Amination of Alkenes. *Chem. – Eur. J.* **2013**, *19*, 12771–12777.

([20]) Grigg, R. D.; Rigoli, J. W.; Van Hoveln, R.; Neale, S.; Schomaker, J. M. Beyond Benzyl Grignards: Facile Generation of Benzyl Carbanions from Styrenes. *Chem. – Eur. J.* **2012**, *18*, 9391–9396.

([21]) Chatalova-Sazepin, C.; Wang, Q.; Sammis, G. M.; Zhu, J. Copper-Catalyzed Intermolecular Carboetherification of Unactivated Alkenes by Alkyl Nitriles and Alcohols. *Angew. Chem. Int. Ed.* **2015**, *54,* 5443–5446.

CHAPTER 3: *Synthesis of Novel Borylated Ibuprofen Derivative through Suzuki Cross-Coupling and Boracarboxylation Methodologies.*

3.1 Introduction

Through the years boron has been a keystone in chemical synthesis. Reactions such as hydroboration oxidation,[1] halogenation,[2] amination,[3] and Suzuki Cross-Coupling have been at the forefront of chemical innovation. In fact, the Suzuki Cross Coupling accounts for 40% of all carbon-carbon bond forming reactions in the pursuit of drug candidates.[4] The Suzuki Cross coupling reaction allows direct access to vinyl arenes in one step from the halogenated arene precursor.[5] Typically these products are accessed from the aldehyde through Wittig methodologies, which have poor atom economy due to the triphenylphosphineoxide byproduct being generated stoichiometrically. In a world where green chemistry is at the forefront of research, the use of greener methods to access synthetic targets is of utmost importance.

We envisioned that a regioselective hetero(element)carboxylation of vinyl arenes would allow for direct access to novel hetero(element) containing NSAIDs. However, hetero(element)carboxylations are exceedingly rare, and until 2016 were limited to alkynyl and allenyl substrates.[6,7,8] Extension of the boracarboxylation reaction to vinyl arenes would provide boron functionalized NSAIDs, and boron based pharmaceutical candidates (Figure 3.1) have been gaining popularity marked by recent decisions by the FDA to approve the chemotherapeutic bortezomib, antifungal tavaborole, and anti-inflammatory crisaborole. The Lewis acidity of boron is interesting from a drug design standpoint due to the capability to readily bind Lewis bases such as diols, hydroxyl groups on carbohydrates, or nitrogen-bases in RNA and DNA. [9] All of these Lewis bases are important due to their roles in physiological and pathological processes[9].

Our approach to boracarboxylation relies upon borylcupration of the alkene by a Cu-Boryl, followed by CO_2 insertion into the resulting Cu-alkyl species. Sadeghi and coworkers reported the boryl cupration of styrene derivitives through use of (NHC)Cu-boryls,[10] and carboxylation of Cu-alkyl species has also been observed.[11] In 2016, we developed a new synthetic approach to achieve mild difunctionalization, of vinyl arenes using a (NHC)Cu-boryl catalyst and only a single atmosphere of gaseous carbon dioxide (Chapter 1, Scheme 1.1).[12] Using this method, the α-aryl propionic acid pharmacophore is directly accessed in a single step, and a novel unexplored class of boron-modified NSAIDs can be prepared in excellent yields. In 2019 we demonstrated that catalytic additives lead to improved catalyst efficiency and broadening of substrate scope, which included two more novel borylated NSAIDs (Figure 3.1).[13]

Previous borylative carboxylation reactions of alkenes could only be achieved under stringent air and moisture free conditions with use of a prefuntionalized copper(I) precatalyst. However, a benchtop method wherein borylated Ibuprofen can be accessed using simple reagents is more desirable. We sought to develop reaction conditions that allowed for boracarboxylation of vinyl arenes, particularly isobutyl styrene, to proceed from the *in-situ* generation of copper precatalyst, and without the need for use of a glovebox. The boracarboxylation method described in Chapter 2 provides the copper precatalyst directly from SIMesHCl (13 mol%) and CuCl (12 mol%), which is then carried foward to generate the active SIMesCuOtBu catalyst *in-situ*.

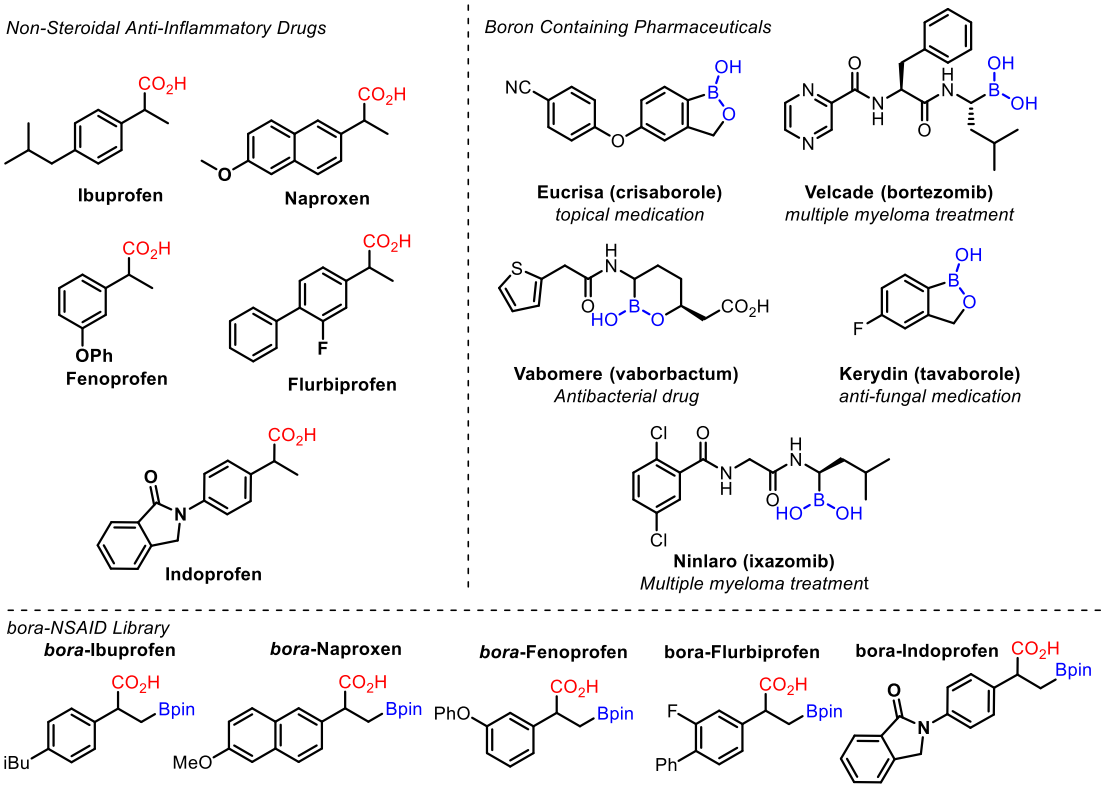

Figure 3.1 Medicinal relevance of boracarboxylation

Using this method, α-methyl styrene was boracarboxylated to afford 95% yield of the desired product, albeit with use of a glovebox. Inspired by this result, we used a modified procedure where the entire reaction was setup and ran without using a nitrogen filled glovebox, to boracarboxylate tBu-styrene. The desired boracarboxylated tert-butyl styrene product was afforded in 90% yield on a 1.5-gram scale. Gratifyingly, this method was also able to be applied to isobutyl styrene to afford *bora*-Ibuprofen NSAID derivative in moderate yield.

Non-steroidal anti-inflammatory drugs (NSAIDs) (Figure 3.1) are among the most common drugs used for the management and treatment of pain, however when taken for chronic pain, they can cause severe gastrointestinal events such as ulcers, bleeding, or perforation of the stomach lining as well as induced chronic kidney disease.[14,15,16,17,18] The α-aryl propionic acid pharmacophore is the core motif amongst NSAIDs, therefore synthetic strategies that allow direct access to this motif are highly desirable chemical transformations. In fact, identification of methods to synthesize unexplored classes of NSAIDs may lay the foundation for novel non-addictive chronic pain management strategies. In this chapter, we present a synthetic pathway to access a novel *bora*-Ibuprofen NSAID derivative from an abundant, cheap 4-isobutylbromobenzene starting material (~$2.50/1g) in moderate yield in two steps, without the need for a glovebox.

3.2 Reaction Protocols:

1. Synthesis of 4-Isobutylstyrene through Suzuki Cross Coupling of 4-isobutylbromobenzene with vinylboronic acid pinacol ester

Scheme 3.1 Synthesis of *bora*-Ibuprofen precursor

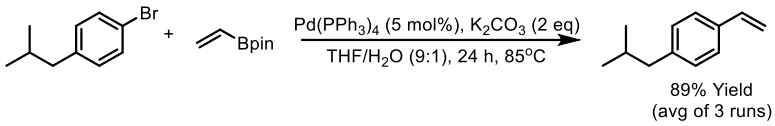

1.1. Add 144 mg of palladium(0) tetrakistriphenylphosine (5 mol %), 1.04 g of anhydrous potassium carbonate (2 equiv.), and magnetic stirbar (0.5 x 0.125 in.), to a 40 mL scintillation vial then seal with a pressure relief cap. Tape around the seal with electrical tape until the seal is completely encapsulated.

1.1.1. Purge the reaction mixture with argon for 2 minutes. After the 2 minutes has finished, 1.07 g of 4-isobutylbromobenzene (1 equiv), then add 13 mL of anhydrous THF obtained from while continuously purging, then commence magnetic stirring.

1.1.2. Add 1.5 mL of argon-sparged deionized water to the solution, followed by 0.72 mL of vinylboronic acid pinacol ester (1.5 equiv), then purge the reaction mixture with argon for an addition 5 minutes.

1.1.3. Once the purge has finished, commence heating at 85 ^{o}C for 24 hours.

1.1.4. After 24 hours has passed, remove a small aliquot from the reaction and dilute it with 2 mL dichloromethane in a 4-dram vial, then run TLC using hexane to ensure reaction completion (Rf=0.9 reactant, Rf=0.91 product).

1.2. Upon confirmation of aryl bromide **3** consumption, add the reaction mixture to a 125 mL separatory funnel, then add 30 mL deionized water. Rinse the vial 3x with 5 mL dichloromethane, adding each individual rinse to the separatory funnel, shake vigorously, then extract the organic layer into a 125 mL Erlenmeyer flask, leaving the aqueous layer behind.

1.2.1. Extract 3x with 5 mL dichloromethane, then add the organic extracts to the 125 mL Erlenmeyer flask, then discard the aqueous layer.

1.2.2. Transfer the organic extracts into the separatory funnel then wash with 30 mL of brine, then discard the brine.

1.2.3. Transfer the organic layer to a 125 mL Erlenmeyer flask then add 5 g of sodium sulfate, and swirl the flask for 20 seconds.

1.2.4. Vacuum filter the solution into a 125 mL filter flask, using a glass funnel plugged with cotton

1.2.5. Transfer the organic layer to a 100 mL roundbottom flask, then concentrate the reaction *in vacuo* to a pale-yellow viscous oil.

1.3. The crude reaction mixture was subjected to column chromatography using 50 g of SilicaFlash P60 silica gel, and pure hexane as the eluent, which provided the pure product in 89% yield (average of 3 reactions).

NOTE: *p*-isobutyl styrene is subject to polymerization at room temperature under light, so once isolated it is

imperative that the product is stored in a dark place at a temperature of -20°C or lower until needed. It is also possible to use a small amount of butylated hydroxytoluene (BHT) as an inhibitor for polymerization if necessary.

2. Large scale synthesis of *bora*-Ibuprofen

Scheme 3.2 Synthesis of *bora*-Ibuprofen

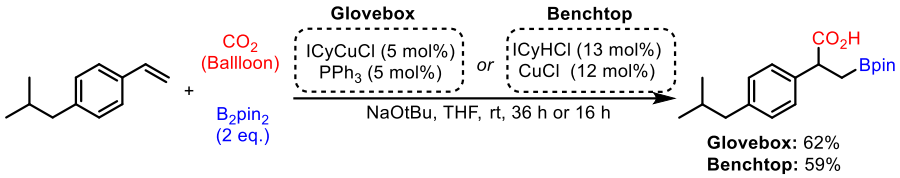

NOTE: This reaction is prepared inside a nitrogen filled glove box. All chemicals are dried or purified before moving into the box. The *p*-isobutyl styrene is freeze pump thawed prior to use. All vials and glassware are dried and heated in a 180°C oven for at least 24 hours prior to use.

2.1. Add 160 mg of ICyCuCl (5 mol %), 131 mg of triphenylphosphine (5 mol %), 1.92 g of sodium tert-butoxide (2 equiv.), 20 mL of anhydrous, degassed THF, and a 0.5 x 0.125 in. magnetic stirbar to a 20 mL scintillation vial, then seal with an air-tight septum, and stir the resulting solution for 20 minutes.

2.1.1. After 20 minutes has passed, the pre-prepared catalyst solution was transferred to a 60 mL syringe, and the needle was plugged using a septum.

2.1.2. Add 2.79g of bis(pinacolato)diboron (1.1 equiv.), 1.87 mL of 4- Isobutylvinylbenzene (1 equiv), 140 mL of THF, and a 2 x 0.3125 in. magnetic stir bar to a 500 mL roundbottom flask, seal with a septum, then tape around the septum until the seal is encapsulated.

NOTE: It is imperative that the addition of the styrene to the 500 mL roundbottom flask is done immediately before the removal of the catalyst solution and styrene solution from the glovebox, as it is subject to rapid polymerization in THF. Also, the catalyst solution is subject to rapid decomposition, so it is necessary to have little downtime between removal from the glovebox and catalyst addition to the 500 mL roundbottom flask.

2.2. The 500 mL RB containing the styrene solution and the 60 mL syringe containing the catalyst solution were removed from the glovebox and moved to a fume hood.

2.2.1. While purging the 500 mL round bottom flask with dry carbon dioxide, the catalyst solution was added over 30 seconds then the reaction was stirred at ambient temperature for 3 hours.

2.2.2. After 3 hours reaction was again purged with dry carbon dioxide (Matheson bone dry carbon dioxide) for 15 minutes and then stirred at ambient temperature for 33 hours.

2.3. Upon reaction completion, the reaction mixture was concentrated in vacuo, then acidified with 30 mL 1.0 M HCl.

2.3.1. 50 mL of diethyl ether is then added to the roundbottom flask containing the 30 mL of 1.0 M HCl solution, and swirled for 10 seconds, then the solution is transferred to a 500 mL separatory funnel, where, then the aqueous layer is removed from the and then discarded.

2.3.2. The ether solution is then extracted with saturated $NaHCO_3$ (8 x 50 mL) into a 500 mL Erlenmeyer flask.

2.3.3. The combined aqueous layers were carefully acidified with 12 M HCl (to pH ≤ 1.0 by litmus paper) and subsequently transferred to a 500 mL separatory funnel, then extracted with dichloromethane (8 x 50 mL) into a 500 mL Erlenmeyer flask.

2.3.4. Add 50 g of sodium sulfate and swirl the flask for 20 seconds.

2.3.5. Filter the solution into a 500 mL roundbottom flask, using a 500 ml separatory funnel plugged with cotton.

2.3.6. Concentrate the solution in vacuo

2.4. Dissolve the residue in 10 mL of HPLC grade Heptane, then store in a freezer (-20 ^{o}C) overnight to afford pure recrystallized *bora*-Ibuprofen in 62% yield (average of 2 reactions).

3. Benchtop large scale synthesis of *bora*-Ibuprofen

NOTE: This reaction is prepared without the use of a nitrogen filled glovebox. All chemicals were used as received or as synthesized without further purification (drying, distilling, etc.). All vials and glassware are dried and heated in a 180^{o}C oven for at least 24 hours prior to use and cooled under argon to room temperature immediately before reaction setup.

3.1. Add 334 mg of ICy-HCl (13 mol %), 2.92 g of sodium tert-butoxide (3 equiv.), and a 0.5 x 0.125 in. magnetic stirbar to a 20 mL scintillation vial, then seal with an air-tight septum and immediately purge with argon for 5 minutes.

3.1.1. Add 20 mL of anhydrous, degassed THF to the weighed-out ligand and base mixture and purge the resulting solution for 5 minutes with argon, then stir for 30 minutes.

3.1.2. Add 119 mg of CuCl (12 mol%), and a 0.5 x 0.125 in. magnetic stirbar to a 20 mL scintillation vial, then seal with an air-tight septum, and immediately purge with argon for minutes. After the ligand solution from 3.1.1 has stirred for 30 minutes, add it to the CuCl, and stir the resulting solution for 1 hour.

NOTE: When weighing out CuCl, take care to place it directly in the center of the bottom of the scintillation vial, as it tends to get stuck around the inside corner edges of the vial, resulting in poor reactivity with the ligand solution.

3.2. Add 5.08 g of bis(pinacolato)diboron (2 equiv.) and a 2 x 0.3125 in. magnetic stir bar to a 500 mL roundbottom flask and seal with a septum, then tape around the septum until the seal is encapsulated. Once sealed, add 140 mL of THF, 1.78 mL of 4- Isobutylvinylbenzene (1 equiv) to the flask, then purge with argon for 5 minutes.

3.2.1. Immediately following the argon purge, begin purging the 500 mL round bottom flask with dry carbon dioxide (Matheson bone dry carbon dioxide). Then add the catalyst solution from 3.1.2 over 30 seconds and purge with dry carbon dioxide for 15 minutes. The reaction was stirred at ambient temperature for 16 hours

3.3. Upon reaction completion, the reaction mixture was concentrated in vacuo, then acidified with 50 mL 1.0

M HCl.

3.3.1. The ether solution is then extracted with saturated $NaHCO_3$ (6 x 50 mL) into a 500 mL Erlenmeyer flask.

3.3.2. The combined aqueous layers were carefully acidified with 12 M HCl (to pH ≤ 1.0 by litmus paper) and subsequently transferred to a 500 mL separatory funnel, then extracted with dichloromethane (6 x 50 mL) into a 500 mL Erlenmeyer flask.

3.3.3. Add 50 g of sodium sulfate and swirl the flask for 20 seconds.

3.3.4. Filter the solution into a 500 mL roundbottom flask, using a 500 ml separatory funnel plugged with cotton.

3.3.5. Concentrate the solution in vacuo.

3.4. Dissolve the residue in 10 mL of HPLC grade Heptane, then store in a freezer (-20 ºC) overnight to afford pure recrystallized *bora*-Ibuprofen in 59% yield.

3.3 Representative Results

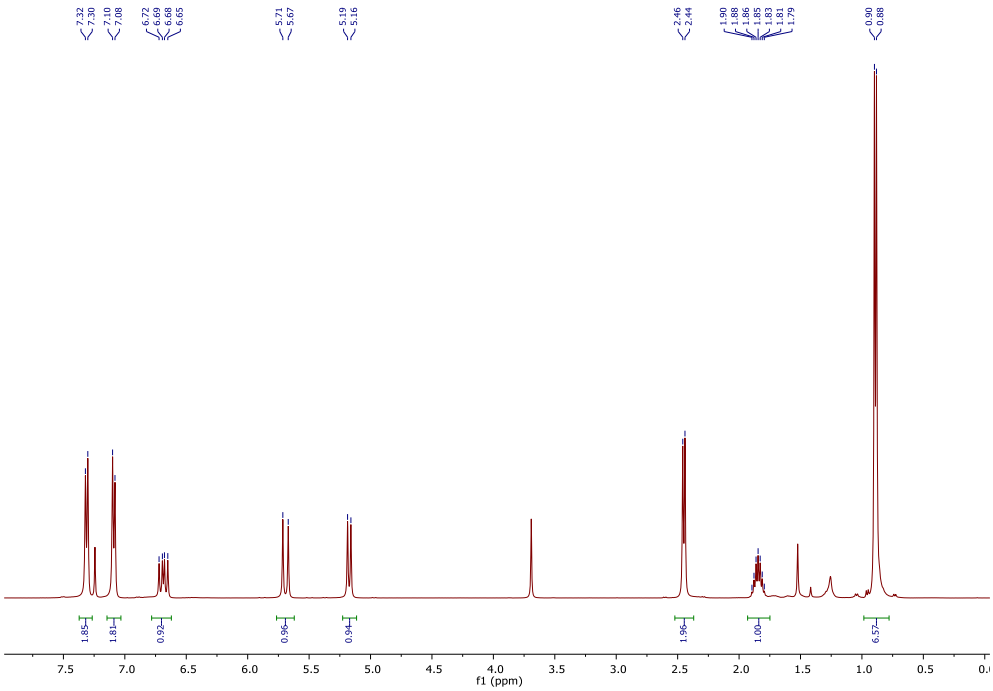

Figure 3.2 ^{1}H NMR spectrum of *p*-Isobutyl Styrene

4-Isobutylstyrene was characterized by ^{1}H, NMR spectroscopy, and *bora*-Ibuprofen was characterized by ^{1}H, ^{13}C and ^{11}B NMR spectroscopy to confirm the product structure and assess purity. Key data for representative compounds is described in this section.

Spectral data are in good agreement with the styrene structure 2 (Figure 3.2). The ^{1}H NMR spectrum shows the characteristic ABX splitting pattern seen for monosubstituted styrene derivatives. These signals are observed as a doublet at 5.69 (d, J = 17.6 Hz,1H), doublet at 5.17 (d, J = 10.9 Hz, 1H) and a doublet of doublets at 6.62 – 6.78 (dd,

J = 10.9, 17.6 Hz 1H) (Figure 4). A second identifiable characteristic feature is the isobutyl methine proton, which appears as a septet at 2.37 – 2.52(m, 2H) and the corresponding methyl groups show up as a doublet at 0.89 (d, J = 6.6 Hz, 6H) (Figure 4).

Synthesis of *p*-Isobutyl styrene via our protocol reliably provides direct access to the product in 89% yield (average of 3 reactions, 5 mmol scale), however, deviation from any of the key reaction conditions such as temperature and time significantly impact the efficiency of the reaction. It is important that the reaction be heated at no less than 85 ^{o}C, and to verify the reaction has run to completion by TLC after 24 hours has passed.

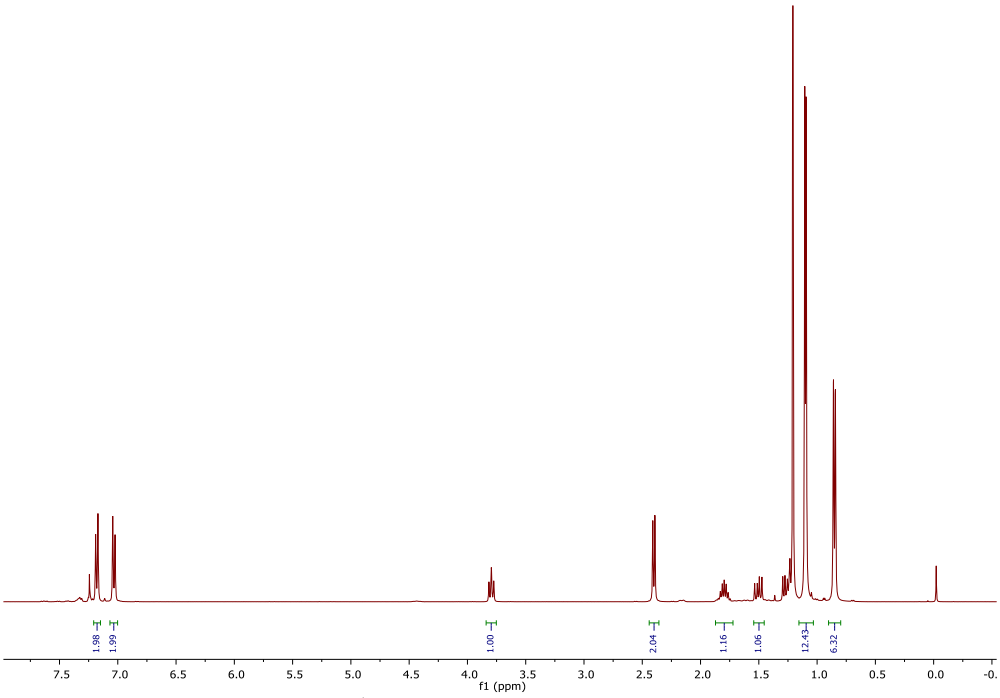

Figure 3.3 ^{1}H NMR spectrum of *bora*-Ibuprofen

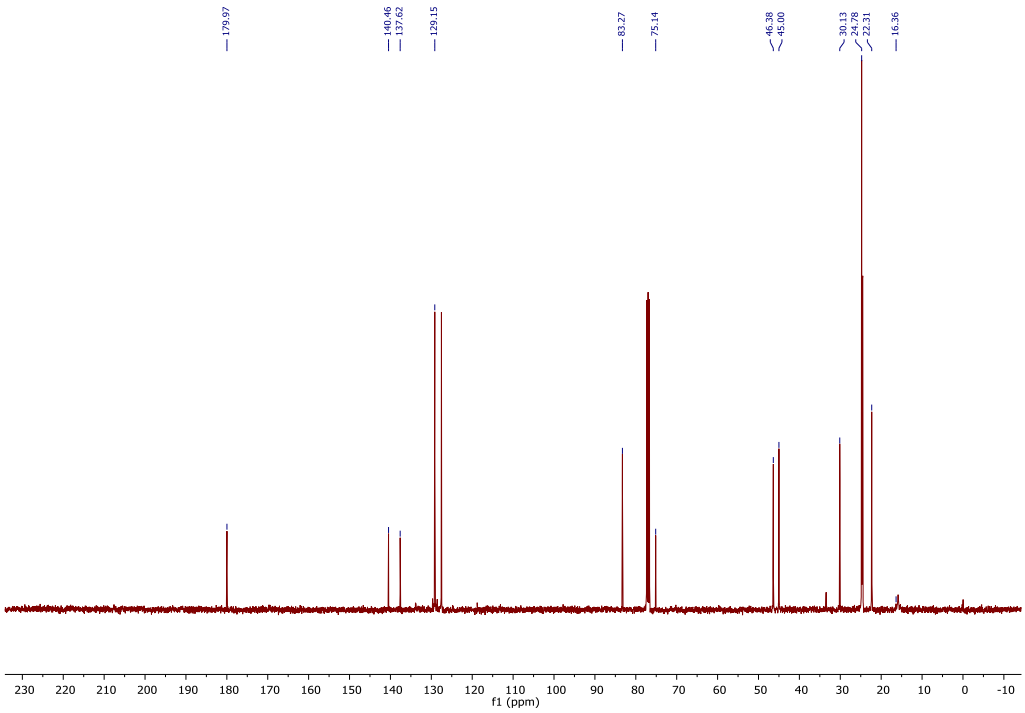

Figure 3.4 ^{13}C NMR spectrum of *bora*-Ibuprofen

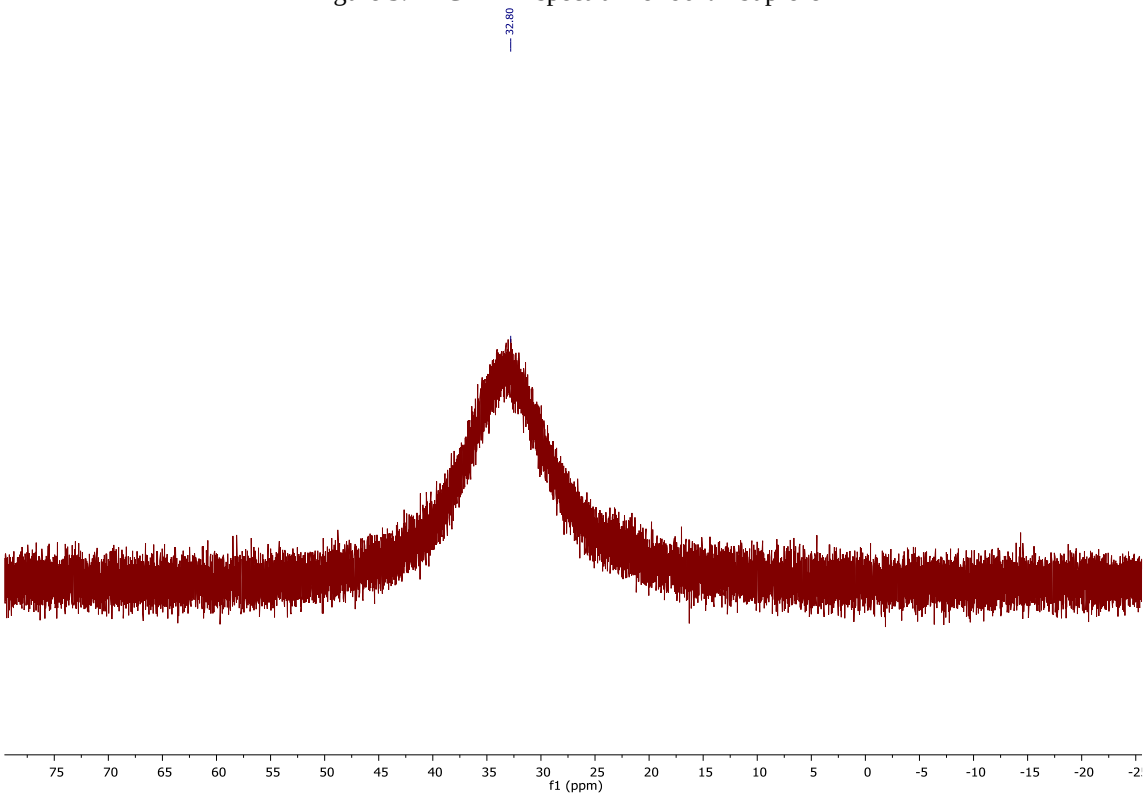

Figure 3.5 ^{11}B NMR spectrum of *bora*-Ibuprofen

Spectral data are in good agreement with the boracarboxylated product 3 (Scheme 3.2). As with the previous substrate the ^{1}H NMR spectrum (Figure 3.3) shows an ABX splitting pattern, but this pattern occurs due to diastereotopic methylene protons, as a result of the newly generated chiral center. These signals are observed as a doublet of doublets

at 1.53 (dd, *J* = 16.0, 9.1 Hz,1H), 1.29 (dd, *J* = 16.0, 7.6 Hz, 1H).The proton at 3.82 (dd, *J* =9.1, 7.6 Hz, 1H) is significantly deshielded, which indicates that it should be alpha to the carboxylic acid. Another key resonance is the doublet at 1.12 (s, 6H), 1.11 (s, 6H) which corresponds to the now diastereotopic methyl groups of the pinacolato boron moiety.

The ^{13}C NMR spectrum of the boracarboxylated product (Figure 3.4) shows a very broad signal at 16 ppm, which is characteristic of a boron-bound carbon, due to the quadrupolar broadening from the boron. Another key resonance is the signal at 180.75 ppm which corresponds to the carboxylic acid.

The ^{11}B NMR spectrum (Figure 3.5) shows one key broad resonance at 33.4 ppm, which is characteristic of a trivalent boron.

The synthesis of *bora*-Ibuprofen via our protocol reliably provides direct access to the product in 62% yield (average of 2 reactions, 2.05 g isolated), however, this reaction is far more sensitive than the previous Suzuki cross coupling reaction. Any deviation that occurs from the reported protocol will result in significantly diminished yields. Particular attention needs to be paid to the air sensitive nature of this reaction. Using our benchtop protocol, the large-scale synthesis of *bora*-Ibuprofen provides the desired product in 59% yield (1.95 g isolated) which is comparable to the glovebox method.

3.4 Discussion and concluding remarks:

p-Isobutyl styrene can be obtained via a Suzuki Cross Coupling reaction between cheap, commercially available 4-bromoIsobutylbenzene, and vinylboronic acid pinacol ester. This allows for access to the product in a greener, more atom economical manner then the conventional Wittig approach. However, it is imperative that before workup of the reaction, to verify that the reaction has gone to completion. If the reaction has not gone to completion, then the separation from the *p*-Isobutyl styrene is exceedingly difficult.

Boracarboxylation of 4-Isobutylstyrene with a copper(I) NHC catalyst at ambient temperature using a pincolato diboron reductant under an atmosphere of gaseous CO_2 provides *bora*-Ibuprofen in moderate yield. It is important to note that the styrene must be freeze pump thawed to the point where there is no air present in the solution, or the air trapped in the compound will diminish reactivity significantly. This reaction is air and moisture sensitive, and even small quantities of air and moisture will cause catalyst decomposition, providing a sky-blue colored reaction Notably, when the catalyst is added to the reaction, it turns a cloudy white color with a very slight hint of pink, and then after addition of the CO_2 and 3 hours have passed the reaction turns brown or light green. The catalyst must be added to the reaction mixture quickly due its air sensitive nature. The reaction can tolerate gentle heating up to 45 ^{o}C. Any higher will result in decomposition and diminished yields.

When the benchtop protocol for the boracarboxylation of 4-isobutylstyrene is employed, the desired *bora*-Ibuprofen product is obtained in comparable yield to the glovebox protocol. However, the reagents utilized in this transformation were used with minimal to no purification, which demands higher catalyst loading (12 mol%) then the

glovebox protocol (5 mol% ICyCuCl and 5 mol% triphenylphosphine). The reaction cannot be stored for any amount of time and must immediately purified. The resulting end color of the reaction is either brown or light green, and if left too long it will turn sky blue, indicating decomposition. At this point it is still possible to isolate the product at the cost of significantly diminished yields. *bora*-Ibuprofen cannot be isolated by column chromatography of any type and must be isolated following the acid-base workup protocol. This product will decompose rapidly on a silica gel column. Once isolated the *bora*-Ibuprofen is an air stable white solid. Upon the first acid base workup, there is a small amount of B_2pin_2 that is isolated along with the product. To remove this impurity, a second acid base workup, followed by a recrystallization in heptane can be employed. In the future we expect that *bora*-Ibuprofen will provide access to a host of other functionalized ibuprofen derivatives, thus allowing for their study as potential therapeutic targets for pain management.

3.5 Experimental Methods

General Information

All the air and moisture sensitive experiments were set up in a nitrogen-filled MBraun 200B dual-port glovebox, and before each experiment the atmosphere was tested using diethyl zinc. The cross coupling and boracarboxylation reactions were performed in 500 mL roundbottom flasks purchased from Chemglass and were dried in an oven at 180 ^oC for at least 24 hours prior to use. All glassware used in the glovebox was dried for at least 24h in the 180 ^oC oven prior to use. The magnetic stirbars in these reactions were new, unused, and purchased from VWR (1/2 by 1/8 in. disposable stirbar CAT. NO:58947-140) and dried for at least 24h at 180 ^oC prior to use. The dry solvent used for all experiments was dried on a Glass Contour solvent purification system, and further dried over 4Å mol sieves. The liquid reagents used in the glovebox were degassed using a freeze/pump/thaw method on a Schlenk line prior to use. $CDCl_3$ was purchased from Cambridge Isotope Laboratories, Inc. NMR spectra were recorded on either a 400 MHz Agilent or 600 MHz Agilent NMR spectrometer. ^1H, ^{13}C, ^{11}B, and ^{19}F NMR experiments were acquired in $CDCl_3$ using tetramethylsilane as a reference in quartz NMR tubes. ^{11}B NMR was referenced to an external $BF_3{\cdot}OEt_2$ standard.

Characterization of isolated compounds

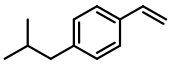

4-Isobutylstyrene is in agreement with previously reported characterization data

^1H NMR (400 MHz, $CDCl_3$) δ 7.36 – 7.28 (m, 2H), 7.13 – 7.06 (m, 2H), 6.69 (dd, *J* = 17.6, 10.9 Hz, 1H), 5.70 (dd, *J* = 17.6, 1.0 Hz, 1H), 5.18 (dd, *J* = 10.9, 1.0 Hz, 1H), 2.46 (d, *J* = 7.2 Hz, 2H), 1.85 (dp, *J* = 13.6, 6.8 Hz, 1H), 0.90 (d, *J* = 6.6 Hz, 6H)[12].

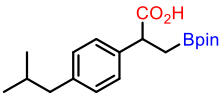

3-boronic acid pinacol ester-2-phenyl propionic acid is in agreement with previously reported characterization data[12]. ^{1}H NMR (400 MHz, $CDCl_3$) δ 7.22 – 7.15 (m, 2H), 7.07 – 7.01 (m, 2H), 3.80 (dd, *J* = 9.1, 7.6 Hz, 1H), 2.41 (d, *J* = 7.2 Hz, 2H), 1.79 (dt, *J* = 13.5, 6.7 Hz, 1H), 1.50 (dd, *J* = 15.9, 9.1 Hz, 1H), 1.32 – 1.23 (m, 1H), 1.22 (s, 1H), 1.10 (s, 6H), 1.08 (s, 6H), 0.86 (dd, *J* = 6.6, 1.3 Hz, 6H). ^{13}C NMR (101 MHz, $CDCl_3$) δ 180.44, 140.55, 137.59, 129.22, 127.58, 83.30, 46.45, 45.05, 33.32, 30.17, 24.84, 24.64, 24.53, 22.36, 22.33. ^{11}B NMR (128 MHz, $CDCl_3$) δ 32.95.

3.6 References

1. J. M. Clay, E. Vedejs, Hydroboration with Pyridine Borane at Room Temperature. *J. Am. Chem. Soc.*, **127**, 5766-5767 (2005).
2. Brown, H. C.; Rathke, M. W.; RogiC´, M. M.; De Lue, N. R., Organoboranes for Synthesis. 9. Rapid Reaction of Organoboranes with Iodine under the Influence of Base. a Convenient Procedure for the Conversion of Alkenes into Iodides via Hydroboration. *Tetrahedron.*, **44** (10), 2751–2762 (1988).
3. R. P. Rucker, A. M. Whittaker, H. Dang, G. Lalic., Synthesis of Tertiary Alkyl Amines from Terminal Alkenes: Copper-Catalyzed Amination of Alkyl Boranes. *J. Am. Chem. Soc.*, **134**, 6571-6574 (2012).
4. Roughley, S. D.; Jordan, A. M. The Medicinal Chemist's Toolbox: An Analysis of Reactions Used in the Pursuit of Drug Candidates. *J. Med. Chem*., **54**, 3451−3479 (2011).
5. Miyaura, N; Suzuki, A. Palladium-Catalyzed Cross-Coupling Reactions of Organoboron Compounds. *Chem. Rev.*, **95** (7): 2457–2483 (1995).
6. Fujihara, T.; Tani, Y.; Semba, K.; Terao, J.; Tsuji, Copper-Catalyzed Silacarboxylation of Internal Alkynes by Employing Carbon Dioxide and Silylboranes Y. *Angew. Chem., Int. Ed*., **51**, 11487− 11490 (2012).
7. Tani, Y.; Fujihara, T.; Terao, J.; Tsuji, Y. Copper-Catalyzed Regiodivergent Silacarboxylation of Allenes with Carbon Dioxide and a Silylborane. *J. Am. Chem. Soc*, **136**, 17706−17709 (2014).
8. Zhang, L.; Cheng, J.; Carry, B.; Hou, Z. Catalytic boracarboxylation of alkynes with diborane and carbon dioxide by an N-heterocyclic carbene copper catalyst. *J. Am. Chem. Soc.*, **134**, 14314−14317 (2012).
9. Draganov, A.; Wang, D. Z.; Wang, B. H., The Future of Boron in Medicinal Chemistry: Therapeutic and Diagnostic Applications. In Atypical Elements in Drug Design, Schwarz, J., Ed.; **17**, 1-27 (2016).
10. Laitar, D. S.; Tsui, E. Y.; Sadighi, J. P. Copper(I) β-Boroalkyls from Alkene Insertion: Isolation and Rearrangement. Synthesis, Structure, and CO2 Reactivity of a Two-Coordinate (Carbene)copper(I) Methyl Complex. *Organometallics.*, **25**, 2405−2408 (2006).
11. Mankad, N. P.; Gray, T. G.; Laitar, D. S.; Sadighi, J. P. *Organometallics.*, **23**, 1191−1193 (2004).
12. Butcher, T. W.; McClain, E. J.; Hamilton, T. G.; Perrone, T. M.; Kroner, K. M.; Donohoe, G. C.; Akhmedov, N. G.; Petersen, J. L.; Popp, B. V. Regioselective Copper-Catalyzed Boracarboxylation of Vinyl Arenes. *Org. Lett.*, **18** (24), 6428–6431 (2016).
13. Perrone, T. M.; Gregory, A. S.; Knowlden, S. W.; Ziemer, N. R.; Alsulami, R. N.; Petersen, J. L.; Popp, B. V. Beneficial Effect of a Secondary Ligand on the Catalytic Difunctionalization of Vinyl Arenes with Boron and CO2.**. 11** (23), 5814-5820 (2019).
14. Wolfe MM, Lichtenstein DR, Singh G: Gastrointestinal toxicity of non-steroidal anti-inflammatory drugs. *N. Engl. J. Med.*, **340**. 1888–1899 (1999).
15. Singh G, Ramey DR, Morfeld D, et al.: Gastrointestinal tract complications of non-steroidal anti-inflammatory drug treatment in rheumatoid arthritis: a prospective observational cohort study. *Arch. Intern. Med.*, **156**. 1530–1536 (1996).
16. Singh G, Triadafilopoulus G: Epidemiology of NSAID-induced GI complications. *Rheumatology.*, **26**. 18–24 (1999).

17. Lichtenstein DR, Syngal S, Wolfe MM: Non-steroidal anti-inflammatory drugs and the gastrointestinal tract: the double-edged sword. *Arthritis. Rheum.*, **38**. 5–18 (1995).
18. Hernandez-Diaz S, Rodriguez LAG: Association between non-steroidal anti-inflammatory drugs and upper gastrointestinal tract bleeding/perforation: an overview of epidemiologic studies published in the 1990s. *Arch. Intern. Med.*, **160**. 2093–2099 (2000).

CHAPTER 4: *Regioselective Boracarboxylation of Unactivated Alkenes Enabled by Catalytic Xantphos Additive*

4.1 Introduction

Transition metal catalyzed reductive hydrocarboxylation of alkynes[1] and alkenes[2] wherein CO_2 is utilized as a C_1 synthon to afford are powerful synthetic transformations. These catalytic methodologies take ubiquitous and abundant chemical feedstocks and provide value-added acrylic[3] and aliphatic[4] carboxylic acid substrates. Typically, these reactions proceed using a hydride source as a reductant to afford the desired carboxylic acid product directly. Furthermore, when a non-hydride reductant is employed the value of the transformation increases. Carbo-,[5] amino-,[6] thio-,[7] phosphono-,[8] sila-[9], and bora-[10] carboxylative difunctionalization reactions have been reported with alkynes and activated alkene substrates. Despite this, reports in which unactivated alkenes are carboxylatively difunctionalized are limited.[5f] In 2016, the Popp group reported a first of its kind borylative carboxylation of electron-rich and neutral vinyl arenes with limited reactivity of electron-poor substrates.[11] This method provides direct access to borylated α-aryl carboxylic acid derivatives from vinyl arenes using mild copper(I) catalysis, 1 atm of CO_2, and bispinacolato diboron (B_2pin_2). The scope of boracarboxylation was expanded to electron-deficient vinyl arene substrates in 2019 through use of PPh_3 as a catalytic additive, and by increasing the concentration of the alkene.[12] Follow up mechanistic studies demonstrated that under these phosphine-mediated carboxylation conditions, a S_E pathway becomes operative, resulting in a more facile carboxylation when electron-deficient substrates are employed.[13] Guided by the mechanistic insight obtained from the previous mechanistic study the Popp group reported, Chapter 2 described further improvement to the catalytic boracarboxylation methodology to expand the scope to a variety of α-substituted vinyl arenes. By altering the N-heterocyclic carbene (NHC) Cu^I catalyst along with the base, and changing the CO_2 and B_2pin_2 concentrations, electron-poor, -rich, and -neutral α-substituted vinyl arenes were boracarboxylated in moderate yields. However, reactivity with unactivated alkenes such as α-olefins and other aliphatic alkenes remained elusive in this catalytic system.

Scheme 4.1 Previous carboxylative and carbonylative difunctionalization work

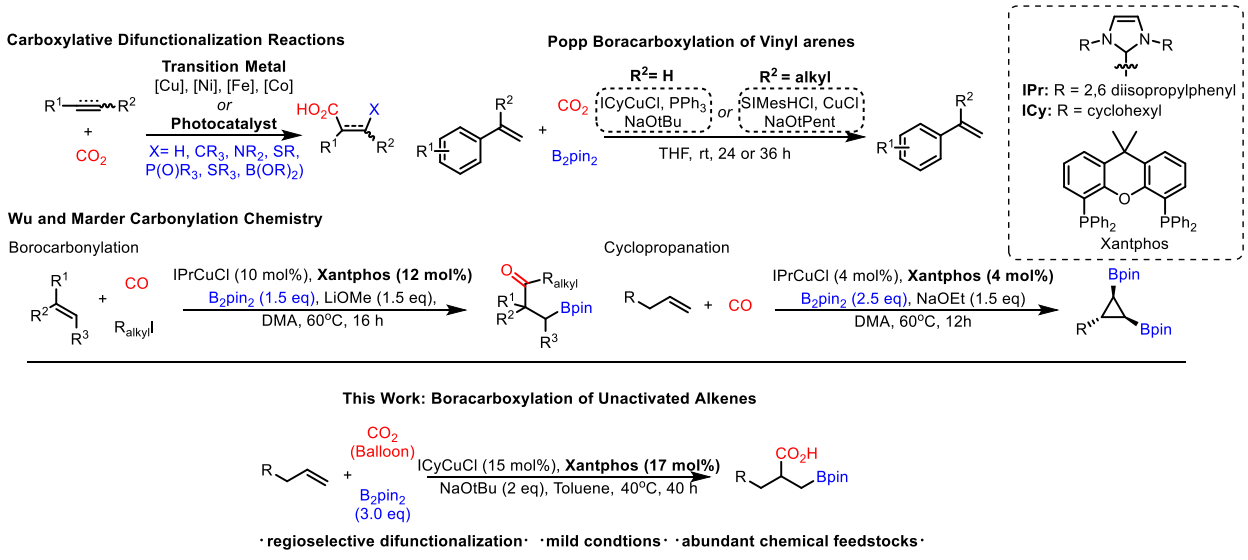

Table 4.1 Wu's borocarbonylation:[14] selected reaction optimization examples highlighting Xantphos effect

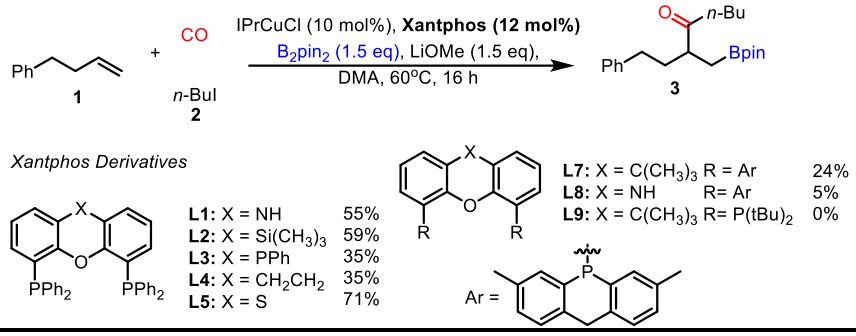

Entry	Deviation from conditions above	3 (%)
1	**none**	**84**
2	No Xantphos	0
3	CuCl (10 mol%) instead of IPrCuCl	9
4	$IMesCuBF_4$ (10 mol%) instead of IPrCuCl	14
5	IMesCuCl (10 mol%) instead of IPrCuCl	31
6	PPh_3 or $BuPAd_2$ or DPPP or DPPF (12 mol%) instead of Xantphos	0
7	Xantphos derivatives (12 mol%) instead of Xantphos	0 - 59
8	(Xantphos)CuCl (10 mol%) instead of IPrCuCl and Xantphos	16
9	(Xantphos)CuCl (10 mol%) and IPrHCl (10 mol%) instead of IPrCuCl and Xantphos	65
10	(Xantphos)CuCl (5 mol%) and IPrCuCl (5 mol%) instead of IPrCuCl and Xantphos	40

Inspired by our previous work on catalytic phosphine additives,[11,12] we sought to explore other additives to enhance the reactivity of unactivated alkenes in the catalytic boracarboxylation system. When searching through relevant literature we found that in 2020, the Wu group published a copper(I)-catalyzed regioselective borocarbonylative coupling reaction,[14] wherein unactivated alkenes were borylatively carbonylated through a catalytic system that employed NHC-ligated IPrCuCl precatalyst in tandem with Xantphos, a bidentate phosphine ligand (Table 4.1). They demonstrated that other copper(I) precatalysts such as CuCl, IMesCuCl and $IMesCuBF_4$ were poor for this transformation (Table 4.1, entires 3-5). When various phosphine ligands were screened it was evident that Xantphos is crucial to obtain the desired product, as the other phosphine ligands led to no desired product (Table 4.1, entry 6). When examining bite-angle effects, the Wu group found that other bidentate Xantphos derivatives lead to diminished reactivity. Consequently, the Wu group examined the unique effect that Xantphos has in their catalytic system (Table 4.1). They performed a series of experiments in which they altered the catalytic system used in their transformation. Under the standard conditions (entry 1, Table 4.1) 84% yield of the desired product was obtained. When (Xantphos)CuCl was employed with no ligand additive, 16% yield of the desired product was obtained, which is in line with results obtained by generating the (Xantphos)CuCl *in-situ* (9%, entry 3). Notably, when a (Xantphos)CuCl was utilized in tandem with an IPrHCl ligand, 65% of the desired product was obtained, further demonstrating the cooperativity of the Xantphos and NHC ligand in this catalysis.

The Wu group also observed this Xantphos effect in their synthesis of sterodefined cyclopropyl bis(boronates).[15] In the absence of Xantphos, the reaction proceeded poorly (Table 4.2, entry 2). Interestingly, in this protocol when the Wu group altered the copper(I) precatalyst from IPrCuCl to CuCl, the yield only decreased moderately from 71% to 48% (Table 4.2, entries 1 and 3) unlike in their borocarbonylation system where reactivity was nearly suppressed. Other copper precatalysts such as CuBr (36%) and $CuCl_2$ (52%) also gave comparable yields. However, when phosphine ligands that did not bear a similar structure to Xantphos were employed, reactivity was suppressed significantly, whereas in the case of Xantphos derivatives moderate reactivity was observed. Moreover, Xantphos derivatives bearing smaller or larger bite angles lead a decrease in yield, which is in line with the borocarbonylation system. Both reports by the Wu group exemplify a unique Xantphos effect in copper(I)-catalyzed methodologies wherein unactivated alkenes are utilized. Encouraged by this work, we hypothesized that a catalytic Xantphos additive would lead to expansion of the boracarboxylation scope to unactivated alkene substrates.

Table 4.2 Wu's cyclopropanation:[15] selected reaction optimization examples highlighting Xantphos effect

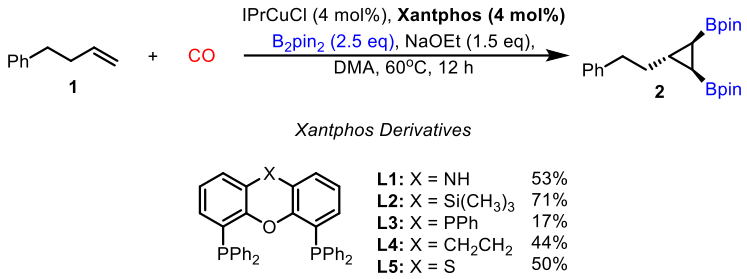

Entry	Deviation from conditions above	3 (%)
1	**none**	**71**
2	No Xantphos and NaOtBu (1.5 eq) instead of NaOEt	7
3	CuCl (10 mol%) and NaOtBu (1.5 eq) instead of IPrCuCl and NaOEt	48
4	$CuCl_2$ (10 mol%) and NaOtBu (1.5 eq) instead of IPrCuCl and NaOEt	52
5	CuBr (10 mol%) and NaOtBu (1.5 eq) instead of IPrCuCl and NaOEt	36
6	PPh_3 or $BuPAd_2$ or CyJohnphos	<5
7	Xantphos derivatives (4 mol%) instead of Xantphos	17-71

4.2 Reaction Optimization

We began our reaction optimization studies with allyl benzene, and ICyCuCl precatalyst, and a NaOtBu base in the closed-system reaction manifold from Chapter 2. Also in Chapter 2, higher concentration of the diboron reductant was necessary, resulting from B_2pin_2 being consumed via a CO_2 reduction pathway. Therefore, high B_2pin_2 loading was employed, expecting this CO_2 reduction pathway to be competitive in the catalytic system also. However, even at high B_2pin_2 concentration and increased catalyst loading, trace yield of the desired product was obtained. Moderate yields of byproducts **3** (diboration), **4** (anti-Markovnikov protoboration), and **5** (markovnikov protoboration) were observed, with trace yields of **6** (hydroxy-borylation). However, when Xantphos was employed as a catalytic additive, moderate yield of the boracarboxylated product was obtained. Notably, none of product **5** was obtained, while product **3** was obtained in comparable yields to boracarboxyled product **2**.

Table 4.3 Reaction stoichiometry optimization[a]

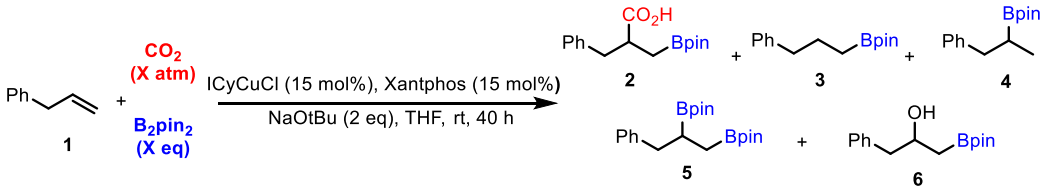

Entry	Stoichiometry	2 (%)	3 (%)	4 (%)	6 (%)	conv (%)
1[b]	1 atm CO_2, 5 eq B_2pin_2, No Xantphos	4	40	11	<5	78
2	1 atm CO_2, 5 eq B_2pin_2	46	32	0	0	>99
3	1 atm CO_2, 4 eq B_2pin_2	41	37	0	0	>99
4	1 atm CO_2, 3 eq B_2pin_2	44	35	0	0	>99
5	1 atm CO_2, 2.5 eq B_2pin_2	28	50	>10	<5	>99
6	1 atm CO_2, 2 eq B_2pin_2	30	32	0	0	>99
7[c]	**1 atm CO_2, 3 eq B_2pin_2**	**50**	**40**	**0**	**0**	**>99**
8	1.25 atm CO_2, 3 eq B_2pin_2	32	22	0	0	>99
9	2 atm CO_2, 3 eq B_2pin_2	16	12	0	0	>99
10	CO_2 Balloon, 3 eq B_2pin_2	42	30	0	0	>99
11	1 atm CO_2, 2 eq Allyl Benzene, 1 eq B_2pin_2	24	16	0	0	ND
12	1 atm CO_2, 5 eq Allyl Benzene, 1 eq B_2pin_2	25	36	0	0	ND

[a]Reactions ran at 0.025 mmol scale with respect to allyl benzene, all yields were determined by ^{1}H NMR spectroscopy using mesitylene as the internal standard. [b]50% yield of product 5 [c]17 mol% Xantphos

Next, we sought to investigate reaction stoichiometry. In the previous iterations of boracarboxylation,[11,12] the B_2pin_2 loading, and CO_2 pressure were shown to alter reactivity of various activated alkenes. Electron deficient styrenes required higher styrene loading to obtain moderate yields, while α-substituted vinyl arenes required high

B_2pin_2 loading and CO_2 pressure. Thus, those are the parameters we initially investigated. Also, product **5** was omitted for clarity, as it is only observed in the absence of Xantphos. The loading of B_2pin_2 could be dropped to **3** equivalents from 5 equivalents with no significant decline in yield (Table 4.3, entries 1 – 3). However, when the B_2pin_2 loading was dropped below 3 equivalents, the yield decreased from 46% to 28%. This suggests that competitive CO_2 and alkene insertion pathways could be operative in this system, because if the alkene favorably inserted into the Cu^I-boryl then the loading of B_2pin_2 would be more in line with the previously reported catalytic boracarboxylation methodologies[11,12] (1.1 equivalents) and not Chapter 2. As the CO_2 pressure increases from balloon to 2 atm, yield declines from 50% to 16% (entries 6-9). The high B_2pin_2 loading along with decreased yield at higher CO_2 pressure further points to CO_2 reduction as a competitive reaction pathway. Changing the limiting reagent to B_2pin_2 and increasing alkene concentration led to lower yields (entries 10 and 11). The ideal conditions are reflected in Table 4.3, entry 7.

Next, we began optimization of the catalyst and additive loading. Initially, when equimolar amounts of copper(I) precatalyst and Xantphos additive was used, 44% yield of the desired product was obtained (Table 4.4, entry 1). The Wu group previously reported a slight excess of Xantphos in their borocarbonylation protocol.[14]

Table 4.4 ICyCuCl and Xantphos loading optimization[a]

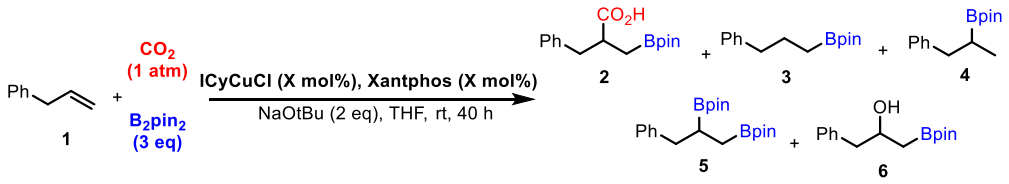

Entry	[ICyCuCl] and [Xantphos]	2 (%)	3 (%)	4 (%)	6 (%)	conv (%)
1	15 mol% ICyCuCl, 15 mol% Xantphos	44	35	0	0	>99
2	**15 mol% ICyCuCl, 17 mol% Xantphos**	**50**	**40**	**0**	**0**	**>99**
3	12 mol% ICyCuCl, 12 mol% Xantphos	42	35	0	<5	>99
4	12 mol% ICyCuCl, 8 mol% Xantphos	24	27	0	<5	>99
5	12 mol% ICyCuCl, 4 mol% Xantphos	20	23	ND	<5	>99
6[b]	12 mol% ICyCuCl, 0 mol% Xantphos	3	10	<5	<5	>99
7	8 mol% ICyCuCl, 12 mol% Xantphos	8	40	10	<5	>99
8	4 mol% ICyCuCl, 12 mol% Xantphos	2	40	<10	<5	>99
9	20 mol% ICyCuCl, 20 mol% Xantphos	30	44	<5	<5	>99
10	15 mol% ICyCuCl, 30 mol% Xantphos	28	40	<5	6	>99

[a]Reactions ran at 0.025 mmol scale with respect to allyl benzene, all yields were determined by ^1H NMR spectroscopy using mesitylene as the internal standard. [b]50% yield of product 5

When we increased Xantphos loading to 17 mol% the yield of product **2** increased from 44% to 50% (Table 4.4, entry 2). Lower copper and Xantphos loading were employed resulting in a yield decrease from 50% to 42% (Table 4.4, entry 3). Furthermore, yield of the desired product decreases as Xantphos loading decreases, and when the copper(I) precatalyst loading is decreased to 8 mol% and 4 mol%, low yields of product **2** are observed (Table 4.4, entries 3 – 8). When the catalyst and additive loading were increased, the yield of product **2** decreased, while the yield of product **3** remained the same as previous entries. The same trend is observed when the Xantphos concetration is increased from 17% to 30% (Table 4.4, entries 9 and 10). These catalyst and additive loading results demonstrate the sensitive nature of this catalytic system, as even small alterations of catalyst and additive can lead to significant changes in yield of the desired product. Interestingly, the yield of product **3** (Table 4.4, entries 3 – 6, 35%, 27%, 23%, and 10% respectively) decreases with the Xantphos loading and remains in line with the yield of product 2 (Table 4.4, entries 3 - 6, 42%, 24%, 20%, 3% respectively). Product **3** is the anti-Markovnikov protoboration product resulting from protodemetallation obtained from a 2,1 migratory insertion of allyl benzene into the Cu^{I}-boryl. At first glance, these preliminary results suggest that Xantphos could be playing a role in the insertion step of the mechanism. In 2013, the Ito group reported a copper(I)-catalyzed borylative exo-cyclization of alkenyl halides.[16] This method demonstrated computationally that the copper(I)-Xantphos species is controlling the regiochemistry of the *exo*-cyclization reaction. One major issue with the reactions performed in the closed system is that there is a product which we have yet to identify or isolate that is present in all the reactions in yields from 1 to 10%. However, this product was not present when we ran the reaction using a balloon of CO_2. Subsequently, we decided to change to a reaction setup to be more in line with previous boracarboxylation methodologies in which a balloon of CO_2 is used.

Upon changing the reaction setup from a closed system to using a balloon for CO_2, we decided to investigate the role that solvent and temperature play in this catalytic system. Previously, we demonstrated that an increase in temperature can lead to higher yield of unfavorable substrates.[11,12] Despite this, when using a balloon in tandem with a solvent with a high vapor pressure such as THF, solvent was lost to evaporation/condensation when heating at temperatures above 40°C. Consequently, we looked to solvents with higher boiling points, such as toluene and dioxane. The yield of the 2 major products observed, product **2** and **3**, were comparable between THF and toluene at room temperature (Table 4.5, entries 1 and 2). A 1:1 mixture of toluene and THF provided the desired product 2 in 60% yield (Table 4.5, entry 3), with 21% yield of product **3**. One problem with this solvent mixture is the formation of products 4 and 6 in low yield (<5%) whereas when only toluene is utilized as the solvent at 40°C the yield of product 2 remains at 60%, and none of products **4** and **6** are observed (Table 4.5, entry 6). Dioxane proved to be a poor solvent choice for this transformation, even when paired with toluene (Table 4.5, entries 4 and 5). Moreover, when the temperature is increased from 40°C to 80°C, there is no discernable change in yield until at 80°C or at 0°C, when the yield decreases significantly (Table 4.5, entries 7-10). This yield decrease could be attributed to the formation of a new unidentified side product observed only at higher temperatures.

Table 4.5 Solvent and temperature optimization[a]

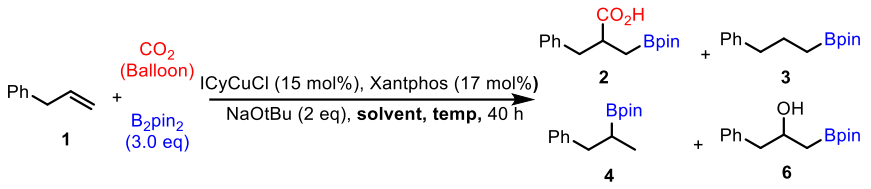

Entry	Solvent/Temp	2 (%)	3 (%)	4 (%)	6 (%)	conv (%)
1	Toluene, rt	46	37	<5	0	>99
2	THF, rt	44	32	<5	<5	>99
3	THF/Toluene 1:1, 40°C	60	21	<5	<5	>99
4	Dioxane, 40°C	28	45	0	0	>99
5	7:1 Diox:Tol, 40°C	36	32	6	0	>99
6	**Toluene, 40°C**	**60**	**15**	**0**	**0**	**>99**
7	Toluene, 50°C	60	17	0	0	>99
8	Toluene, 60°C, 0.025 M	52	12	0	<5	>99
9	Toluene, 70°C	60	18	0	<5	>99
10	Toluene, 80°C	14	18	<10	ND	>99
11	Toluene, 0°C	34	45	0	<5	>99

[a]Reactions ran at 0.025 mmol scale with respect to allyl benzene, all yields were determined by ^{1}H NMR spectroscopy using mesitylene as the internal standard.

Currently, the ideal reaction condition is displayed in Table 4.6, entry 1. Following the solvent optimization, we decided to explore the copper(I) precatalyst employed in this protocol to determine whether or not the NHC-ligated copper(I) precatalyst is necessary for this transformation (shown previously by the Wu group in their carbonylation chemistry[14,15]), or if other copper(I) precatalysts will suffice. Initially, when other NHC-Ligated copper(I) precatalysts are utilized, the yield of product **2** decreases from 60% to 16 – 36% (depending on the NHC), and the yield of side product **3** increases from 15% to 29 – 46% (Table 4.6, entries 2-5). Small amounts of products **4** and **6** are also observed when other NHC-Cu precatalysts are employed (Table 4.6, entries 3-5). When we employ other common copper precatalysts 13% of product **2** or less is observed along with small amounts of products **4** and **6** (Table 4.6, entries 7-13). However, significant amounts of protodemetallation product **3** are observed when these other copper precatalysts are utilized, with CuCl and $CuCl_2$ leading to the highest yields (70% and 65% respectively, Table 4.6 entries 7 and 11). Furthermore, following the boracarboxylation methodologies used in chapters 2 and 3, entry 14 shows that the active catalyst can be generated *in-situ* from ICyHCl and CuCl to afford 56% yield of product **2**, which is comparable to the ICyCuCl precatalyst result of 60% yield; however slightly higher yield of product **3** is obtained (26% vs 15% for ICyCuCl). Nevertheless, this provides a synthetic route that is accessible to those who are unable to synthesize the ICyCuCl precatalyst due to equipment constraints. Notably, when $Cu(MeCN)_4PF_6$ and ICyHCl (16 mol%) is used as the copper catalyst system, the yield of product **2** (entry 15, 14%)

is comparable to when $Cu(MeCN)_4PF_6$ is employed without ICyHCl (entry 13, 13%), implying problematic active catalyst formation.

Table 4.6 Copper precatalyst optimization[a]

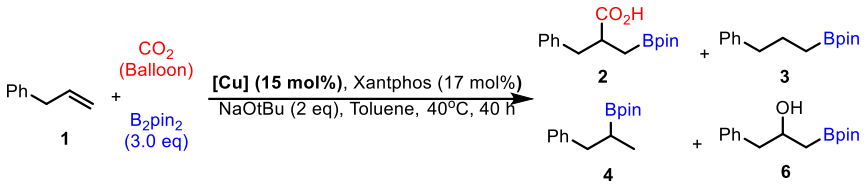

Entry	[Cu]	2 (%)	3 (%)	4 (%)	6 (%)	conv (%)
1	**ICyCuCl**	**60**	**15**	**0**	**0**	**>99**
2	SICyCuCl	36	29	0	0	>99
3	IMesCuCl	24	38	<5	<5	96
4	SIMesCuCl	26	46	<10	<5	88
5	IPrCuCl	16	ND	<10	0	>99
7	CuCl	10	70	<10	0	>99
8	CuBr	<10	50	<10	0	80
9	$CuBr(Me_2S)$	<5	41	<5	0	78
10	CuI	0	<10	<5	0	54
11	$CuCl_2$	12	65	<10	0	>99
12	$Cu(OMe)_2$	3	20	<5	<5	98
13	$Cu(MeCN)_4PF_6$	13	57	8	0	>99
14	CuCl + ICyHCl (16 mol%)	56	26	0	<5	>99
15	$Cu(MeCN)_4PF_6$ + ICyHCl (16 mol%)	14	61	0	<5	>99

[a]Reactions ran at 0.025 mmol scale with respect to allyl benzene, all yields were determined by ^1H NMR spectroscopy using mesitylene as the internal standard.

When comparing the catalytic systems employed, the disparity in reactivity between entries 1 and 7 is quite interesting. When an NHC-ligated copper(I) ICyCuCl precatalyst is utilized, 60% yield of desired boracarboxylated product **2** is obtained, and only 15% of undesired protodemetallation product **3** is observed. Yet when ligandless CuCl is employed, only 10% of product **2** is obtained, while product **3** is obtained in a high yield of 70%. These results suggest that Xantphos could be necessary for a regioselective 2,1 migratory insertion to occur, while the NHC ligand plays a large role in the carboxylation. In Table 4.4, preliminary results suggested that Xantphos could be responsible for facilitating a regioselective 2,1 insertion, due to the amounts of products **2** and **3** observed as Xantphos concentration decreased. The results observed in entries 7-13 further support this hypothesis, as minor quantities of the 1,2 protodemetallation product are observed, while large quantities of the 2,1 protodemetallation product are observed.

In order to determine the role whether or not the Xantphos additive was crucial in this transformation, we explored other phosphine ligands. Previously, we have demonstrated that electron rich phosphine ligands result in higher yields of boracarboxylated product.[11] However, when the more electron rich CyXantphos derivative was utilized as an additive low yields of all products were obtained, and the conversion of allyl benzene was significantly lower than any other result (Table 4.7, entry 2). Next, we sought to explore phosphines that have been shown to be competent additives in catalytic boracarboxylation in the past. When PPh_3 and PCy_3 were employed as the additives similar reactivity was observed (Table 4.7, entries 3 and 4). Trace yield of desired product **2** was observed, while moderate yields of protoboration products **3** and **4** were observed, and moderate yield of diboration product **5** was observed. Notably, PPh_3 and PCy_3 provided the first reactions where significant yield of the Markovnikov protoboration product **4** is obtained. In both cases the yield of product **4** is double that of product **3**, suggesting that under these conditions 1,2 insertion can potentially become favorable over 2,1 insertion allyl benzene insertion into the copper(I)-boryl.

Table 4.7 Phosphine additive optimization[a]

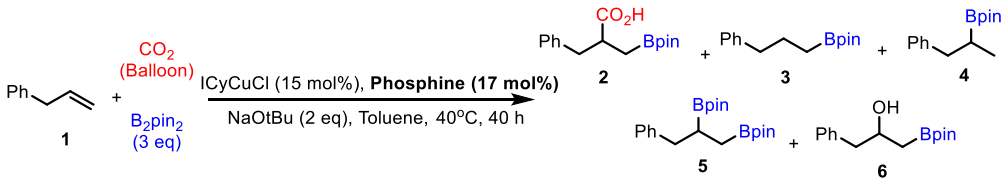

Entry	Phosphine	2 (%)	3 (%)	4 (%)	5 (%)	6 (%)	conv (%)
1	**Xantphos**	60	15	0	0	**0**	>99
2	CyXantphos	2	<5	<5	ND	0	68
3	PCy_3, THF	<5	22	48	34	0	>99
4	PPh_3, THF	<5	24	48	40	0	>99
5	CyDPEPhos	5	28	25	26	<5	>99
6	DPEPhos	16	30	6	40	<5	>99
7	DPPF	8	30	ND	ND	ND	98

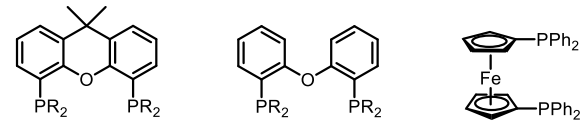

[a]Reactions ran at 0.025 mmol scale with respect to allyl benzene, all yields were determined by ^{1}H NMR spectroscopy using mesitylene as the internal standard.

We then decided to screen other bidentate phosphine ligands (Table 4.7, entries 5 – 7). When CyDPEPhos was utilized, lower yield of desired product 2 was obtained (5%) than when DPEPhos was screened as an additive

(16%), yet the yield of product **4** differed significantly in both ligand systems (25% for CyDPEPhos, and 6% for DPEPhos). All non-Xantphos ligands yielded moderate amounts of diboration product **5**, whereas none of the reactions where Xantphos is employed yielded any of product 5. Diboration is thought to proceed through a base catalyzed pathway.[17] Specifically, base catalyzed diboration of allyl benzene has been previously reported by Wen and coworkers in 2018.[18] If unactivated alkene insertion into copper(I)-boryl is a slow process, then competing side reactions would become operative in this system. Since none of product 5 is observed in any reaction when a Xantphos additive is employed, this implies that a competitive diboration of alkene pathway cannot proceed. Potentially, this suggests that Xantphos could play a role in accelerating alkene insertion, while also controlling regiochemistry.

In chapter 2 we saw that the choice of base can significantly alter reactivity in the catalytic boracarboxylation of α-substituted vinyl arenes. Thus, various bases were screened to determine whether base had a significant effect on reactivity in this system. NaOtBu has been the ideal base for this methodology, so unsurprisingly it provided the desired product in 60%, with minimal low yield of side product **3** (Table 4.8, entry 1). However, when other tert-butoxide bases are employed, reactivity diminished significantly (Table 4.8, entry 2 and 3). When LiOtBu was employed, low conversion of allyl benzene was observed. While KOtBu provided similar yield of product **3** to when NaOtBu was used (14% and 15%), low yield of the desired boracarboxylated product **2** was observed also.

Table 4.8 Base optimization[a]

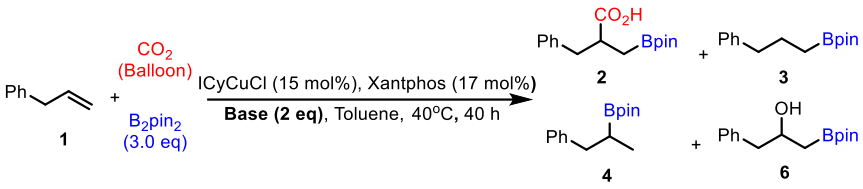

Entry	Base	2 (%)	3 (%)	4 (%)	6 (%)	conv (%)
1	NaOtBu	60	15	0	**0**	>99
2	LiOtBu, 50C	8	11	0	14	68
3	KOtBu	14	14	<2	0	>99
4	NaOMe	5	4	0	<5	>99
5	NaOEt	15	61	<5	0	>99
6	NaOtPent	12	13	0	<5	>99
7	NaOTMS	<5	70	<10	0	98

[a]Reactions ran at 0.025 mmol scale with respect to allyl benzene, all yields were determined by ^{1}H NMR spectroscopy using mesitylene as the internal standard.

When other sodium alkoxides were utilized in this transformation, low yield of product **2** was obtained (Table 4.8, entries 4-6). Interestingly, NaOEt provided moderate yield of protoboration product **3**, whereas none of

the other sodium alkoxides delivered this product in any appreciable yield. Similar protoboration favorability was observed when NaOTMS was employed, and this result agrees with data obtained in chapter **2**, as large amounts of protoboration were observed in the case of α-substituted vinyl arenes when NaOTMS was used. Overall, any deviation of the base from NaOtBu resulted in a significant decline in yield.

Table 4.9 Reaction optimization of other parameters

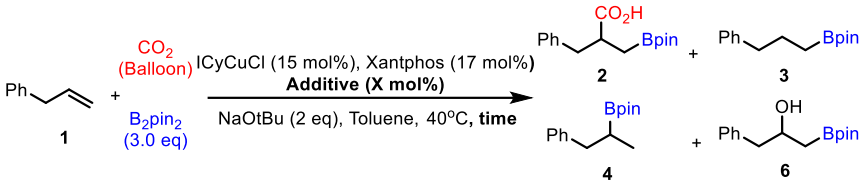

Entry	Time/Additive/Concentration/other	2 (%)	3 (%)	4 (%)	6 (%)	conv (%)
1	40 h, none, 0.06 M	60	15	0	0	>99
2	64 h, none, 0.06 M	38	28	0	0	>99
3	40 h, 20 mol% $MgCl_2$, 0.06 M	60	30	0	<5	>99
4	40 h, 50 mol% $MgCl_2$, 0.06 M	60	28	0	<5	>99
5	40 h, 20 mol% $ZnBr_2$, 0.06 M	34	40	0	<5	>99
6	40 h, none, 0.13 M	40	35	0	0	>99
7	40 h, none, 0.03 M	36	43	0	0	>99
8	40 h, none, 0.06 M, 3ml catalyst solution	65	35	0	1	>99
9	40 h, none, 0.025 M, 25 mol% ICyCuCl, 27 mol% Xantphos	65	16	0	<5	>99
10	16 h, none, 0.06 M, 10 min CO_2 purge instead of balloon	24	52	<5	<5	>99
11	36 h, none, 0.06 M, 10 min CO_2 purge instead of balloon	13	7	0	0	80
12	40 h, none, 0.06 M, 10 min CO_2 sparge and balloon	12	10	0	<5	82

[a]Reactions ran at 0.025 mmol scale with respect to allyl benzene, all yields were determined by ^{1}H NMR spectroscopy using mesitylene as the internal standard.

In an attempt to obtain higher than 60% yield of product **2**, we screened other reaction conditions such as time, concentration, other additives, and also different methods in which CO_2 is introduced into the system. Forty hours was the ideal time for this transformation because time increase led to a decline in yield, presumably due to decomposition of the boralactonate salt (see chapter 3 discussion about product decomposition). Lewis acidic additives such as $MgCl_2$ and $ZnBr_2$ (Table 4.9, entries 3-5) did not lead to higher yield of product 2[19]. Both doubling and halving the concentration resulted in similarly diminished yields (Table 4.9, entries 6 and 7). In chapter 2 and 3, the general methods section calls for the reaction of ICyCuCl and NaOtBu in 2 ml of solvent to generate the active ICyCuOtBu catalyst, which is then added to a solution of B_2pin_2 and alkene. However, decreasing the concentration of catalyst solution resulting in yield increase of product **2** from 60% to 65% (Table 4.9, entry 8), with significantly more of product **3** observed also (from 15% to 35%). Increasing the catalyst loading in tandem with decreasing the concentration of the reaction did not provide any significant changes in yield (Table 4.9, entry 9). Entries 10-12 in

table 4.9 describe different methods in which CO_2 has been introduced into the reaction. In chapters 2 and 3, a method in which the flask was purged with CO_2 for 15 minutes then sealed was described. In this method, yields comparable to when a balloon was used could be obtained in significantly lower reaction times. Yet when this method was used for this catalytic system, the yield of product **2** diminished significantly. In fact, when reaction was ran for 16 h and purged with CO_2, moderate yield of protoboration product 3 was obtained.

4.3 Boracarboxylation of Unactivated Alkenes Reaction Scope

With the optimized reaction conditions in hand, we decided to investigate the scope of the reaction. Much like in chapter 2, and previous reported boracarboxylation methods,[12] product is lost during the work-up procedure, resulting in lower isolated yields for many substrates. Boracarboxylated allyl benezene and allyl anisole were both obtained in 65% crude yield. When a longer chain unactivated alkene substrates homoallyl benzene and 5-hexenyl benzene were employed, the desired products were delivered in a comparable crude yield of 58% and 54% respectively. This is comparable to allyl benzene, implying that longer aliphatic chain unactivated alkenes could also be utilized in this transformation. Gratifyingly, were able to achieve moderate reactivity with the α-olefin substrate **2e**, providing the valuable borylated aliphatic carboxylic acid in 28% crude yield. Next, we sought to screen unactivated alkene substrates bearing a pendant heteroatom, as these substrates could lead to a weak coordination of the heteroatom to the copper catalyst, potentially accelerating the alkene migratory insertion into the copper-boryl[20]. However, this effect was not seen in our catalytic system, as the crude yield did not exceed the yield of substrate 2a in any of these substrates (Table 4.10, **2f** to **2o**). Substrates bearing synthetically useful functional groups such as nitriles (**2i**), alkynes (**2j**), and halides (**2k, 2l, 2m**) were delivered in modest yields. These substrates now have three reaction sites that can provide opportunities for further synthetic elaboration. Notably, for substrate **2j** boracarboxylation occurred exclusively at the alkene moiety, with no competitive alkyne boracarboxylation[10]. Also substrates **2k**, **2l**, and **2m**, mark the first example of halides being tolerated well in the catalytic boracarboxylation methodology. Furthermore, tosyl amine substrate **2n** also marks the first amine containing substrate to be successfully boracarboxylated. When unactivated alkenes bearing distal heteroaromatic substrates such as indole (**2o**, 50%), furan (**2p**, 20%), and thiophene (**2q**, 32%), were employed in this transformation, moderate crude yields were observed. Substrates being multiple alkenes exclusively boracarboxylated the least substituted alkene and, while the other alkene remained unaffected (**2r** and **2s**), leading to boracarboxylated citronella derivative **2s**, albeit at poor yield. Vitamin E derivative **2t** was boracarboxylated in good yield, lending credence to a hypothesis that boracarboxylation can be achieved on other medicinally relevant molecules. In previous iterations of boracarboxylation, internal alkenes proceeded poorly. Thus, it was unsurprising that unactivated internal α-olefin substrate **2t** did not provide any yield. Also, alkyl bromide substrate **2u** did not deliver any boracarboxylated product, likely resulting from competitive reaction pathways[16,20].

Table 4.10 Substrate scope of unactivated alkenes[a]

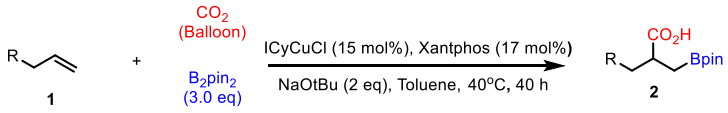

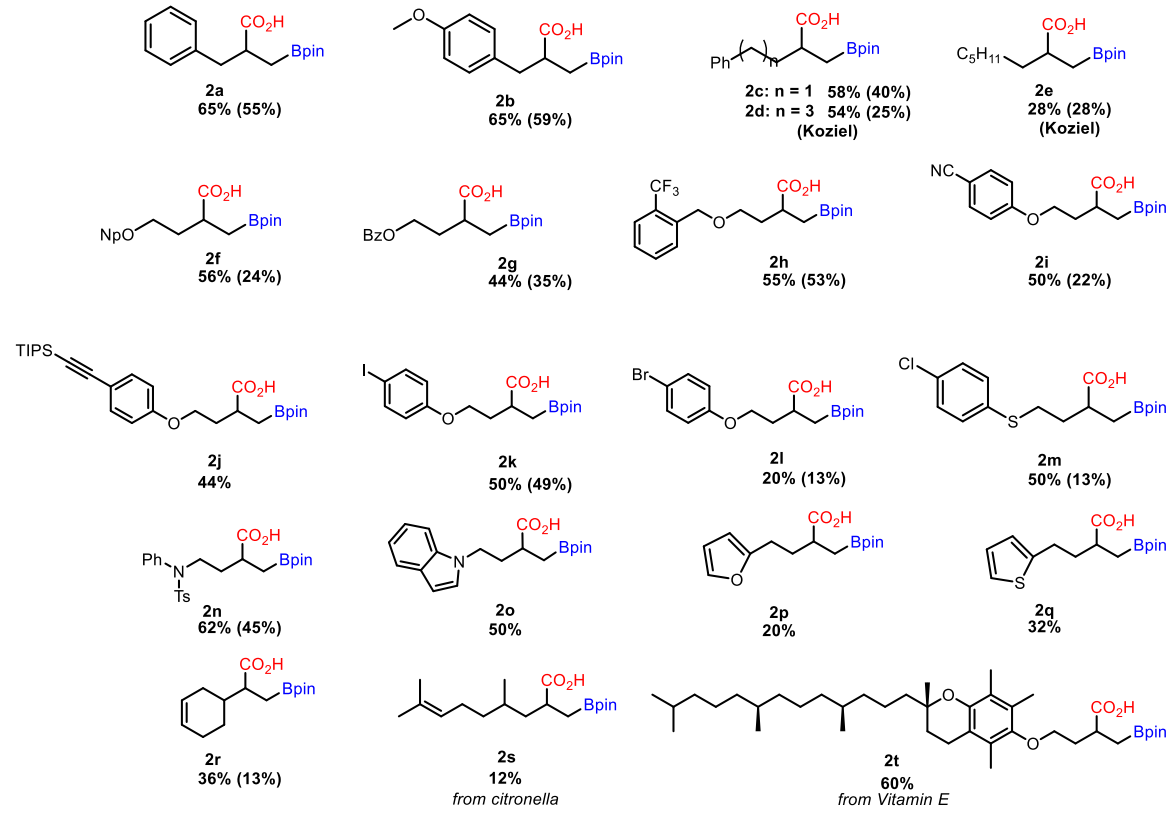

Limitations

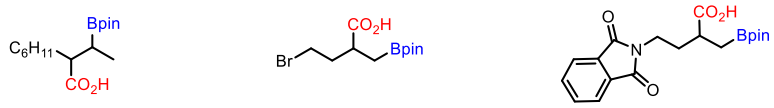

[a]Reactions ran at 0.025 mmol scale with respect to allyl benzene, all yields were determined by ^{1}H NMR spectroscopy using mesitylene as the internal standard, isolated yields are reported in parentheses.

Unexpectedly, substrate **2v** provided a 0% crude yield of product; however, a new unidentified compound was observed in the ^{1}H NMR in 60% yield. Upon further NMR analysis, a new product was identified shown in Figure 4.1. An apparent quartet and triplet were observed through ^{1}H NMR at 3.47 ppm and 3.25 ppm respectively (Figure 4.1, top left). When the triplet frequency at 3.47 ppm was selectively excited through 1D zTOCSY, a spin system including 7 protons was revealed (Figure 4.1, top right). Gratifyingly, the 1D zTOCSY spectrum matched the calculated spectrum for the pyrridoisoindoline molecule proposed (Figure 4.1, bottom left). The gHMBCAD spectra provided the missing piece of spectral data required to fully identify the product. ^{1}H - ^{13}C correlation from

the protons alpha to the nitrogen to both the carbonyl carbon (170 ppm, ^{13}C) and the quaternary alcohol carbon (97 ppm, ^{13}C) was observed (Figure 4.1, bottom right). Furthermore, the crosspeak correlating to the signal at 97 ppm in ^{13}C NMR was verified to be a quaternary carbon via gHSQCAD. In the realm of copper(I) boryl chemistry, a protocol in which this functionalized pyriddoisoindoline fused ring system can be accessed in a single step from simple phthalimide starting materials has not yet been reported. In order to test whether this product was synthesized via a pathway that utilizes CO_2, the reaction was ran in the absence of CO2. The pyrridoisoindoline product was obtained in 70% crude yield. Subsequently, a potential pathway in which this product is being formed is proposed in Figure 4.1. Initially, boryl cupration of the alkene will occur, followed by insertion of the phthalimide CO bond to afford the pyrridoisoindoline. An analogous reaction pathway was reported by the Lautens group in 2019 as a method to access enantiopure polycyclic indolines.[21] In this protocol, the Lautens group employed 1,1 diaryl alkenes, with an ortho- substituted succinmide derivative (Figure 4.1, bottom).

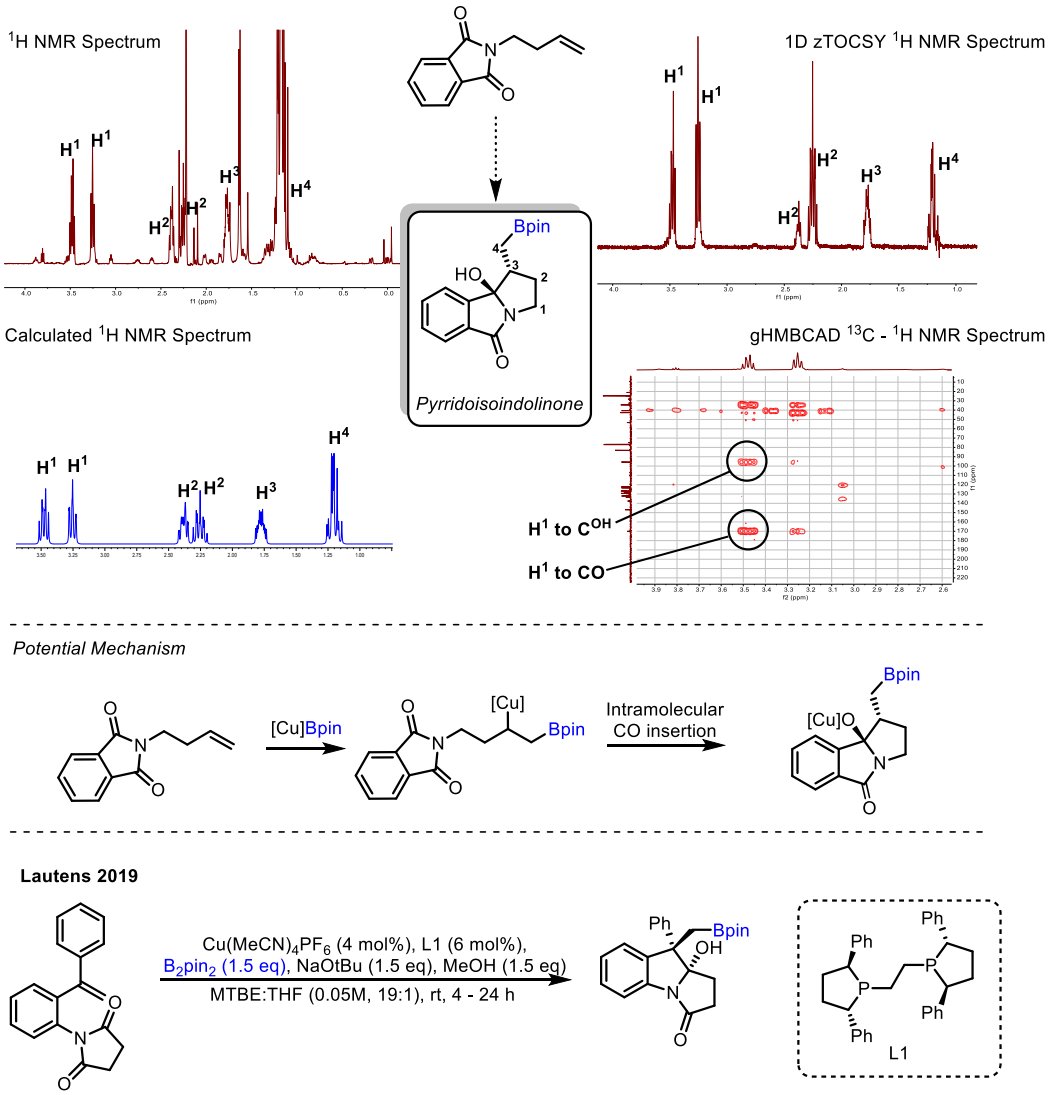

Figure 4.1 Pyrridoisoindolinone characterization data and mechanism

4.4 Conclusions

Chapter 4 has presented a novel methodology wherein a variety of unactivated alkenes can be boracarboxylated to achieve valuable borylated aliphatic carboxylic acid products in moderate to good yields. A unique Xantphos effect is the linchpin of this method, as when the reaction is run in the absence of Xantphos, trace yield of desired boracarboxylated product is obtained, and significant portions of undesired byproducts are synthesized. Moreover, preliminary optimization studies demonstrate that Xantphos could be playing a role in the migratory insertion step of the mechanism. When a phthalimide substrate was employed in this transformation, novel reactivity was observed and a densely functionalized pyrridoisoindolinone polycyclic heterocycle was synthesized in good yield, highlighting further synthetic utility of this method. Further work to screen more substrates and to isolate these products is underway.

4.5 Experimental Section

General Information: All the air and moisture sensitive experiments were set up in a nitrogen-filled MBraun 200B dual-port glovebox, and before each experiment the atmosphere was tested using diethyl zinc. The boracarboxylation reactions were performed in 25 ml roundbottom flask purchased dried in an oven at 180 ^{o}C for at least 24 hours prior to use. All glassware used in the glovebox was dried for at least 24h in the 180 $^{\circ}$C oven prior to use. The magnetic stirbars in these reactions were new, unused, and purchased from VWR (1/2 by 1/8 in. disposable stirbar CAT. NO:58947-140) and dried for at least 24h at 180 $^{\circ}$C prior to use. The balloons used were double walled and stored in a chamber with desiccant for 24 hours prior to use. The dry solvent used for all experiments was dried on a Glass Contour solvent purification system, and further dried over 4Å mol sieves. The liquid reagents were degassed using a freeze/pump/thaw method on a Schlenk line prior to use. CDCl3 was purchased from Cambridge Isotope Laboratories, Inc. NMR spectra were recorded on either a 400 MHz Agilent or 600 MHz Agilent NMR spectrometer. ^{1}H, ^{13}C, ^{11}B, and ^{19}F NMR experiments were acquired in CDCl3 using tetramethylsilane as a reference in quartz NMR tubes. ^{11}B NMR was referenced to an external $BF_3{\cdot}OEt_2$ standard. High-resolution mass spectra were recorded on a Thermo Fisher Scientific Q-Exactive Mass Spectrometer with samples dissolved in acetonitrile.

Synthesis of substrates 2a-2t: In a nitrogen filled glovebox, a 20 ml scintillation vial was charged with ICyCuCl (12.5 mg, 0.0375 mmol, 15 mol%), NaOtBu (48.0 mg, 0.50 mmol, 2.0 eq.) and anhydrous, degassed THF (2 ml). The vial was then capped and stirred for 15 minutes to afford a clear solution. In a separate 20 ml scintillation vial, Xantphos (23.6 mg, 0.0375 mmol, 17 mol%) was added, along with anhydrous degassed THF (1 ml), and then stirred for 15 minutes. Once these 15 minute periods were up, the 20 ml scintillation vial containing the Xantphos solution was added to the 20 ml scintillation vial containing the catalyst solution, and stirred for 1 hour. In a 25 ml roundbottom flask, B_2pin_2 (192.0 mg, 0.75 mmol, 3.0 eq), alkene (0.25 mmol, 1.0 eq) and anhydrous, degassed THF (1 ml) were added then sealed with a rubber septum. The catalyst solution was then loaded into a 5.0 ml Hamilton gas-tight syringe, and then the needle was plugged using a rubber septum. The roundbottom flask and catalyst solution were then removed from the glovebox and the roundbottoms were added to a preheated silicon oil bath at 40^{o}C. A double-walled ballon was purged with CO_2 three times, then capped with a needle. Once the balloon was ready, the catalyst solution was added to the roundbottom flask, followed by immediate balloon addition, and then

the reaction was stirred at 40ºC for 24h. Upon completion of the reaction, the crude mixture was added to a 60 ml separatory funnel containing 20 ml of 1M HCl, and then extracted with DCM (3 x 4 ml) and collected in a 20 ml scintillation vial. The combined organic extracts were concentrated under vacuum, and mesitylene (20 mol%) was added to the crude reaction mixture. The mixture was then dissolved in 1 ml of CDCl3 then analyzed by 1H NMR spectroscopy to obtain an NMR yield. Once the NMR yield was obtained, the crude mixture was taken up in 10 ml of diethyl ether then filtered. The resulting solid was washed with diethyl ether (3 x 3ml). The filtrate was added to a 60 ml separatory funnel, and extracted with saturated $NaHCO_3$ (4 x 3 ml). The aqueous layer was added to a 50 ml Erlenmeyer flask, and acidified by slow addition of 5 ml of 12M HCl, then added back to a 60 ml scintillation vial and extracted with dichloromethane (4 x 3 ml). The organic layer was dried over Na_2SO_4, and the solvent was removed in vacuo to afford the boracarboxylated product.

Characterization data

NOTE – *any missing characterization data (NMR, HRMS, etc.) for the described compounds will be obtained by the graduate student who continues this project. See Apprendix I for NMR Spectral data.*

2a. White solid, (39.8 mg, 55% yield). ^{1}H NMR (400 MHz, $CDCl_3$): δ 7.28 – 7.25 (m, 2H), 7.22 – 7.18 (m, 3H), 3.08 (dd, *J* = 13.4, 6.5 Hz, 1H), 2.91 (ddt, *J* = 8.8, 7.7, 6.4 Hz, 1H), 2.77 (dd, *J* = 13.4, 7.8 Hz, 1H), 1.22 (s, 6H), 1.21 (s, 6H), 1.04 (dd, *J* = 16.0, 8.8 Hz, 1H), 0.94 (dd, *J* = 16.0, 6.1 Hz, 1H).^{13}C NMR (151 MHz, $CDCl_3$): δ 181.7, 139.2, 129.2, 128.3, 126.3, 83.3, 42.7, 39.7, 24.8, 24.6, 13.3 (broad due to quadrupolar broadening from ^{11}B). ^{11}B NMR δ 28.1. HRMS (ESI): m/z calc. for $C_{16}H_{23}BO_4$ [M-H]$^-$: 289.1617, found 289.1616

2b. White solid, (47.0 mg, 59% yield). ^{1}H NMR (400 MHz, $CDCl_3$): δ 7.14 – 7.07 (m, 2H), 6.85 – 6.77 (m, 2H), 3.78 (s, 3H), 3.01 (dd, *J* = 13.4, 6.4 Hz, 1H), 2.85 (dt, *J* = 8.5, 6.5 Hz, 1H), 2.71 (dd, *J* = 13.4, 7.6 Hz, 1H), 1.22 (s, 6H), 1.20 (s, 6H) 1.02 (dd, *J* = 16.0, 8.7 Hz, 1H), 0.92 (dd, *J* = 16.0, 6.1 Hz, 1H). ^{13}C NMR (151 MHz, $CDCl_3$): δ. 182.1, 158.3, 131.4, 130.3, 113.9, 83.4, 55.3, 43.1, 39.0, 24.9, 24.8, 13.5. (broad due to quadrupolar broadening from ^{11}B). ^{11}B NMR δ 33.8.

2c. White solid, (30.0 mg, 40% yield). ^{1}H NMR (400 MHz, $CDCl_3$): δ 7.29 – 7.24 (m, 2H), 7.21 – 7.15 (m, 3H), 2.72 – 2.61 (m, 3H), 2.03 (m, 1H), 1.83 (m, 1H), 1.23 (s, 6H), 1.22 (s, 6H), 1.15 (dd, *J* = 15.9, 8.4 Hz, 1H), 1.02 (dd, *J* = 15.9, 6.6 Hz, 1H). ^{13}C NMR (151 MHz, $CDCl_3$): δ 182.7, 141.9, 128.6, 128.5, 126.0, 83.5, 40.5, 35.8, 33.6, 24.9, 24.8, 14.1. (broad due to quadrupolar broadening from ^{11}B). ^{11}B NMR δ 28.8. ^{19}F NMR (376 MHz, $CDCl_3$) δ HRMS (ESI): m/z calc. for $C_{17}H_{25}BO_4$ [M-H]$^-$: 307.1522, found 307.1520

2d. Yellow solid, (20.8 mg, 25% yield). ^{1}H NMR (400 MHz, $CDCl_3$): δ 2.65 – 2.56 (m, 1H), 1.74 – 1.61 (m, 1H), 1.56 – 1.43 (m, 1H), 1.37 – 1.24 (m, 8H), 1.24 (s, 6H), 1.22 (s, 6H), 1.08 (dd, *J* = 15.9, 8.6 Hz, 1H), 0.96 (dd, *J* = 15.9, 6.6 Hz, 1H), 0.91 – 0.82 (m, 3H). ^{13}C NMR (101 MHz, $CDCl_3$): δ 182.8, 83.4, 40.8, 34.1, 31.8, 29.3, 27.2, 24.9, 24.8, 22.7, 14.2, 14.2. (broad due to quadrupolar broadening from ^{11}B). ^{11}B NMR δ 33.3.

2e. Colorless oil, (19.9 mg, 28% yield). ^{1}H NMR (400 MHz, $CDCl_3$): δ 7.28 – 7.21 (m, 2H), 7.19 – 7.10 (m, 3H), 2.66 – 2.54 (m, 3H), 1.79 – 1.46 (m, 4H), 1.45 – 1.31 (m, 2H), 1.22 (s, 6H), 1.20 (s, 6H), 1.06 (dd, *J* = 15.9, 8.5 Hz, 1H), 0.94 (dd, *J* = 15.9, 6.6 Hz, 1H). ^{13}C NMR (101 MHz, $CDCl_3$): δ 182.8, 142.7, 128.5, 128.4, 125.8, 83.4, 40.8, 35.8, 33.8, 31.5, 26.9, 24.9, 24.8, 14.0. (broad due to quadrupolar broadening from ^{11}B). ^{11}B NMR δ 33.4 HRMS (ESI): m/z calc. for $C_{15}H_{29}BO_4$ $[M\text{-}H]^-$: 283.2086, found 283.2086

2f. Brown solid, (21.4 mg, 24% yield). ^{1}H NMR (400 MHz, $CDCl_3$): δ 7.76 – 7.66 (m, 3H), 7.41 (ddd, *J* = 8.2, 6.9, 1.3 Hz, 1H), 7.31 (ddd, *J* = 8.1, 6.8, 1.2 Hz, 1H), 7.16 – 7.09 (m, 2H), 4.16 (t, *J* = 6.3 Hz, 2H), 2.96 (tt, *J* = 7.9, 6.2 Hz, 1H), 2.29 (ddt, *J* = 14.0, 7.9, 6.2 Hz, 1H), 2.08 (dq, *J* = 14.0, 6.3 Hz, 1H), 1.21 (m, 13H), 1.09 (dd, *J* = 15.9, 6.6 Hz, 1H). ^{13}C NMR (151 MHz, $CDCl_3$): δ 182.3, 156.9, 134.7, 129.5, 129.1, 127.7, 126.9, 126.4, 123.7, 119.1, 106.8, 83.6, 65.7, 37.9, 33.1, 24.9, 24.8, 14.2. (broad due to quadrupolar broadening from ^{11}B). ^{11}B NMR δ 33.6. HRMS (ESI): m/z calc. for $C_{21}H_{27}BO_5$ $[M\text{-}H]^-$: 369.1879, found 369.1879.

2g. White solid, (30.0 mg, 35% yield). ^{1}H NMR (400 MHz, $CDCl_3$): δ 8.10 – 7.98 (m, 2H), 7.57 – 7.50 (m, 1H), 7.42 (dd, *J* = 8.3, 7.0 Hz, 2H), 4.47 – 4.38 (m, 1H), 4.41 – 4.32 (m, 1H), 2.92 – 2.80 (m, 1H), 2.24 – 2.14 (m, 1H), 2.07 – 1.90 (m, 1H), 1.23 – 1.15 (m, 13H), 1.06 (dd, *J* = 16.0, 7.0 Hz, 1H). ^{11}B NMR δ 32.6.

2h. Colorless oil, (53 mg, 53% yield). ^{1}H NMR (400 MHz, $CDCl_3$): δ 7.67 (d, *J* = 7.8 Hz, 1H), 7.59 (d, *J* = 7.8 Hz, 1H), 7.51 (t, *J* = 7.6 Hz, 1H), 7.32 (t, *J* = 7.7 Hz, 1H), 4.65 (s, 2H), 3.58 (td, *J* = 6.4, 1.7 Hz, 2H), 2.81 (p, *J* = 6.9 Hz, 1H), 2.07 (dq, *J* = 13.7, 6.6 Hz, 1H), 1.86 (dt, *J* = 13.8, 6.3 Hz, 1H), 1.21 (s, 6H), 1.19 (s, 6H), 1.10 (dd, *J* = 15.9, 8.3 Hz, 1H), 0.99 (dd, *J* = 15.9, 6.6 Hz, 1H).^{13}C NMR (101 MHz, $CDCl_3$): δ 182.5, 137.4, 132.1, 128.7, 127.4 (q, J = 31.0 Hz) , 127.3, 125.7 (q, J = 5.6 Hz), 124.5 (q, J = 272.0 Hz), 83.5, 68.8 (q, 3.0 Hz), 68.7, 38.1, 33.6, 24.9, 24.8, 14.1. (broad due to quadrupolar broadening from ^{11}B). ^{11}B NMR δ 33.6.

2i. White solid, (19.2 mg, 22% yield). ^{1}H NMR (400 MHz, $CDCl_3$): δ 7.54 (d, *J* = 8.7 Hz, 2H), 6.90 (d, *J* = 8.4 Hz, 2H), 4.07 (t, *J* = 6.3 Hz, 2H), 2.86 (p, *J* = 7.2 Hz, 1H), 2.20 (dq, *J* = 13.9, 6.5 Hz, 1H), 2.01 (dq, *J* = 12.7, 6.1 Hz, 1H), 1.20 (s, 12fH), 1.17 – 1.11 (m, 1H), 1.03 (dd, *J* = 16.0, 6.7 Hz, 1H). ^{13}C NMR (151 MHz, $CDCl_3$): δ 181.9, 162.2, 134.1, 119.4, 115.3, 104.1, 83.7, 66.1, 37.7, 32.8, 24.9, 24.8, 14.1. (broad due to quadrupolar broadening from ^{11}B). ^{11}B NMR δ 33.8.

2k. Brown solid, (54.2 mg, 49% yield). ^{1}H NMR (400 MHz, $CDCl_3$): δ 7.56 – 7.48 (m, 2H), 6.69 – 6.61 (m, 2H), 3.99 (t, *J* = 6.3 Hz, 2H), 2.92 – 2.82 (m, 1H), 2.24 – 2.14 (m, 1H), 2.04 – 1.94 (m, 1H), 1.22 (s, 6H), 1.21 (s, 6H), 1.15 (dd, *J* = 15.9, 8.3 Hz, 1H), 1.03 (dd, *J* = 15.9, 6.7 Hz, 1H). ^{11}B NMR δ 28.5.

2l. Brown solid, (12.5 mg, 13% yield). ^{1}H NMR (400 MHz, $CDCl_3$): δ 7.37 – 7.28 (m, 2H), 6.78 – 6.70 (m, 2H), 3.98 (t, *J* = 6.3 Hz, 2H), 2.87 (p, *J* = 7.4 Hz, 1H), 2.25 – 2.12 (m, 1H), 2.04 – 1.91 (m, 1H), 1.21 (s, 8H), 1.20 (s, 7H), 1.15 (dd, *J* = 16.0, 8.3 Hz, 1H), 1.03 (dd, *J* = 15.9, 6.6 Hz, 1H). ^{13}C NMR (151 MHz, $CDCl_3$): δ 180.9, 158.0, 132.3, 116.5, 113.0, 83.6, 66.0, 37.7, 33.1, 25.0, 24.9, 24.8, 24.7, 14.2. (broad due to quadrupolar broadening from ^{11}B). ^{11}B NMR δ 33.3.

2m. White solid, (12.0 mg, 13% yield). ^{1}H NMR (400 MHz, $CDCl_3$): δ 7.29 – 7.22 (m, 4H), 3.00 – 2.87 (m, 2H), 2.79 (p, *J* = 7.3 Hz, 1H), 2.06 – 1.98 (m, 1H), 1.82 (m, 1H), 1.20 (s, 12H), 1.12 (dd, *J* = 15.9, 8.1 Hz, 1H), 0.98 (dd, *J* = 16.0, 6.8 Hz, 1H).

2n. Clear oil, (53.6 mg, 45% yield). ^{1}H NMR (400 MHz, $CDCl_3$): δ 7.46 – 7.39 (m, 2H), 7.34 – 7.17 (m, 5H), 7.07 – 6.97 (m, 2H), 3.66 – 3.49 (m, 2H), 2.68 (tt, *J* = 7.8, 6.5 Hz, 1H), 2.39 (s, 3H), 1.83 (dtd, *J* = 14.1, 8.1, 6.4 Hz, 1H), 1.59 (ddt, *J* = 14.2, 8.2, 6.2 Hz, 1H), 1.15 (s, 12fH), 1.02 (dd, *J* = 15.9, 8.1 Hz, 1H), 0.93 (dd, *J* = 15.9, 6.7 Hz, 1H).^{13}C NMR (101 MHz, $CDCl_3$): δ 181.3, 143.3, 139.0, 135.1, 129.4, 129.0, 128.7, 127.8, 127.7, 83.4, 48.5, 37.8, 32.0, 24.7, 24.6, 21.5. (broad due to quadrupolar broadening from ^{11}B). ^{11}B NMR δ 32.4.

2o. Maroon solid, (50% NMR yield). ^{11}B NMR δ 33.4.

2r. Yellow oil, (9 mg, 13% yield). ^{1}H NMR (400 MHz, $CDCl_3$): δ 5.63 (s, 2H), 2.57 (m, 1H), 2.14 – 1.78 (m, 5H), 1.74 – 1.68 (m, 1H), 1.31 (m, 1H), 1.22 (s, 6H), 1.19 (s, 6H), 1.05 (m, 1H), 0.92 (m, 1H). ^{13}C NMR (151 MHz, $CDCl_3$): δ 182.1, 127.0, 126.3, 126.3, 83.5, 46.2, 45.9, 37.3, 37.2, 29.4, 28.2, 26.9, 25.8, 25.7, 25.0, 24.7, 10.3 (broad due to quadrupolar broadening from ^{11}B). ^{11}B NMR δ 33.7.

4.6 References

[1](a) Li, S.; Yuan, W.; Ma, S. Highly Regio- and Stereoselective Three-Component Nickel-Catalyzed Syn-Hydrocarboxylation of Alkynes with Diethyl Zinc and Carbon Dioxide. *Angew. Chem. Int. Ed.* **2011**, *50* (11), 2578–2582. (b) Fujihara, T.; Xu, T.; Semba, K.; Terao, J.; Tsuji, Y. Copper-Catalyzed Hydrocarboxylation of Alkynes Using Carbon Dioxide and Hydrosilanes. *Angew. Chem. Int. Ed.* **2011**, *50* (2), 523–527. (c) Wang, X.; Nakajima, M.; Martin, R. Ni-Catalyzed Regioselective Hydrocarboxylation of Alkynes with CO2 by Using Simple Alcohols as Proton Sources. *J. Am. Chem. Soc.* **2015**, *137* (28), 8924–8927. (d) Gaydou, M.; Moragas, T.; Juliá-Hernández, F.; Martin, R. Site-Selective Catalytic Carboxylation of Unsaturated Hydrocarbons with CO2 and Water. *J. Am. Chem. Soc.* **2017**, *139* (35), 12161–12164. (e) Kuge, K.; Luo, Y.; Fujita, Y.; Mori, Y.; Onodera, G.; Kimura, M. Copper-Catalyzed Stereodefined Construction of Acrylic Acid Derivatives from Terminal Alkynes via CO2 Insertion. *Org. Lett.* **2017**, *19* (4), 854–857. (f) Juhl, M.; Laursen, S. L. R.; Huang, Y.; Nielsen, D. U.; Daasbjerg, K.; Skrydstrup, T. Copper-Catalyzed Carboxylation of Hydroborated Disubstituted Alkenes and Terminal Alkynes with Cesium Fluoride. *ACS Catal.* **2017**, *7* (2), 1392–1396. (g) Williams, C. M.; Johnson, J. B.; Rovis, T. Nickel-Catalyzed Reductive Carboxylation of Styrenes Using CO2. *J. Am. Chem. Soc.* **2008**, *130* (45), 14936–14937.

[2] Ohishi, T.; Zhang, L.; Nishiura, M.; Hou, Z. Carboxylation of Alkylboranes by N-Heterocyclic Carbene Copper Catalysts: Synthesis of Carboxylic Acids from Terminal Alkenes and Carbon Dioxide. *Angew. Chem. Int. Ed.* **2011**, *50* (35), 8114–8117. (b) Ohmiya, H.; Tanabe, M.; Sawamura, M. Copper-Catalyzed Carboxylation of Alkylboranes with Carbon Dioxide: Formal Reductive Carboxylation of Terminal Alkenes. *Org. Lett.* **2011**, *13* (5), 1086–1088. (c) Takimoto, M.; Hou, Z. Cu-Catalyzed Formal Methylative and Hydrogenative Carboxylation of Alkynes with Carbon Dioxide: Efficient Synthesis of α,β-Unsaturated Carboxylic Acids. *Chem. – Eur. J.* **2013**, *19* (34), 11439–11445.

[3] (a) Zhu, S.-F.; Zhou, Q.-L. Iridium-Catalyzed Asymmetric Hydrogenation of Unsaturated Carboxylic Acids. *Acc. Chem. Res.* **2017**, *50* (4), 988–1001. (b) Weiss, K. D. Paint and Coatings: A Mature Industry in Transition. *Prog. Polym. Sci.* **1997**, *22* (2), 203–245. (c) Bielawski, C. W.; Jethmalani, J. M.; Grubbs, R. H. Synthesis of Telechelic Polyacrylates with Unsaturated End-Groups. *Polymer* **2003**, *44* (13), 3721–3726. (d) Xu, X.; Lin, J.; Cen, P. Advances in the Research and Development of Acrylic Acid Production from Biomass. *Chin. J. Chem. Eng.* **2006**, *14* (4), 419–427.

[4] (a) Shen, T. Y. Perspectives in Nonsteroidal Anti-inflammatory Agents. *Angew. Chem., Int. Ed. Engl*. **1972**, 11, 460−472. (b) Mueller-Warrant, G. W. Enhanced Activity of Single-Isomer Fenoxaprop on Cool-Season Grasses. *Weed Technology* **1991**, 5, 826− 833. (c) Lassila, T.; Hokkanen, J.; Aatsinki, S.-M.; Mattila, S.; Turpeinen, M.; Tolonen, A. Toxicity of Carboxylic Acid-Containing Drugs: The Role of Acyl Migration and CoA Conjugation Investigated. *Chem. Res. Toxicol.* **2015**, *28* (12), 2292–2303. (d) Ballatore, C.; Huryn, D. M.; Smith III, A. B. Carboxylic Acid (Bio)Isosteres in Drug Design. *ChemMedChem* **2013**, *8* (3), 385–395

[5] (a) Takimoto, M.; Hou, Z. Cu-Catalyzed Formal Methylative and Hydrogenative Carboxylation of Alkynes with Carbon Dioxide: Efficient Synthesis of α,β-Unsaturated Carboxylic Acids. *Chem. – Eur. J.* **2013**, *19* (34), 11439–11445. (b) Nogi, K.; Fujihara, T.; Terao, J.; Tsuji, Y. Carboxyzincation Employing Carbon Dioxide and Zinc Powder: Cobalt-Catalyzed Multicomponent Coupling Reactions with Alkynes. *J. Am. Chem. Soc.* **2016**, *138* (17), 5547–5550 (c) Wang, X.; Liu, Y.; Martin, R. Ni-Catalyzed Divergent Cyclization/Carboxylation of Unactivated Primary and Secondary Alkyl Halides with CO2. *J. Am. Chem. Soc.* **2015**, *137* (20), 6476–6479. (d) Wang, X.; Liu, Y.; Martin, R. Ni-Catalyzed Divergent Cyclization/Carboxylation of Unactivated Primary and Secondary Alkyl Halides with CO2. *J. Am. Chem. Soc.* **2015**, *137* (20), 6476–6479. (e) Yatham, V. R.; Shen, Y.; Martin, R. Catalytic Intermolecular Dicarbofunctionalization of Styrenes with CO2 and Radical Precursors. *Angew. Chem. Int. Ed.* **2017**, *56* (36). (f) Ju, T.; Zhou, Y.-Q.; Cao, K.-G.; Fu, Q.; Ye, J.-H.; Sun, G.-Q.; Liu, X.-F.; Chen, L.; Liao, L.-L.; Yu, D.-G. Dicarboxylation of Alkenes, Allenes and (Hetero)Arenes with CO2 via Visible-Light Photoredox Catalysis. *Nat. Catal.* **2021**, *4* (4), 304–311. (g) For more photocatalytic examples see: Cai, B.; Cheo, H. W.; Liu, T.; Wu, J. Light-Promoted Organic Transformations Utilizing Carbon-Based Gas Molecules as Feedstocks. *Angew. Chem.* **2021**, *133* (35), 19098–19128.

[6] (a) Li, S.; Ma, S. Quadri-Synergetic Effect for Highly Effective Carbon Dioxide Fixation and Its Application to Indoloquinolinone. *Adv. Synth. Catal.* **2012**, *354* (13), 2387–2394. (b) Inamoto, K.; Asano, N.; Nakamura, Y.; Yonemoto, M.; Kondo, Y. Synthesis of 3-Carboxylated Indoles through a Tandem Process Involving Cyclization of 2-Ethynylanilines Followed by CO2 Fixation in the Absence of Transition Metal Catalysts. *Org. Lett.* **2012**, *14* (10), 2622–2625. (c) Didehban, K.; Vessally, E.; Salary, M.; Edjlali, L.; Babazadeh, M. Synthesis of a Variety of Key Medicinal Heterocyclic Compounds via Chemical Fixation of CO2 onto O-Alkynylaniline Derivatives. *J. CO2 Util.* **2018**, *23*, 42–50. (d) Cao, X.; Zhong, H. A.; Zhang, P.; Zheng, H. The Simple System of Fixing CO2 to Synthesize Benzimidazolones at Atmospheric Pressure. *J. CO2 Util.* **2018**, *24*, 250–255.

[7] Ye, J.-H.; Miao, M.; Huang, H.; Yan, S.-S.; Yin, Z.-B.; Zhou, W.-J.; Yu, D.-G. Visible-Light-Driven Iron-Promoted Thiocarboxylation of Styrenes and Acrylates with CO2. *Angew. Chem. Int. Ed.* **2017**, *56* (48), 15416–15420.

[8] (a) Fu, Q.; Bo, Z.-Y.; Ye, J.-H.; Ju, T.; Huang, H.; Liao, L.-L.; Yu, D.-G. Transition Metal-Free Phosphonocarboxylation of Alkenes with Carbon Dioxide via Visible-Light Photoredox Catalysis. *Nat. Commun.* **2019**, *10* (1), 3592. (b) Cu(II)-Catalyzed Phosphonocarboxylative Cyclization Reaction of Propargylic Amines and Phosphine Oxide with CO2. *J. Org. Chem.* **2020**, *85* (21), 14109–14120.

[9] (a) Fujihara, T.; Tani, Y.; Semba, K.; Terao, J.; Tsuji, Y. Copper-Catalyzed Silacarboxylation of Internal Alkynes by Employing Carbon Dioxide and Silylboranes. *Angew. Chem. Int. Ed.* **2012**, *51* (46), 11487–11490. (b) Hou, J.; Ee, A.; Cao, H.; Ong, H.-W.; Xu, J.-H.; Wu, J. Visible-Light-Mediated Metal-Free Difunctionalization of Alkenes with CO2 and Silanes or C(Sp3)−H Alkanes. *Angew. Chem. Int. Ed.* **2018**, *57* (52), 17220–17224.

[10] Zhang, L.; Cheng, J.; Carry, B.; Hou, Z. Catalytic Boracarboxylation of Alkynes with Diborane and Carbon Dioxide by an N-Heterocyclic Carbene Copper Catalyst. *J. Am. Chem. Soc.* **2012**, *134* (35), 14314–14317.

[11] Butcher, T. W.; McClain, E. J.; Hamilton, T. G.; Perrone, T. M.; Kroner, K. M.; Donohoe, G. C.; Akhmedov, N. G.; Petersen, J. L.; Popp, B. V. Regioselective Copper-Catalyzed Boracarboxylation of Vinyl Arenes. *Org. Lett.* **2016**, *18* (24), 6428–6431.

[12] Perrone, T. M.; Gregory, A. S.; Knowlden, S. W.; Ziemer, N. R.; Alsulami, R. N.; Petersen, J. L.; Popp, B. V. Beneficial Effect of a Secondary Ligand on the Catalytic Difunctionalization of Vinyl Arenes with Boron and CO2. *ChemCatChem* **2019**, *11* (23), 5814–5820.

[13] Baughman, N. N.; Akhmedov, N. G.; Petersen, J. L.; Popp, B. V. Experimental and Computational Analysis of CO2 Addition Reactions Relevant to Copper-Catalyzed Boracarboxylation of Vinyl Arenes: Evidence for a Phosphine-Promoted Mechanism. *Organometallics* **2021**, *40* (1), 23–37

[14] Wu, F.-P.; Yuan, Y.; Schünemann, C.; Kamer, P. C. J.; Wu, X.-F. Copper-Catalyzed Regioselective Borocarbonylative Coupling of Unactivated Alkenes with Alkyl Halides: Synthesis of β-Boryl Ketones. *Angew. Chem.* **2020**, *132* (26), 10537–10541.

[15] Wu, F.-P.; Luo, X.; Radius, U.; Marder, T. B.; Wu, X.-F. Copper-Catalyzed Synthesis of Stereodefined Cyclopropyl Bis(Boronates) from Alkenes with CO as the C1 Source. *J. Am. Chem. Soc.* **2020**, *142* (33), 14074–14079.

[16] Kubota, K.; Yamamoto, E.; Ito, H. Copper(I)-Catalyzed Borylative Exo-Cyclization of Alkenyl Halides Containing Unactivated Double Bond. *J. Am. Chem. Soc.* **2013**, *135* (7), 2635–2640.

[17] For base catalyzed diboration reactions see: Wen, Y.; Deng, C.; Xie, J.; Kang, X. Recent Synthesis Developments of Organoboron Compounds via Metal-Free Catalytic Borylation of Alkynes and Alkenes. *Molecules* **2019**, *24* (1), 101.

[18] Deng, C. M.; Ma, Y. F.; Wen, Y. M. Transition-Metal-Free Borylation of Alkynes and Alkenes. *ChemistrySelect* **2018**, *3* (4), 1202–1204.

[19] Wang, J.; Shang, M.; Lundberg, H.; Feu, K. S.; Hecker, S. J.; Qin, T.; Blackmond, D. G.; Baran, P. S. Cu-Catalyzed Decarboxylative Borylation. *ACS Catal.* **2018**, *8* (10), 9537–9542.

[20] Su, W.; Gong, T.-J.; Lu, X.; Xu, M.-Y.; Yu, C.-G.; Xu, Z.-Y.; Yu, H.-Z.; Xiao, B.; Fu, Y. Ligand-Controlled Regiodivergent Copper-Catalyzed Alkylboration of Alkenes. *Angew. Chem. Int. Ed.* **2015**, *54* (44), 12957–12961. (b) Xu, Z.-Y.; Jiang, Y.-Y.; Su, W.; Yu, H.-Z.; Fu, Y. Mechanism of Ligand-Controlled Regioselectivity-Switchable Copper-Catalyzed Alkylboration of Alkenes. *Chem. – Eur. J.* **2016**, *22* (41), 14611–14617.

[21] Whyte, A.; Torelli, A.; Mirabi, B.; Lautens, M. Enantioselective Copper-Catalyzed Borylative Cyclization with Cyclic Imides. *Org. Lett.* **2019**, *21* (20), 8373–8377.

Appendix I NMR Characterization Data

Contents

I. ^{1}H, ^{13}C, ^{11}B and ^{19}F NMR Spectra – Compounds in Chapter 2 84

II. ^{1}H, ^{13}C, ^{11}B and ^{19}F NMR Spectra – Compounds in Chapter 4 154

^{1}H, ^{13}C, ^{11}B and ^{19}F NMR Spectra – Compounds in Chapter 2

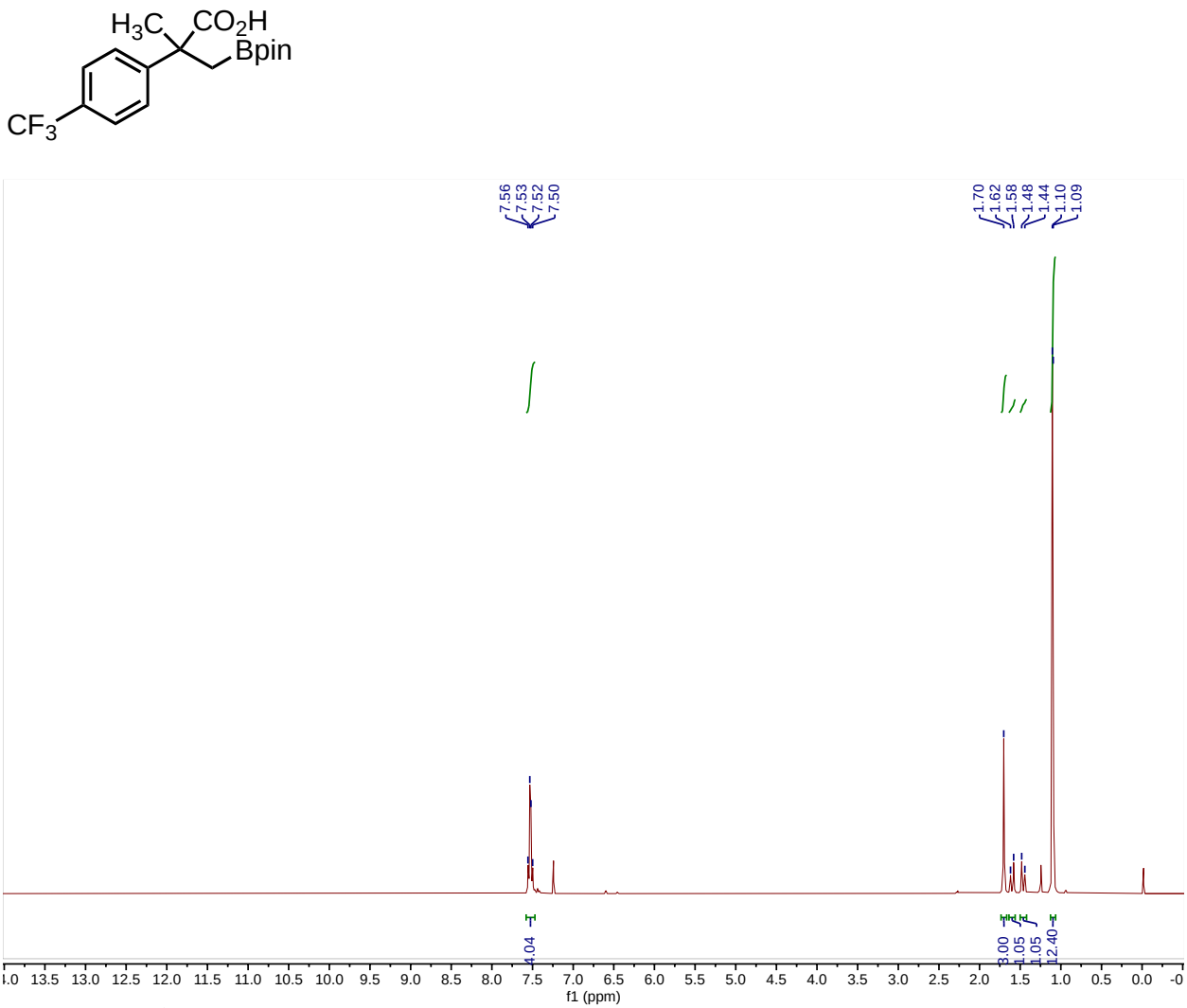

Figure A-1. ^{1}H NMR Spectrum of **2b**.

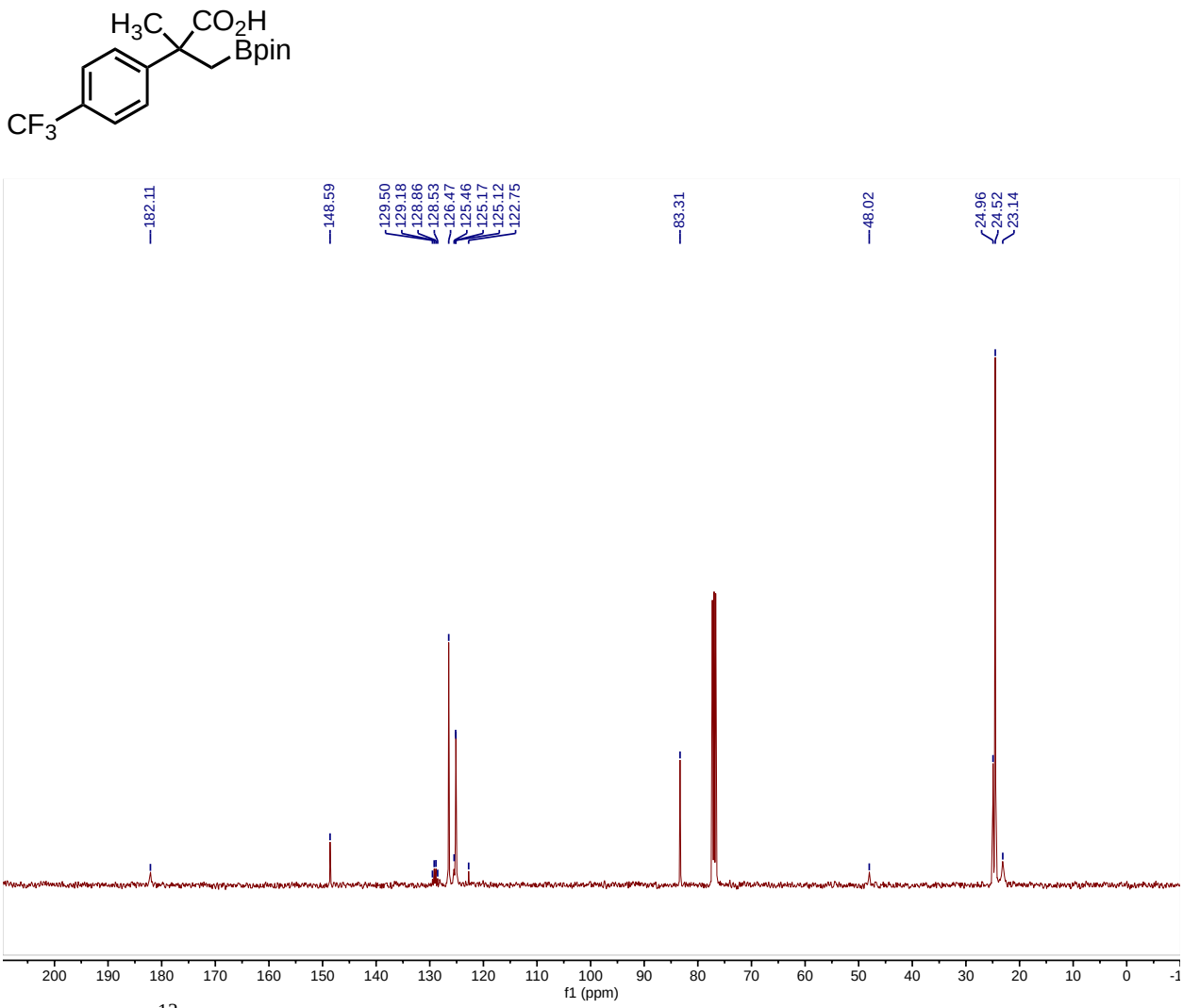

Figure A-2. ^{13}C NMR Spectrum of **2b**.

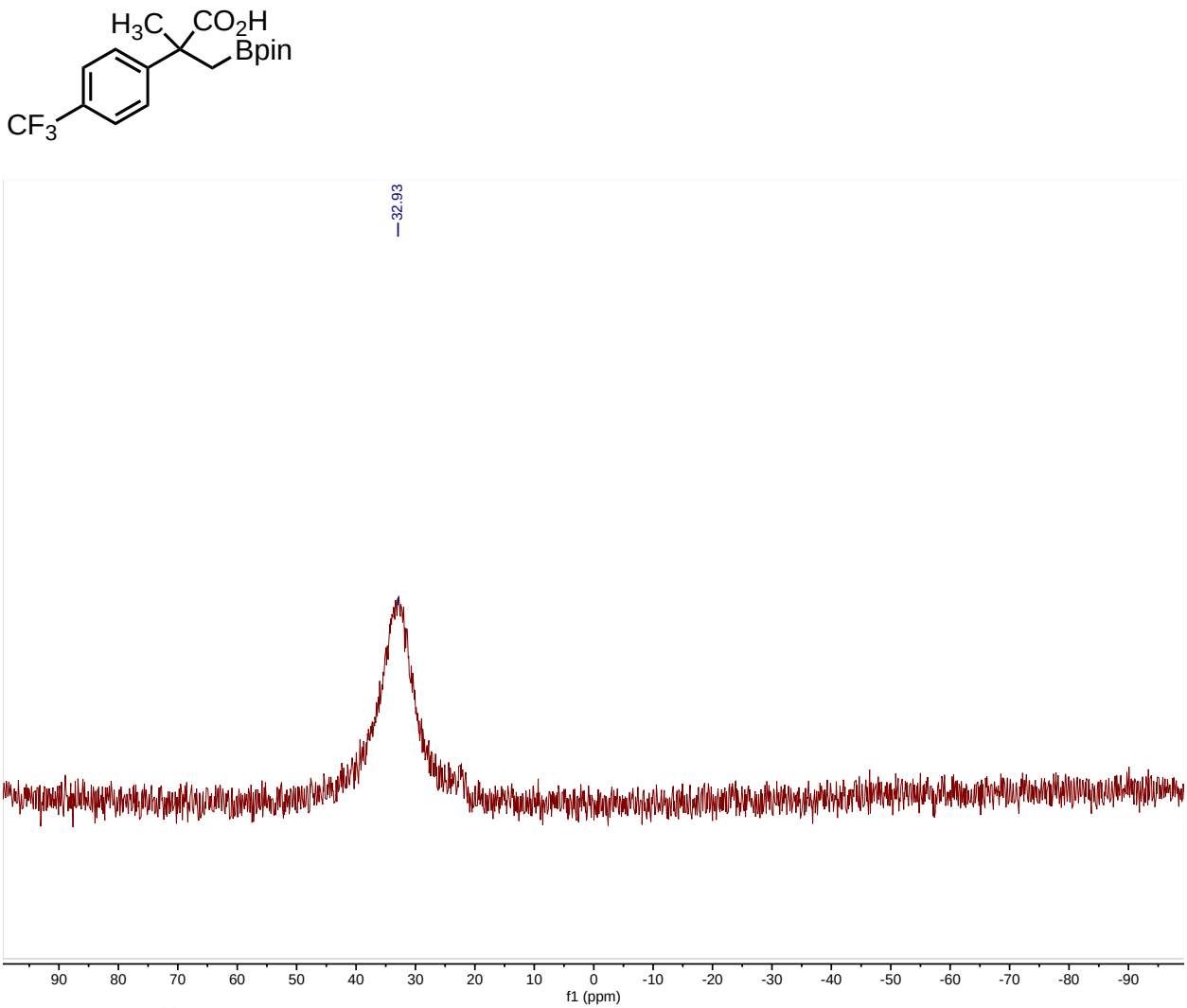

Figure A-3. ^{11}B NMR Spectrum of **2b**.

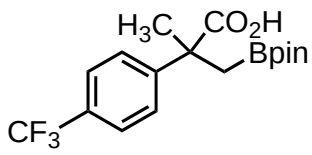

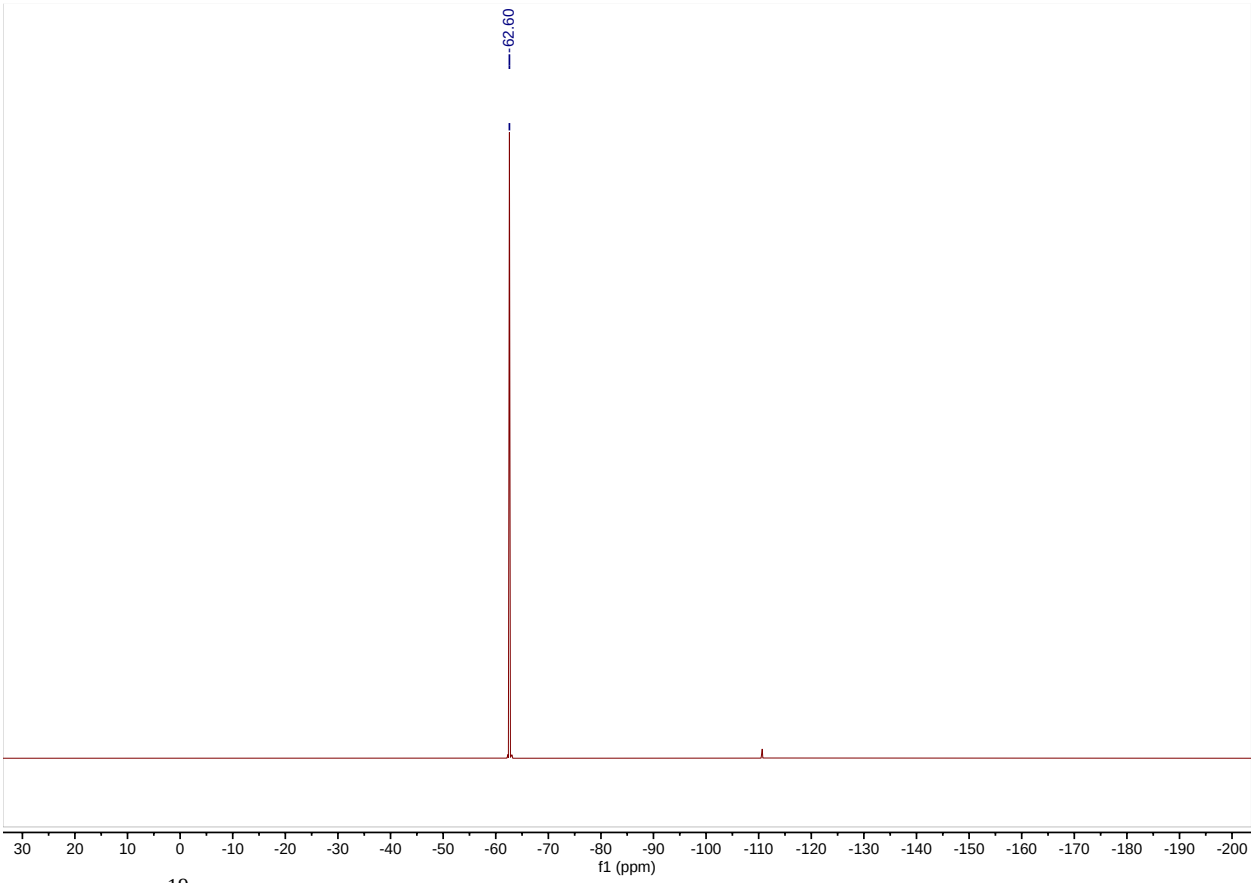

Figure A-4. ^{19}F NMR Spectrum of **2b**.

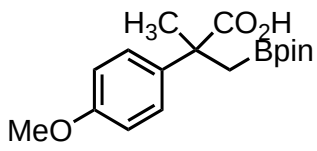

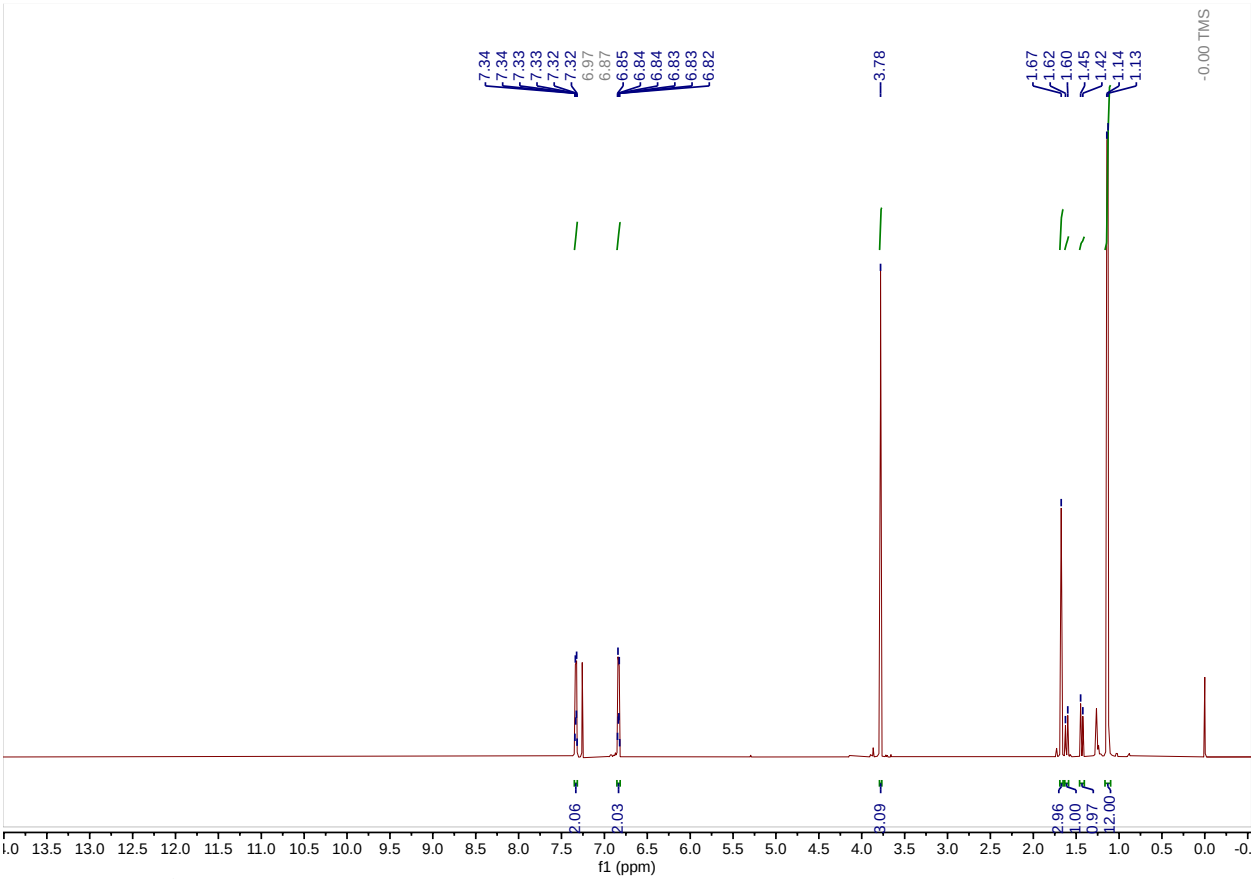

Figure A-5. ^{1}H NMR Spectrum of **2c**.

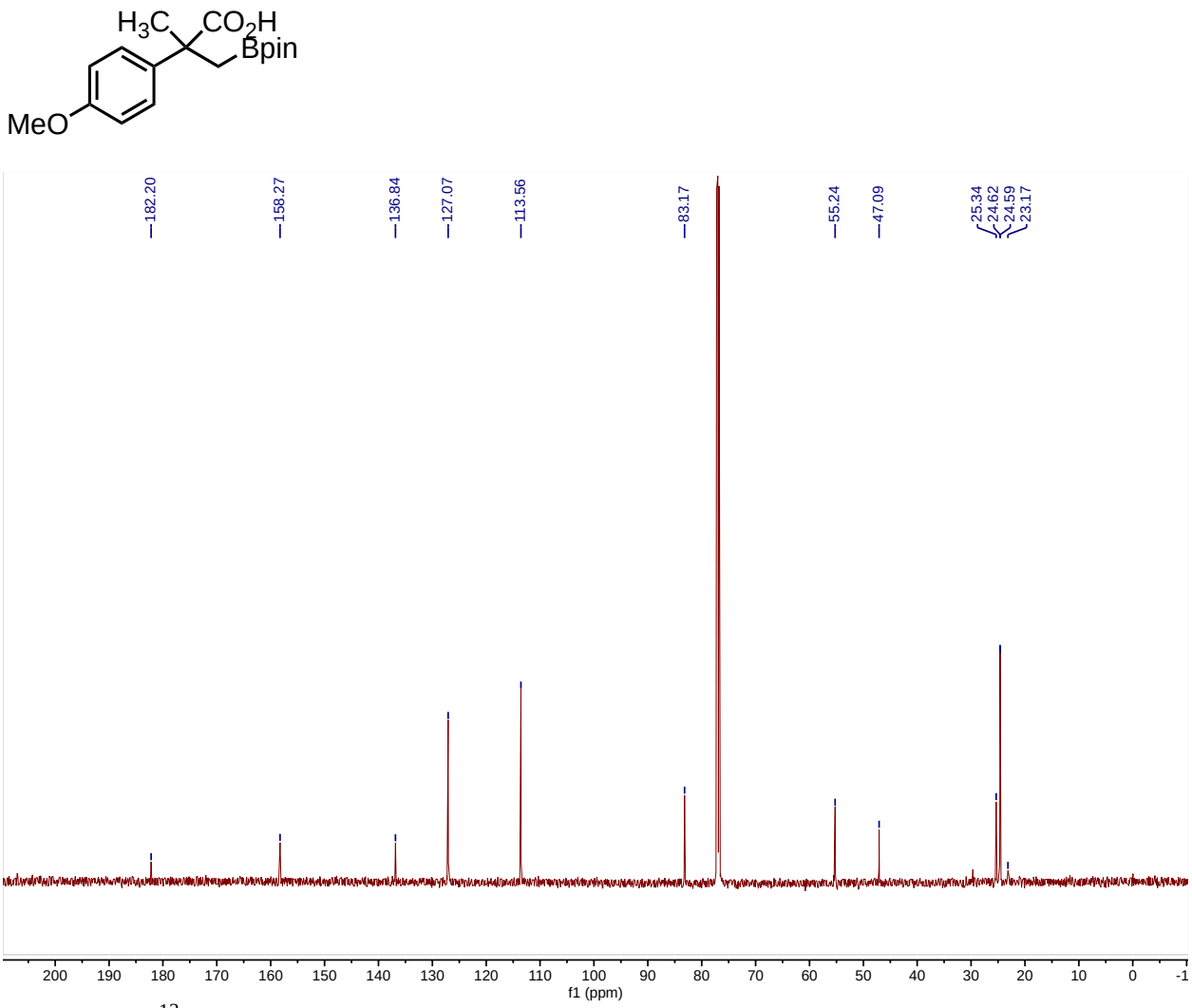

Figure A-6. ^{13}C NMR Spectrum of **2c**.

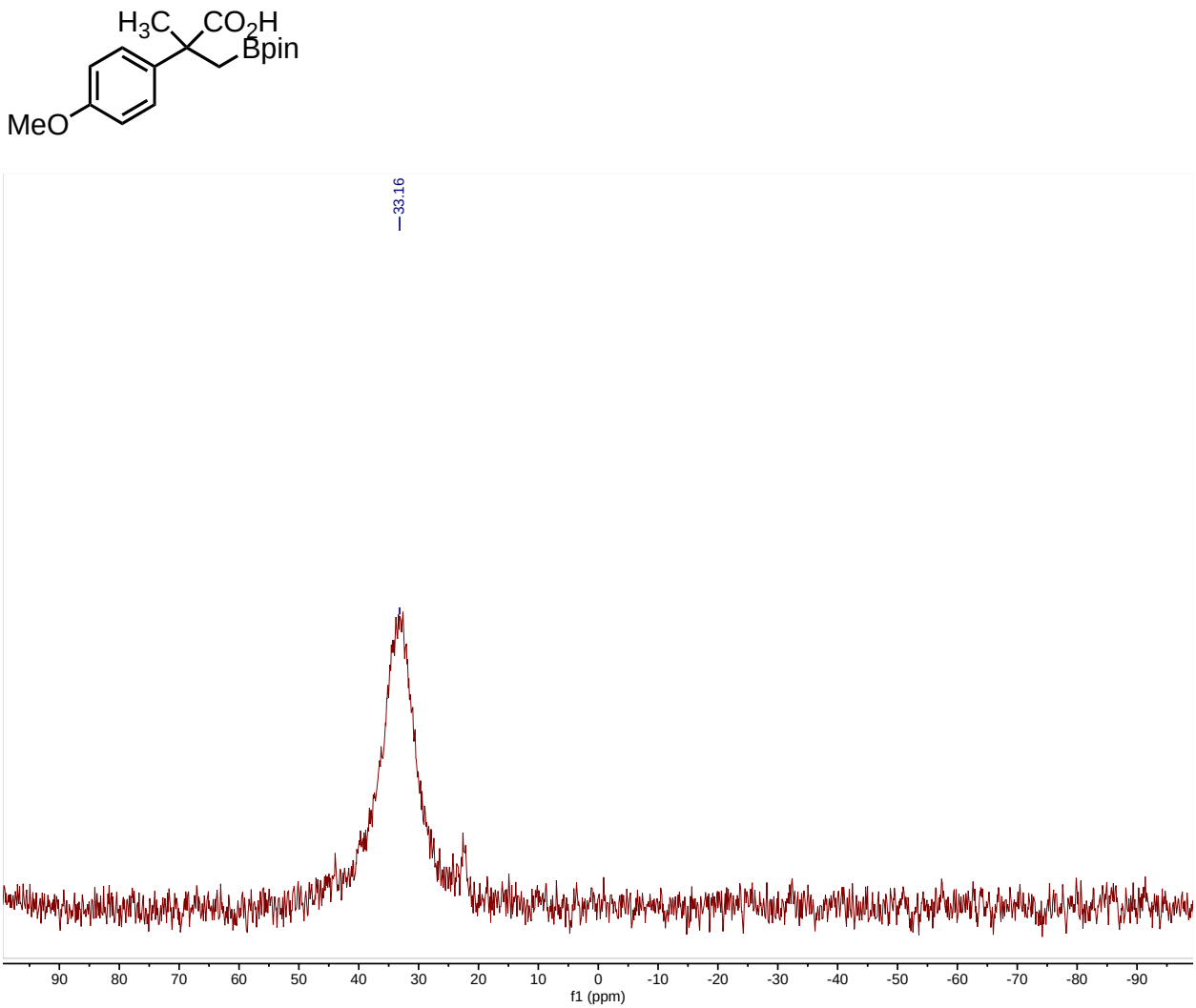

Figure A-7. ^{11}B NMR Spectrum of **2c**.

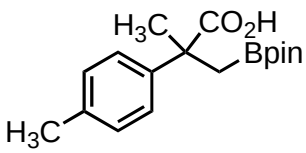

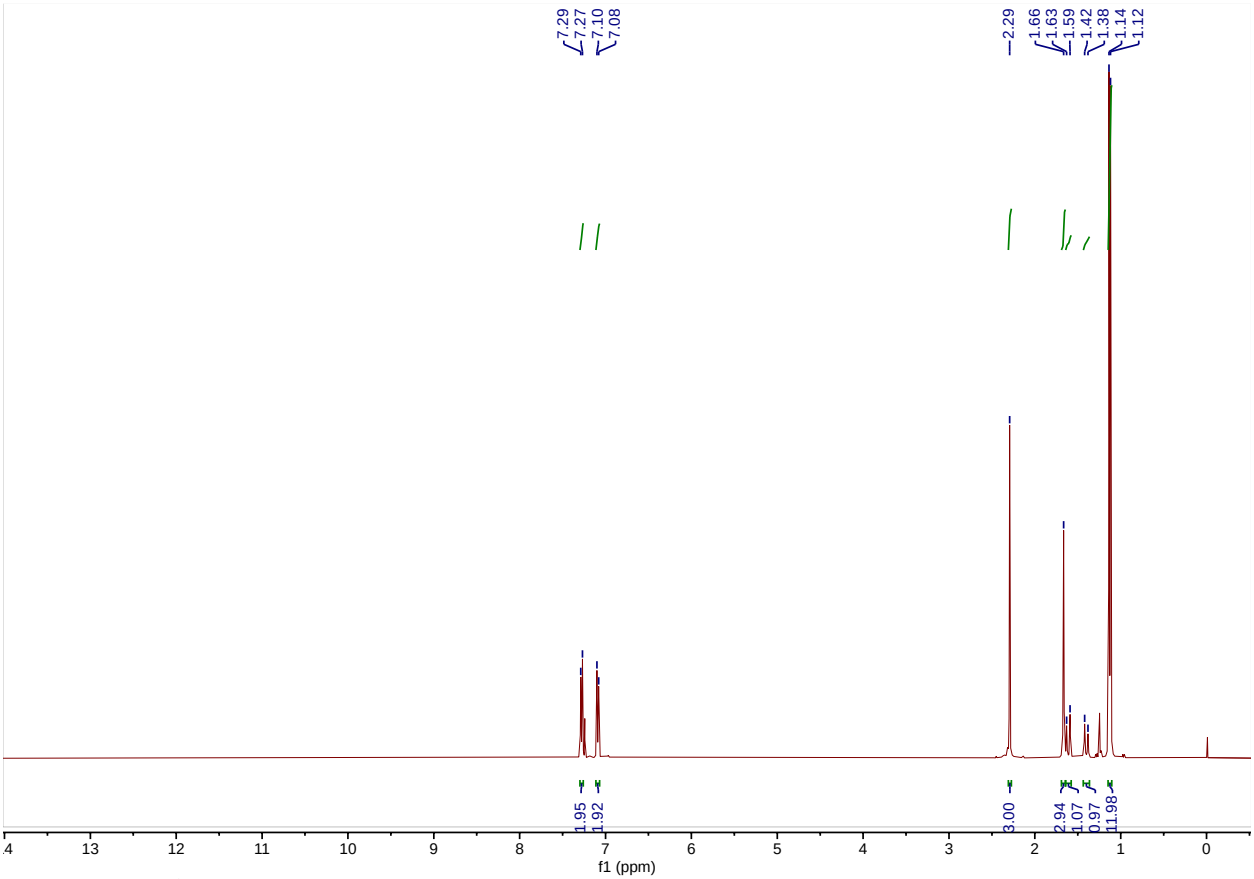

Figure A-8. ^{1}H NMR Spectrum of **2d**.

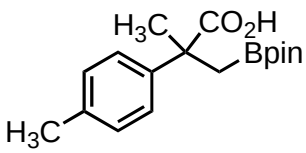

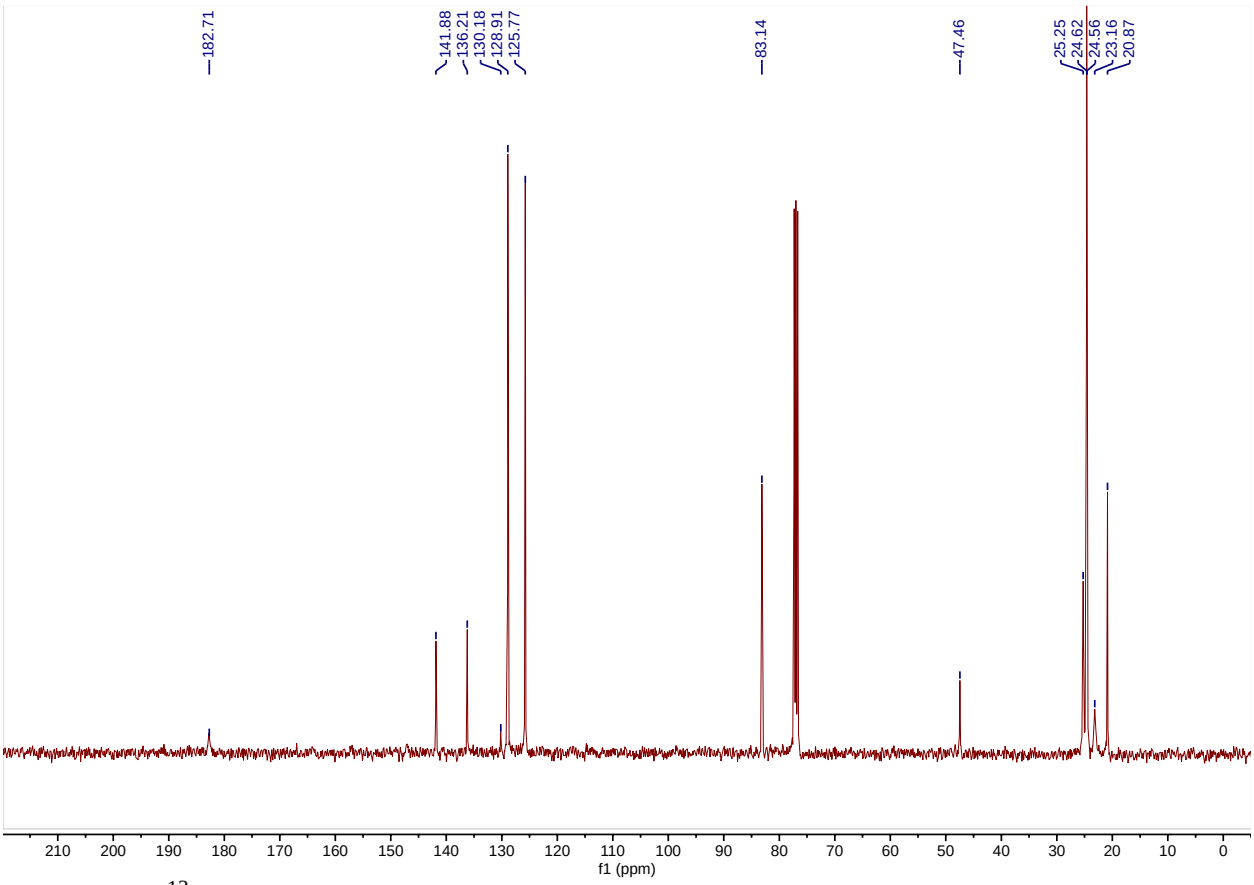

Figure A-9. ^{13}C NMR Spectrum of **2d**.

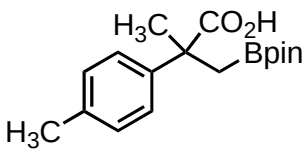

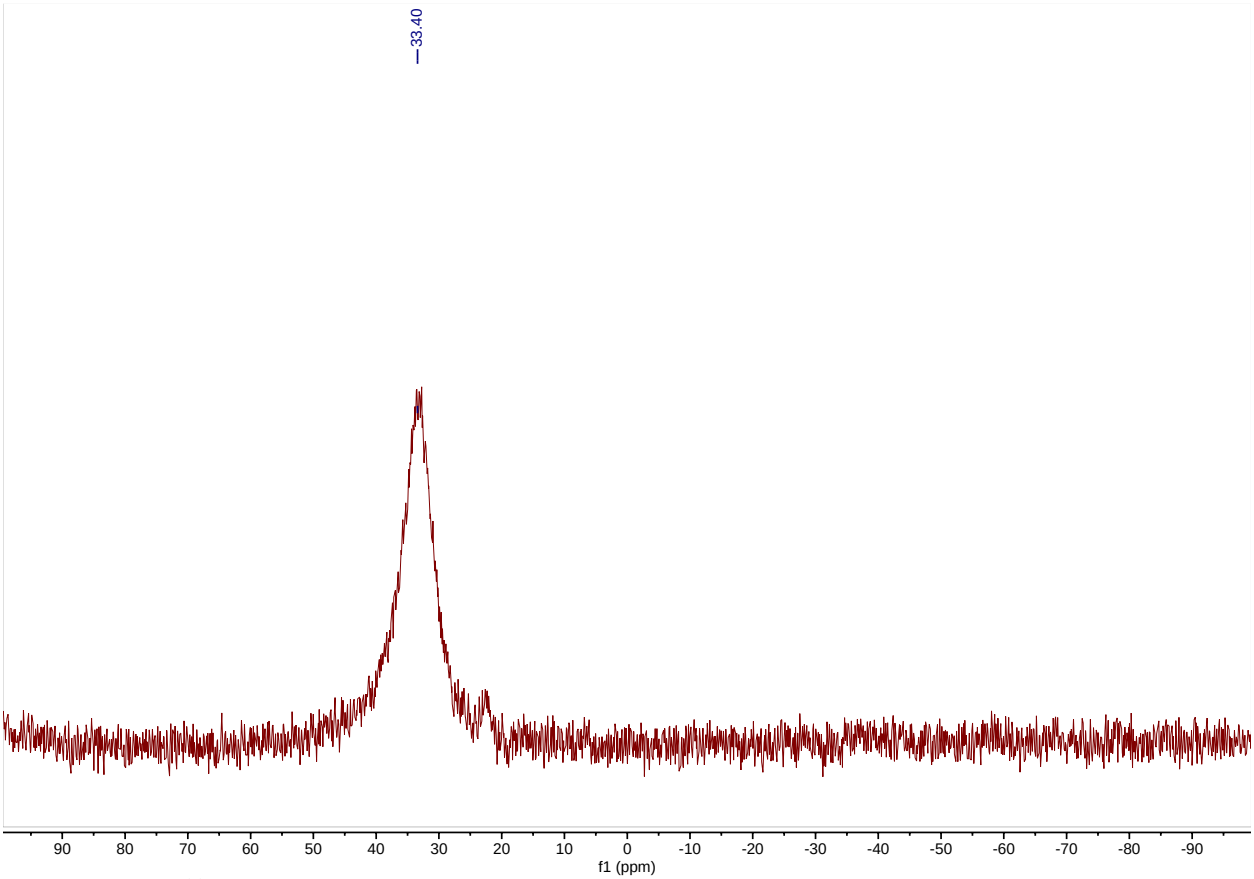

Figure A-10. ^{11}B NMR Spectrum of **2d**.

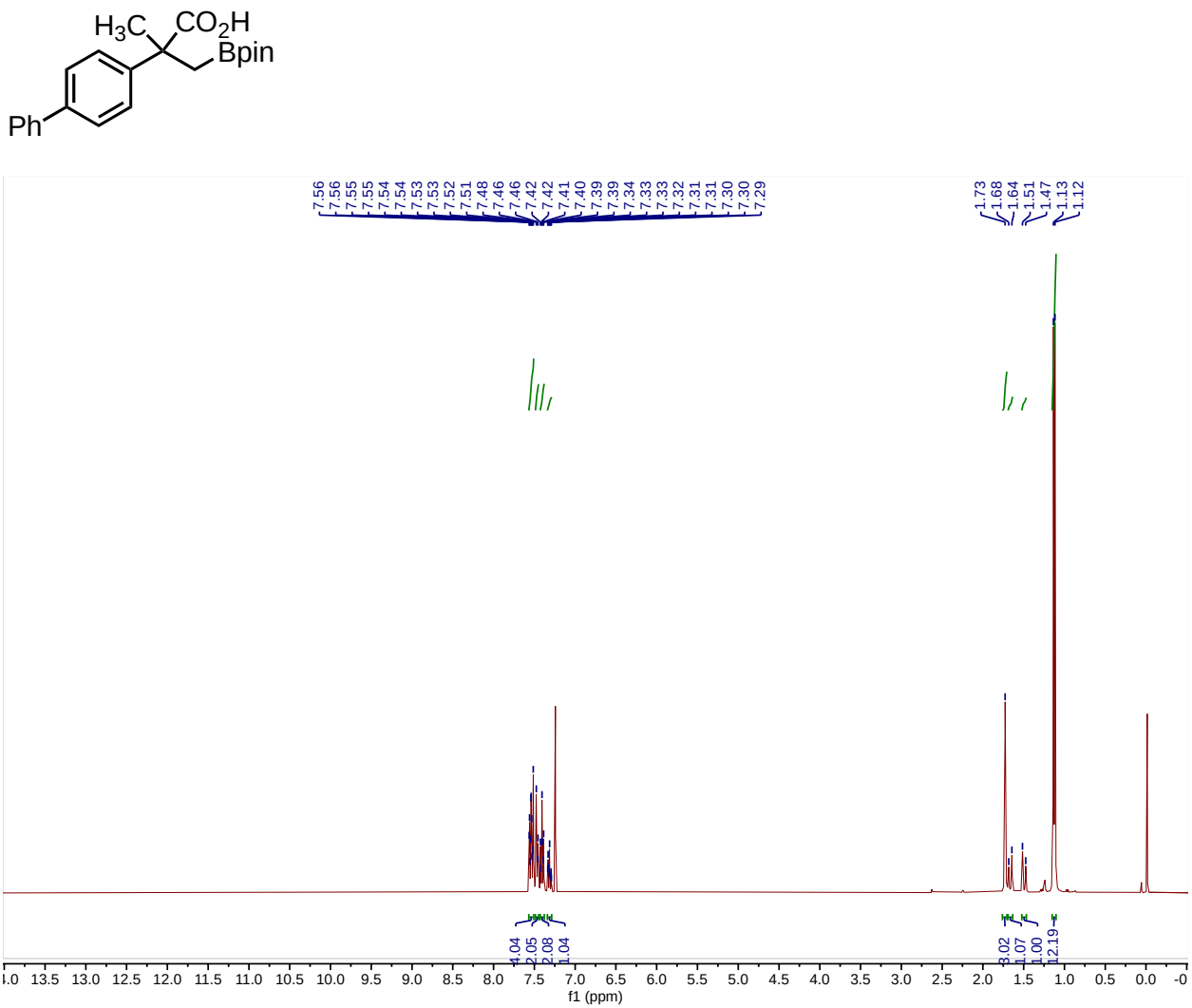

Figure A-11. ^{1}H NMR Spectrum of **2e**.

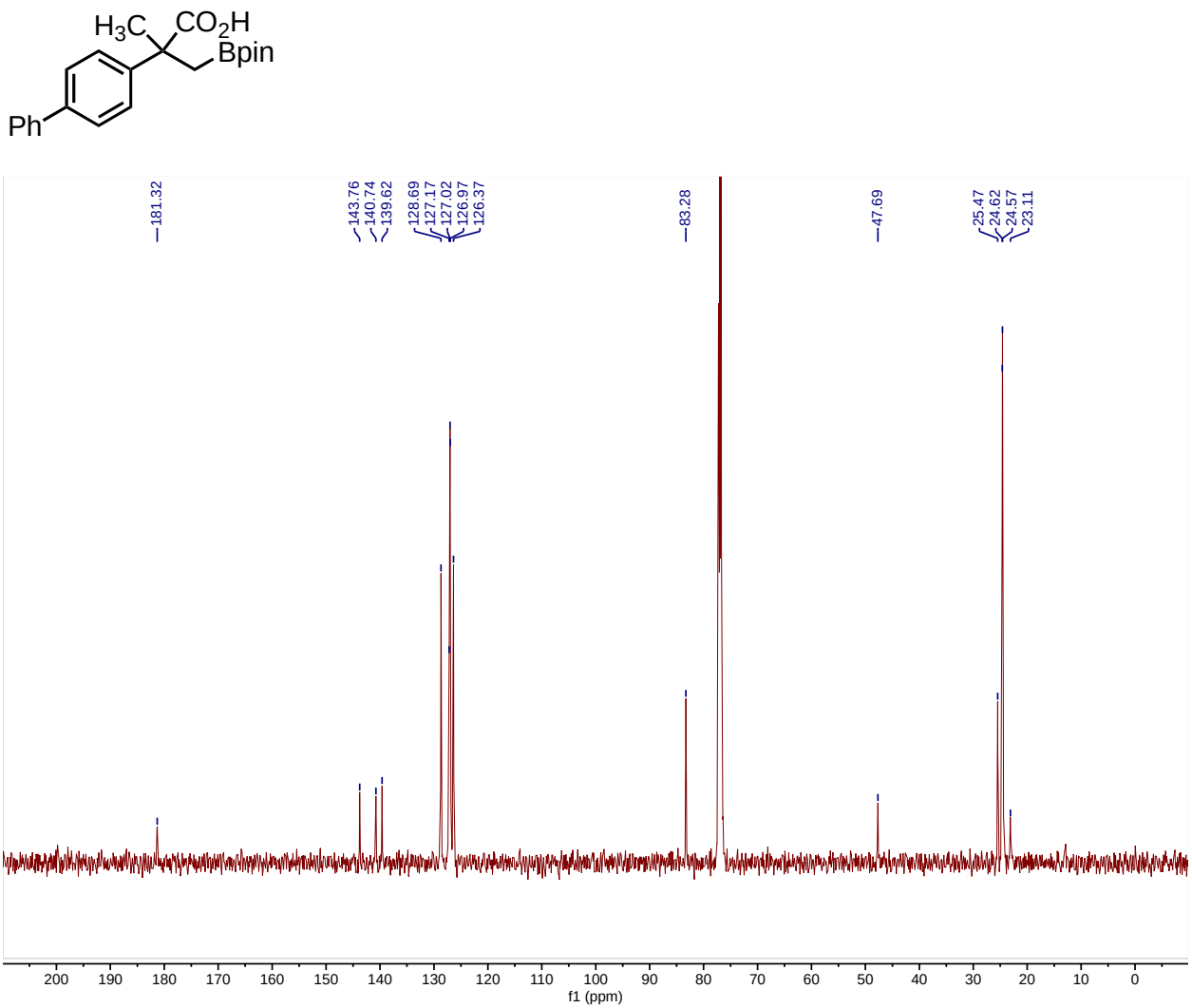

Figure A-12. ^{13}C NMR Spectrum of **2e**.

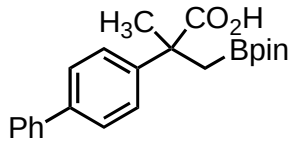

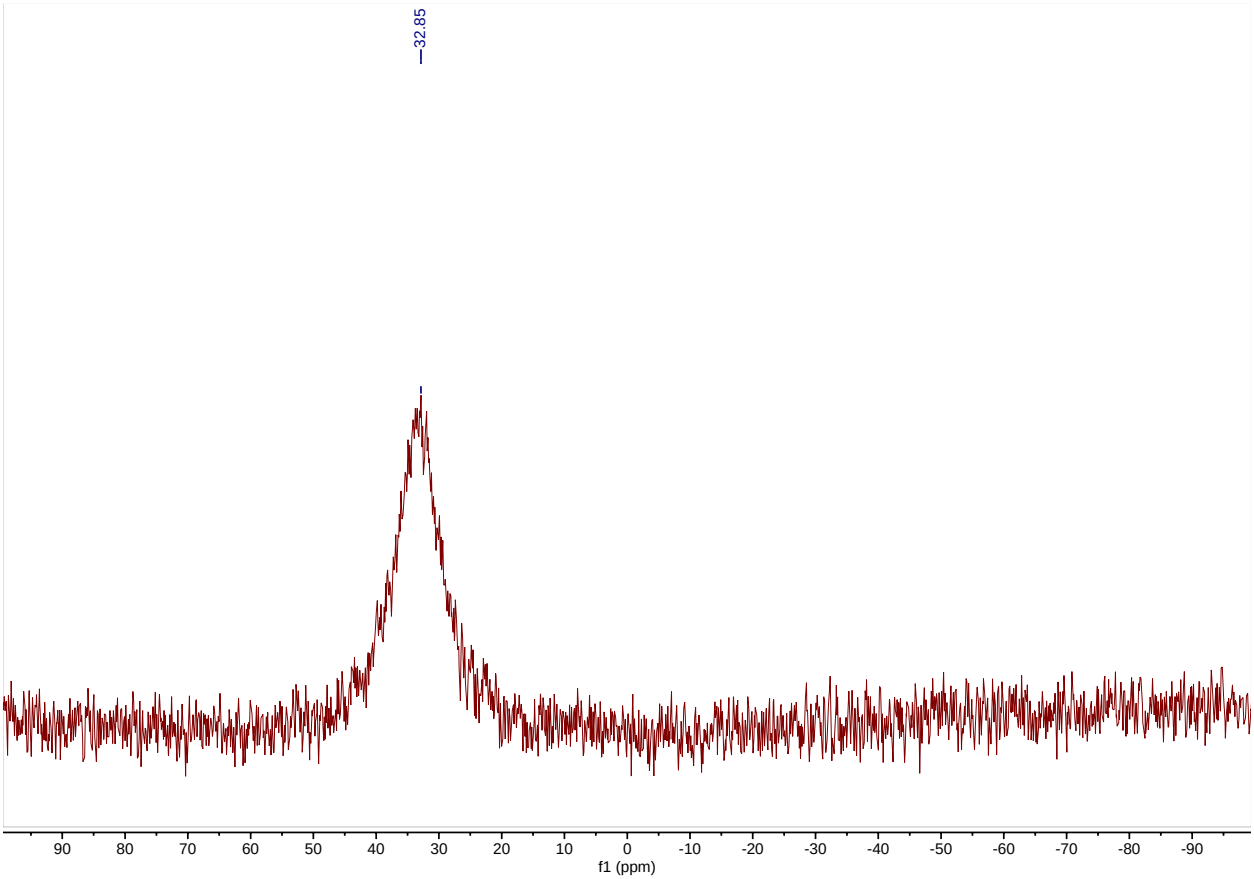

Figure A-13. ^{11}B NMR Spectrum of **2e**.

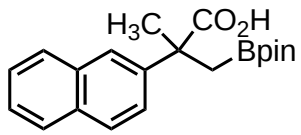

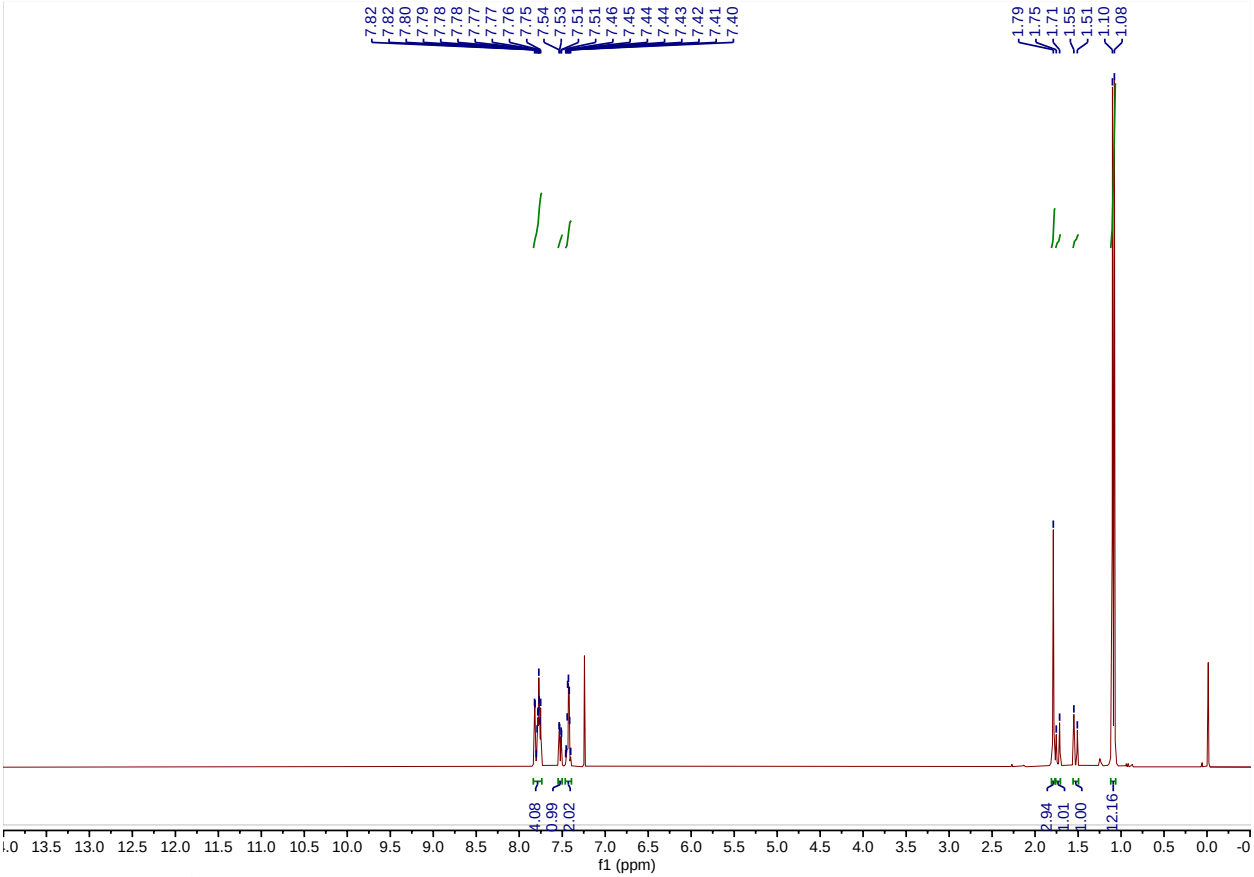

Figure A-14*:* ^{1}H NMR Spectrum of **2f**

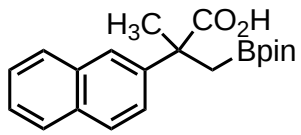

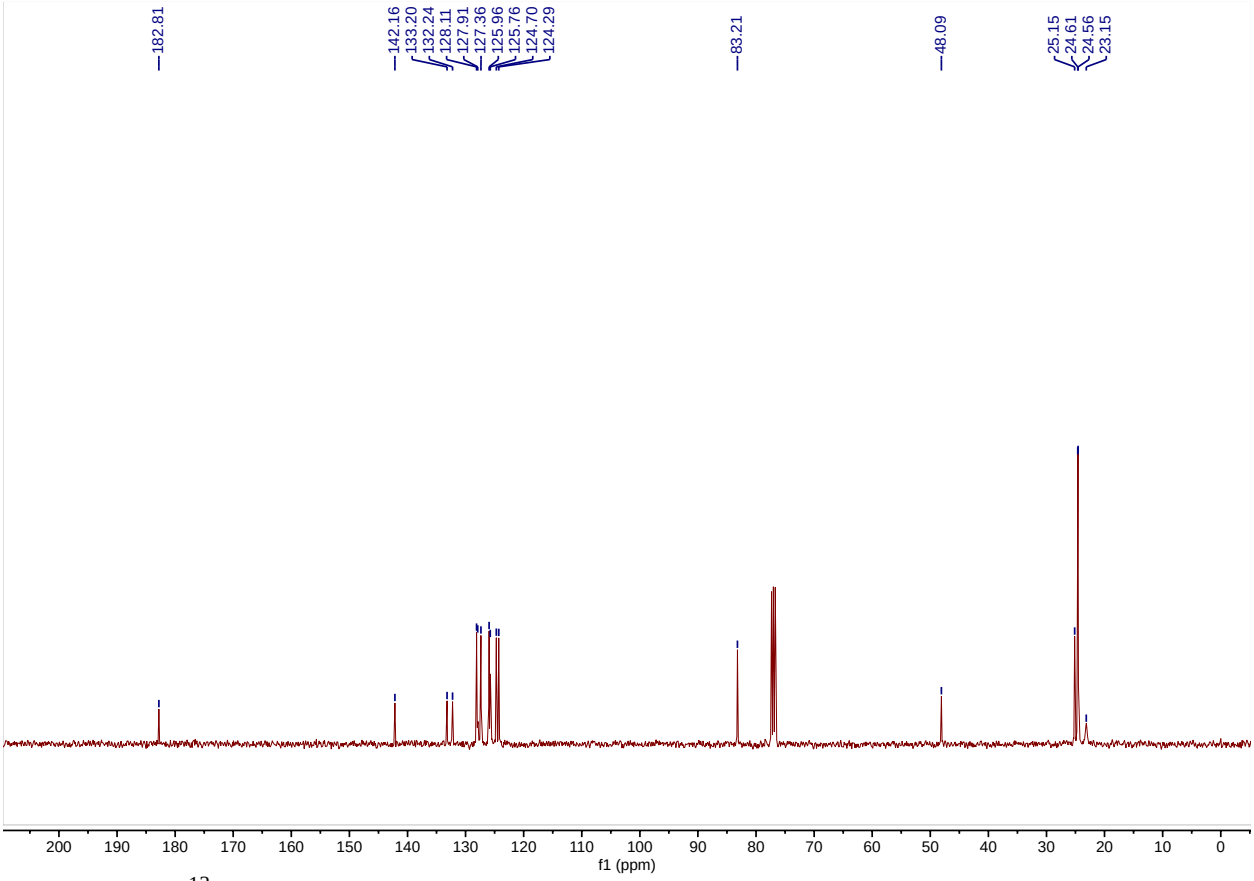

Figure A-15. ^{13}C NMR Spectrum of **2f**.

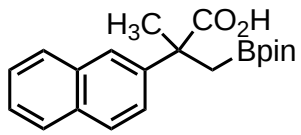

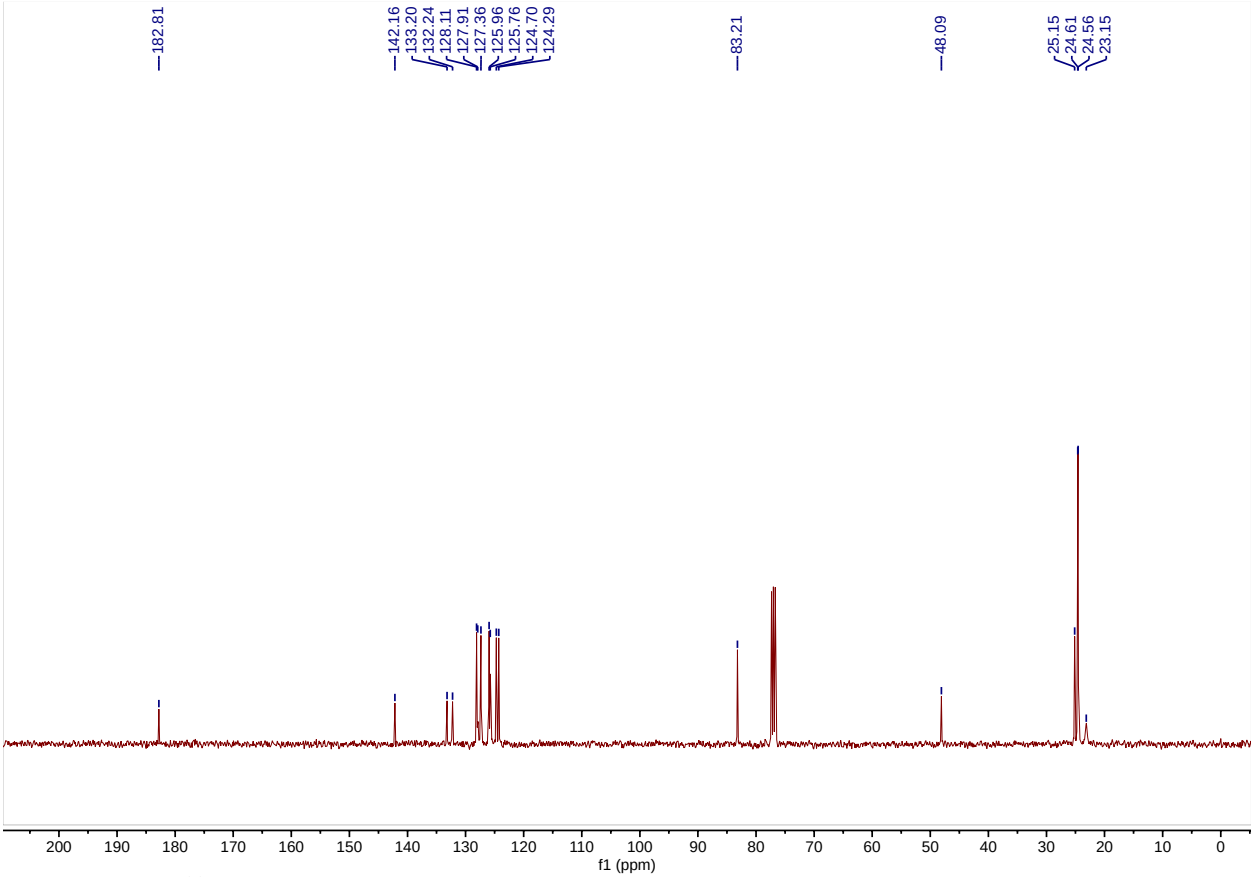

Figure A-16. ^{11}B NMR Spectrum of **2f**.

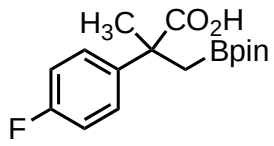

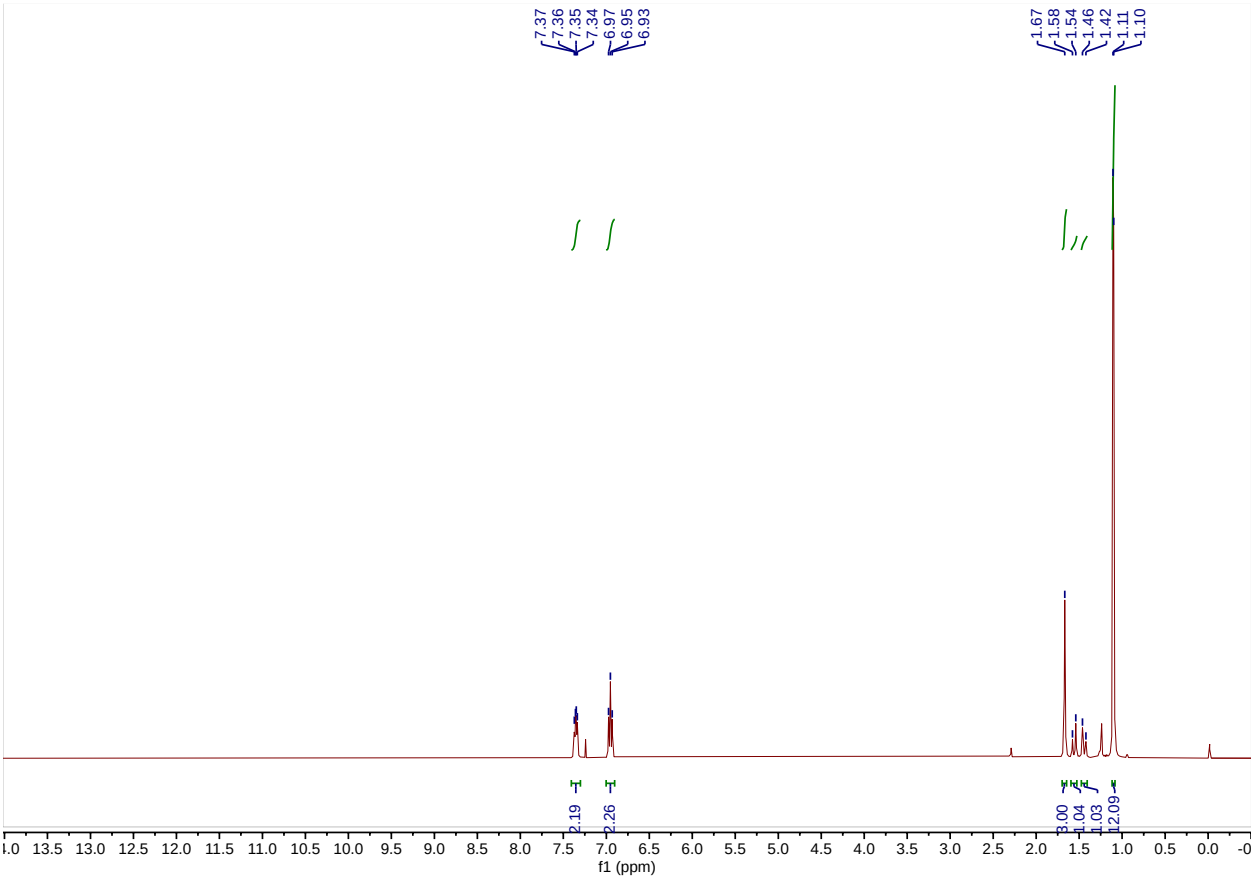

Figure A-17. ^{1}H NMR Spectrum of **2g**.

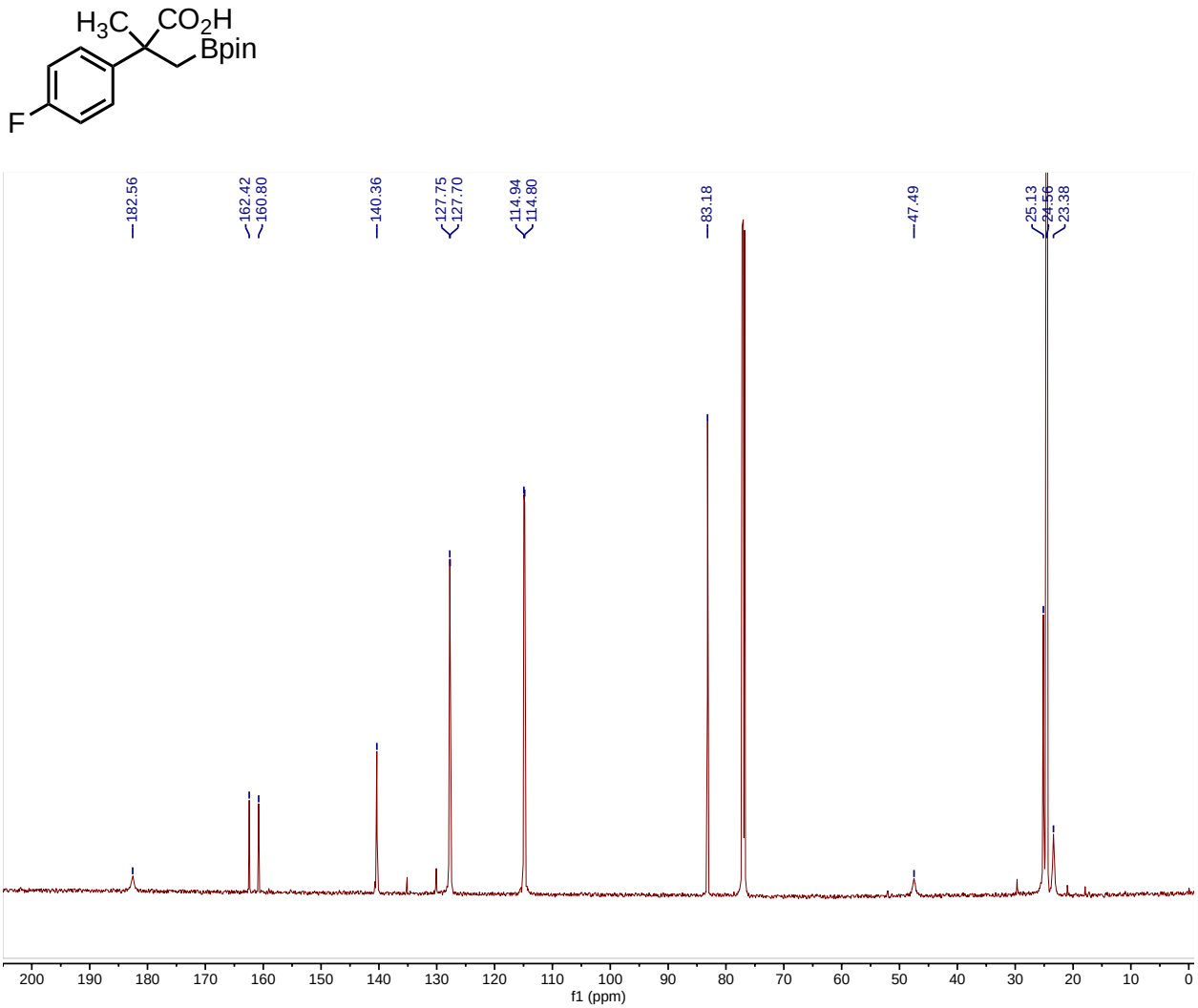

Figure A-18. ^{13}C NMR Spectrum of **2g**.

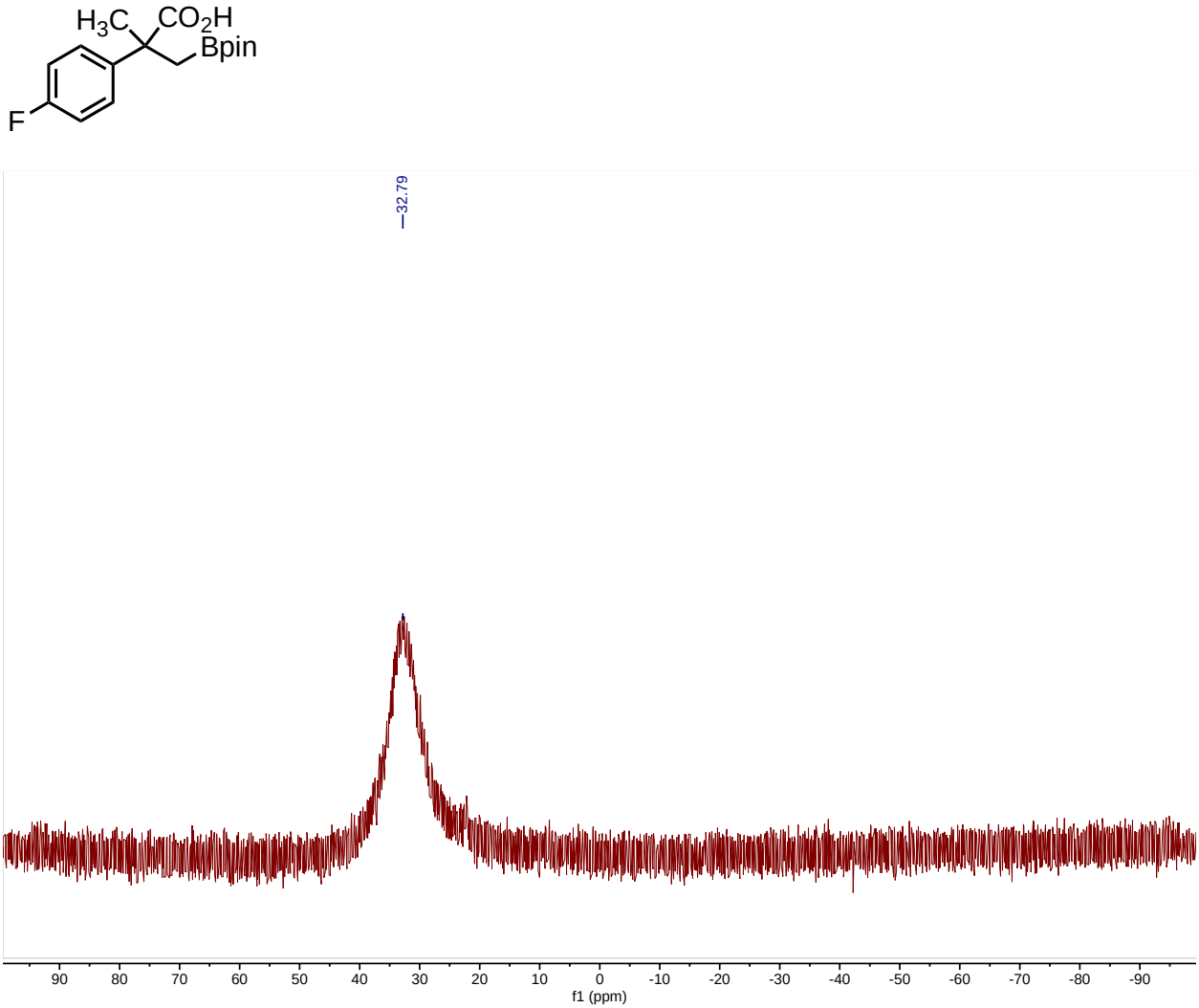

Figure A-19. ^{11}B NMR Spectrum of **2g**.

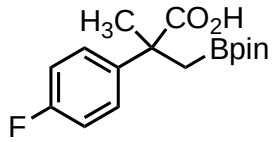

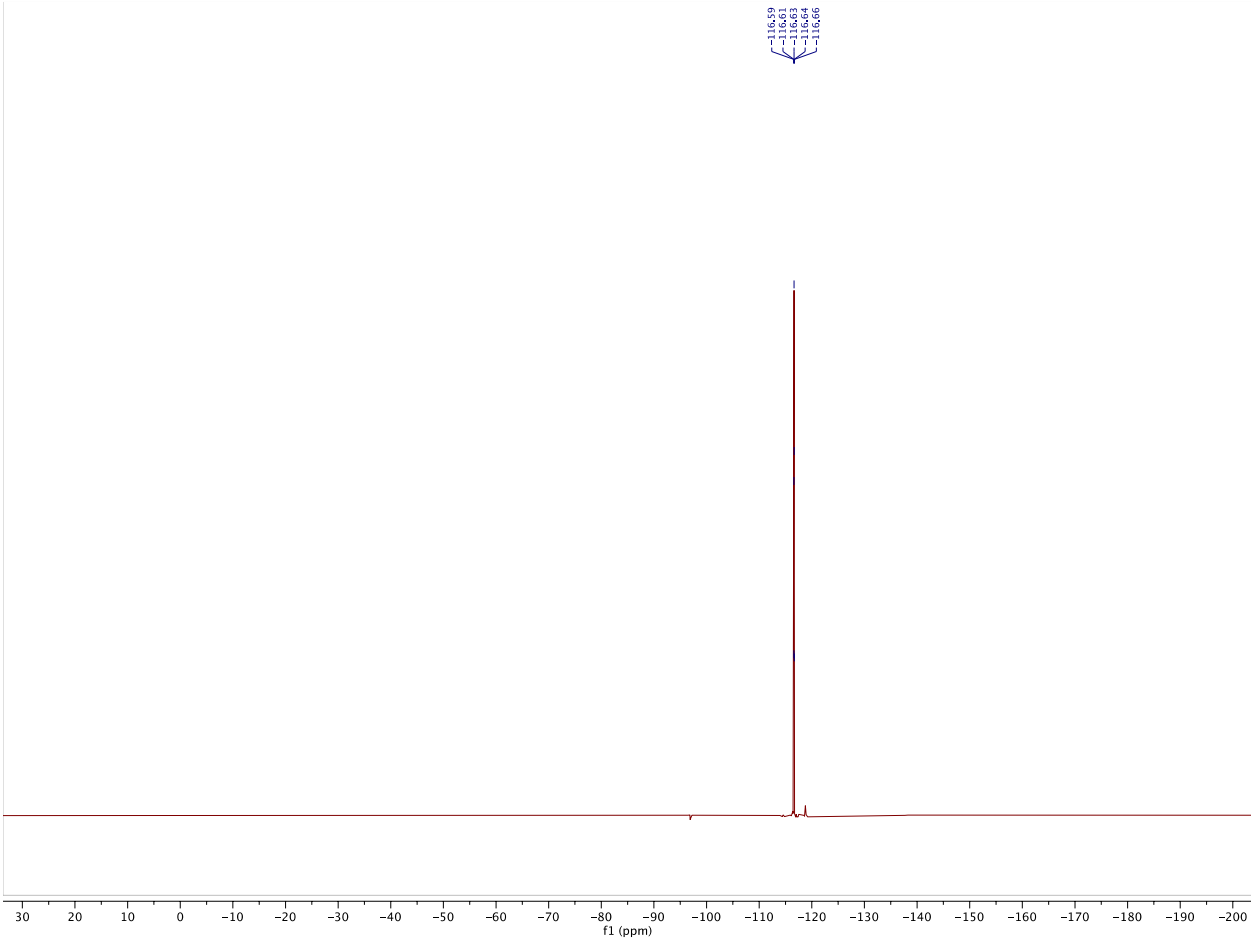

Figure A-20. ^{19}F NMR Spectrum of **2g**.

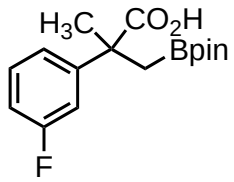

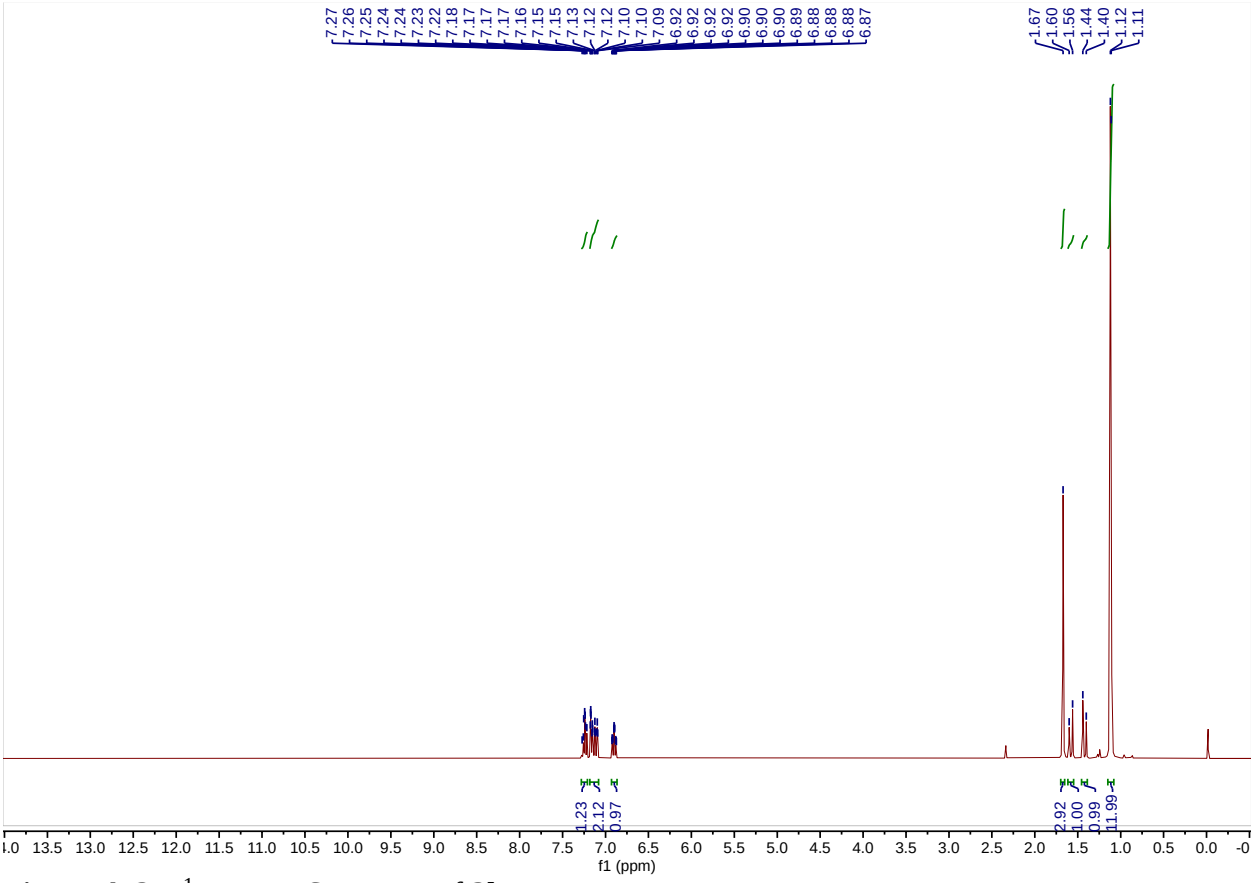

Figure A-21. ^{1}H NMR Spectrum of **2h**.

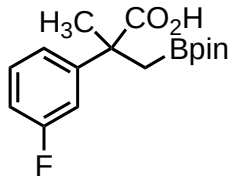

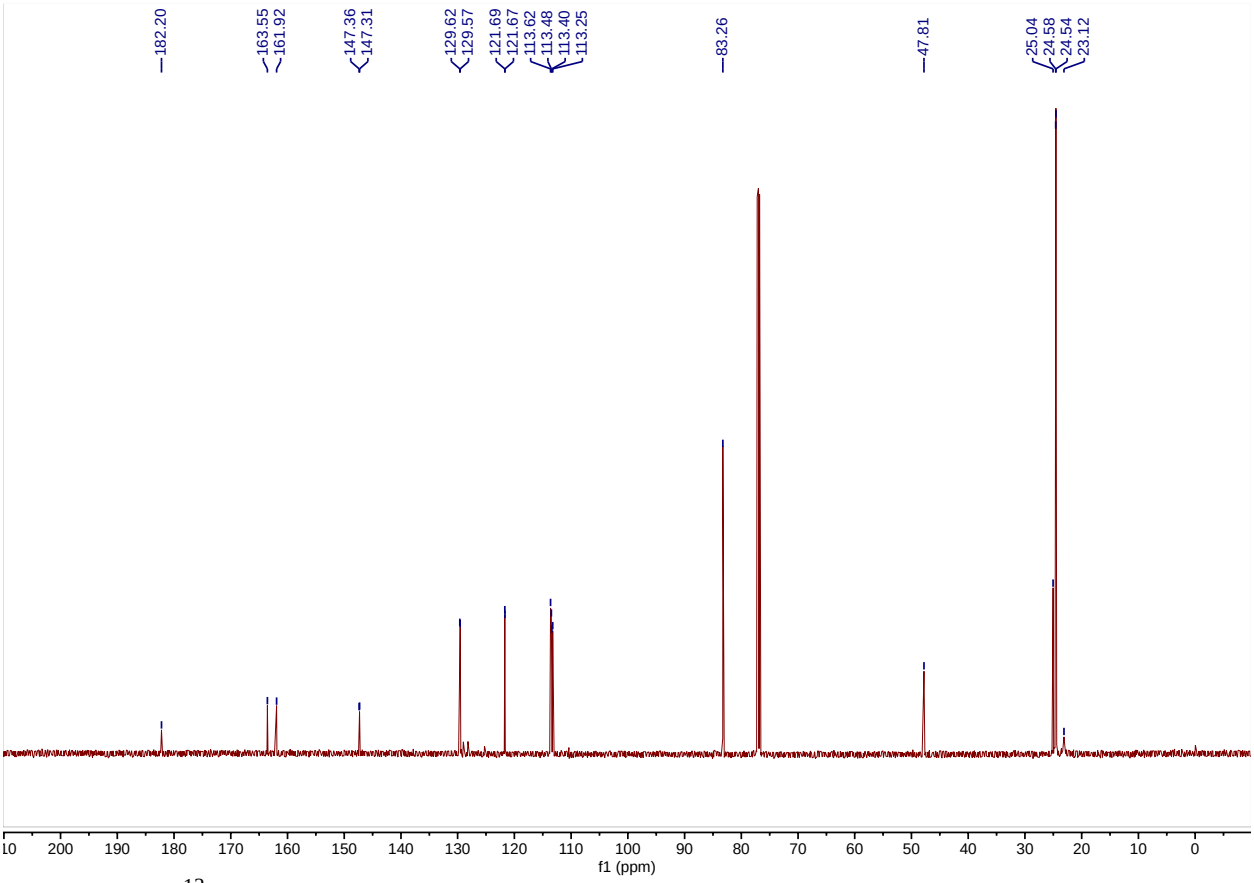

Figure A-22. ^{13}C NMR Spectrum of **2h**.

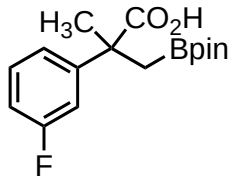

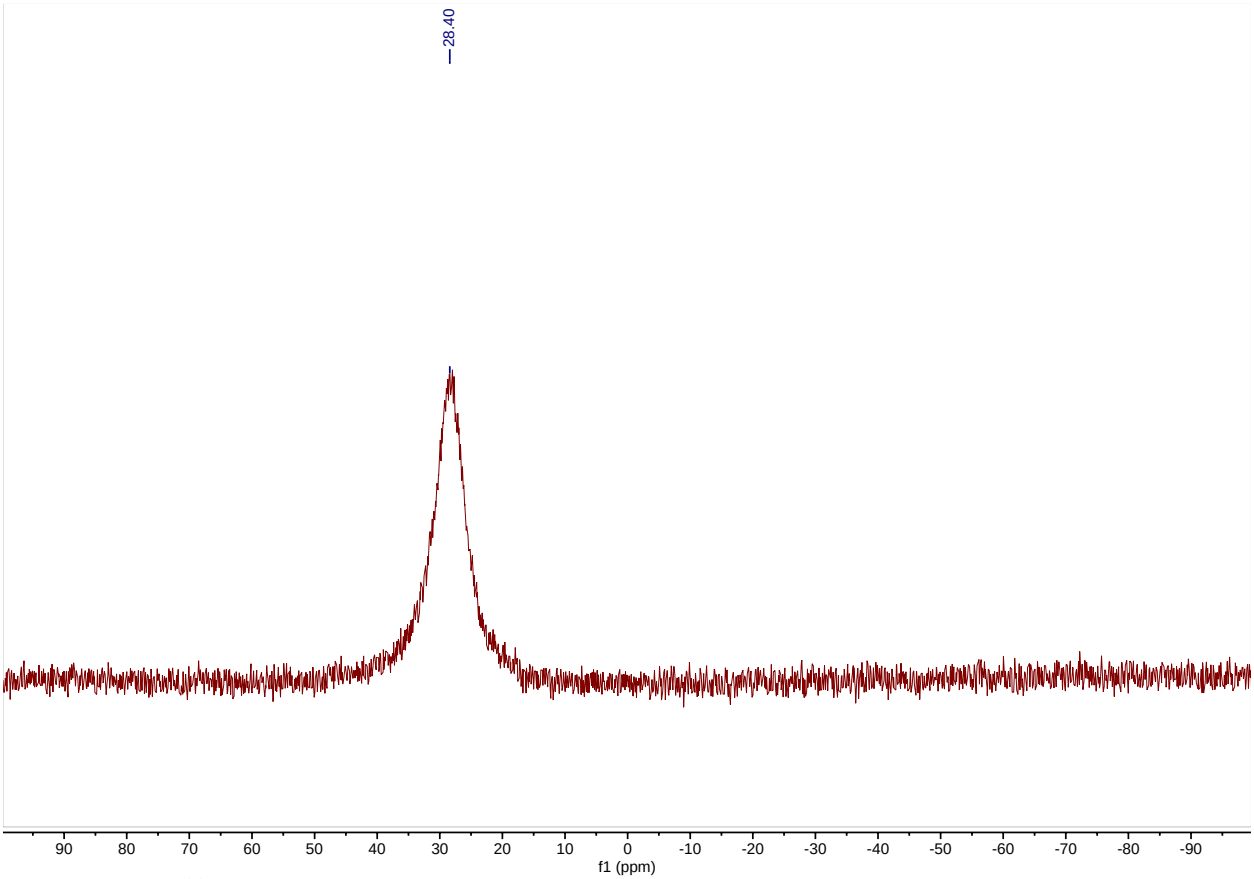

Figure A-23. ^{11}B NMR Spectrum of **2h**.

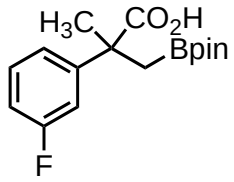

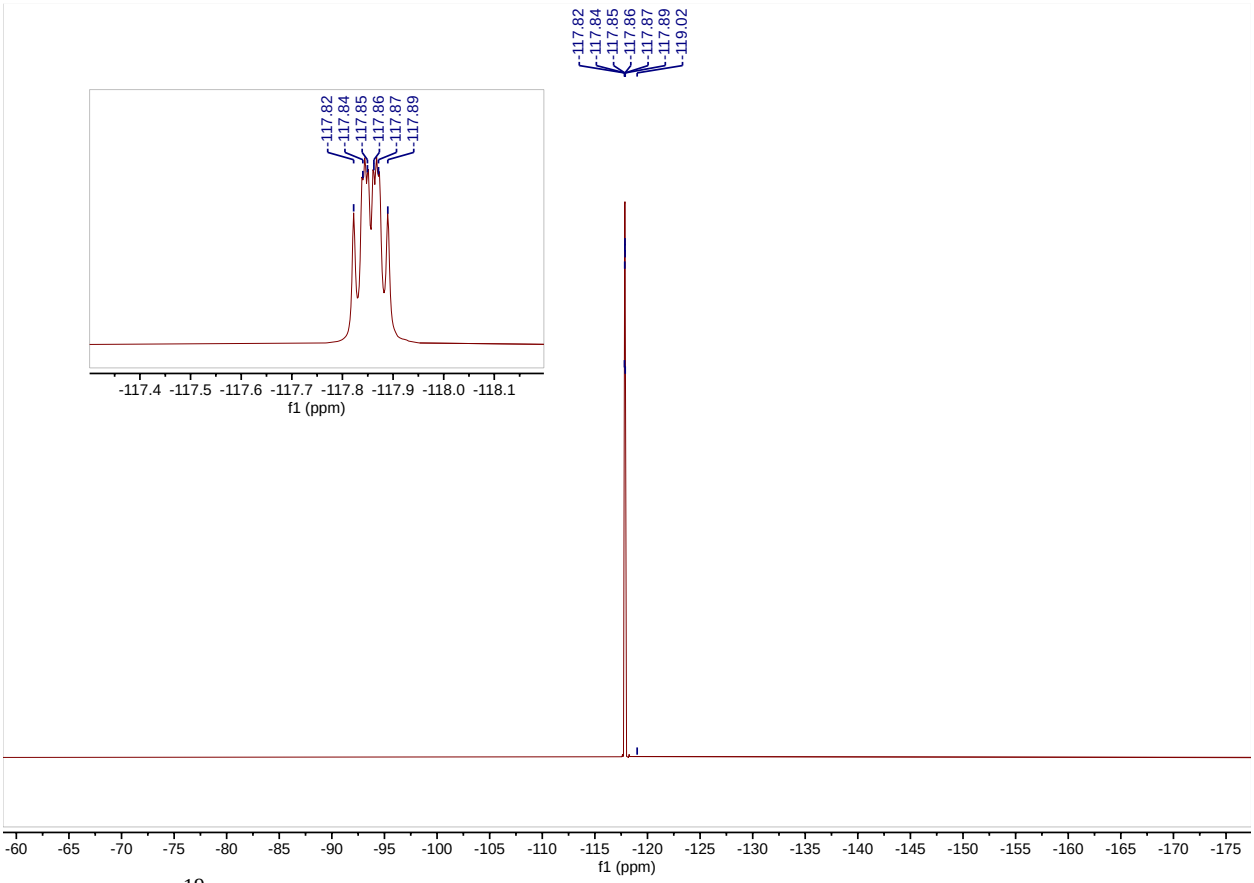

Figure A-24. ^{19}F NMR Spectrum of **2h**.

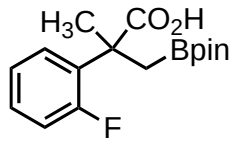

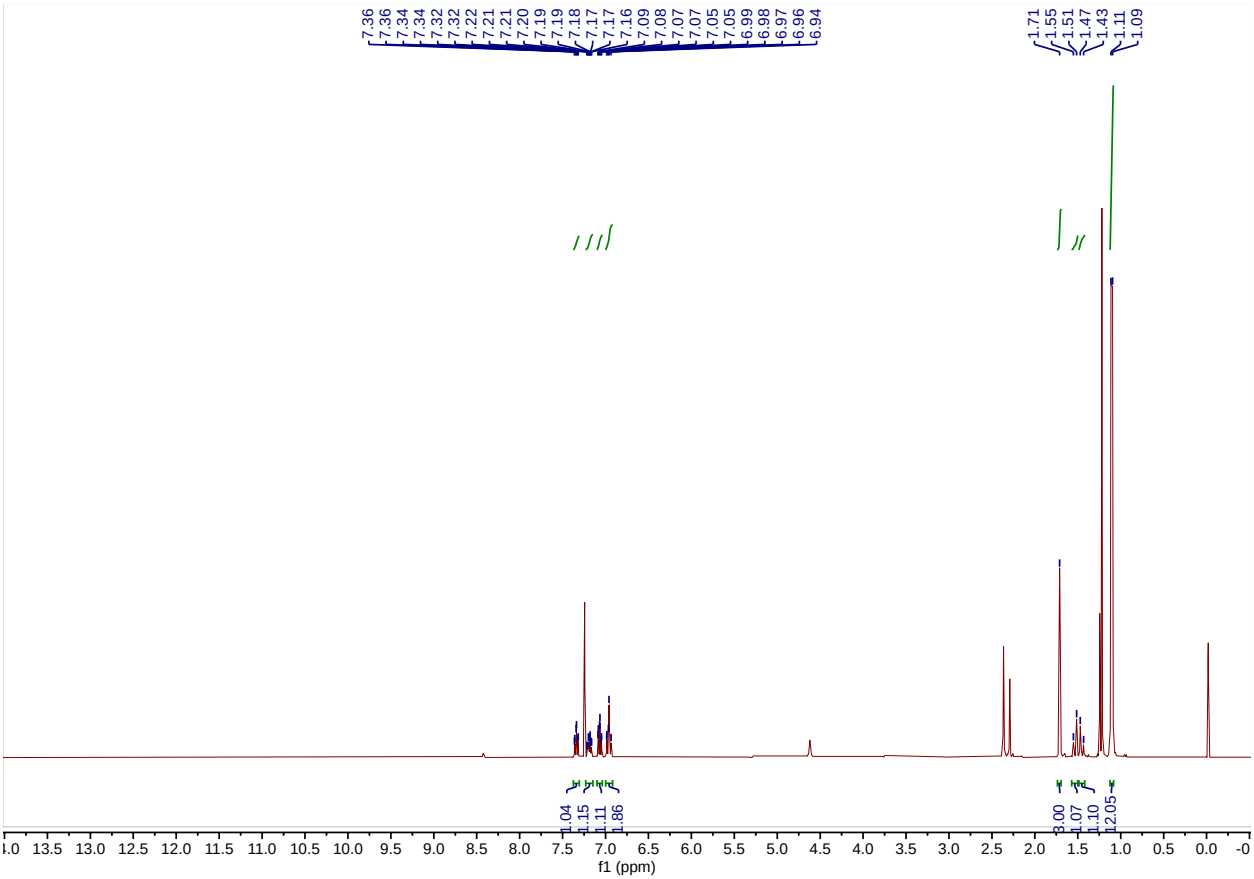

Figure A-25. Crude ^{1}H NMR Spectrum of **2i**.

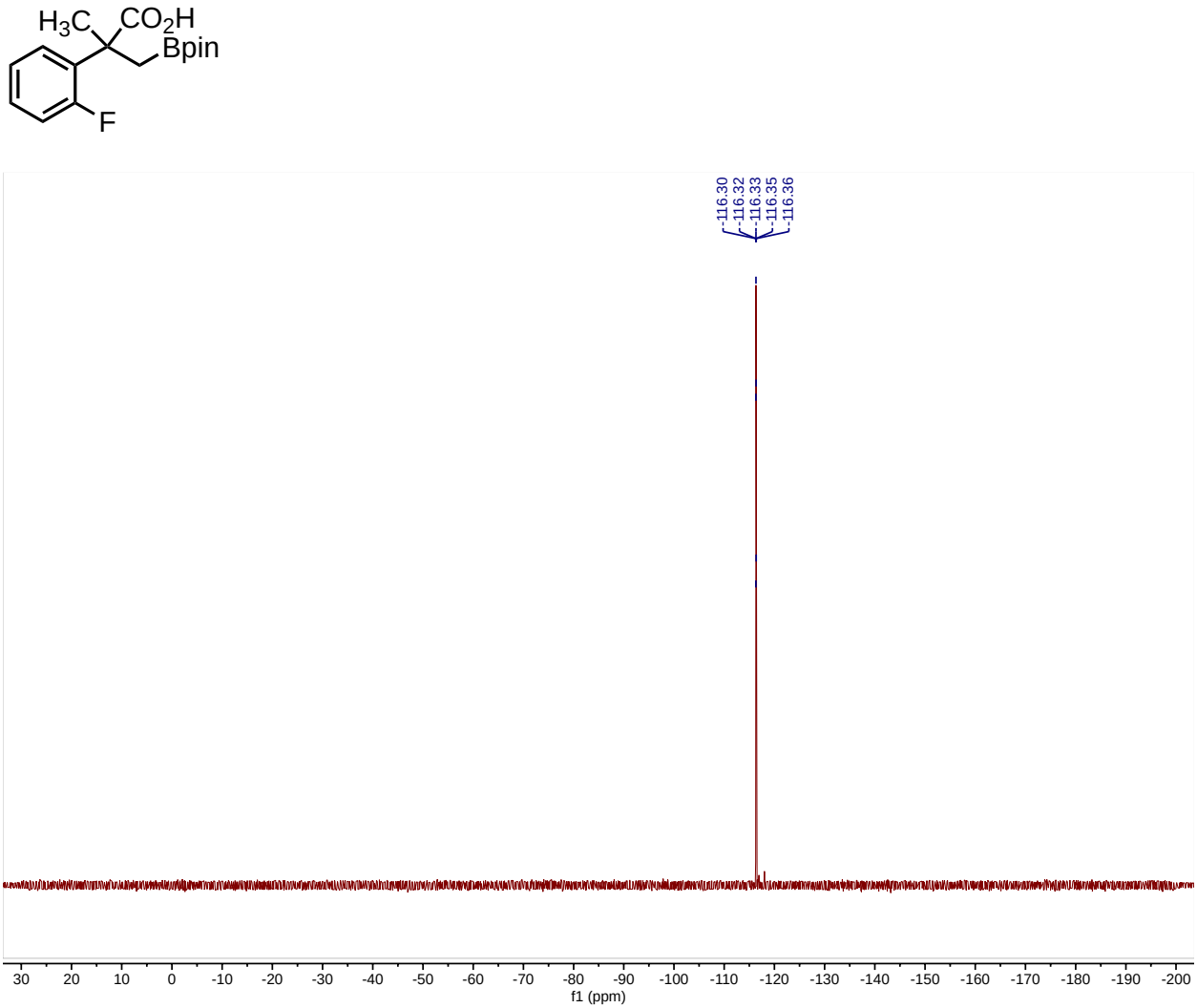

Figure A-26. Crude ^{19}F NMR Spectrum of **2i**.

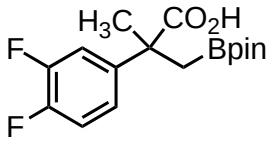

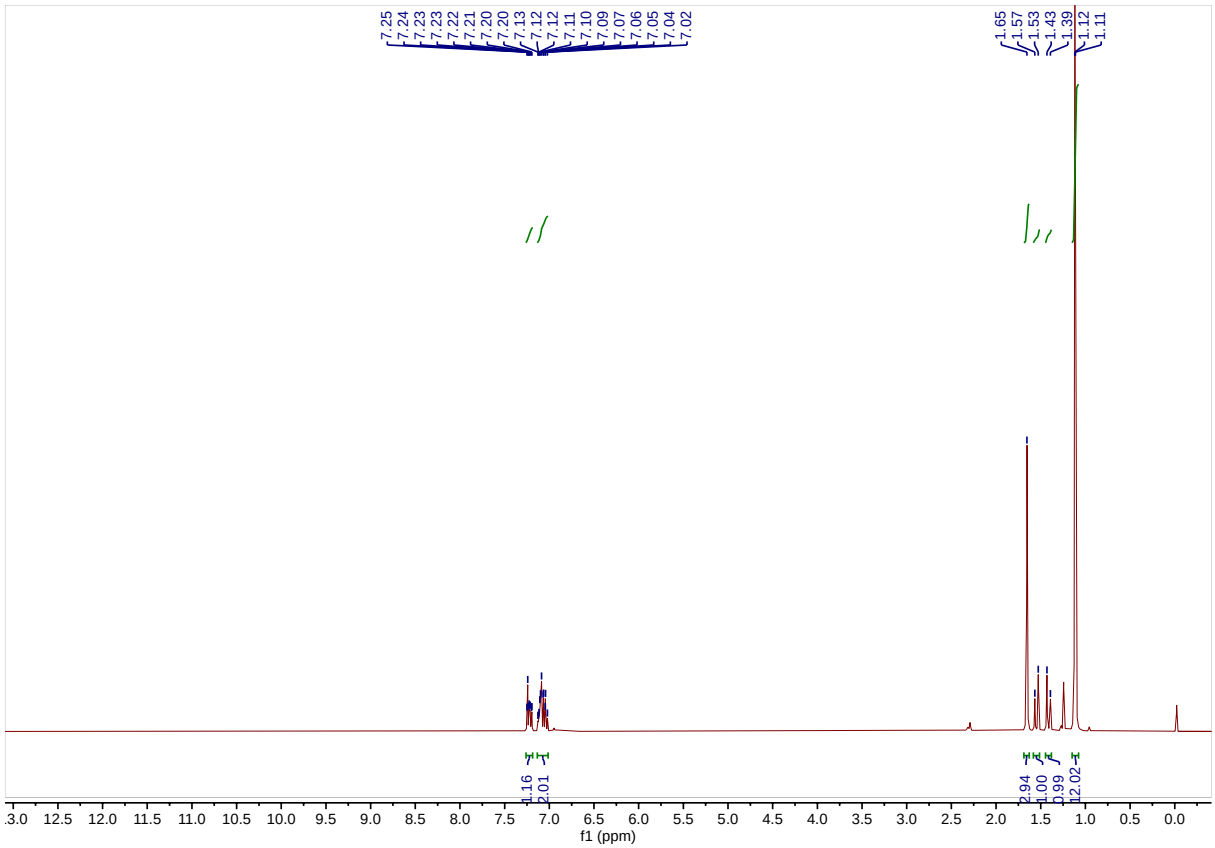

Figure A-27. ^{1}H NMR Spectrum of **2j**.

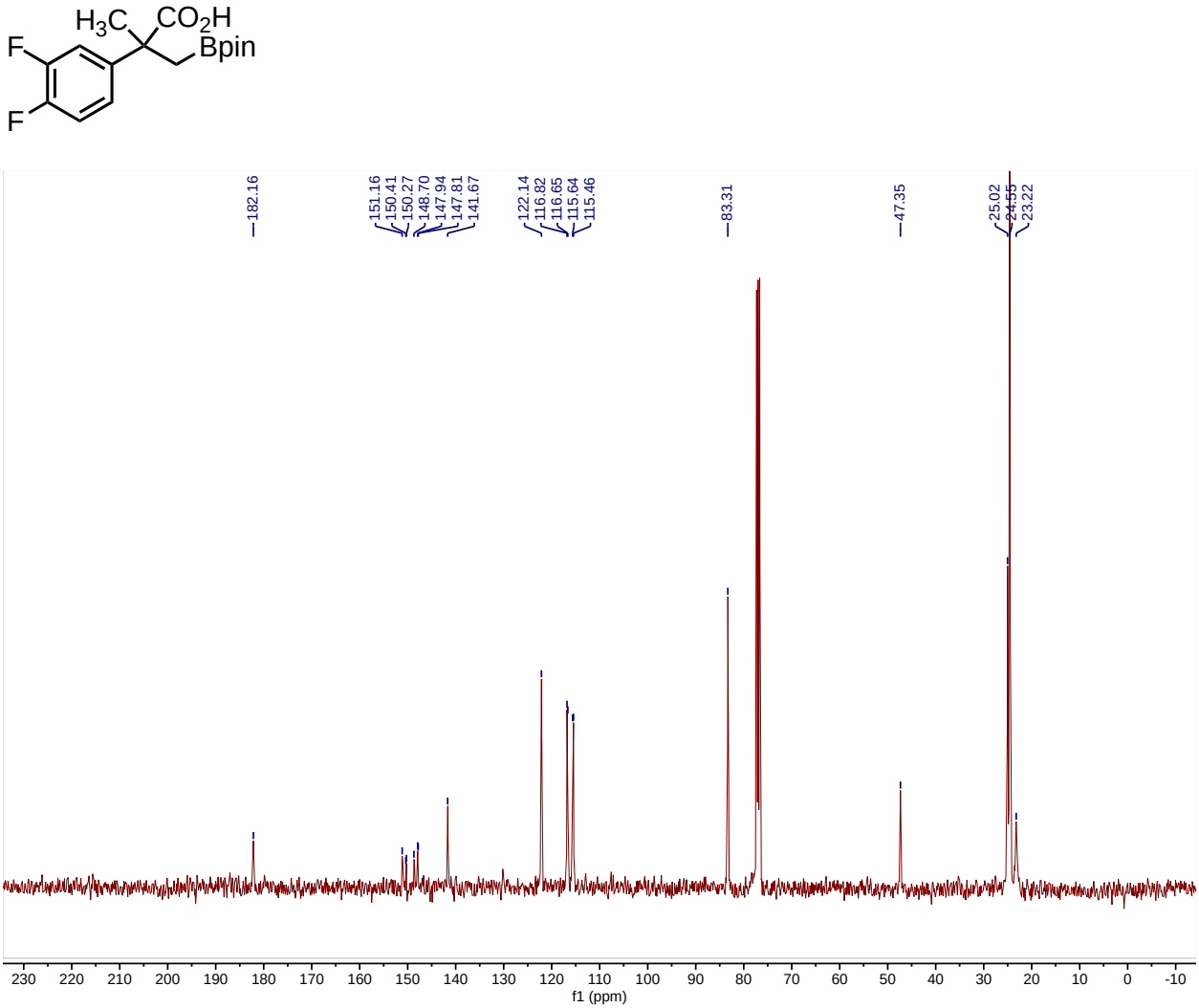

Figure A-28. ^{13}C NMR Spectrum of **2j**.

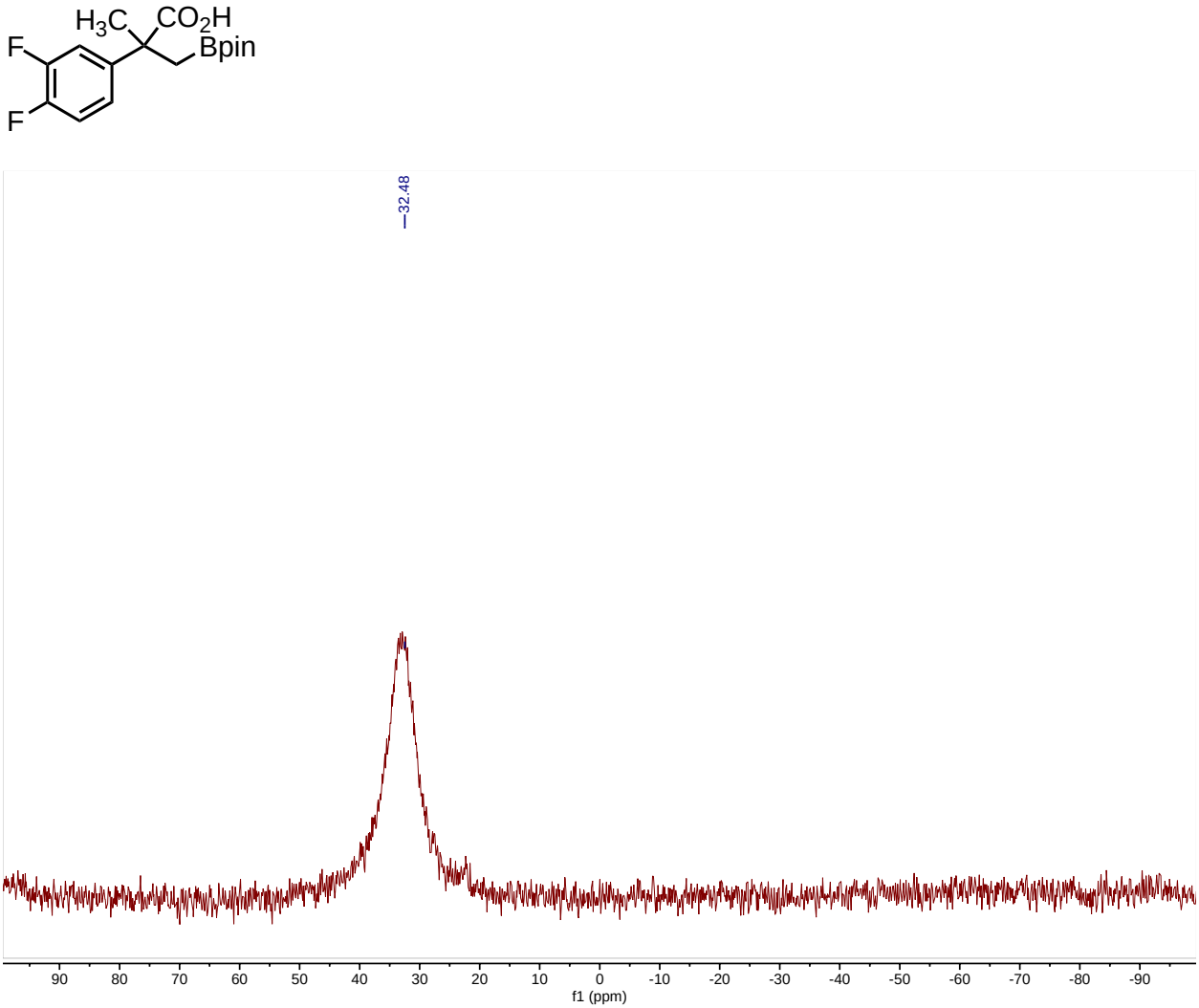

Figure A-29. ^{11}B NMR Spectrum of **2j**.

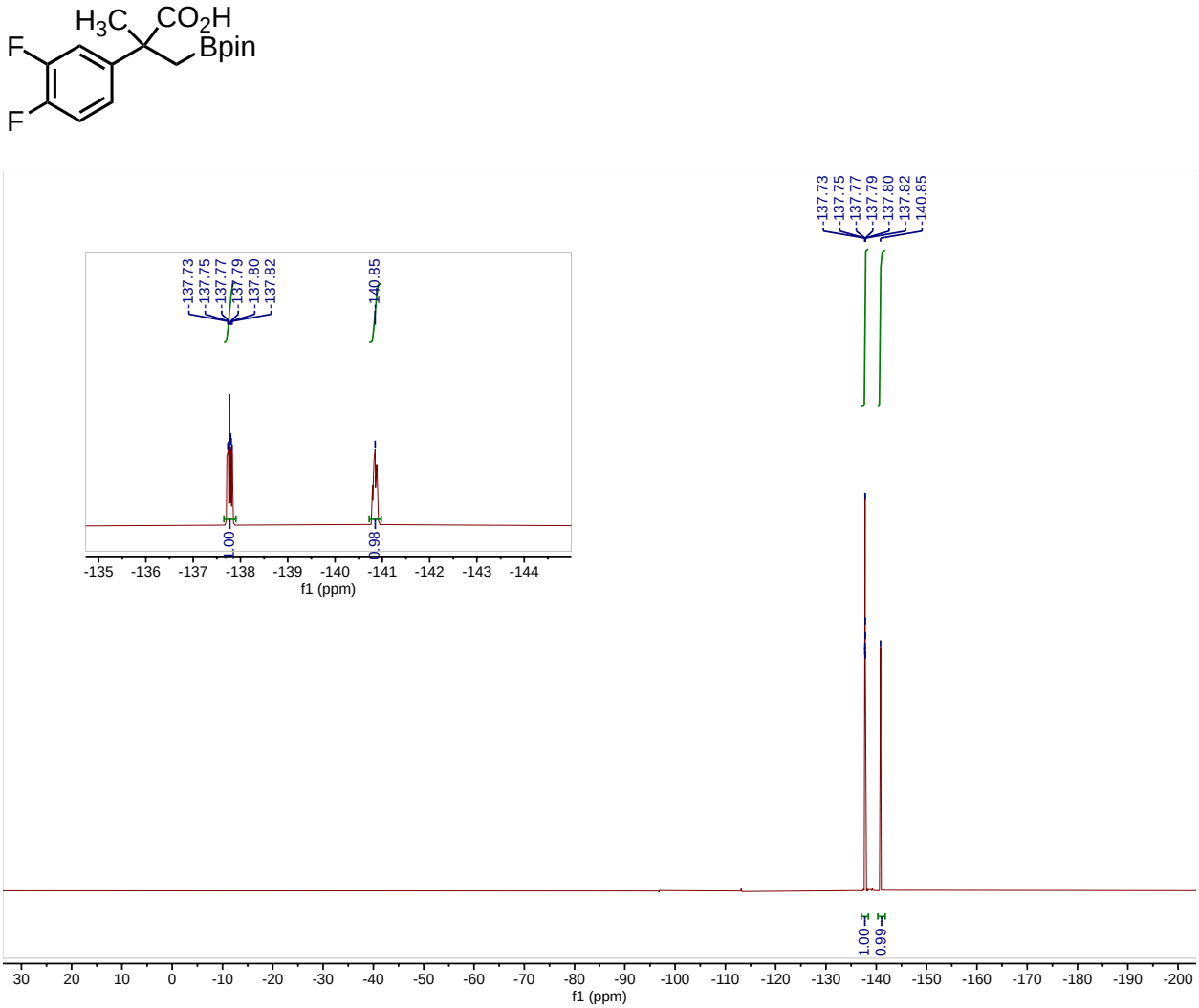

Figure A-30. ^{19}F NMR Spectrum of **2j**.

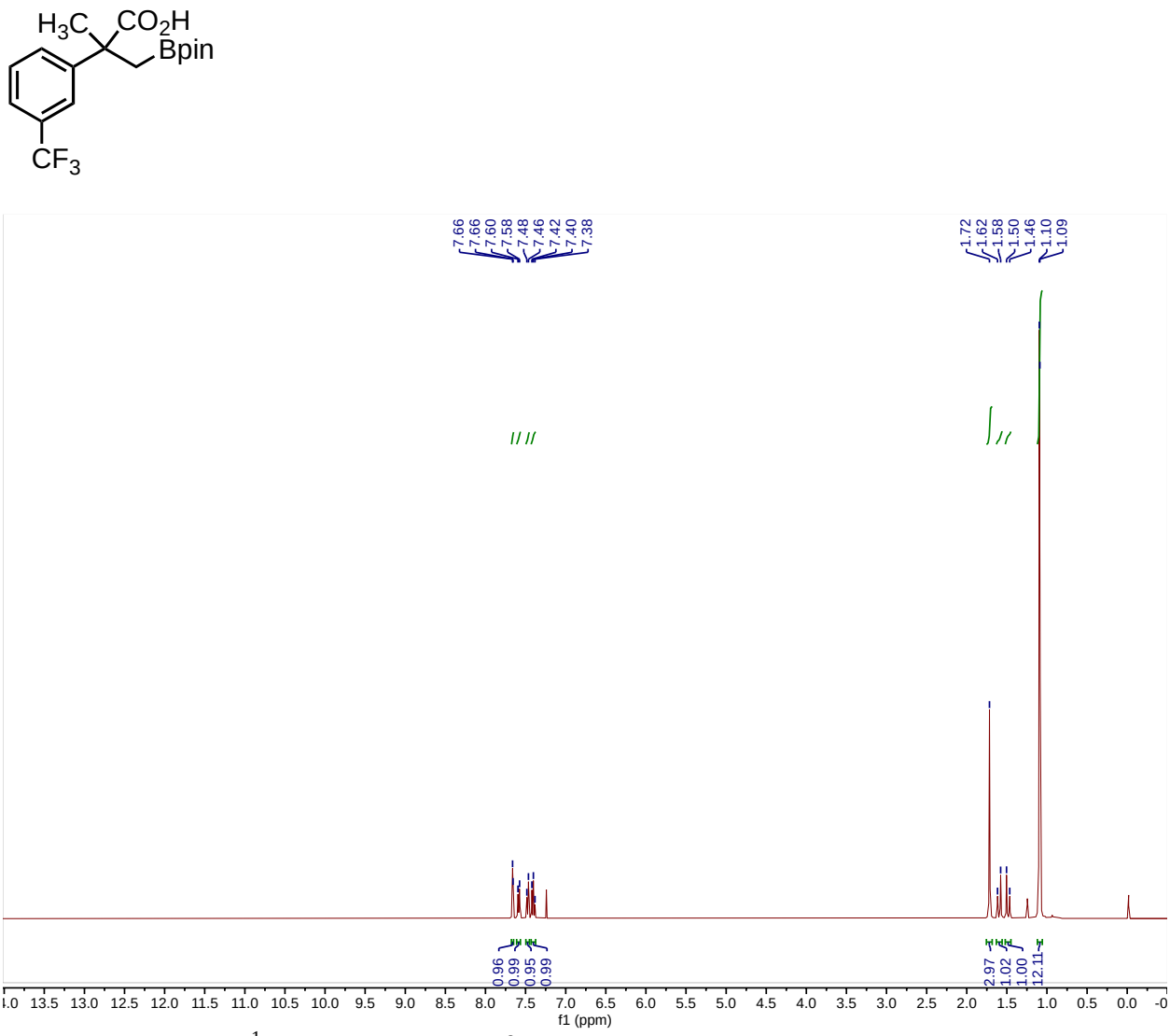

Figure A-31. Crude ^{1}H NMR Spectrum of **2k**.

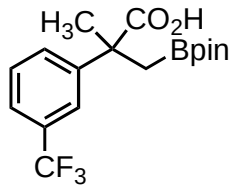

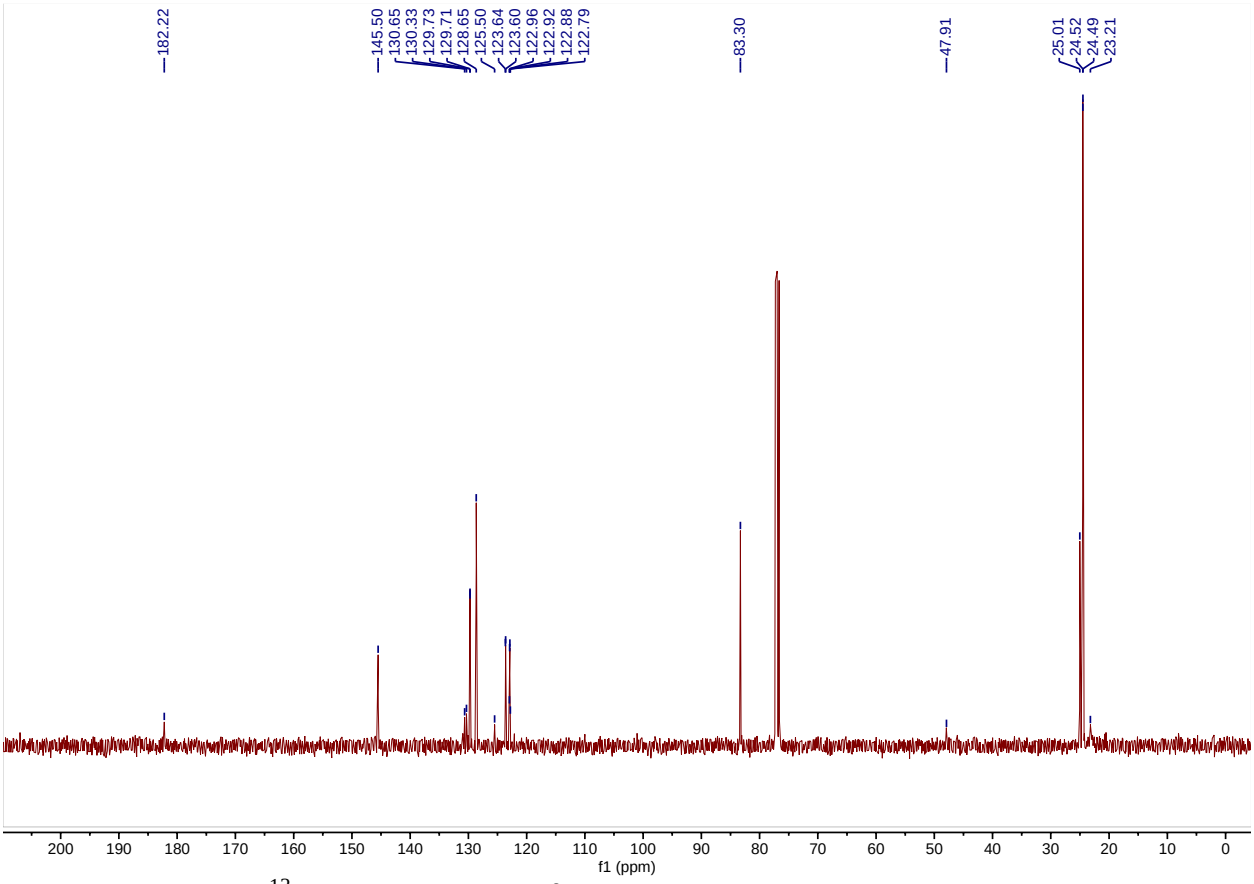

Figure A-32. Crude ^{13}C NMR Spectrum of **2k**.

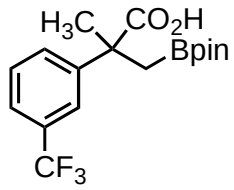

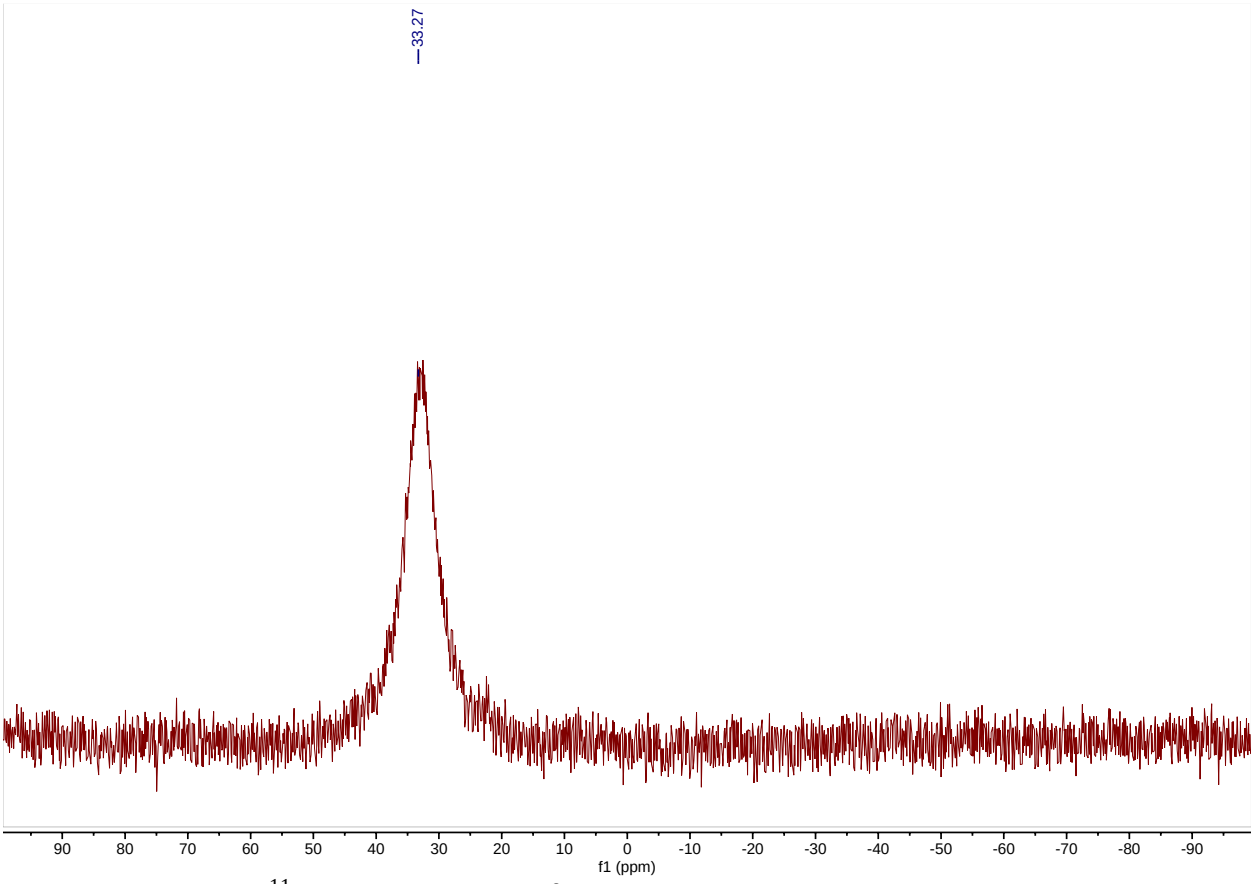

Figure A-33. Crude ^{11}B NMR Spectrum of **2k**.

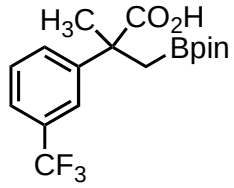

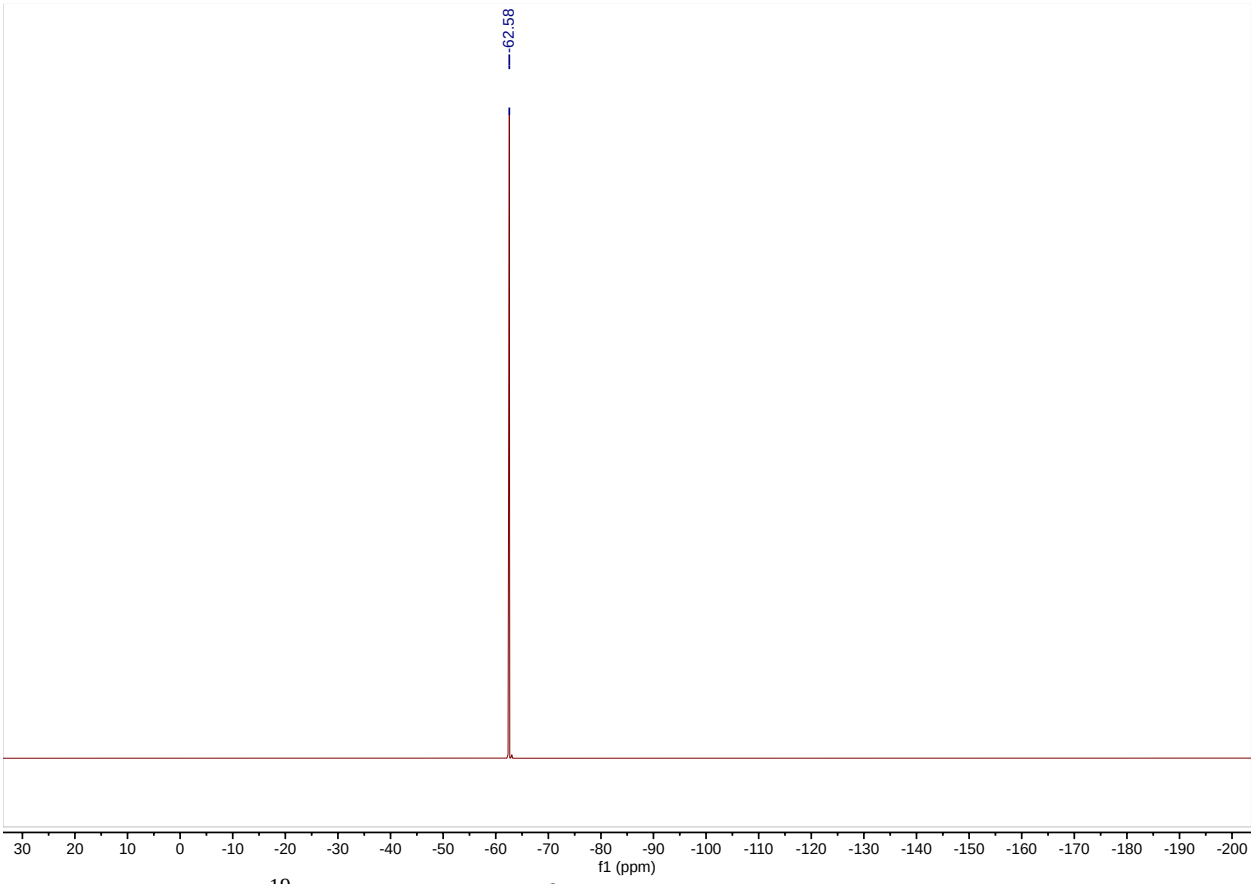

Figure A-34. Crude ^{19}F NMR Spectrum of **2k**.

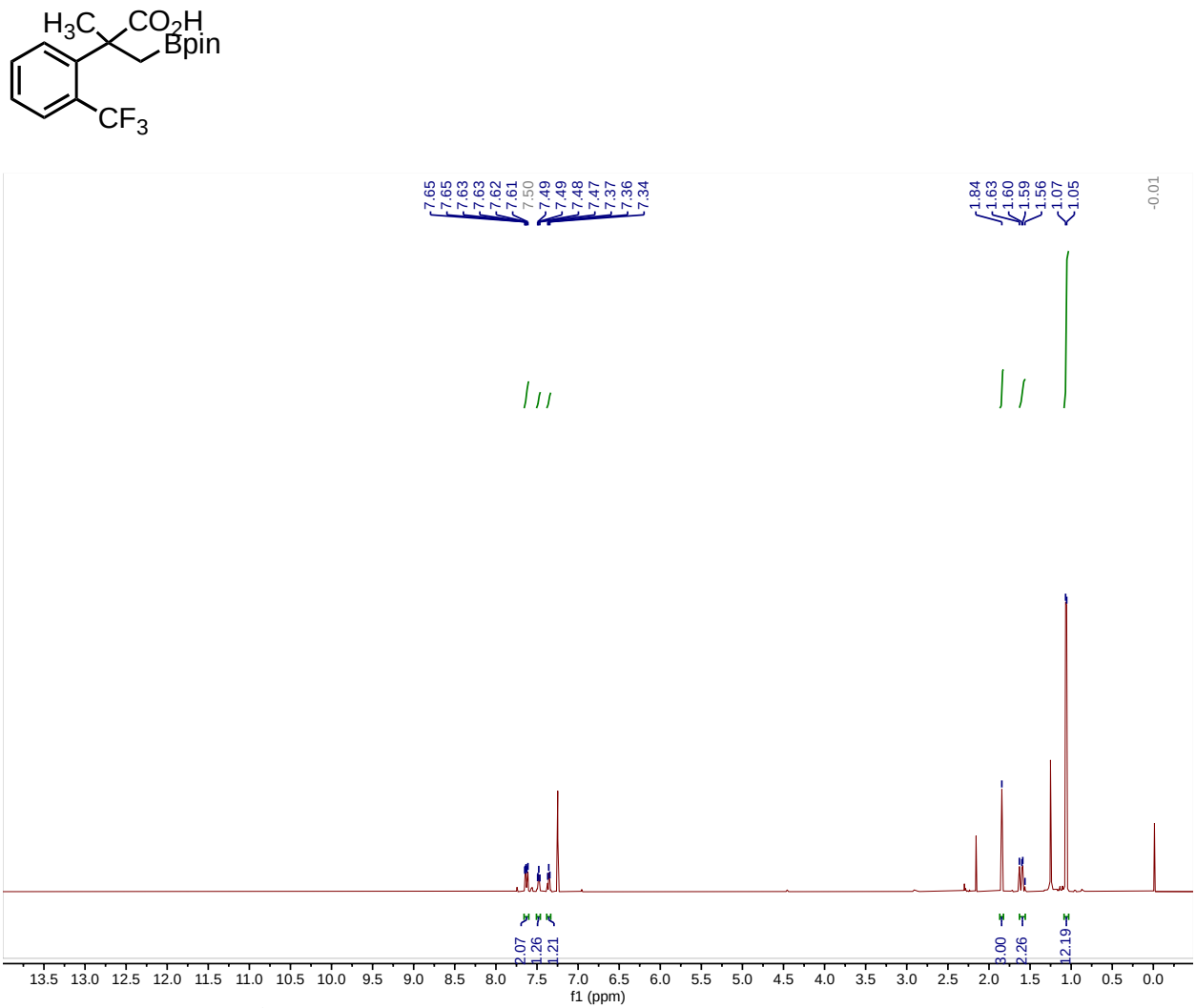

Figure A-35. Crude ^{1}H NMR Spectrum of **2l**.

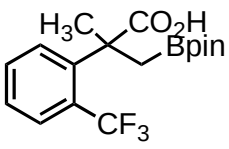

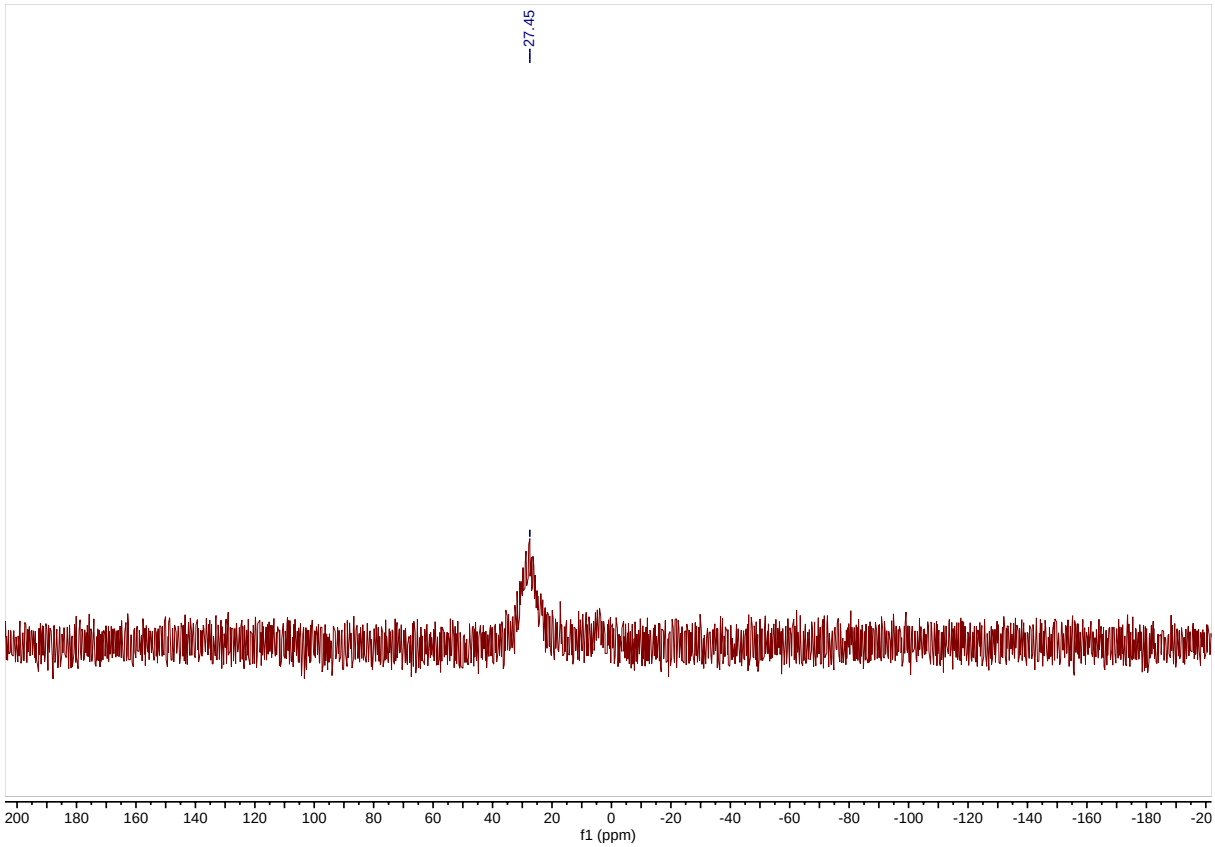

Figure A-36. Crude ^{11}B NMR Spectrum of **2l**.

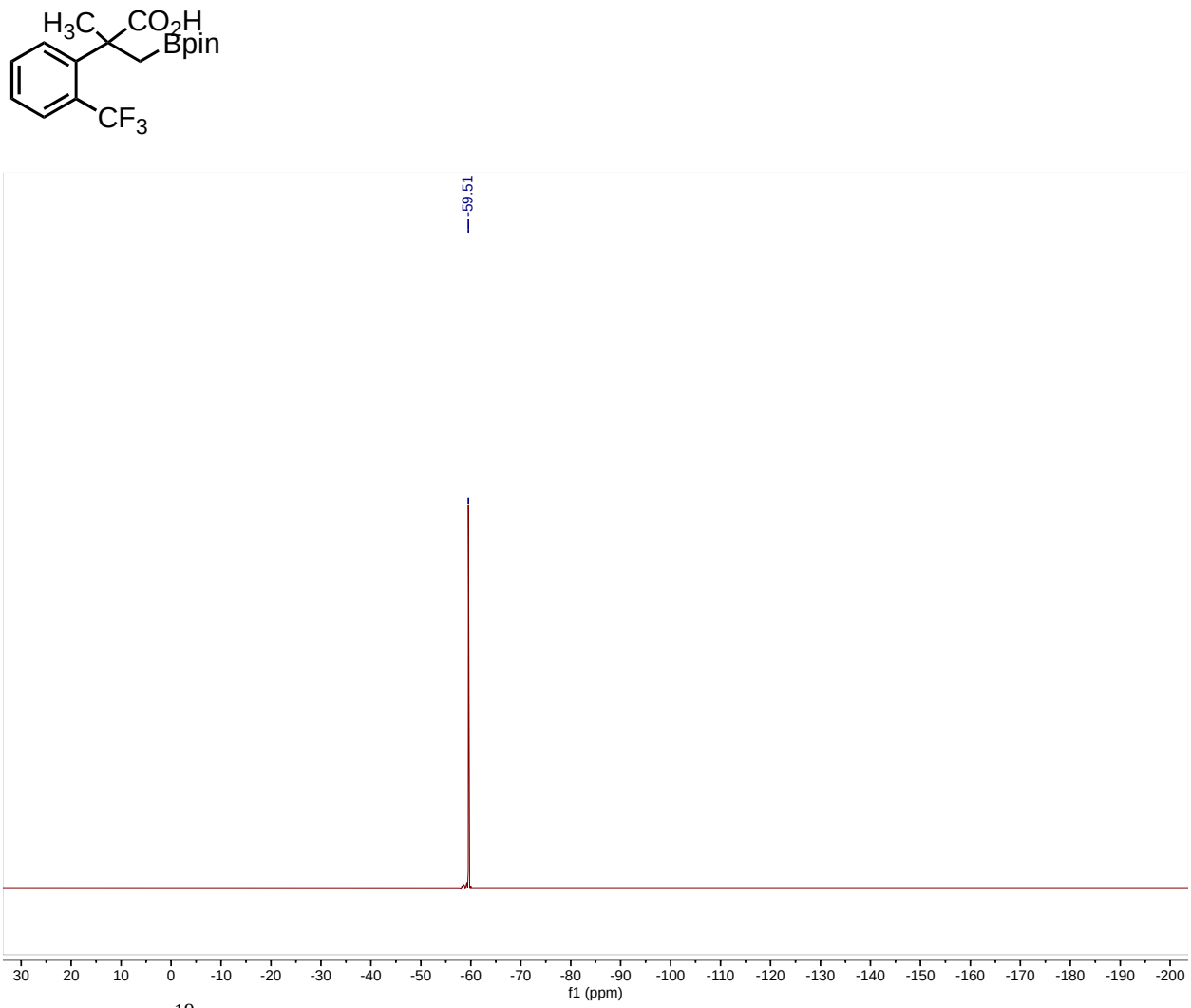

Figure A-37. ^{19}F NMR Spectrum of **2l**.

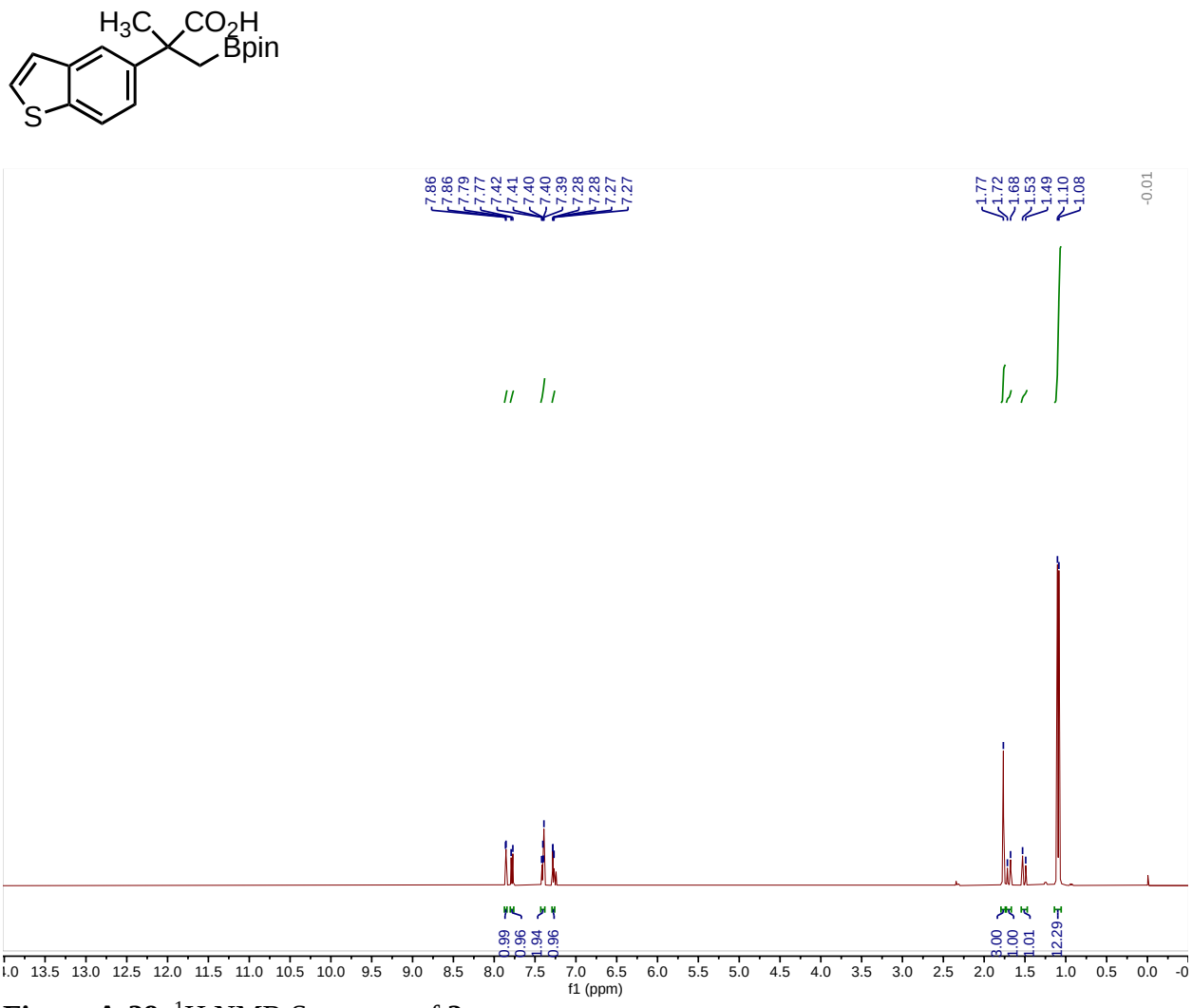

Figure A-38. ^{1}H NMR Spectrum of **2m**.

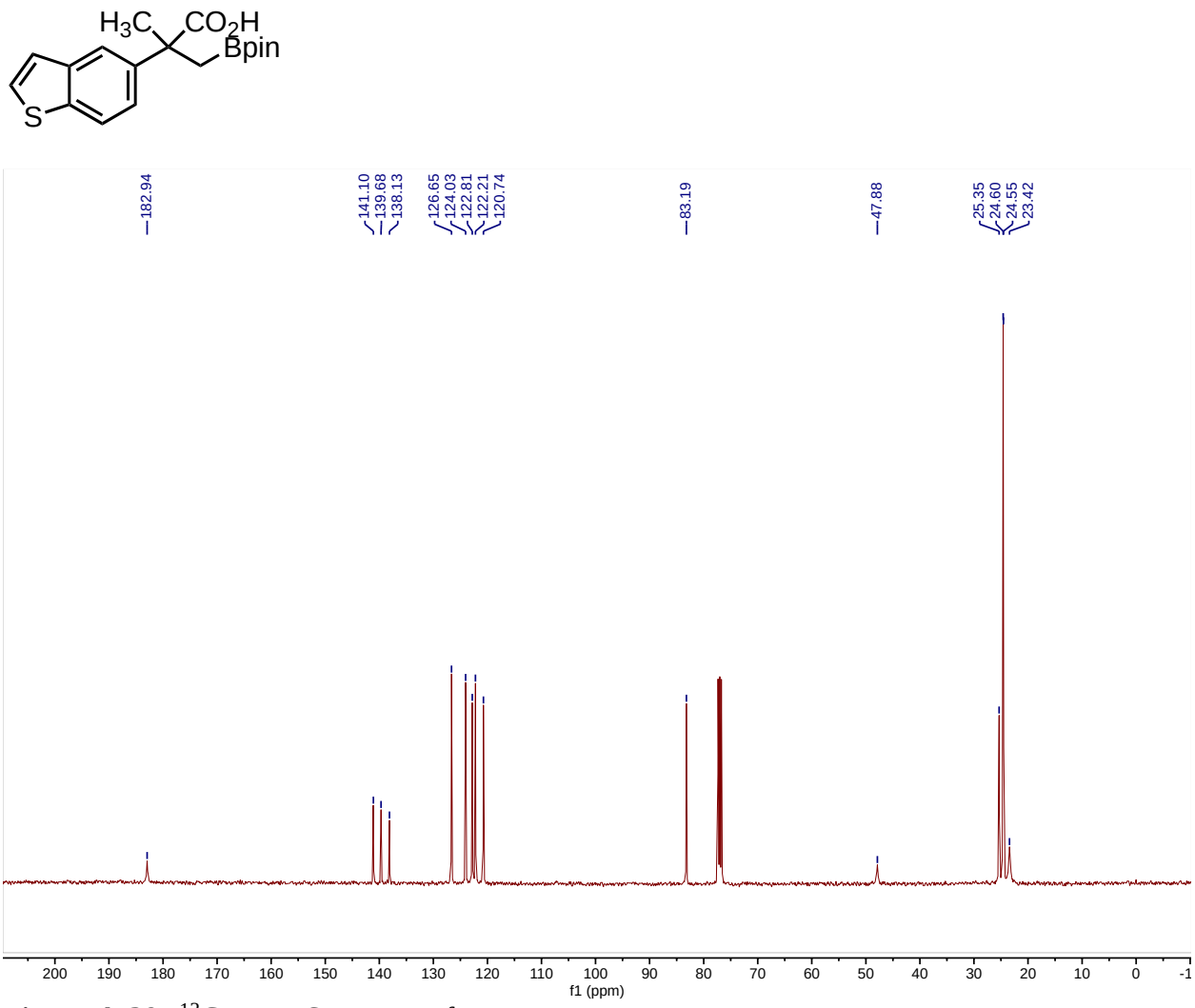

Figure A-39. ^{13}C NMR Spectrum of **1m**.

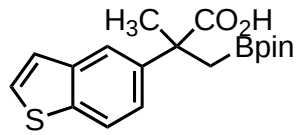

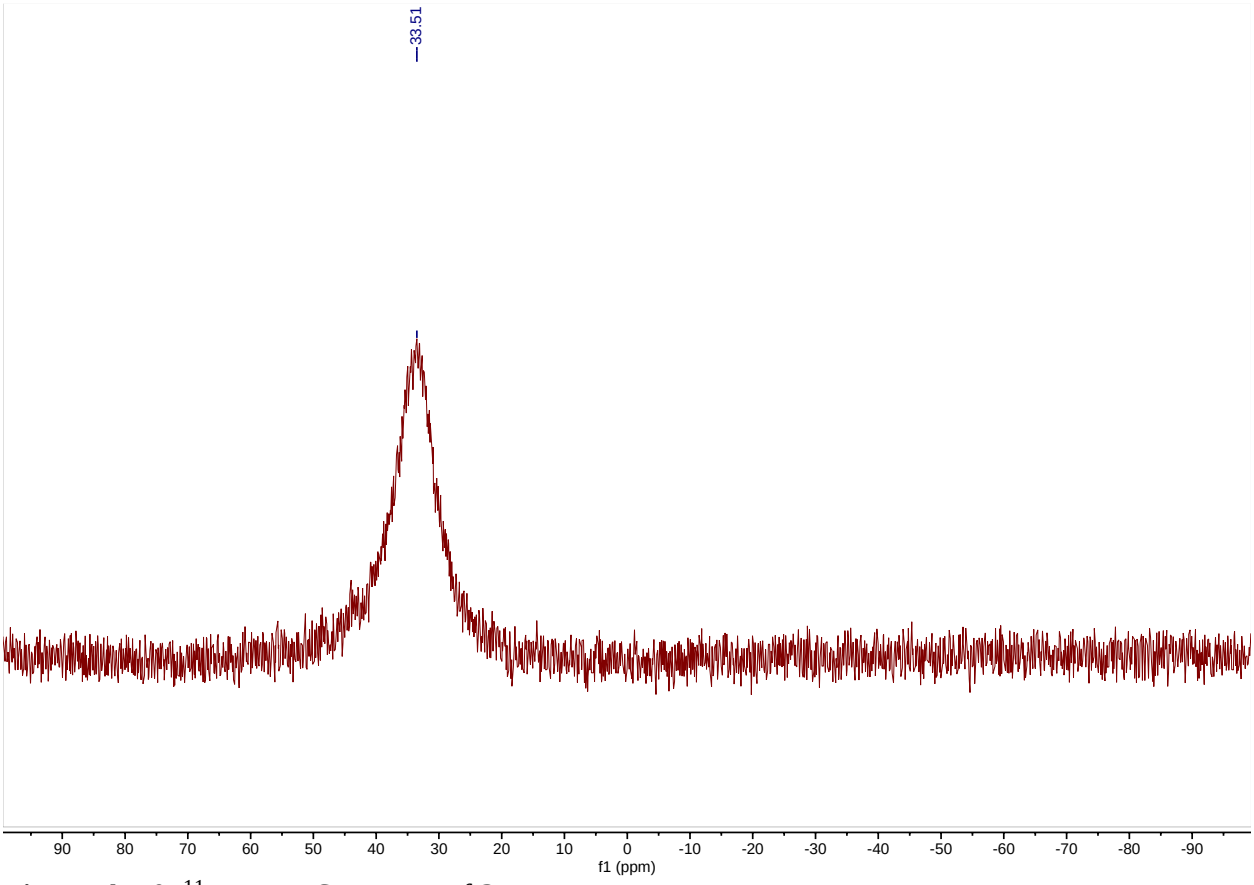

Figure A-40. ^{11}B NMR Spectrum of **2m**.

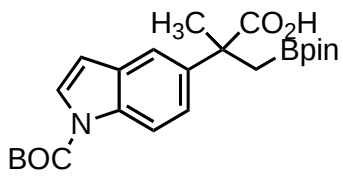

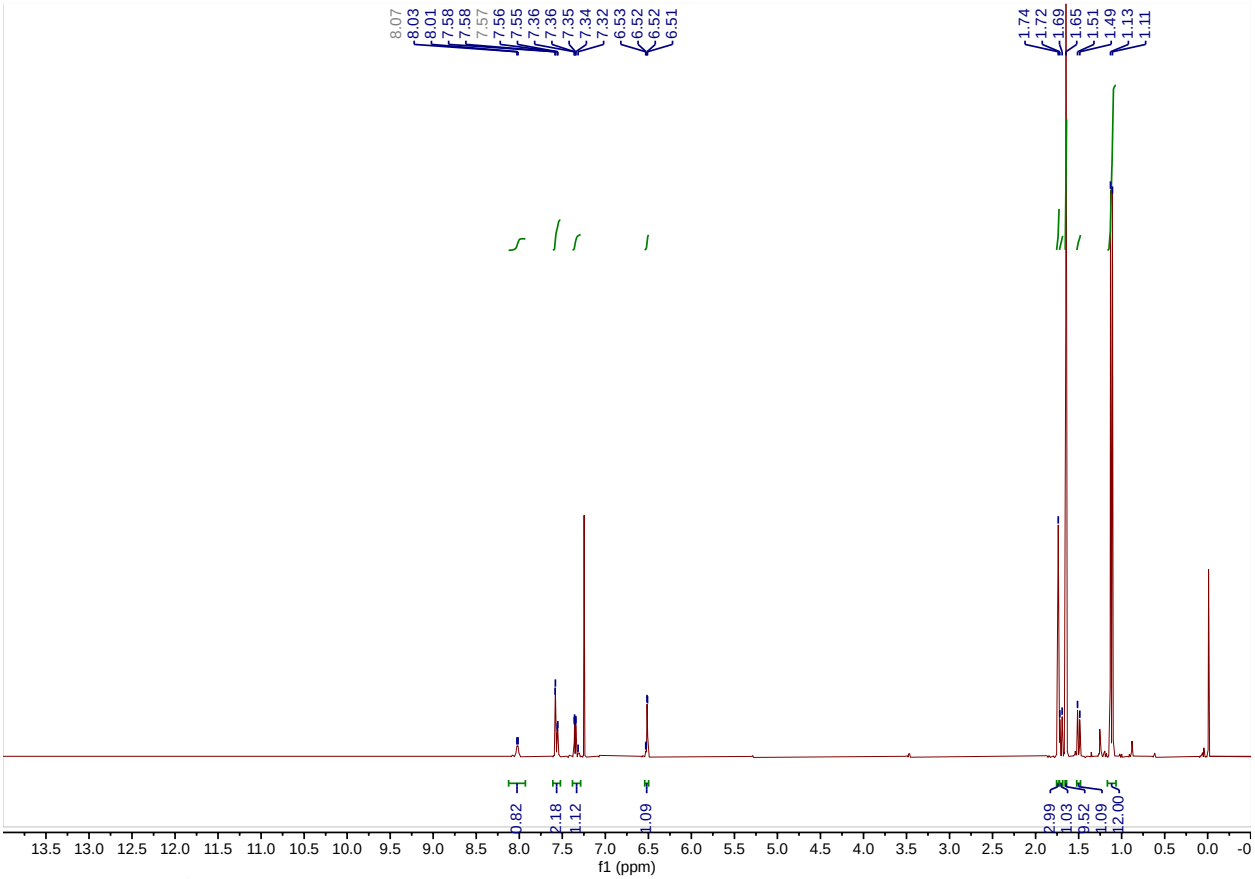

Figure A-41. ^{1}H NMR Spectrum of **2n**.

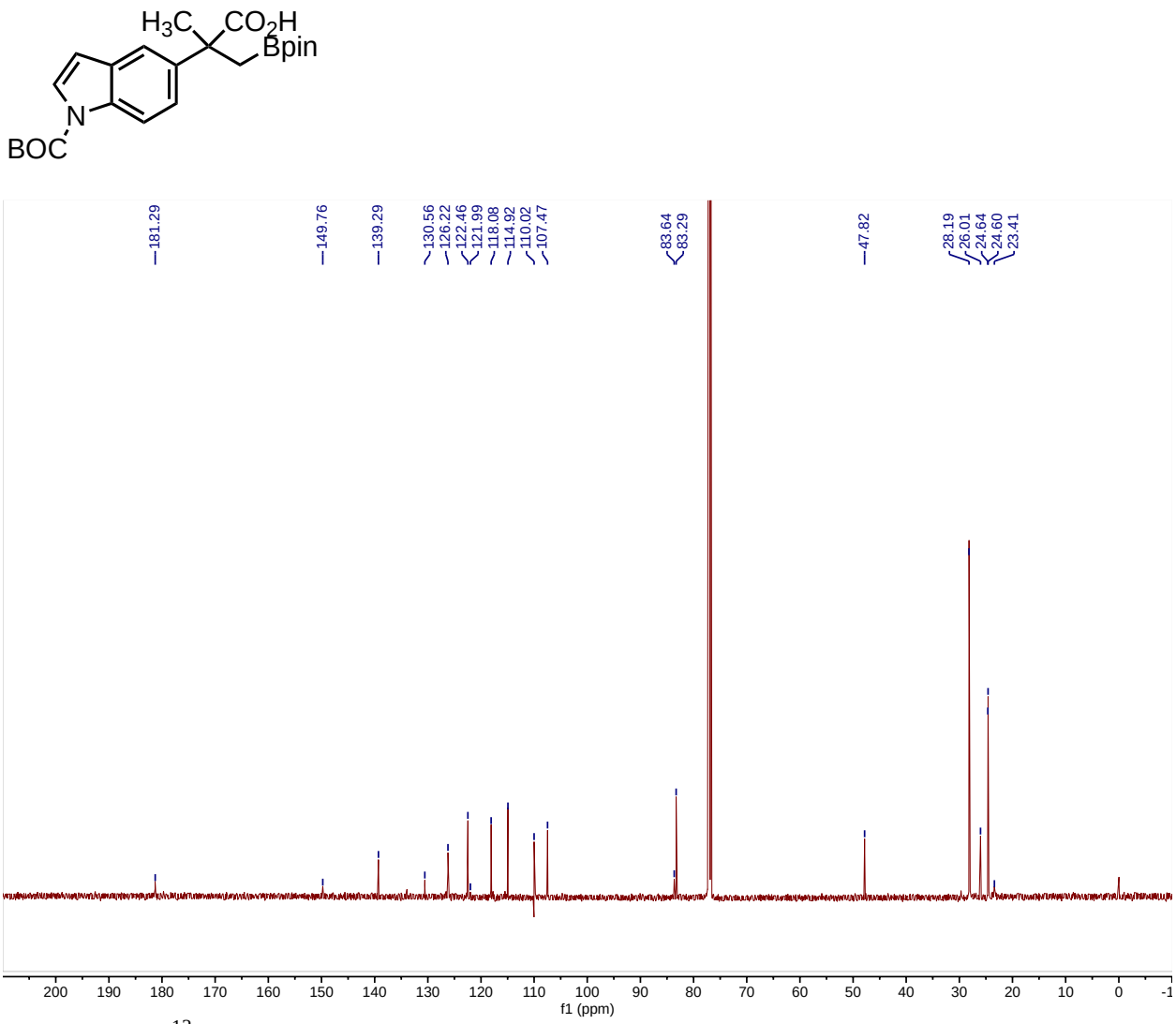

Figure A-42. ^{13}C NMR Spectrum of **2n**.

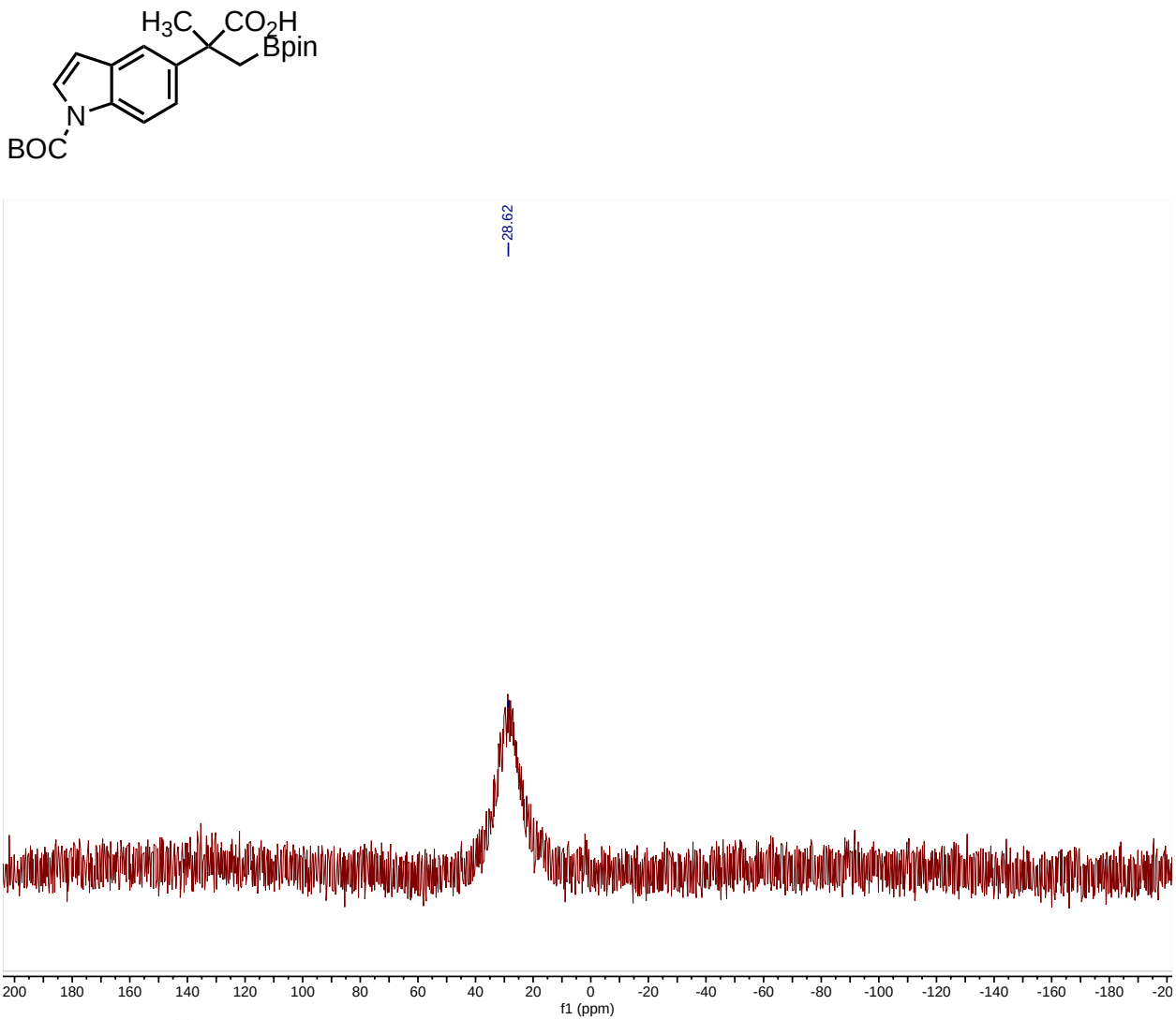

Figure A-43. ^{11}B NMR Spectrum of **2n**.

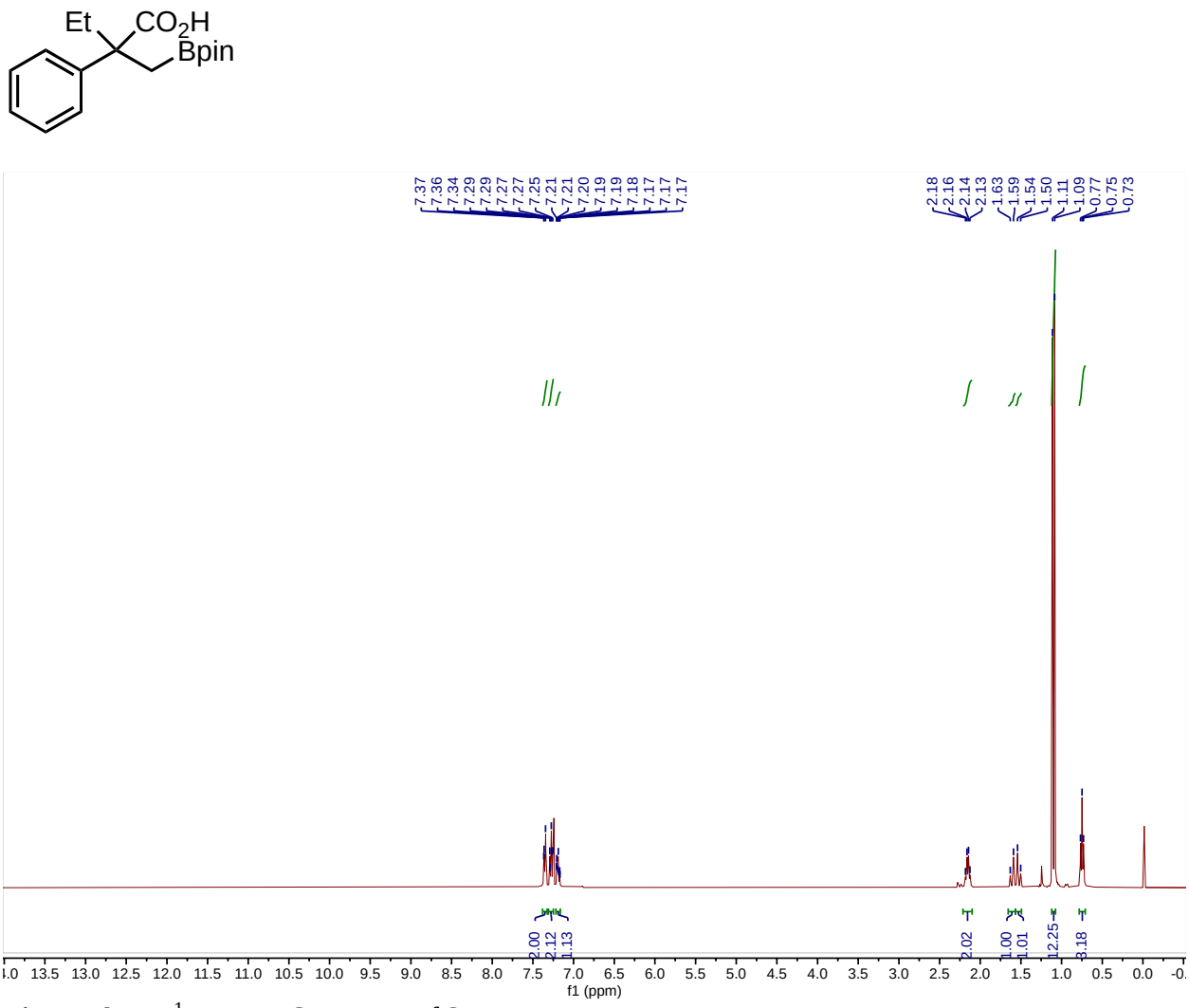

Figure A-44. ^{1}H NMR Spectrum of **2o**.

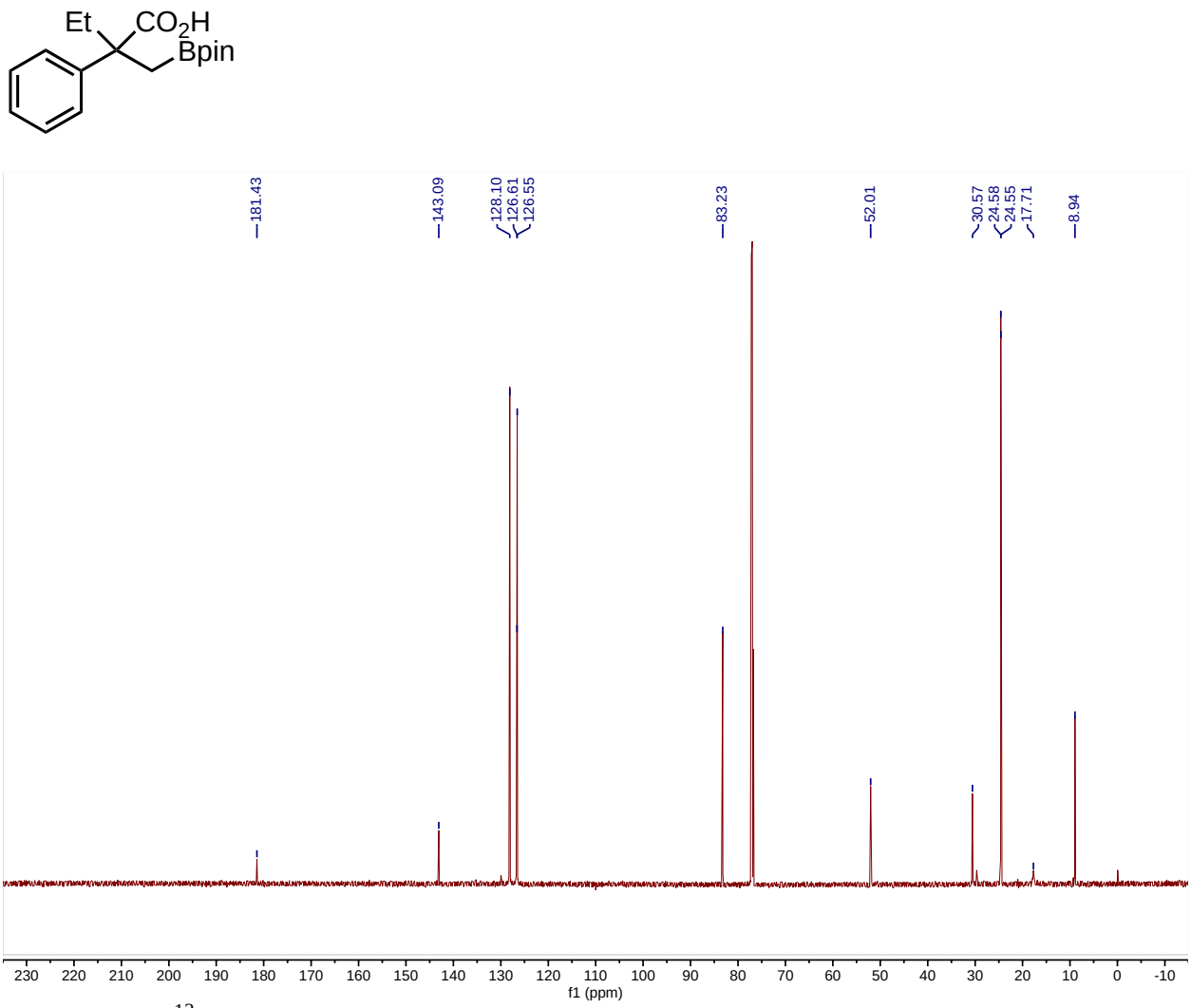

Figure A-45. ^{13}C NMR Spectrum of **2o**.

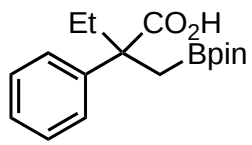

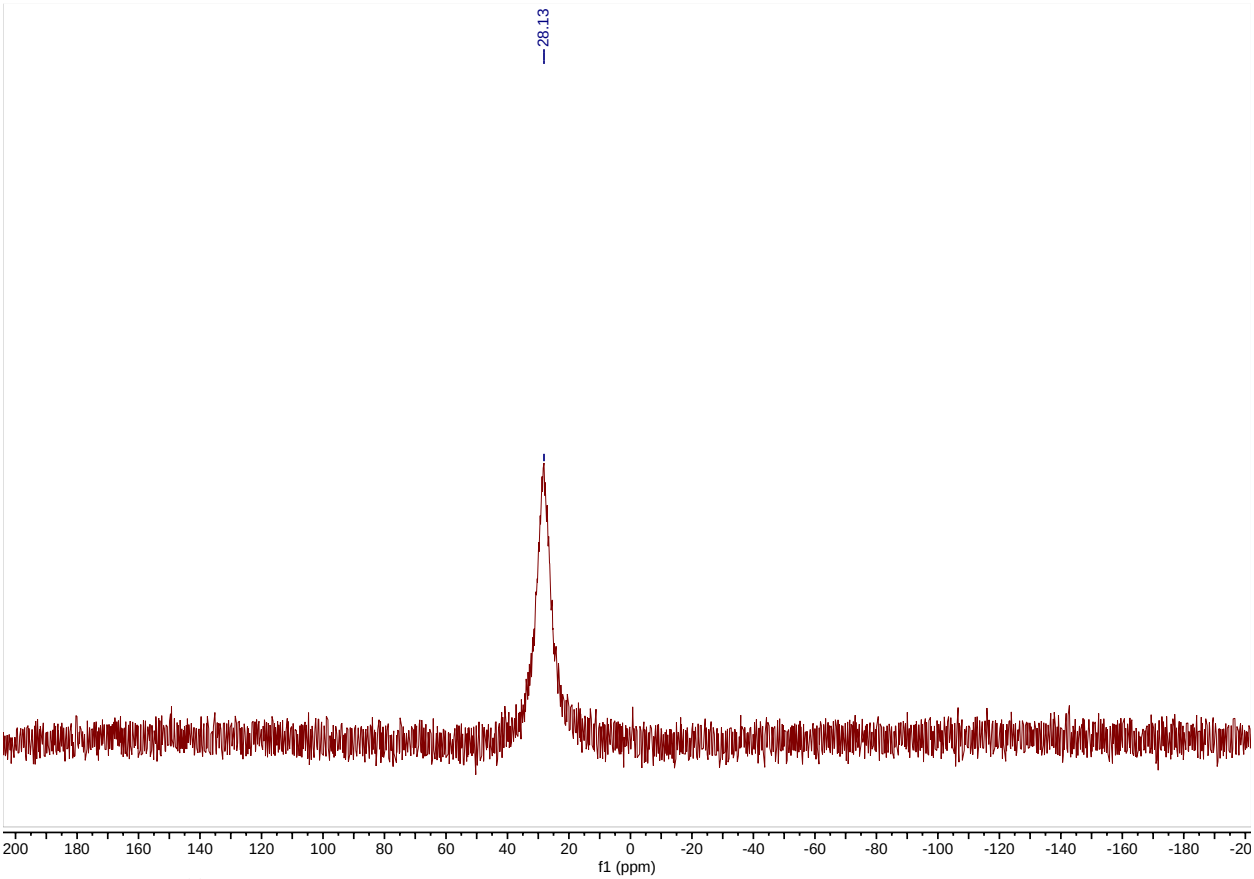

Figure A-46. ^{11}B NMR Spectrum of **2o**.

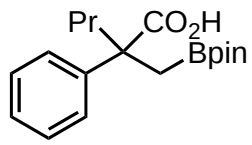

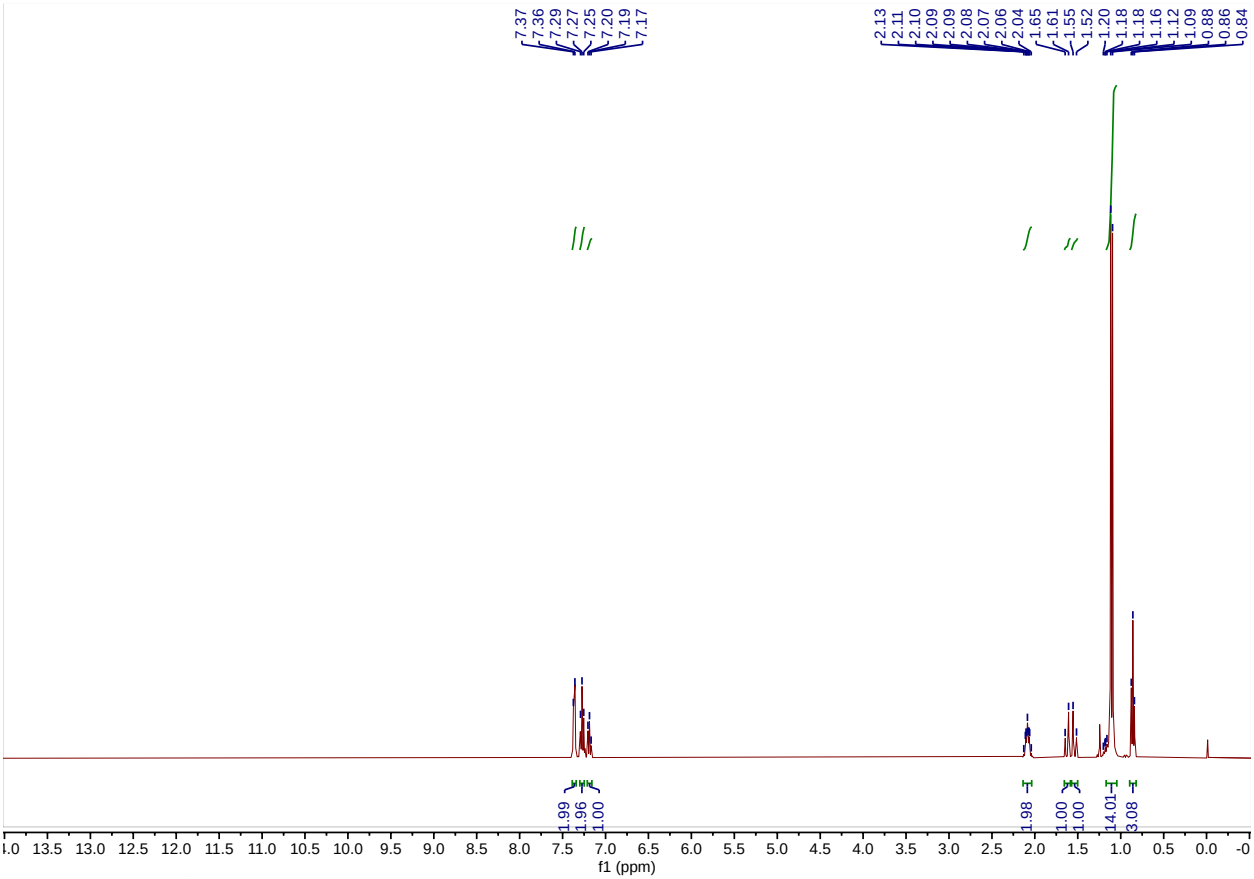

Figure A-47. ^{1}H NMR Spectrum of **2p**.

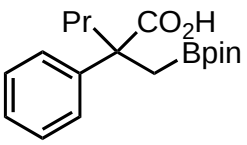

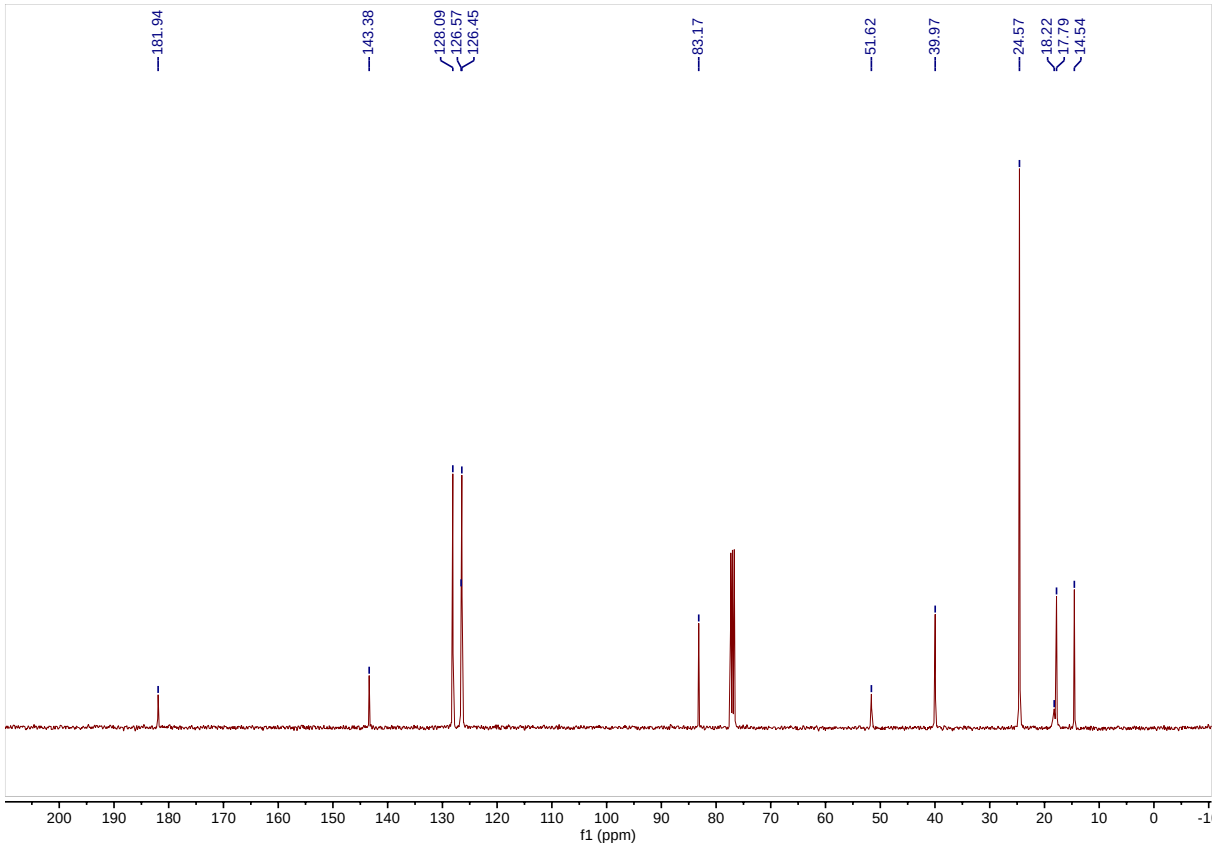

Figure A-48. ^{13}C NMR Spectrum of **2p**.

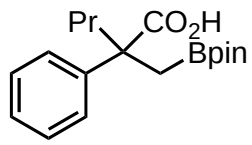

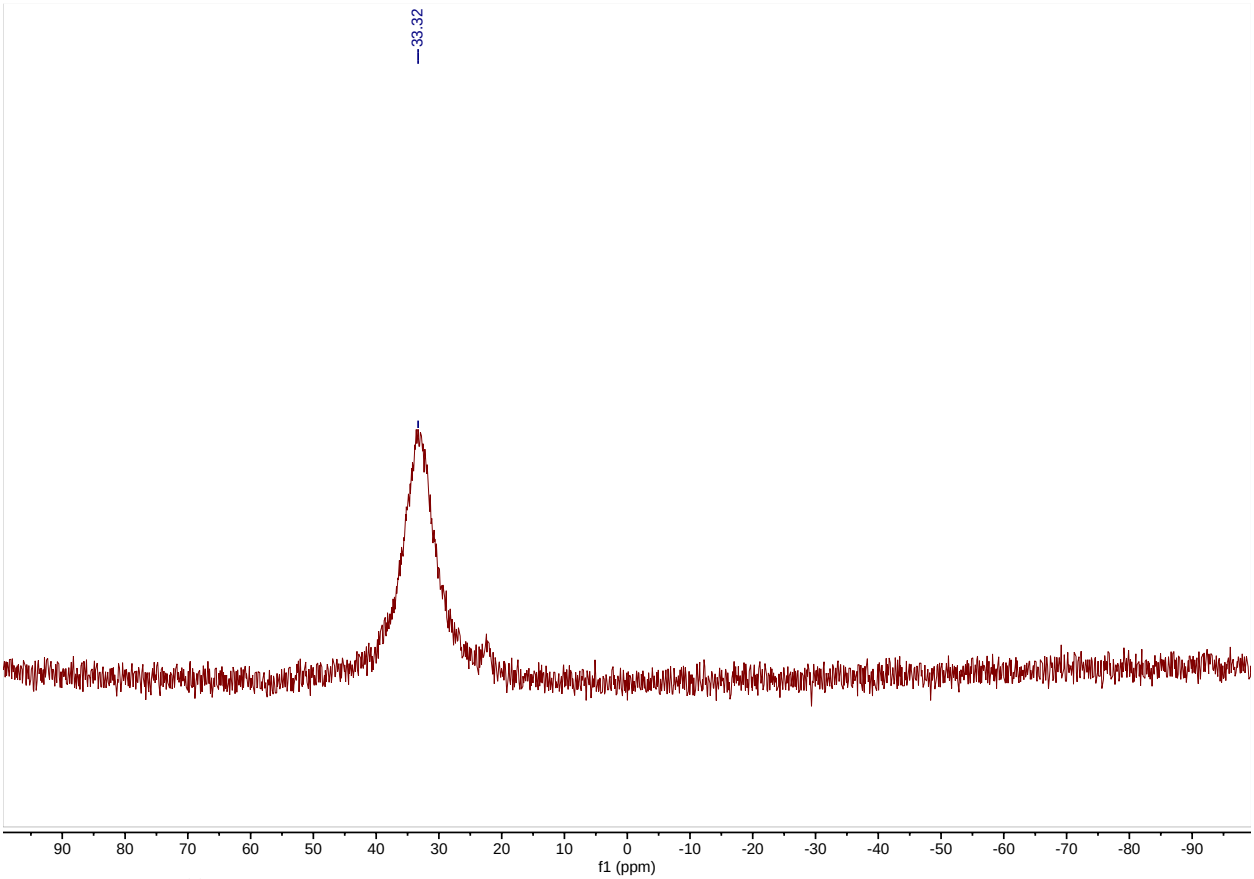

Figure A-49. ^{11}B NMR Spectrum of **2p**.

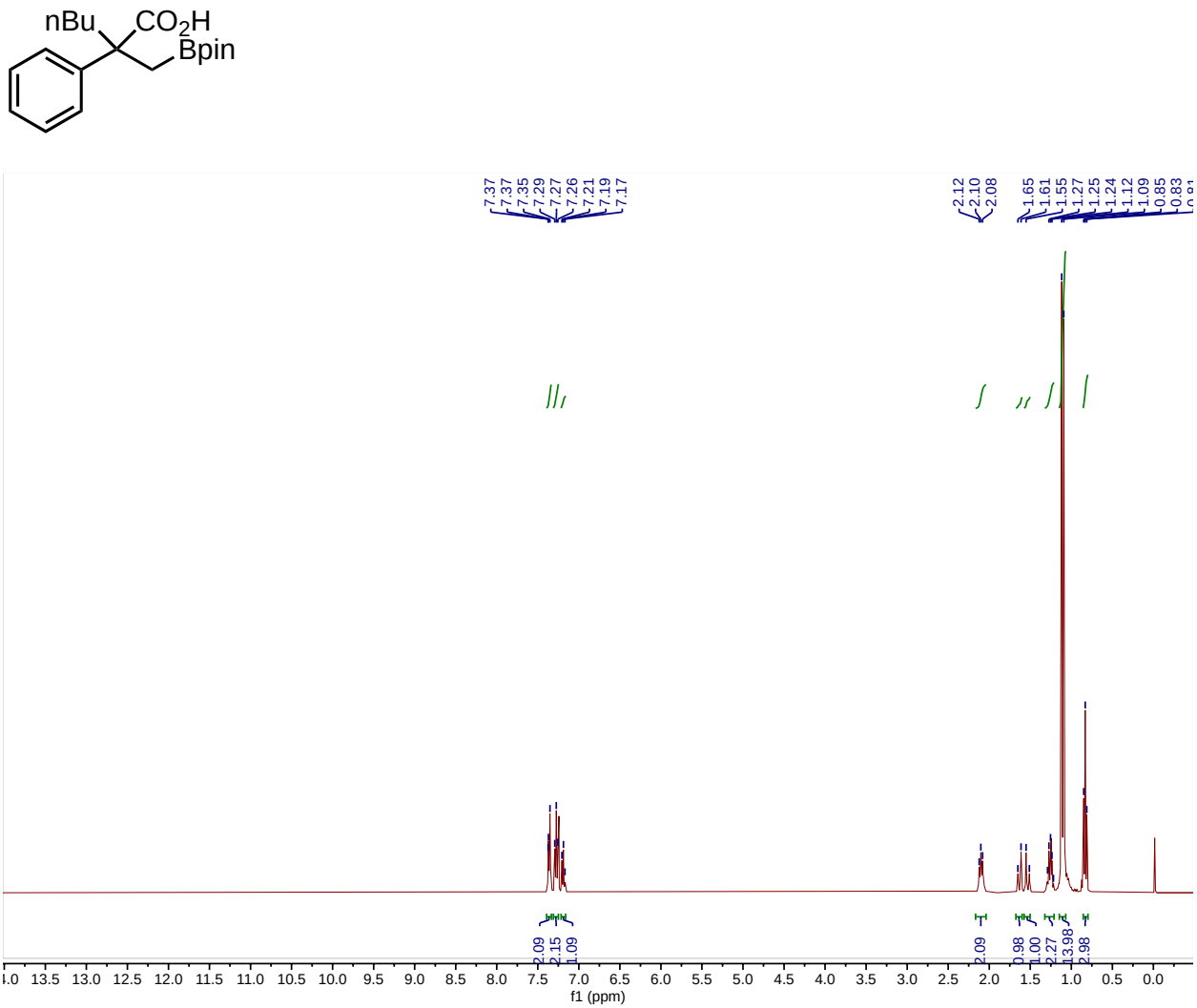

Figure A-50. ^{1}H NMR Spectrum of **2q**.

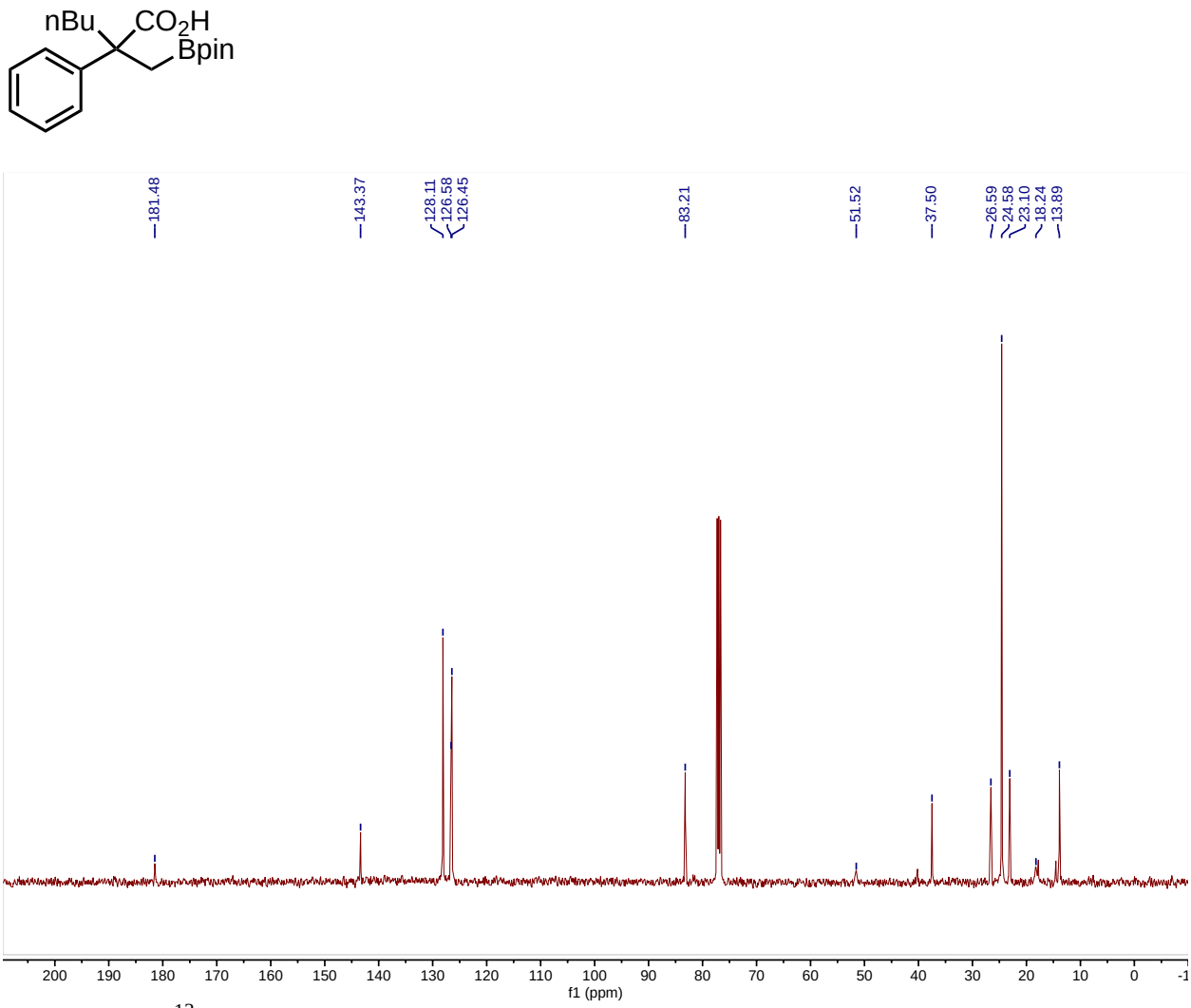

Figure A-51. ^{13}C NMR Spectrum of **2q**.

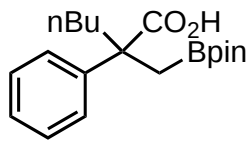

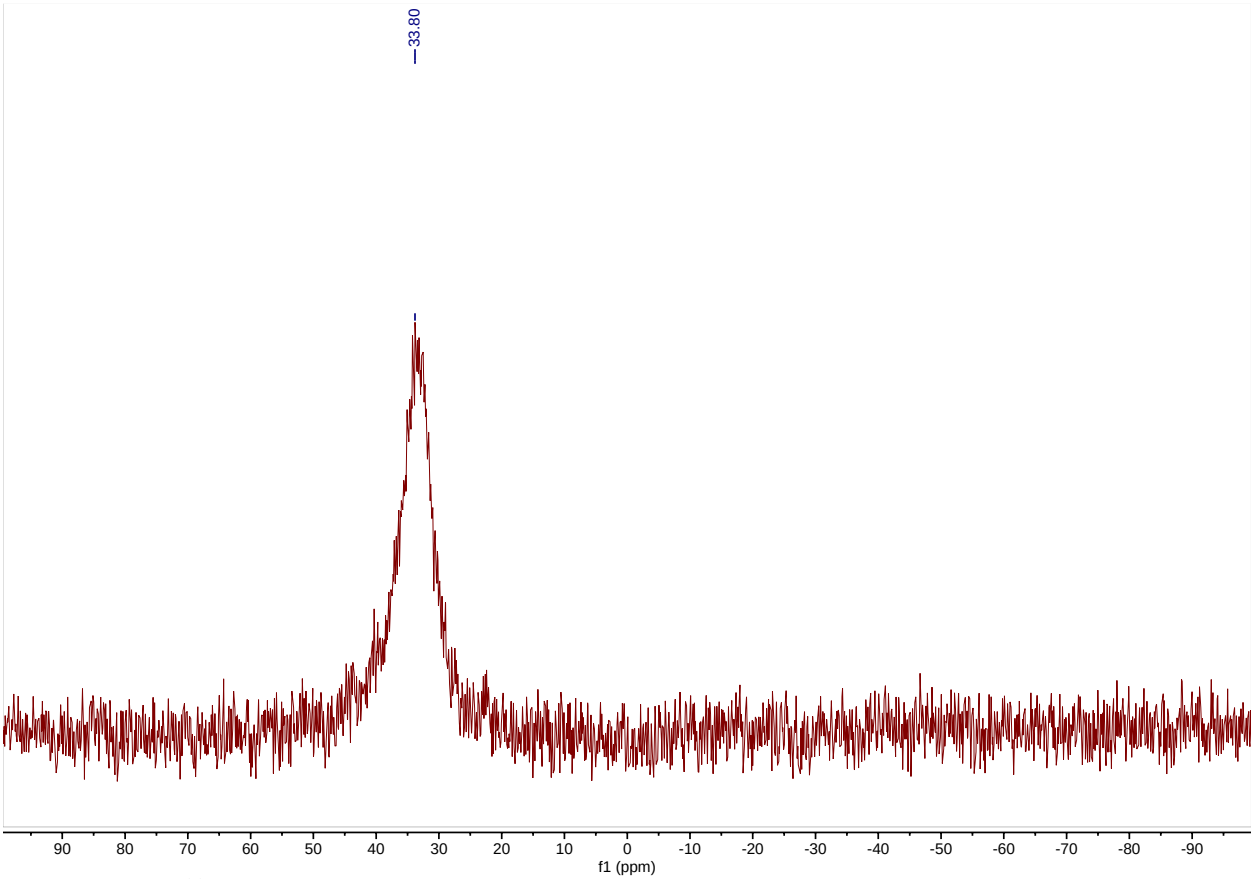

Figure A-52. ^{11}B NMR Spectrum of **2q**.

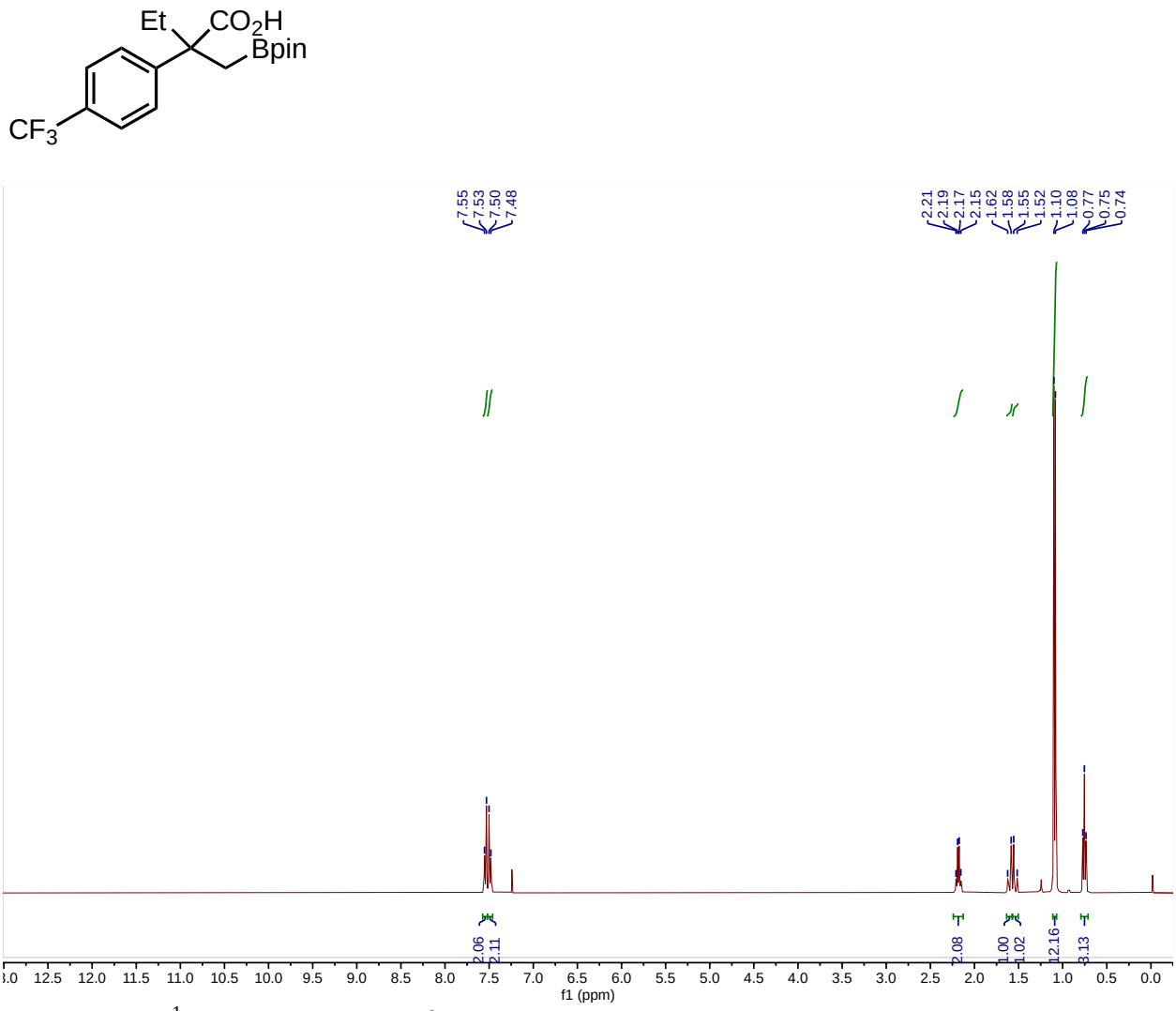

Figure A-53. ^{1}H NMR Spectrum of **2r**.

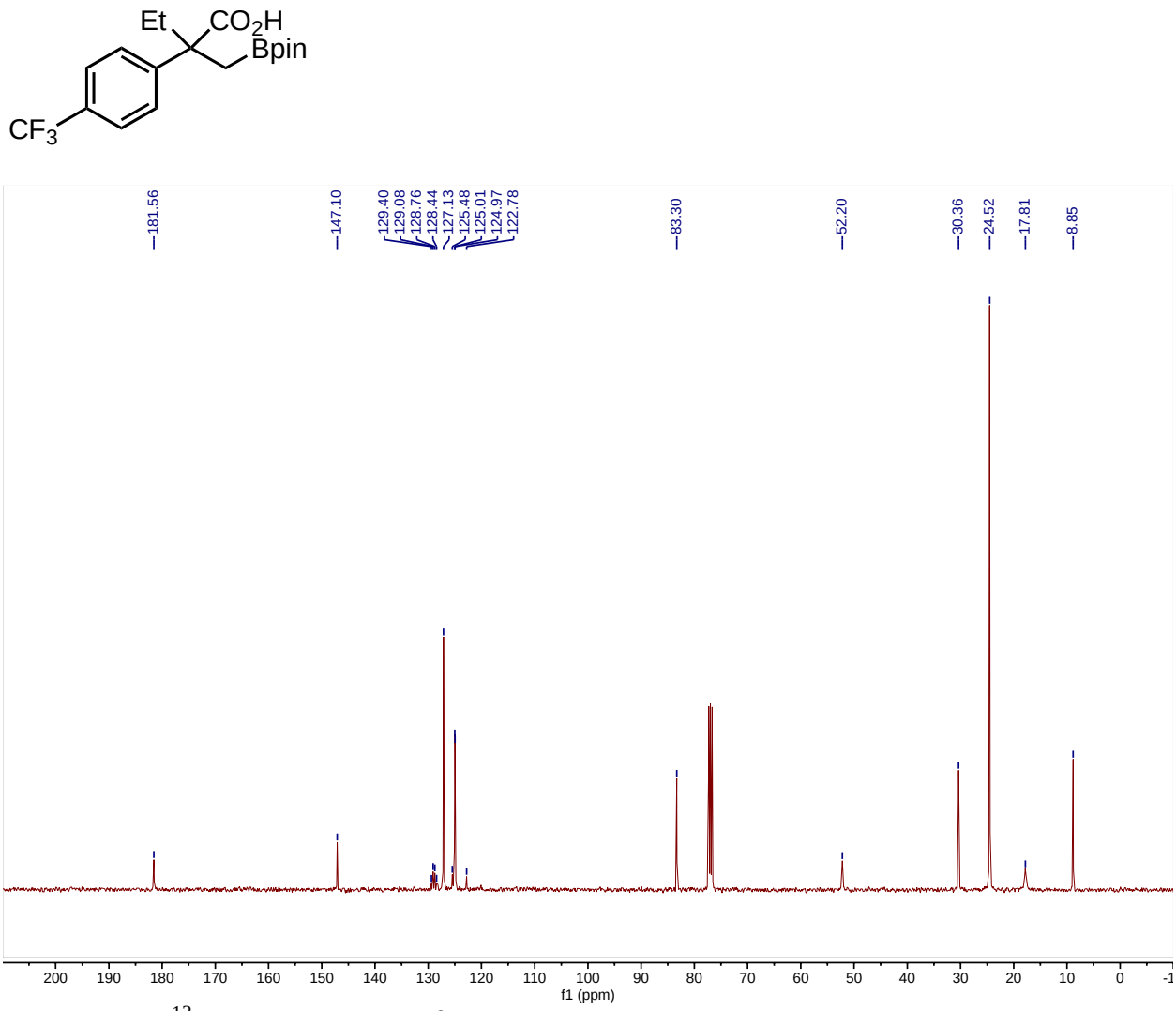

Figure A-54. ^{13}C NMR Spectrum of **2r**.

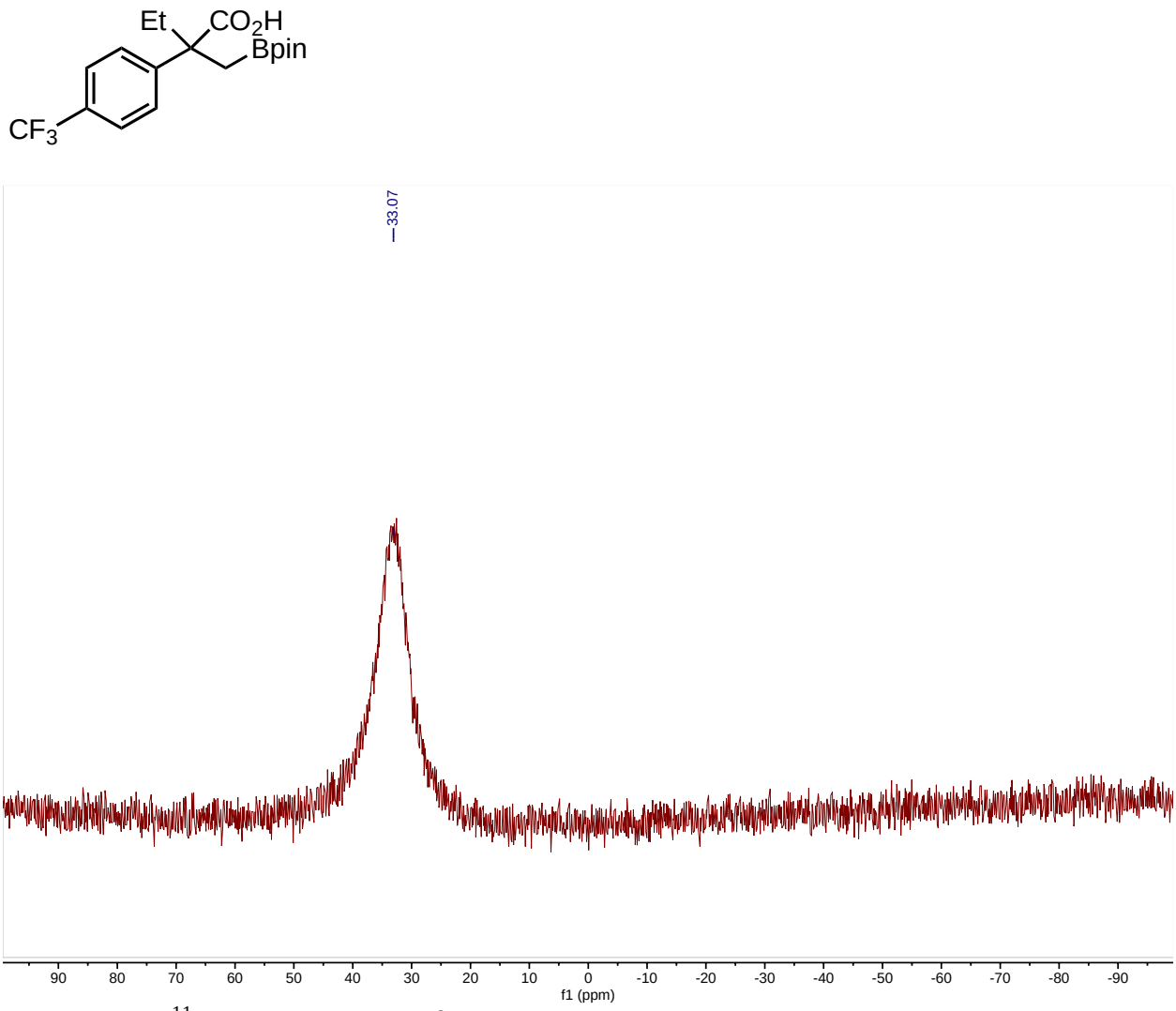

Figure A-55. ^{11}B NMR Spectrum of **2r**.

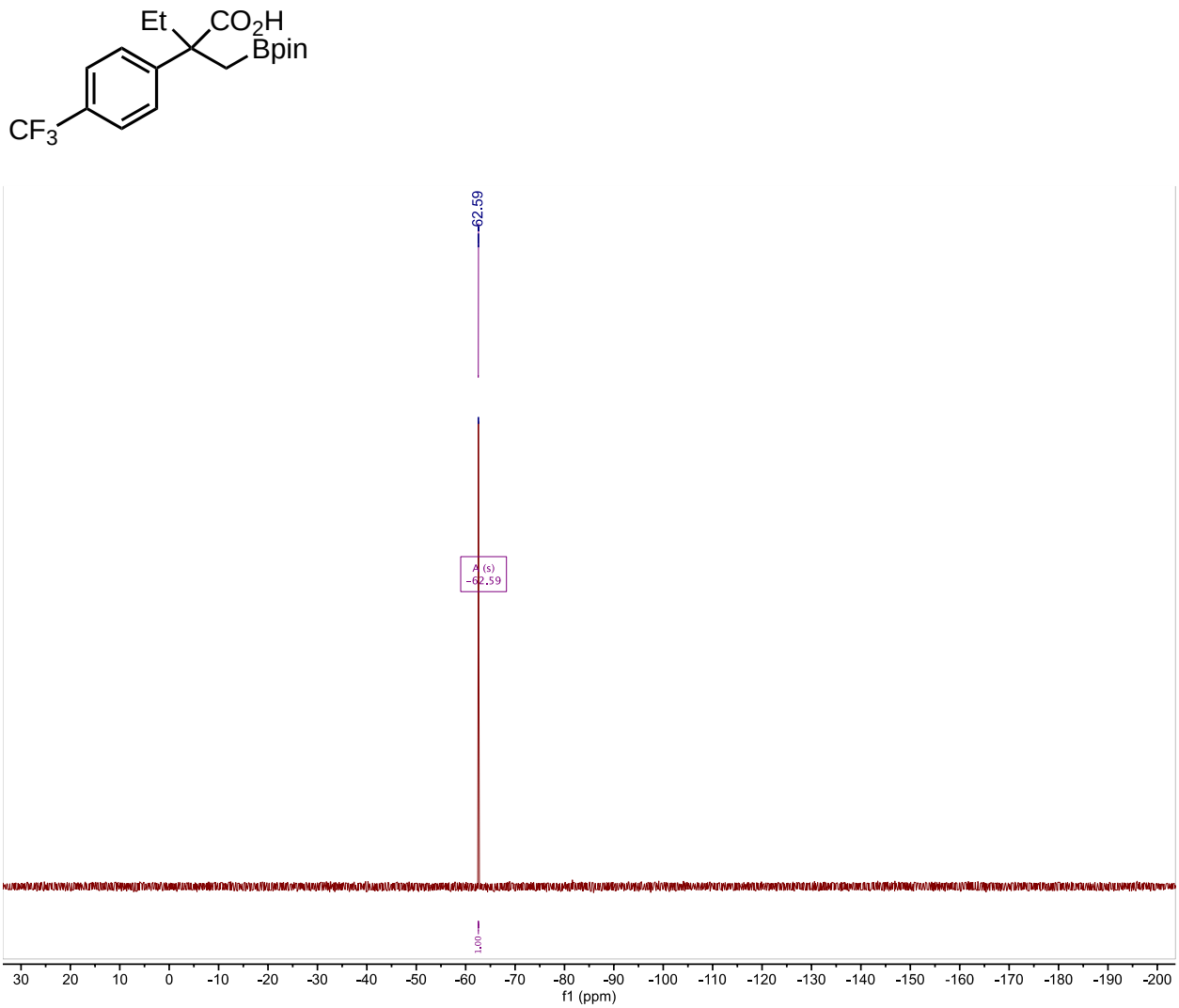

Figure A-56. ^{19}F NMR Spectrum of **2r**.

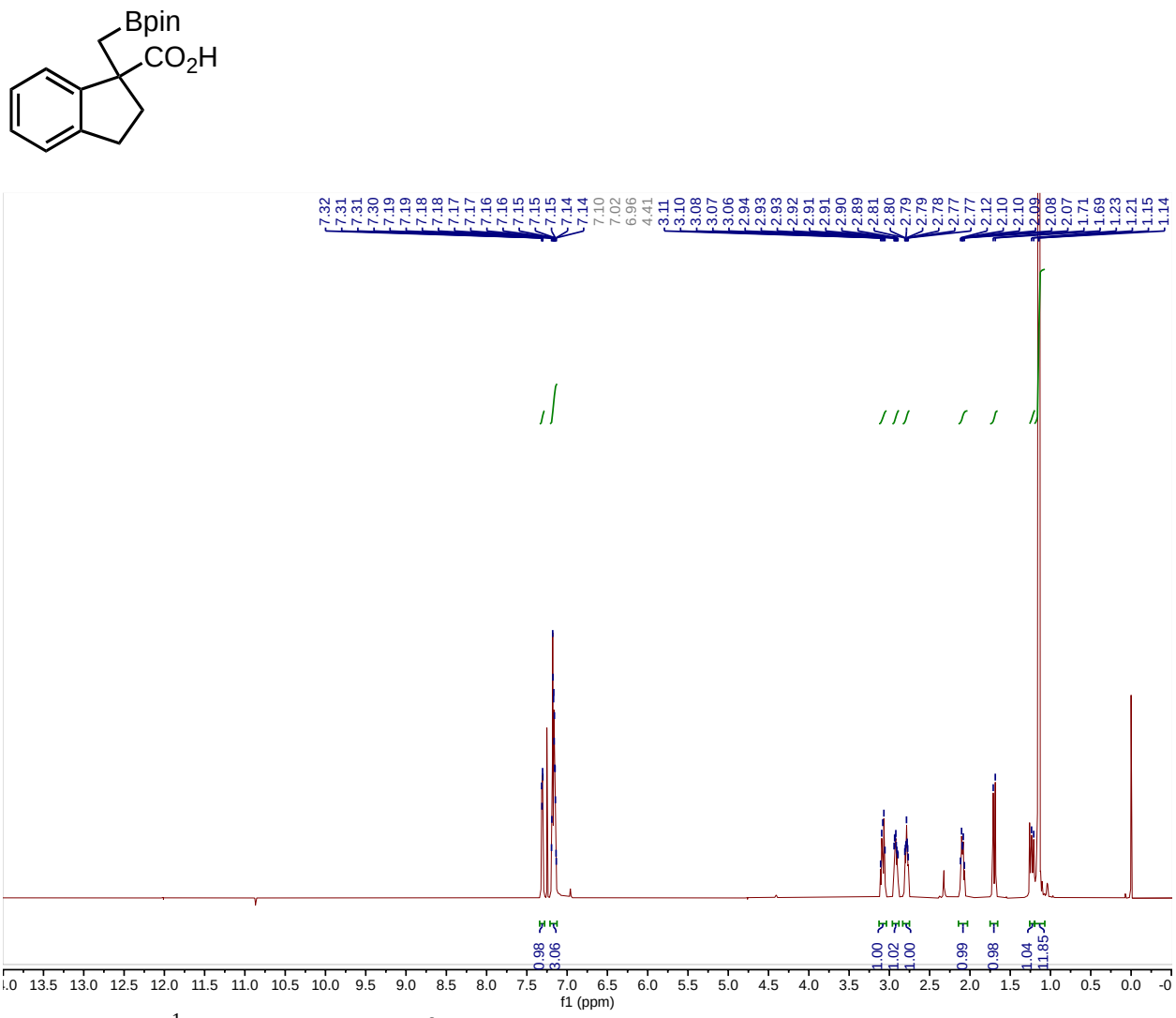

Figure A-57. ^{1}H NMR Spectrum of **2s**.

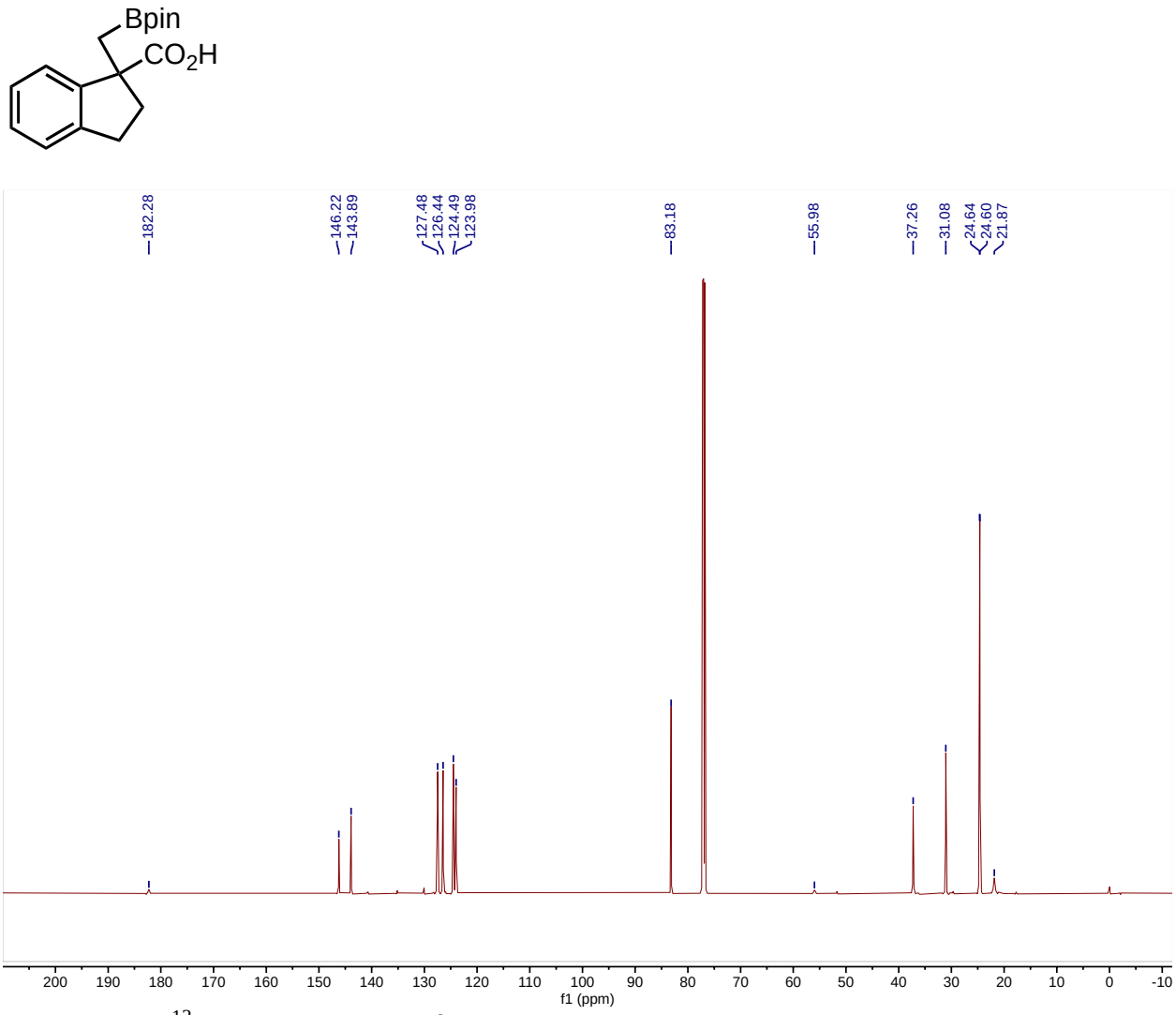

Figure A-58. ^{13}C NMR Spectrum of **2s**.

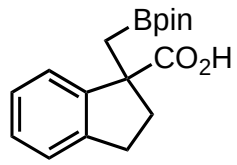

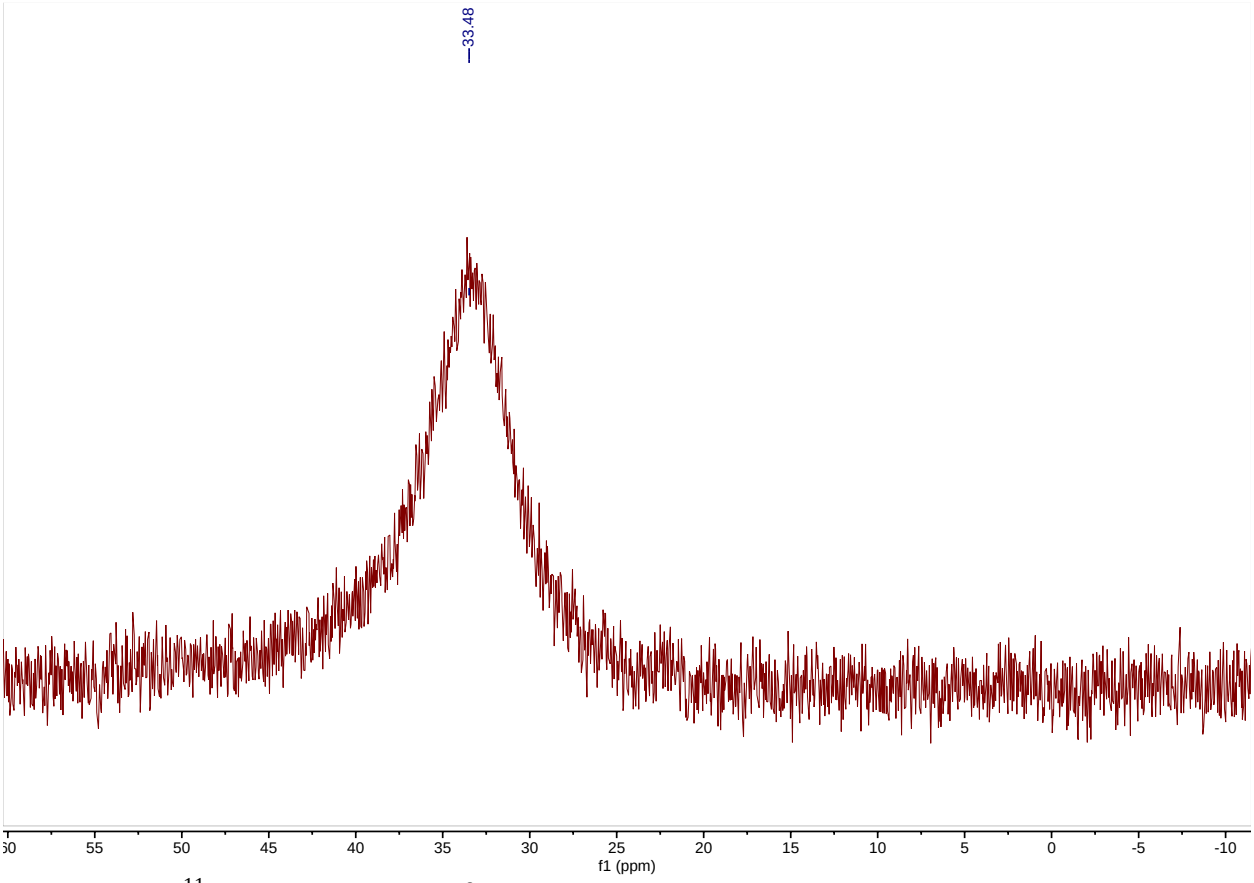

Figure A-59. ^{11}B NMR Spectrum of **2s**.

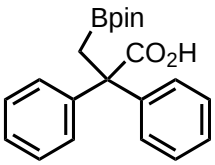

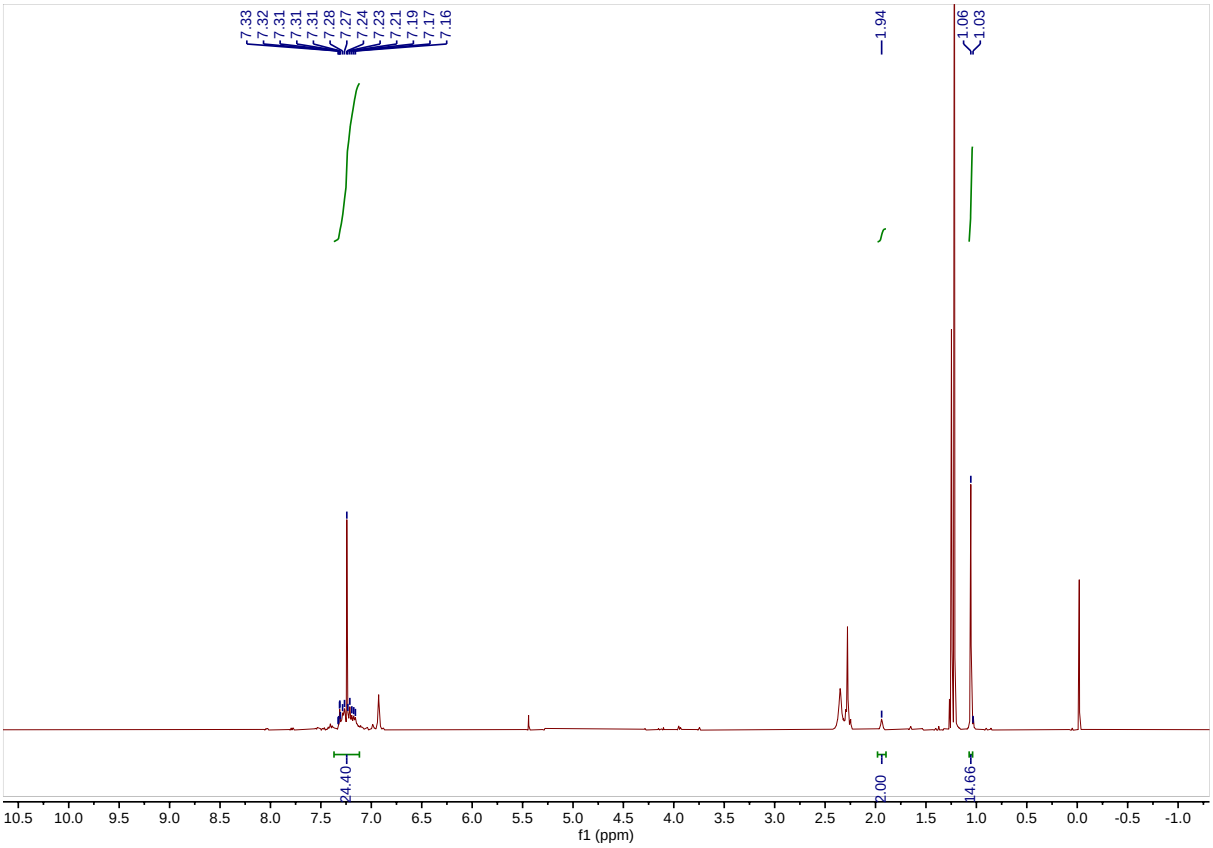

Figure A-60. ^{1}H NMR Spectrum of crude **2t**.

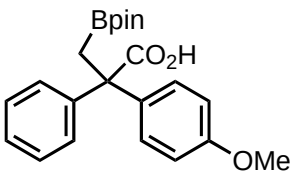

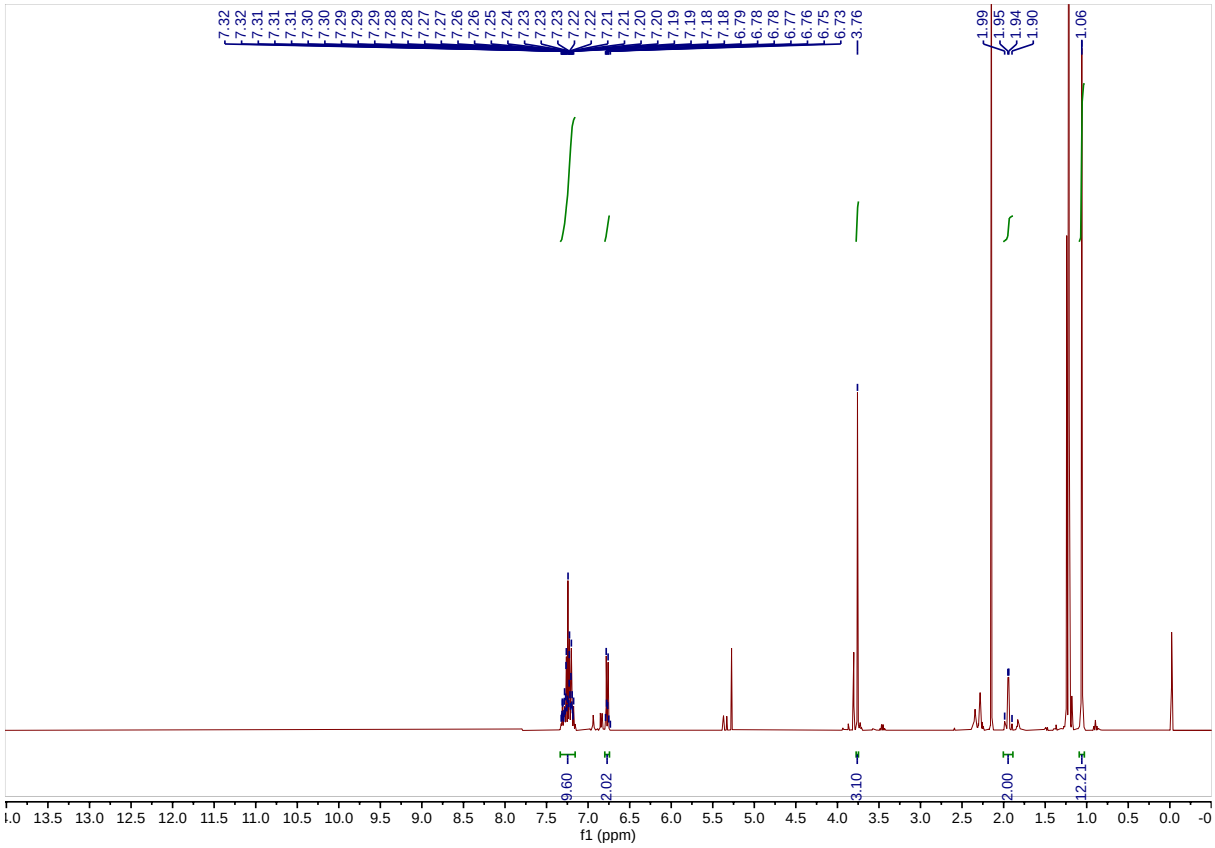

Figure A-61. ^{1}H NMR Spectrum of crude **2u**.

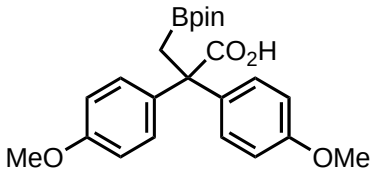

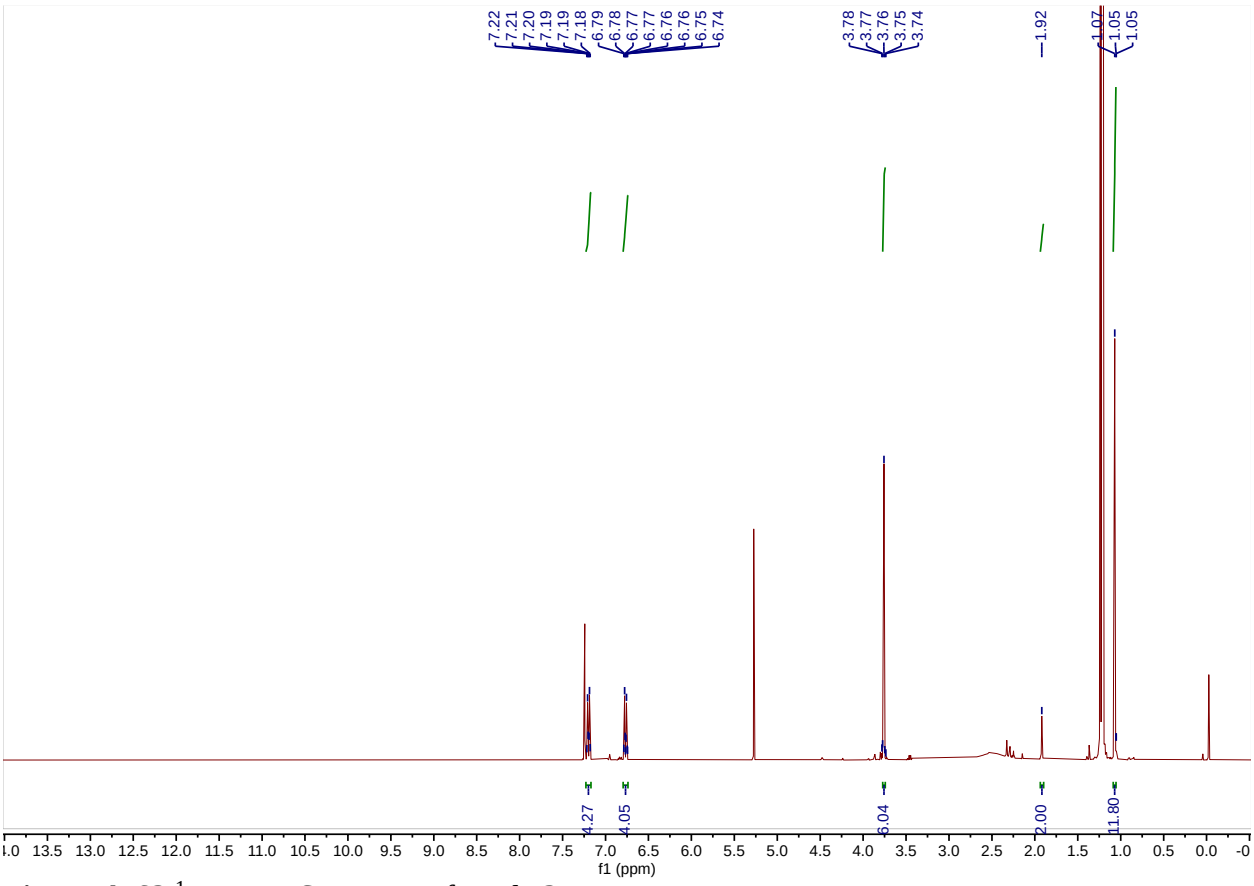

Figure A-62.[1]H NMR Spectrum of crude **2v**.

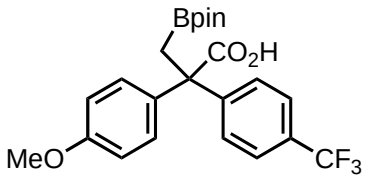

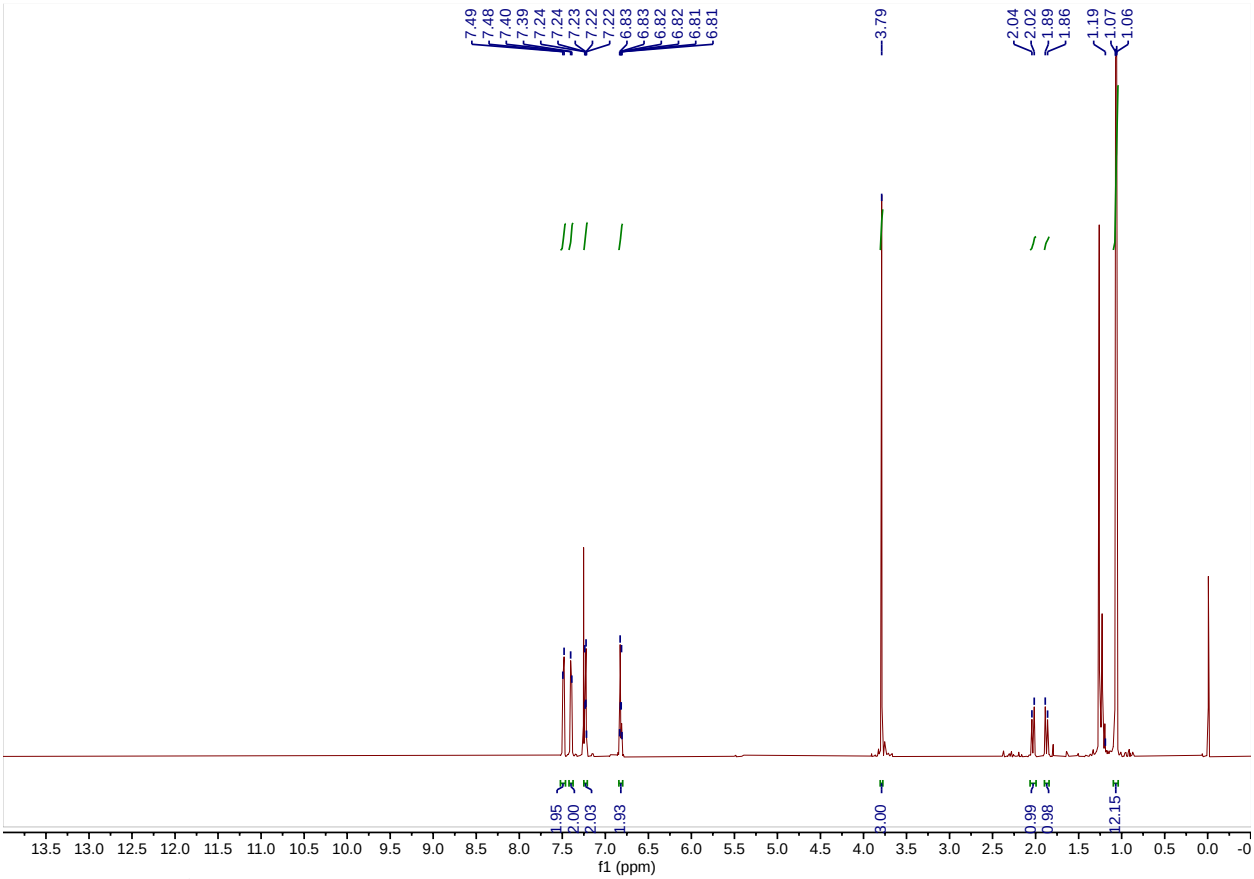

Figure A-63. ^{1}H NMR Spectrum of crude **2w**.

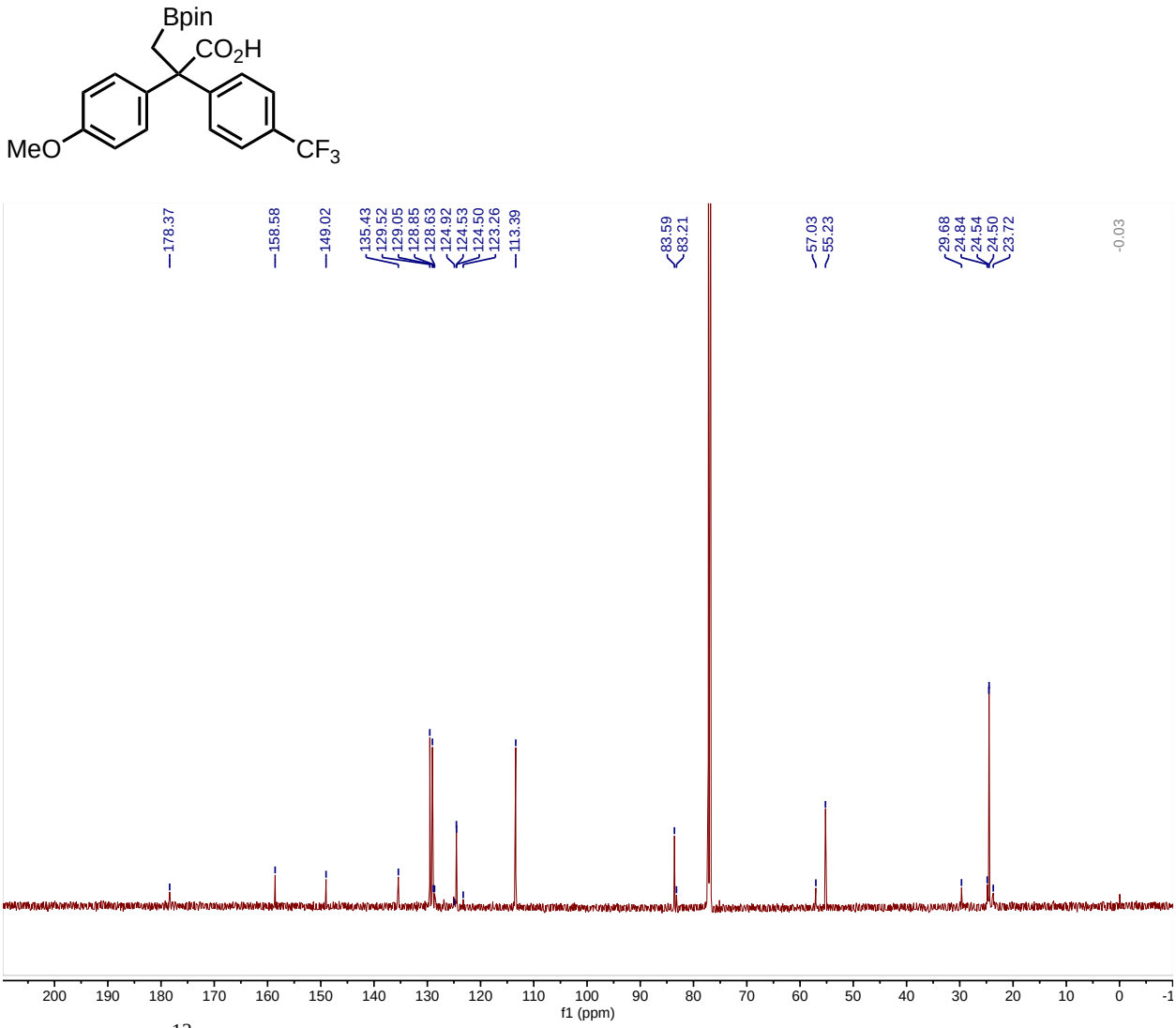

Figure A-64. ^{13}C NMR Spectrum of crude **2w**.

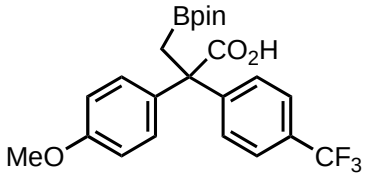

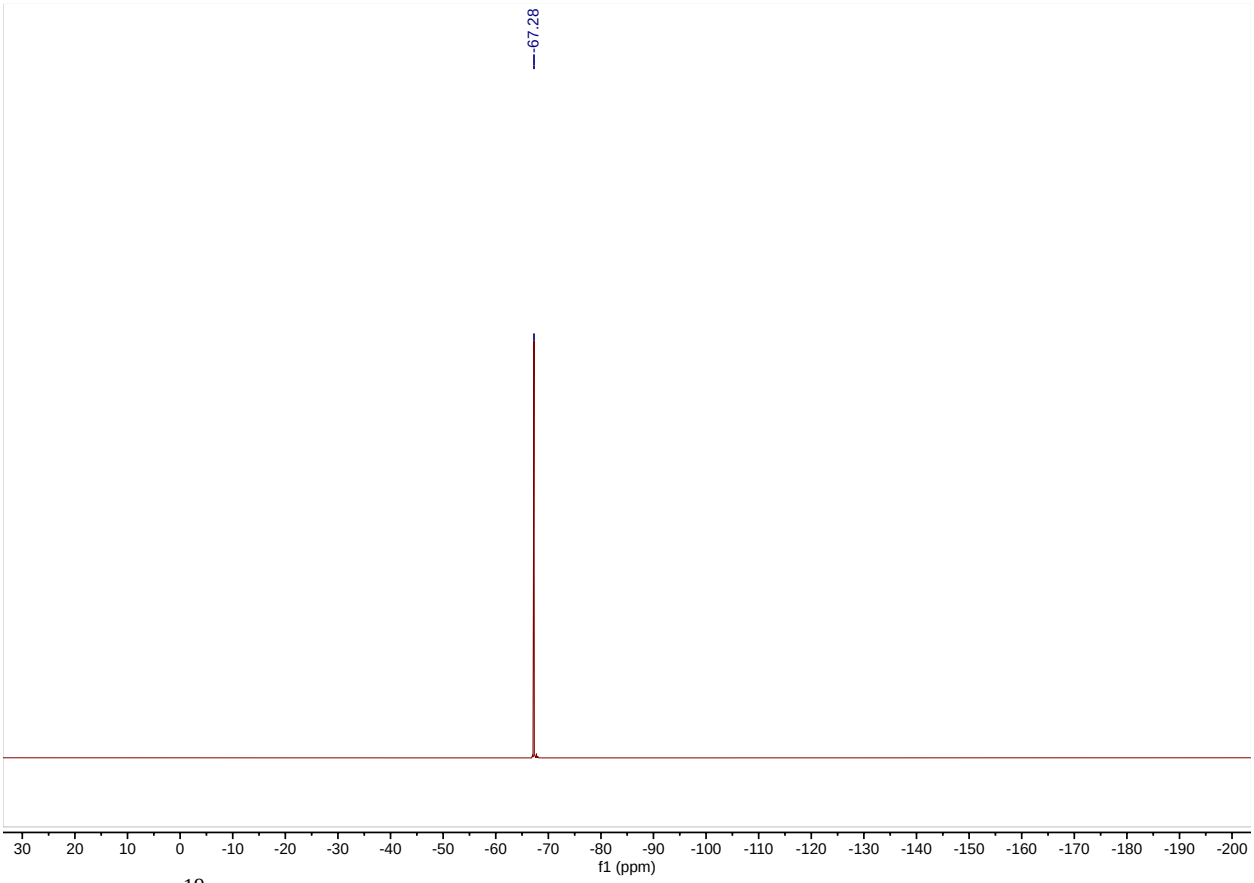

Figure A-65. ^{19}F NMR Spectrum of crude **2w**.

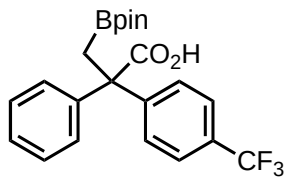

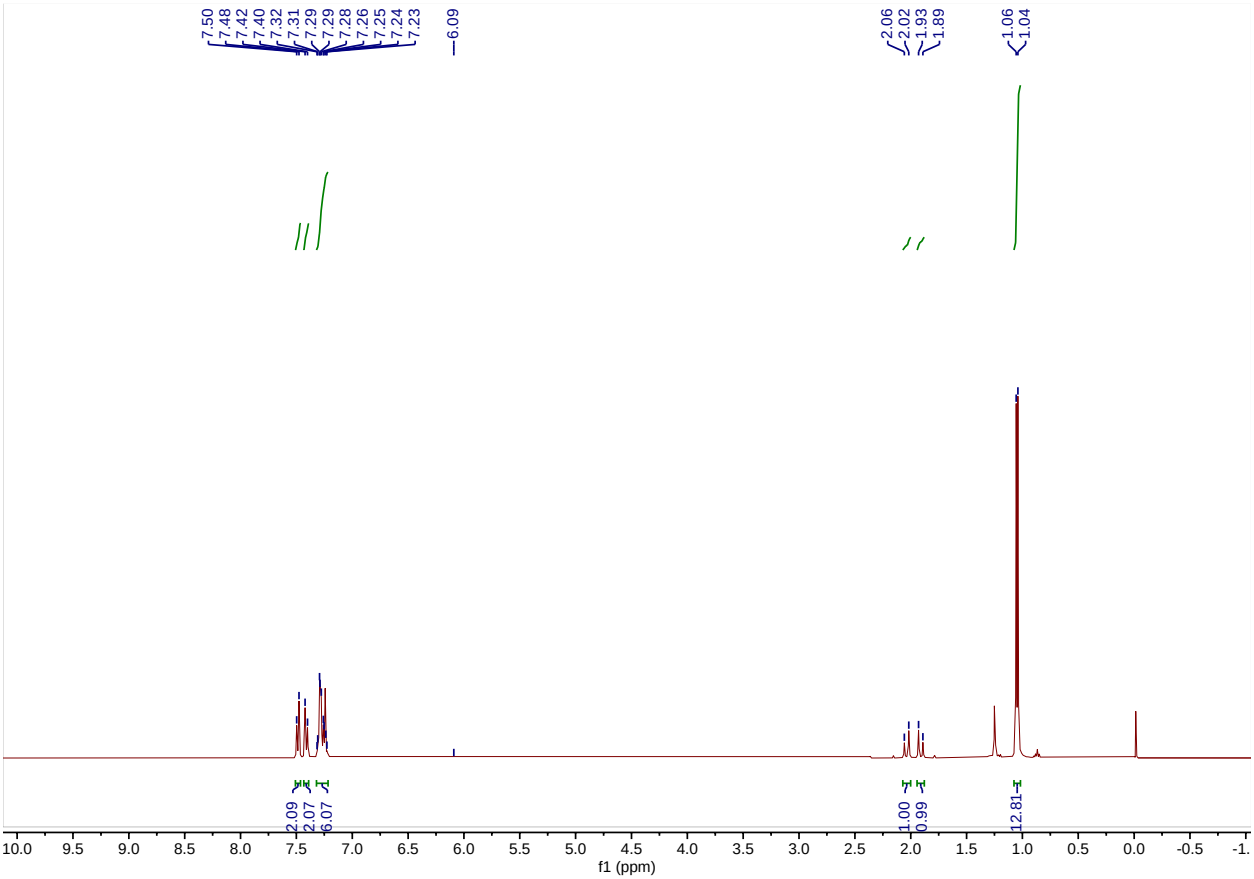

Figure A-66. ^{1}H NMR Spectrum of **2x**.

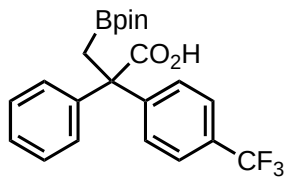

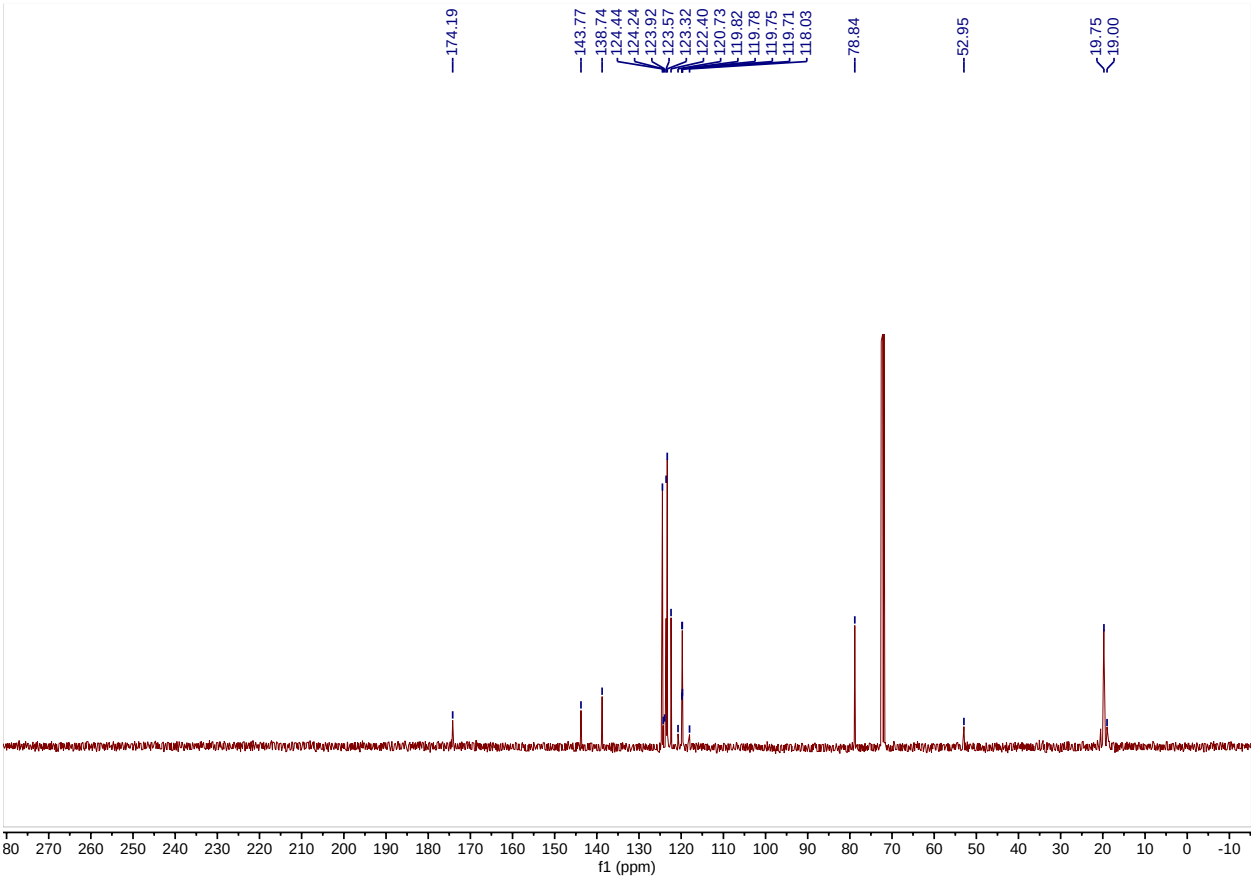

Figure A-67. ^{13}C NMR Spectrum of **2x**.

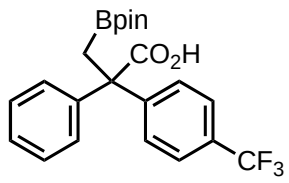

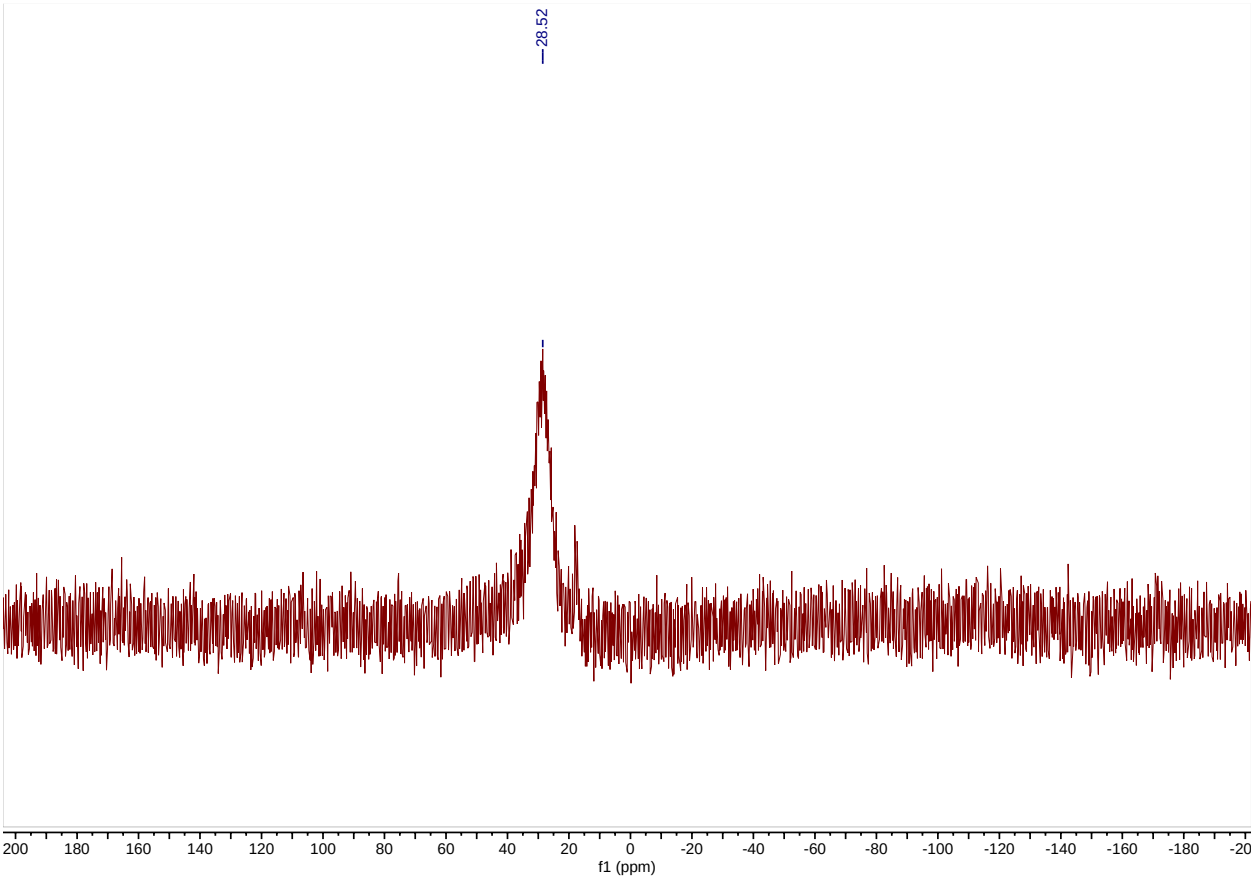

Figure A-68. ^{11}B NMR Spectrum of **2x**.

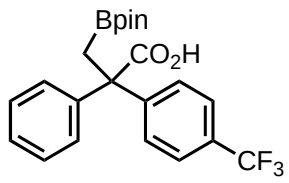

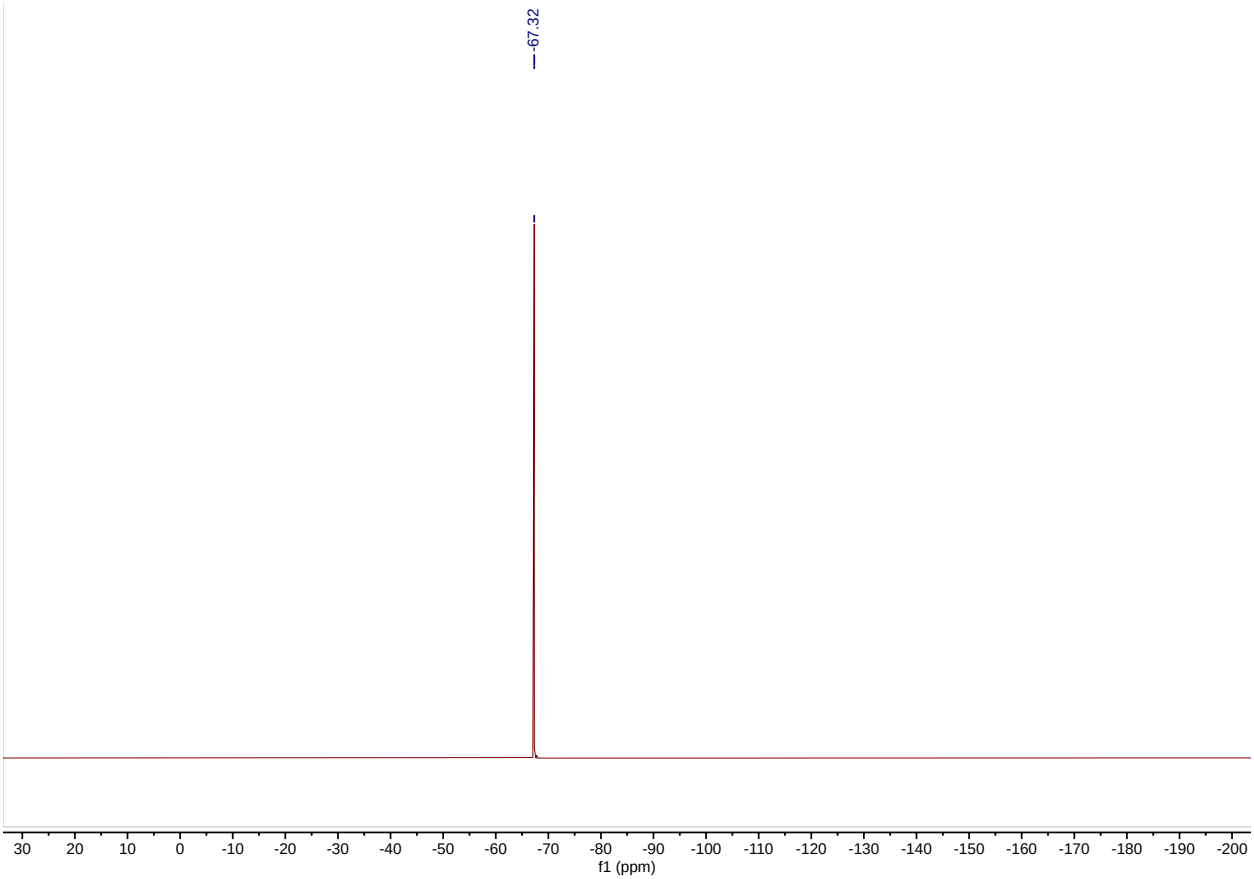

Figure A-69. ^{19}F NMR Spectrum of **2x**.

^{1}H, ^{13}C, ^{11}B and ^{19}F NMR Spectra – Compounds in Chapter 4

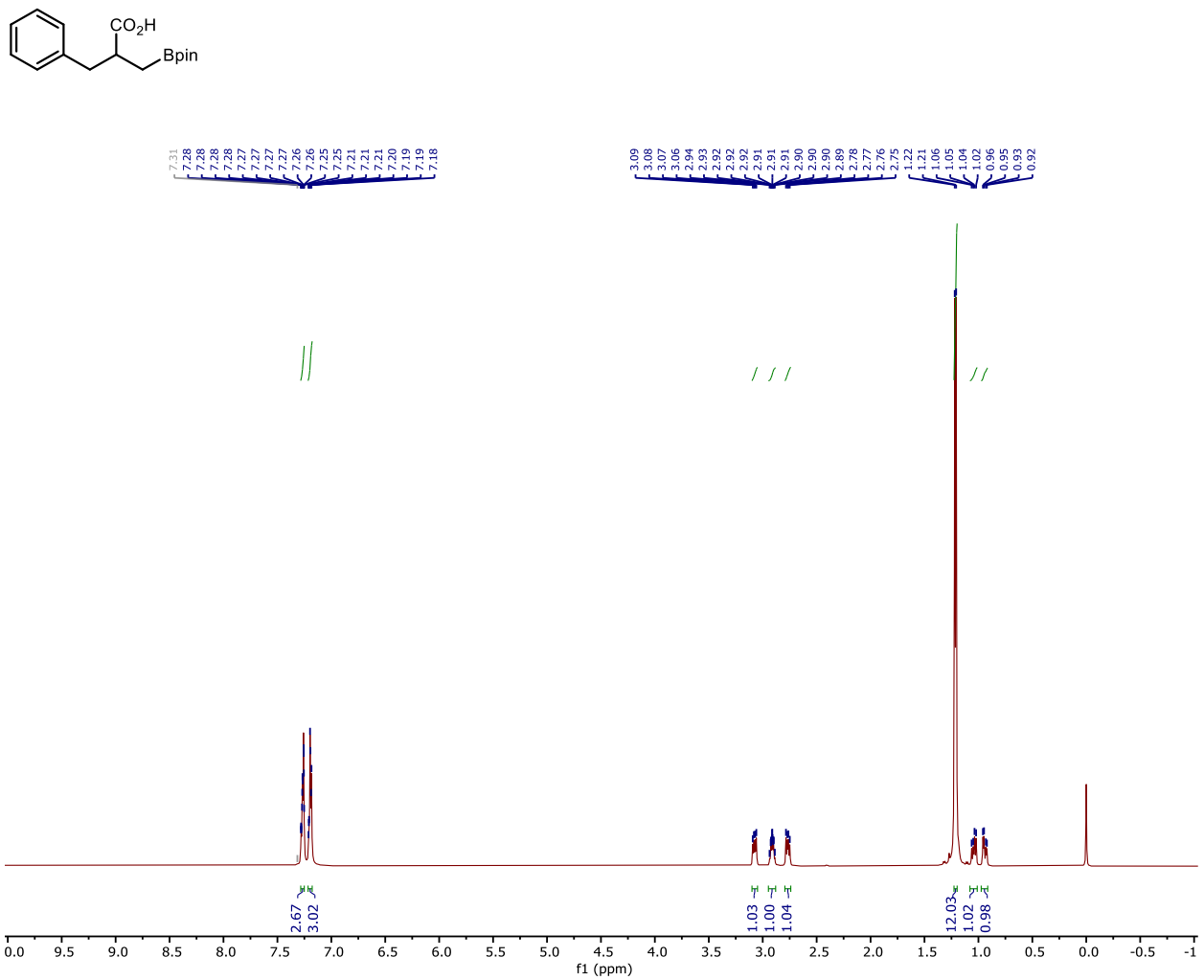

Figure A-70. ^{1}H NMR Spectrum of **2a**.

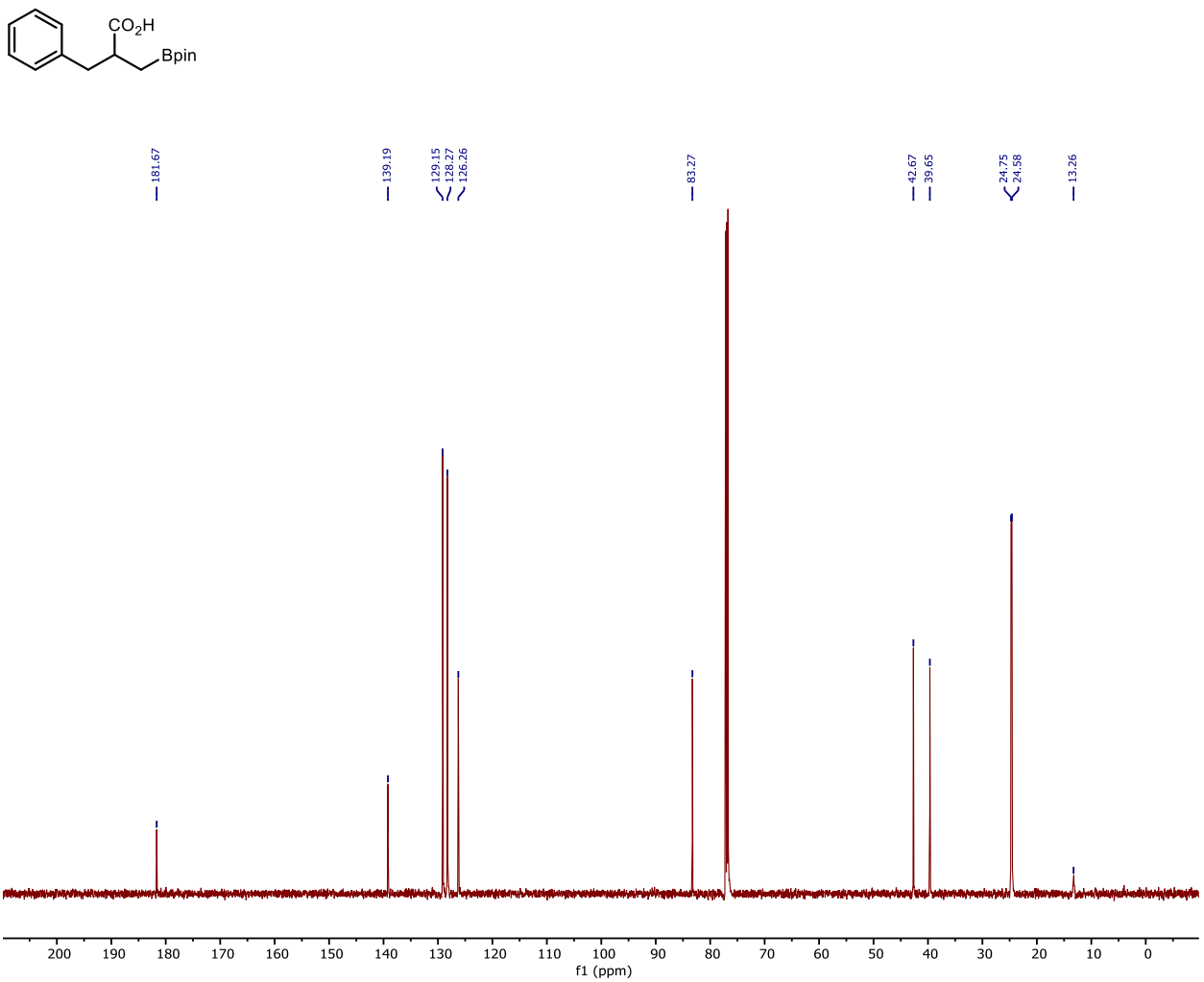

Figure A-71. ^{13}C NMR Spectrum of **2a**.

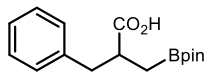

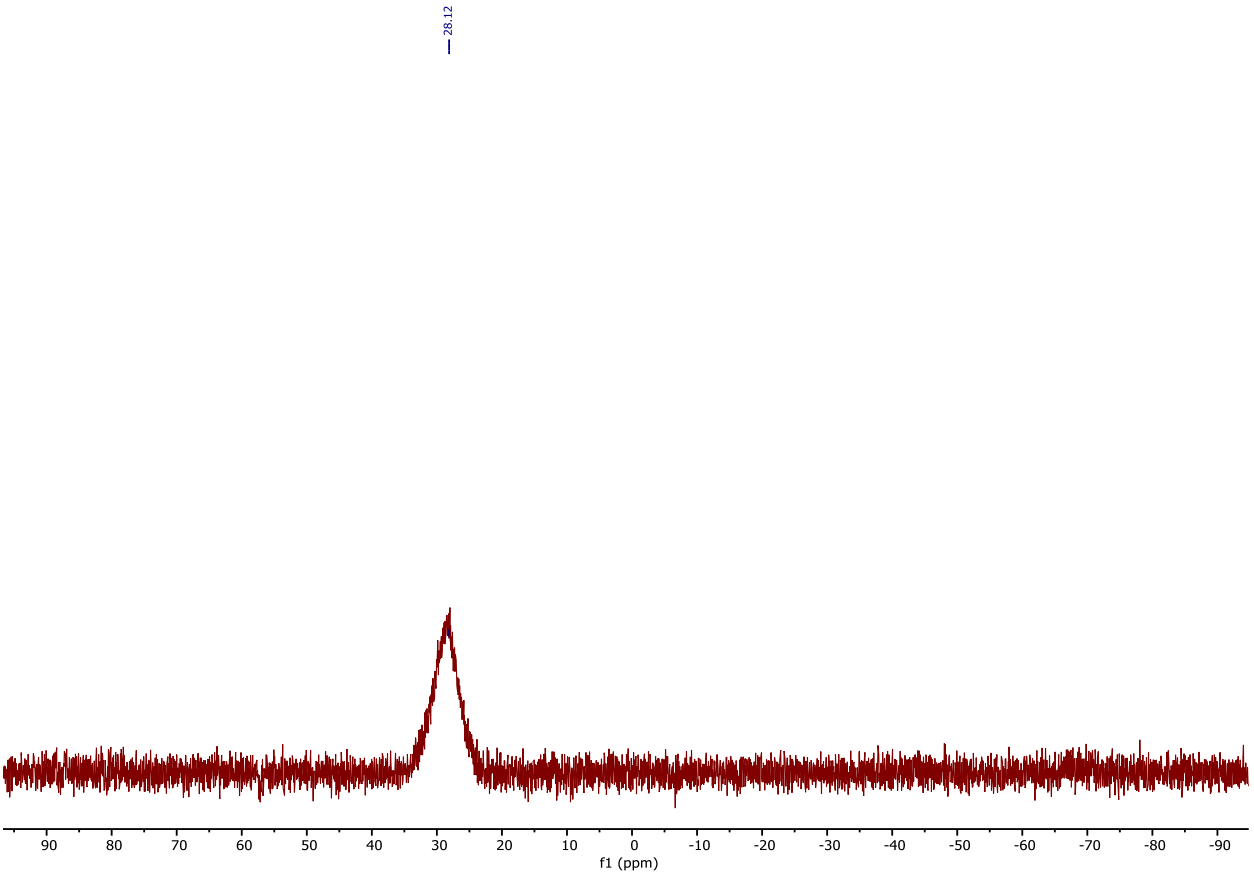

Figure A-72. ^{11}B NMR Spectrum of **2a**.

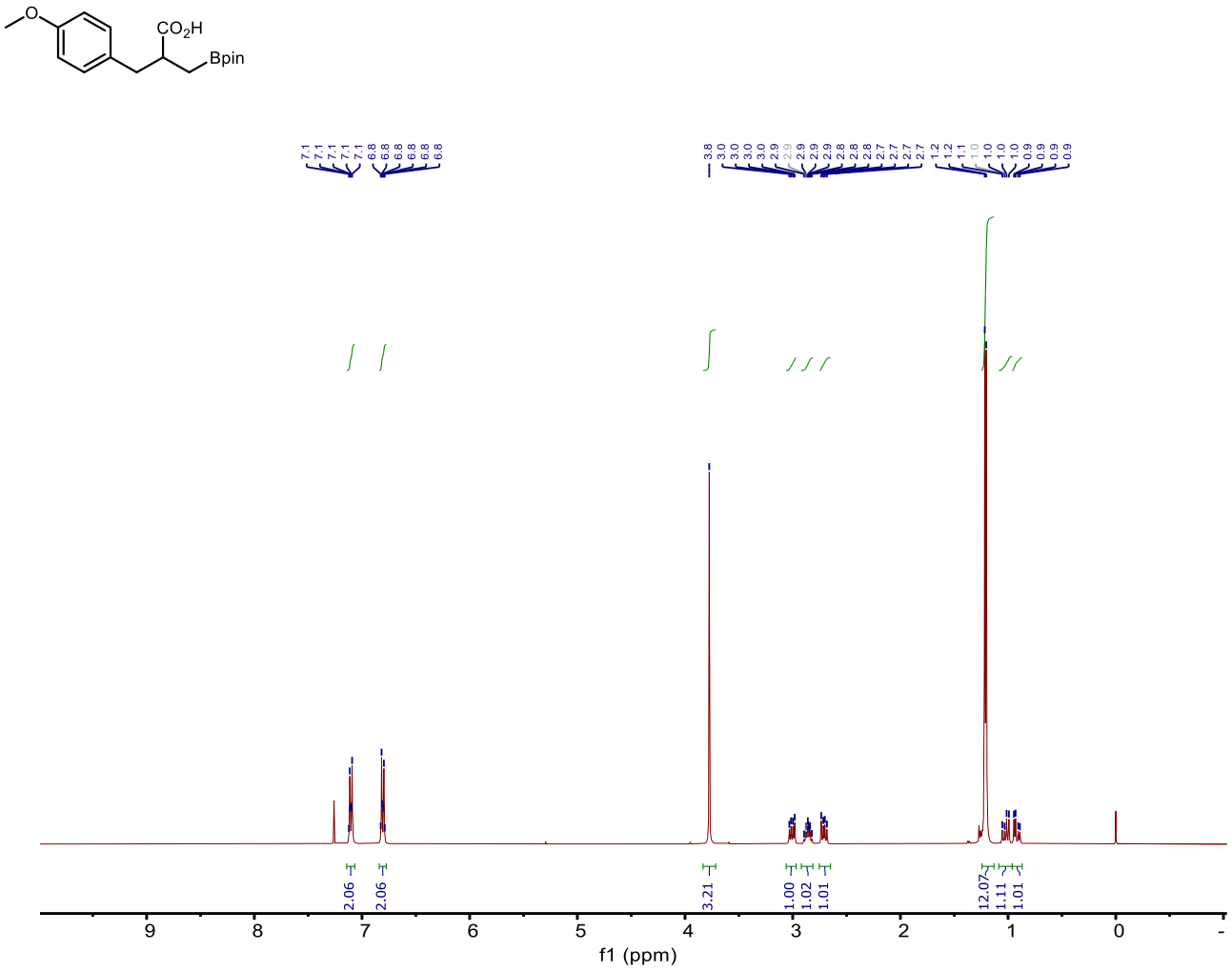

Figure A-73. ^{1}H NMR Spectrum of **2b.**

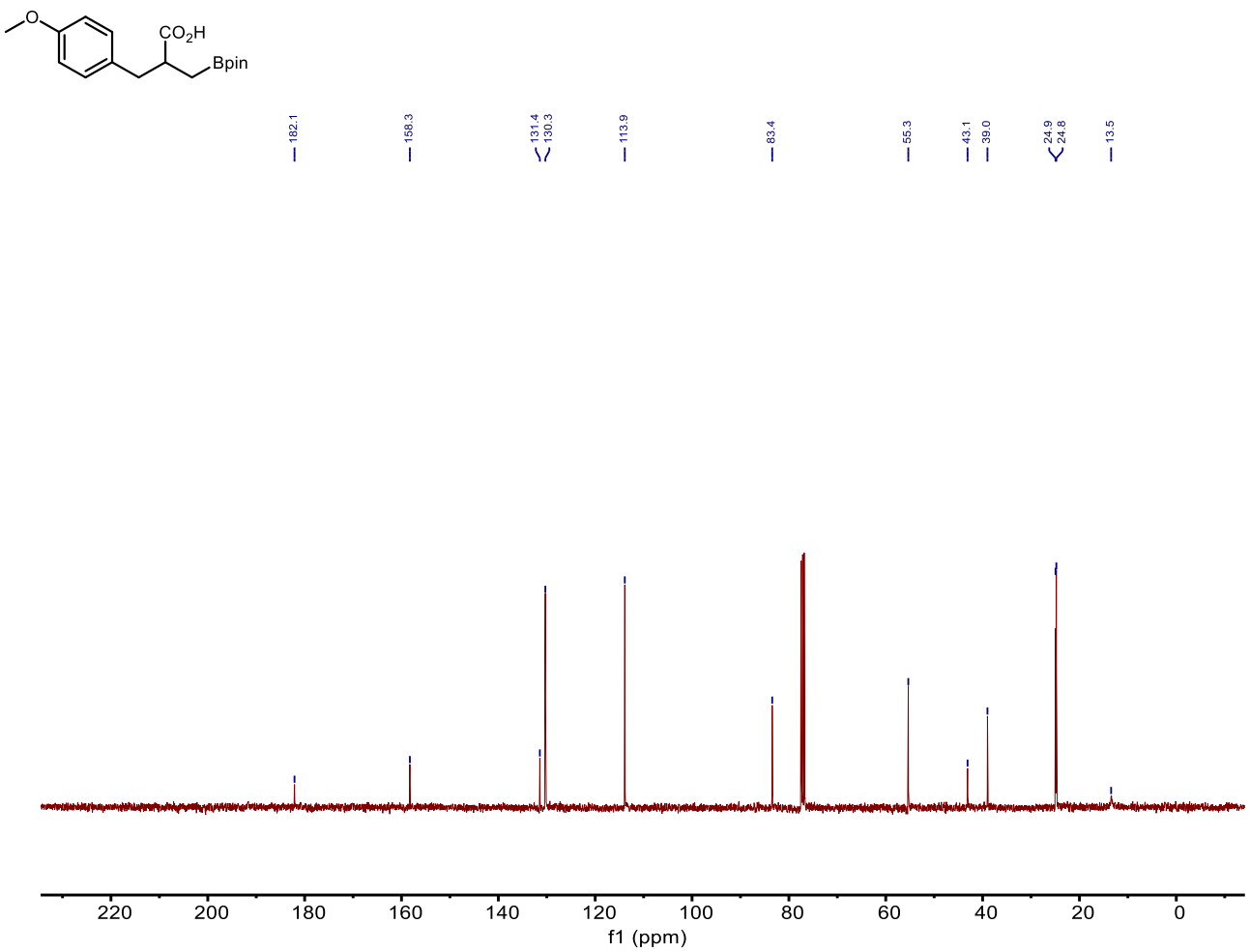

Figure A-74. ^{13}C NMR Spectrum of **2b.**

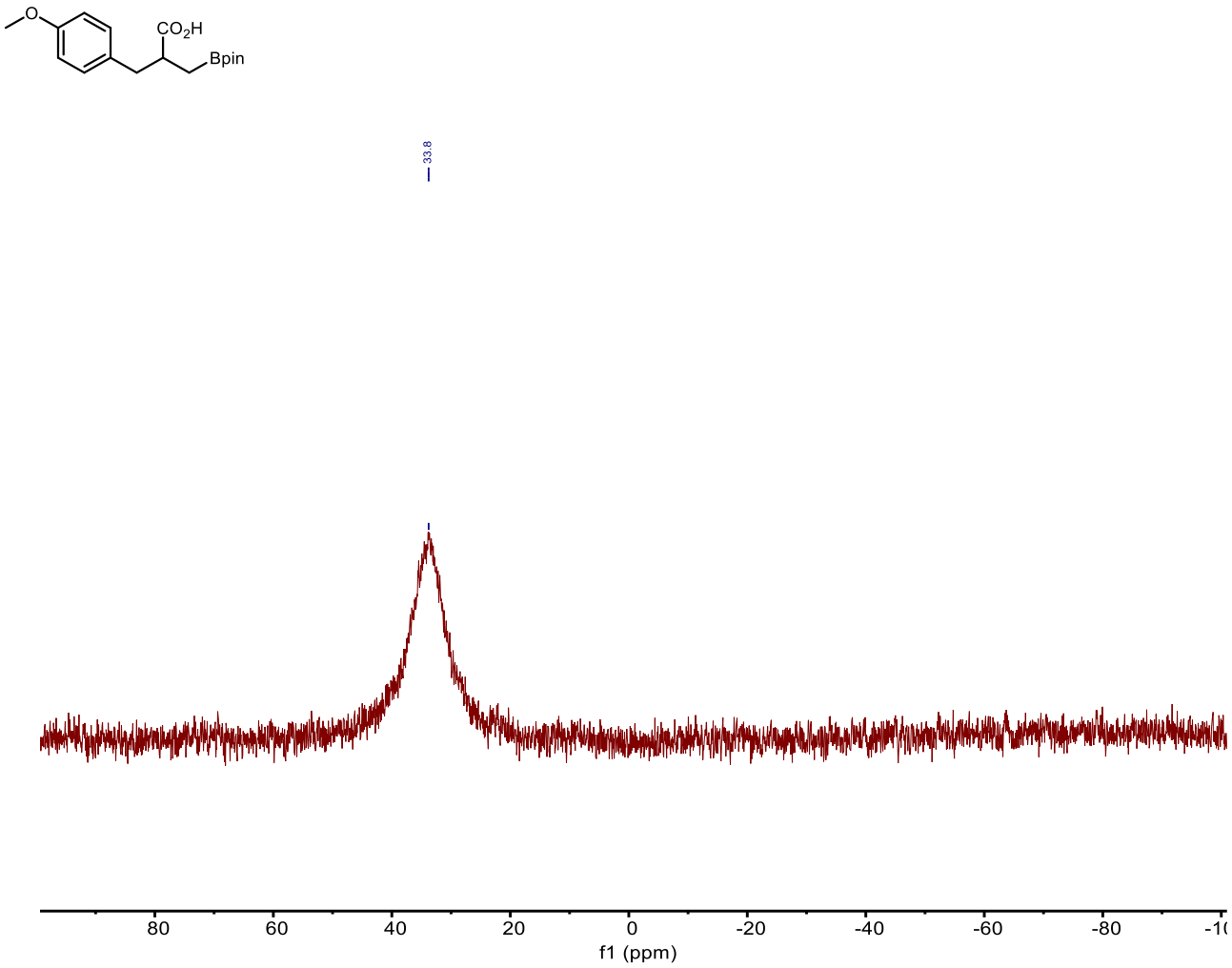

Figure A-75. ^{11}B NMR Spectrum of **2b.**

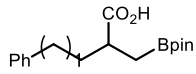

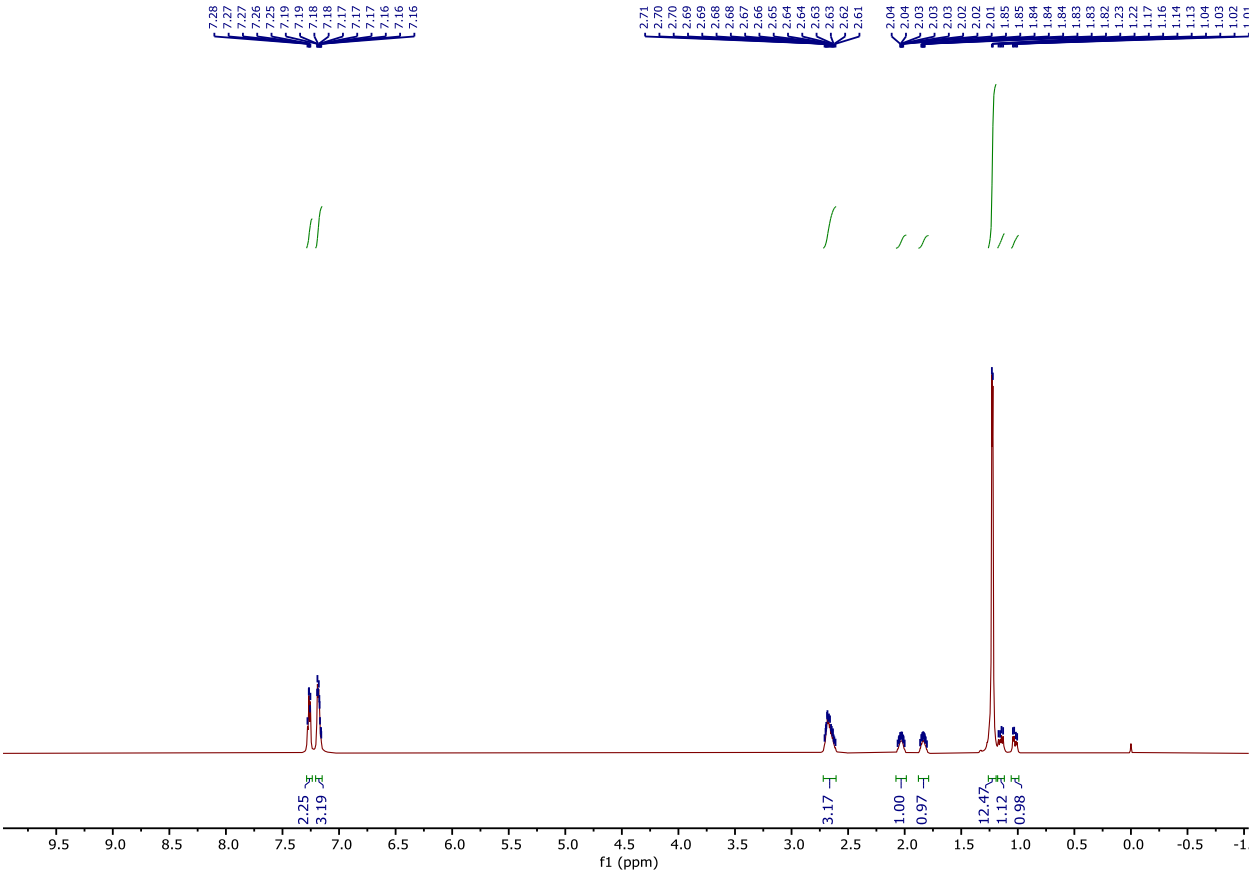

Figure A-76. ^{1}H NMR Spectrum of **2c.**

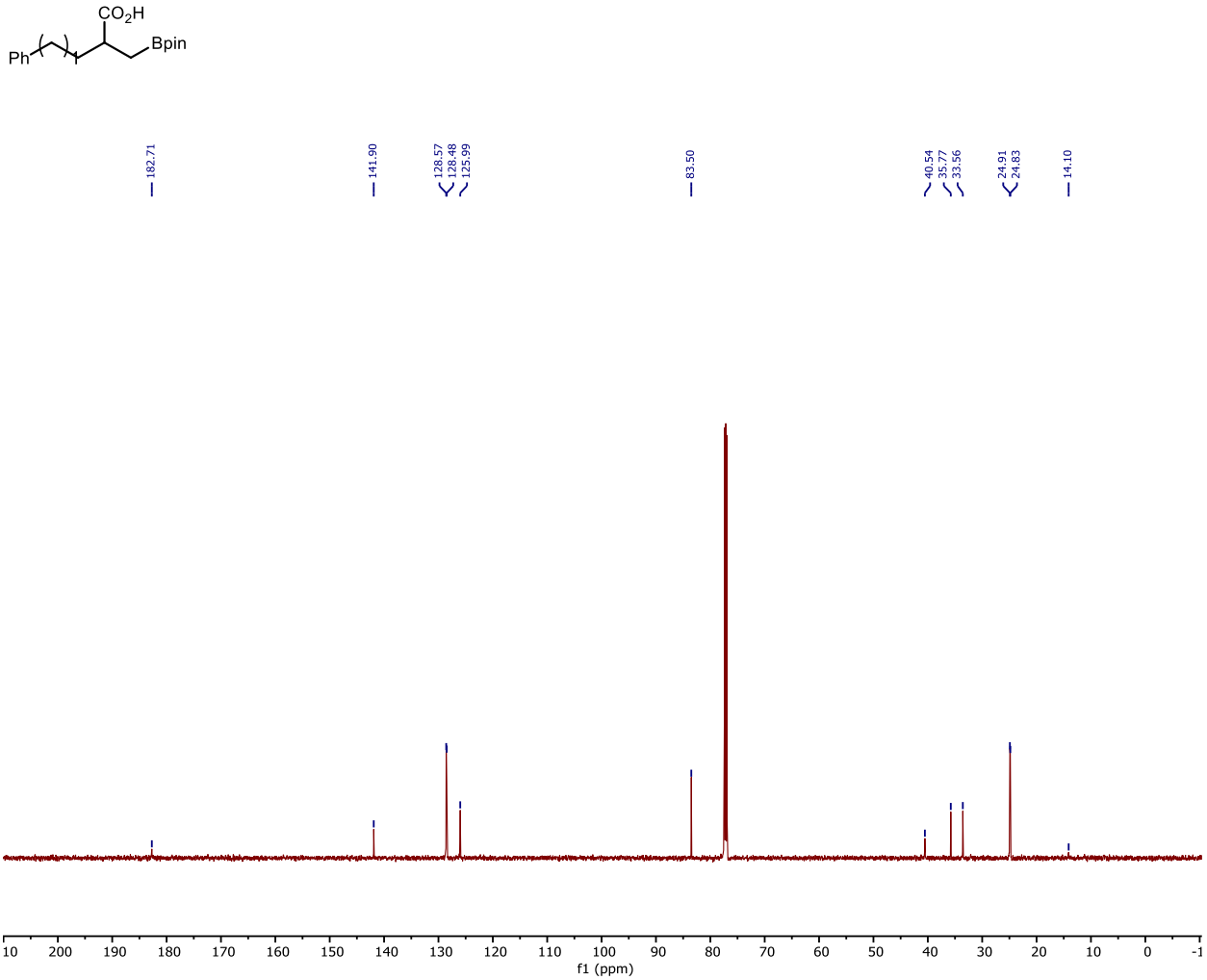

Figure A-77. ^{13}C NMR Spectrum of **2c.**

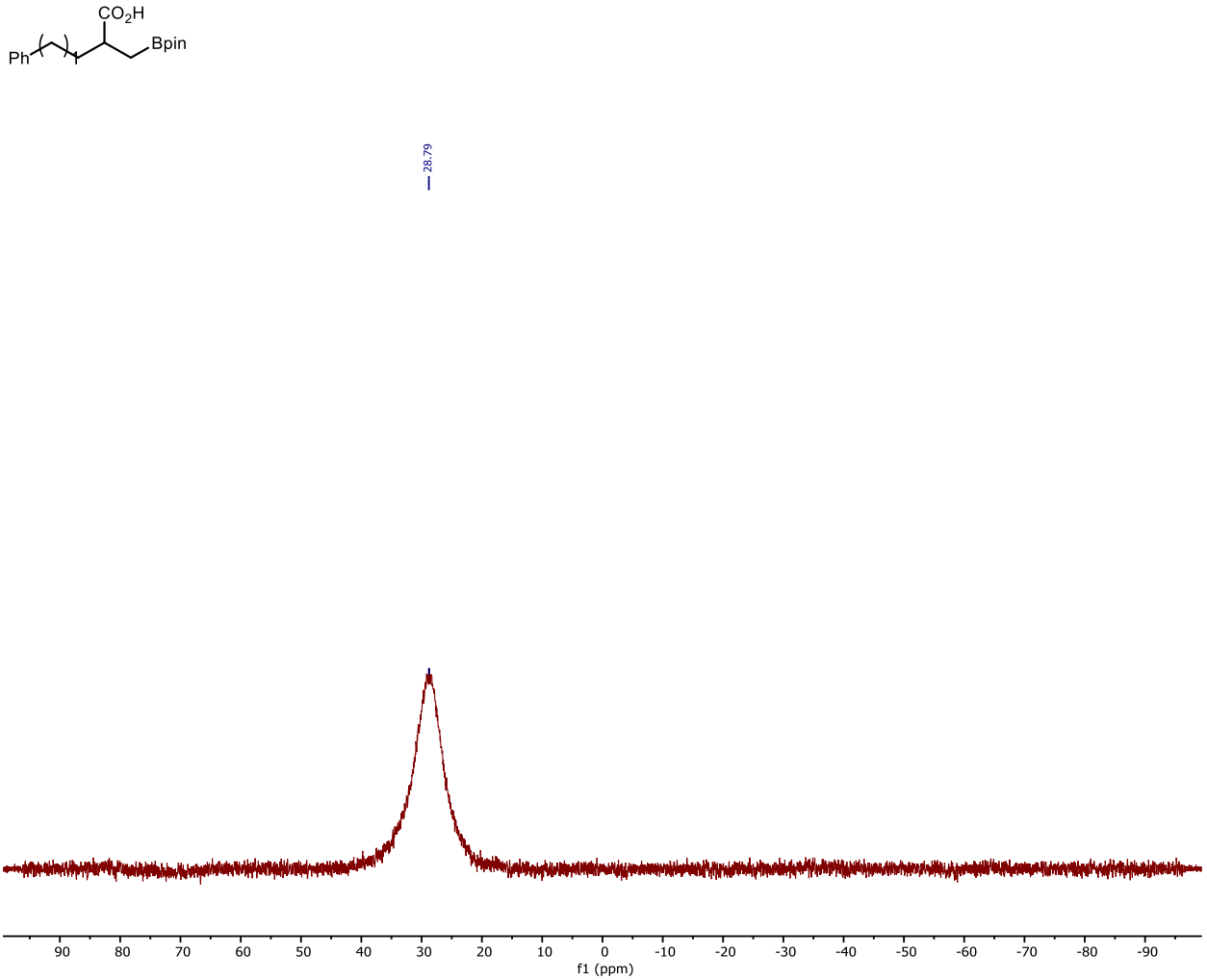

Figure A-78. ^{11}B NMR Spectrum of **2c.**

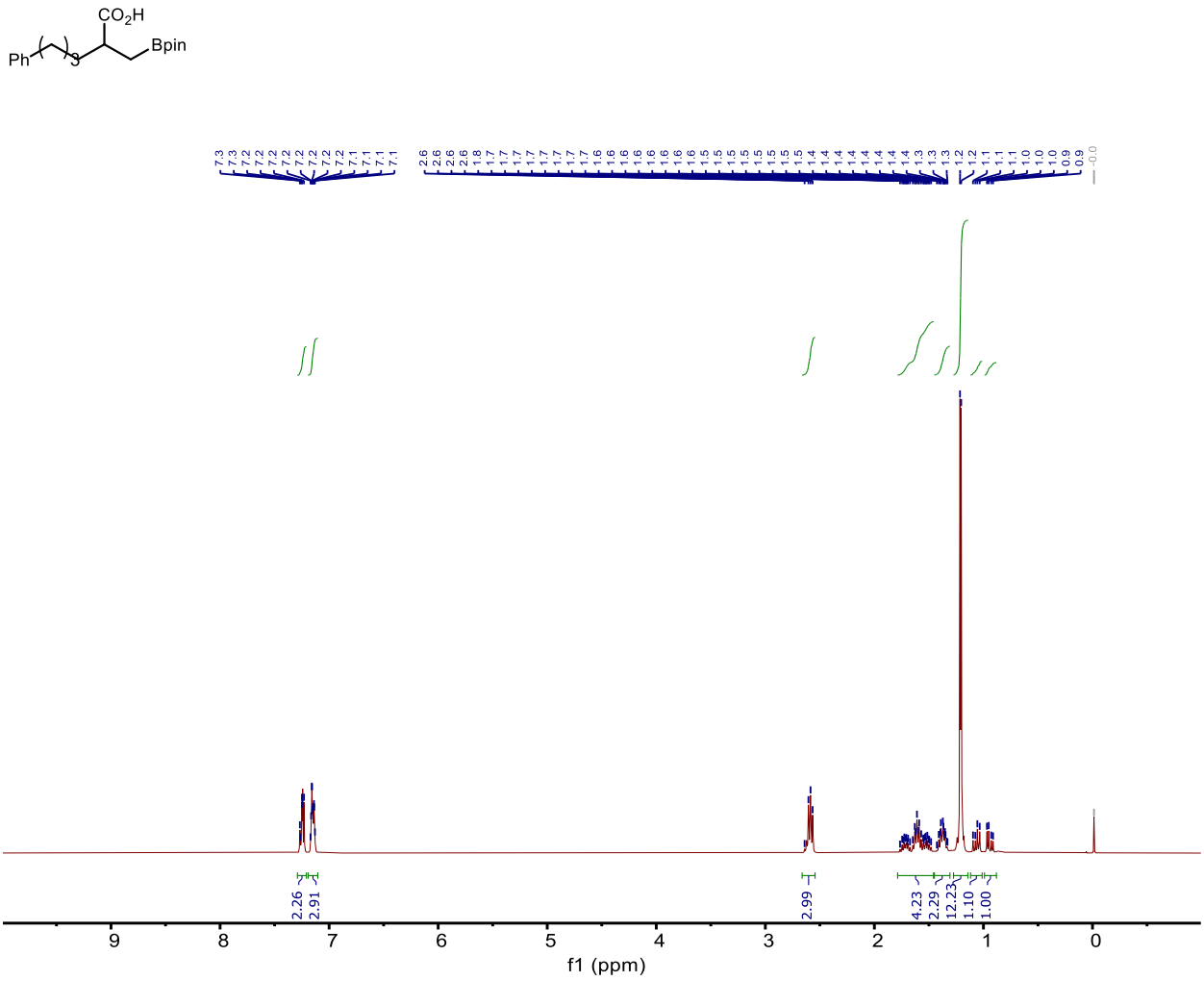

Figure A-79. ^{1}H NMR Spectrum of **2d**.

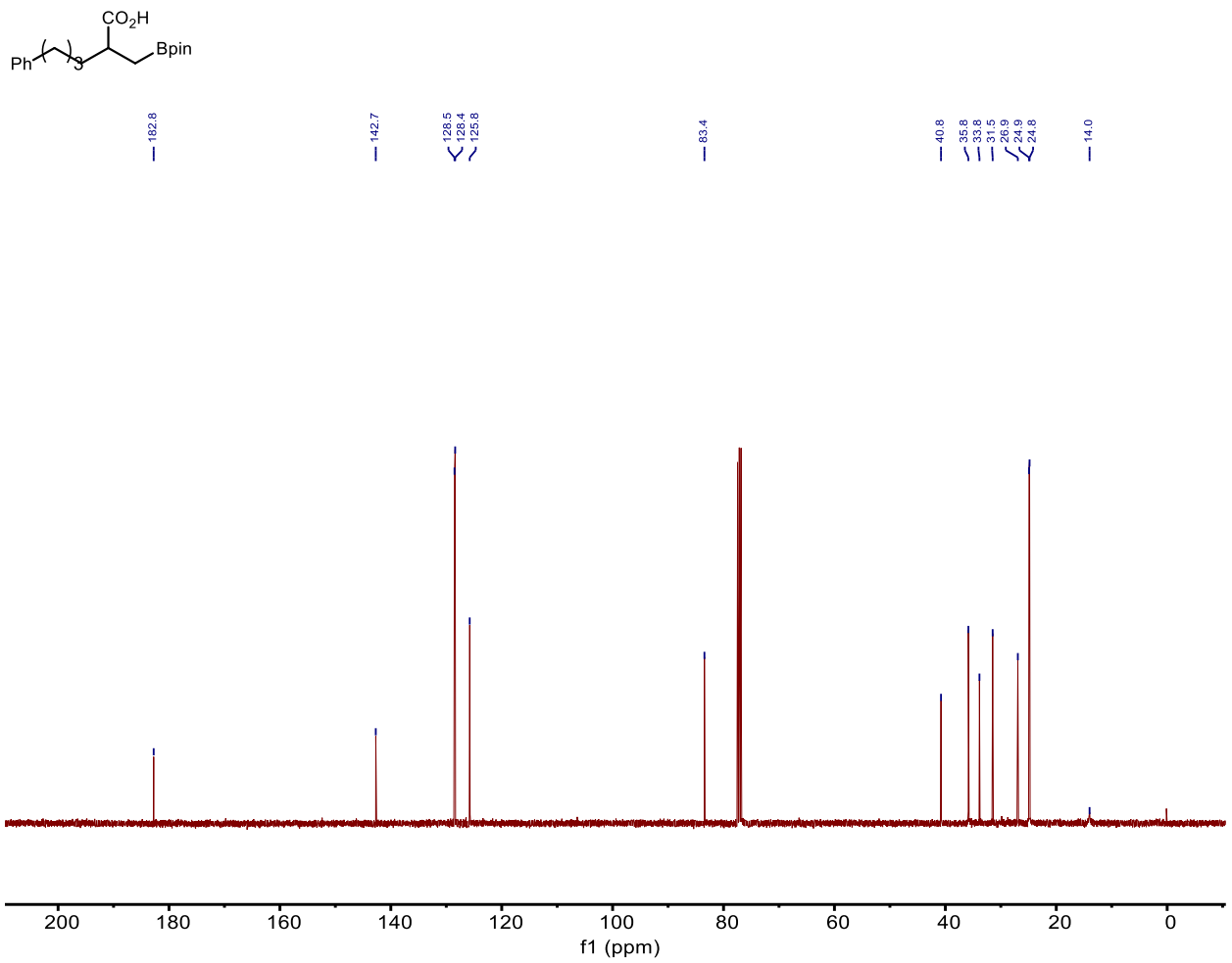

Figure A-80. ^{13}C NMR Spectrum of **2d**.

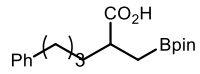

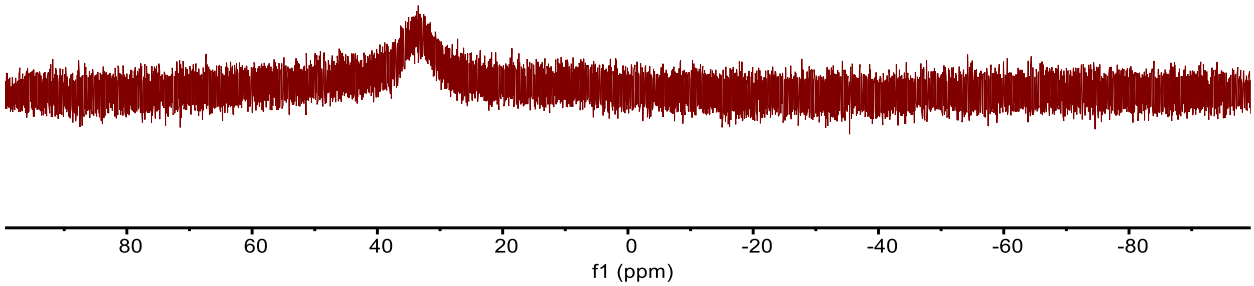

Figure A-81. ^{11}B NMR Spectrum of **2d.**

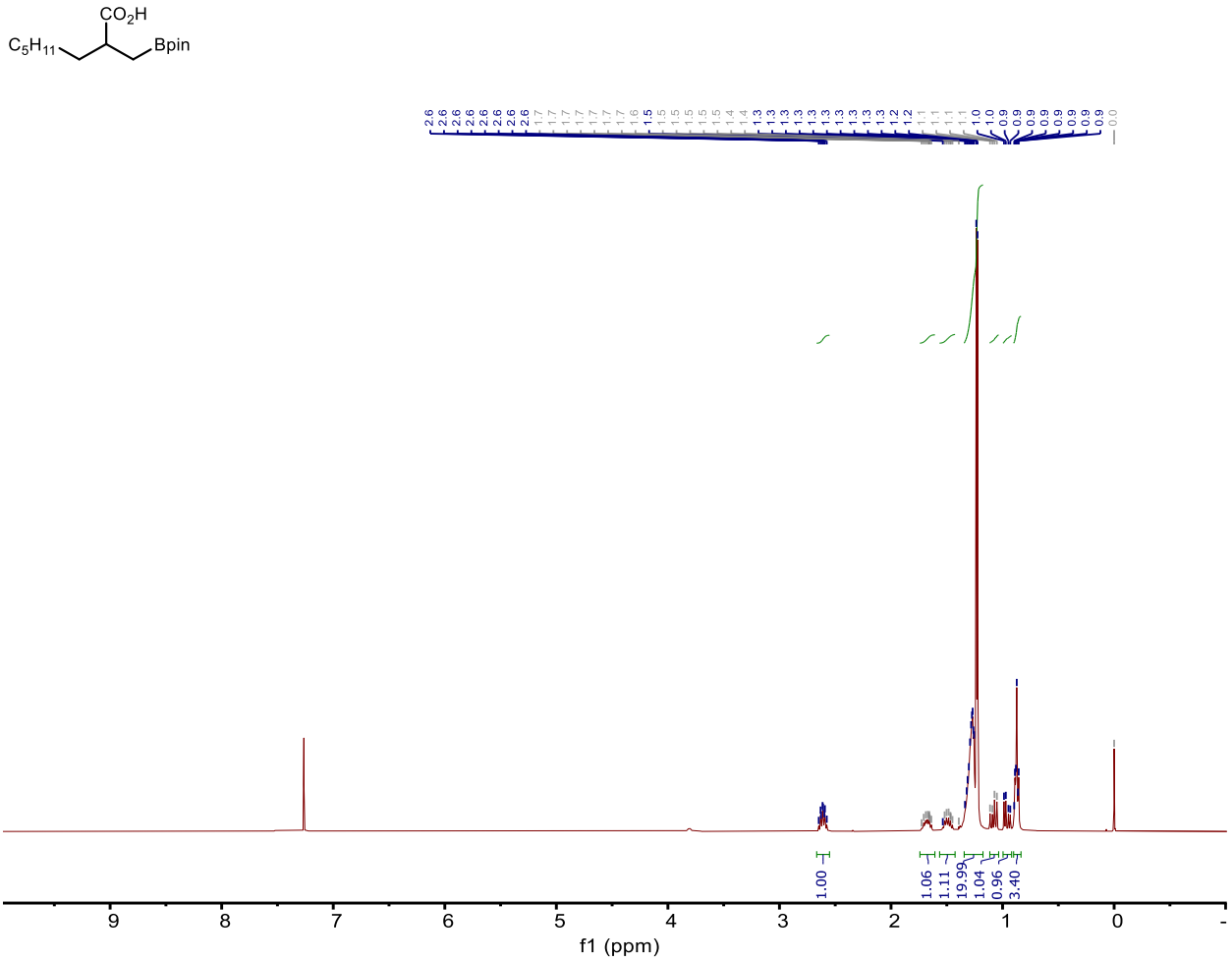

Figure A-82. ^{1}H NMR Spectrum of **2e**.

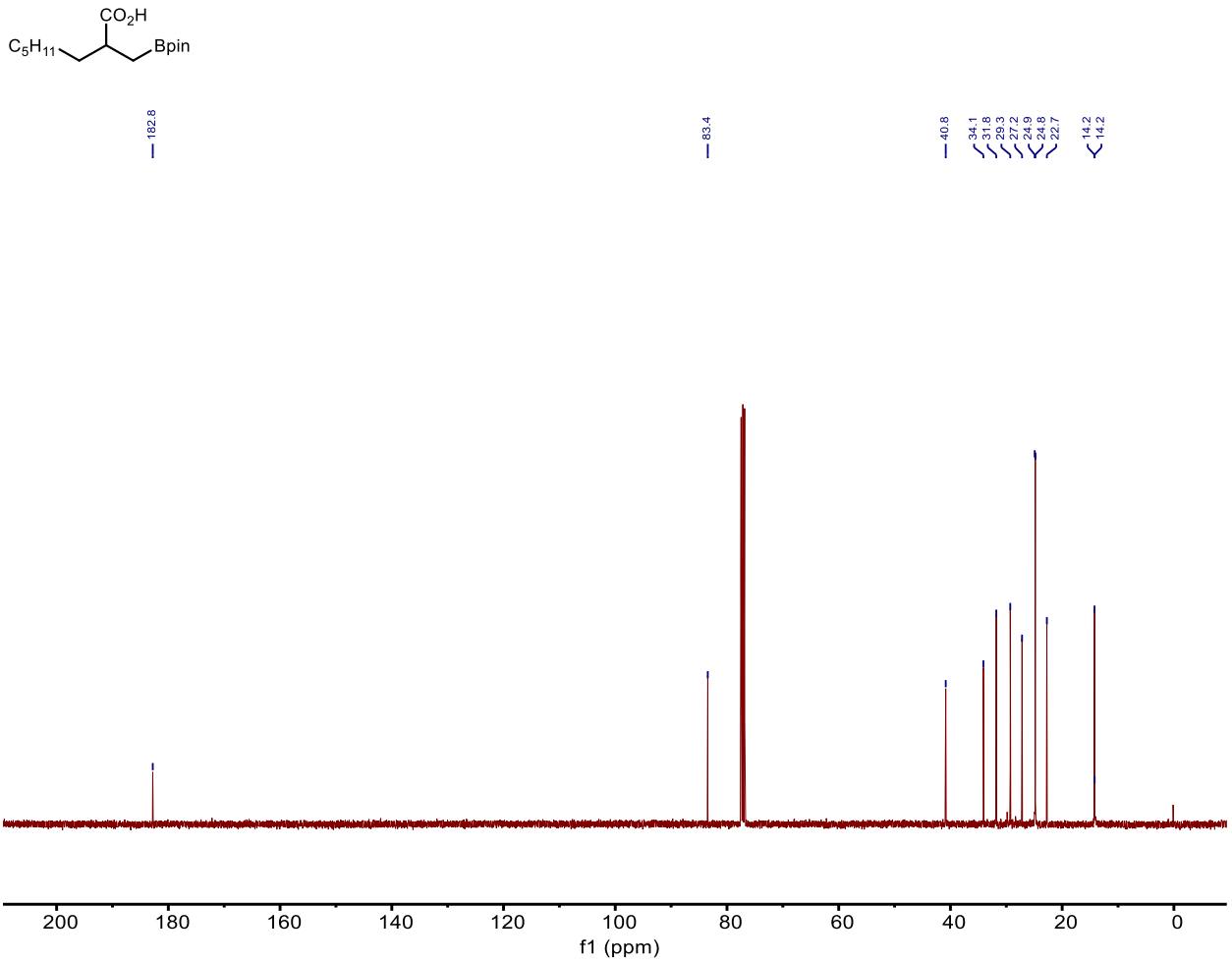

Figure A-83. ^{13}C NMR Spectrum of **2e**.

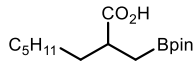

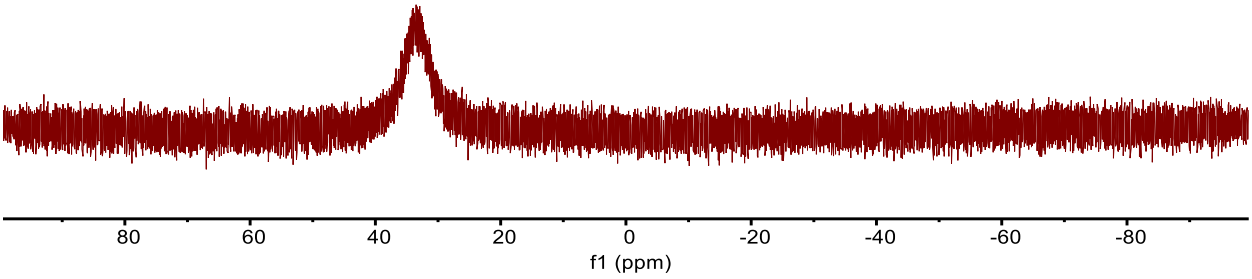

Figure A-84. ^{11}B NMR Spectrum of **2e.**

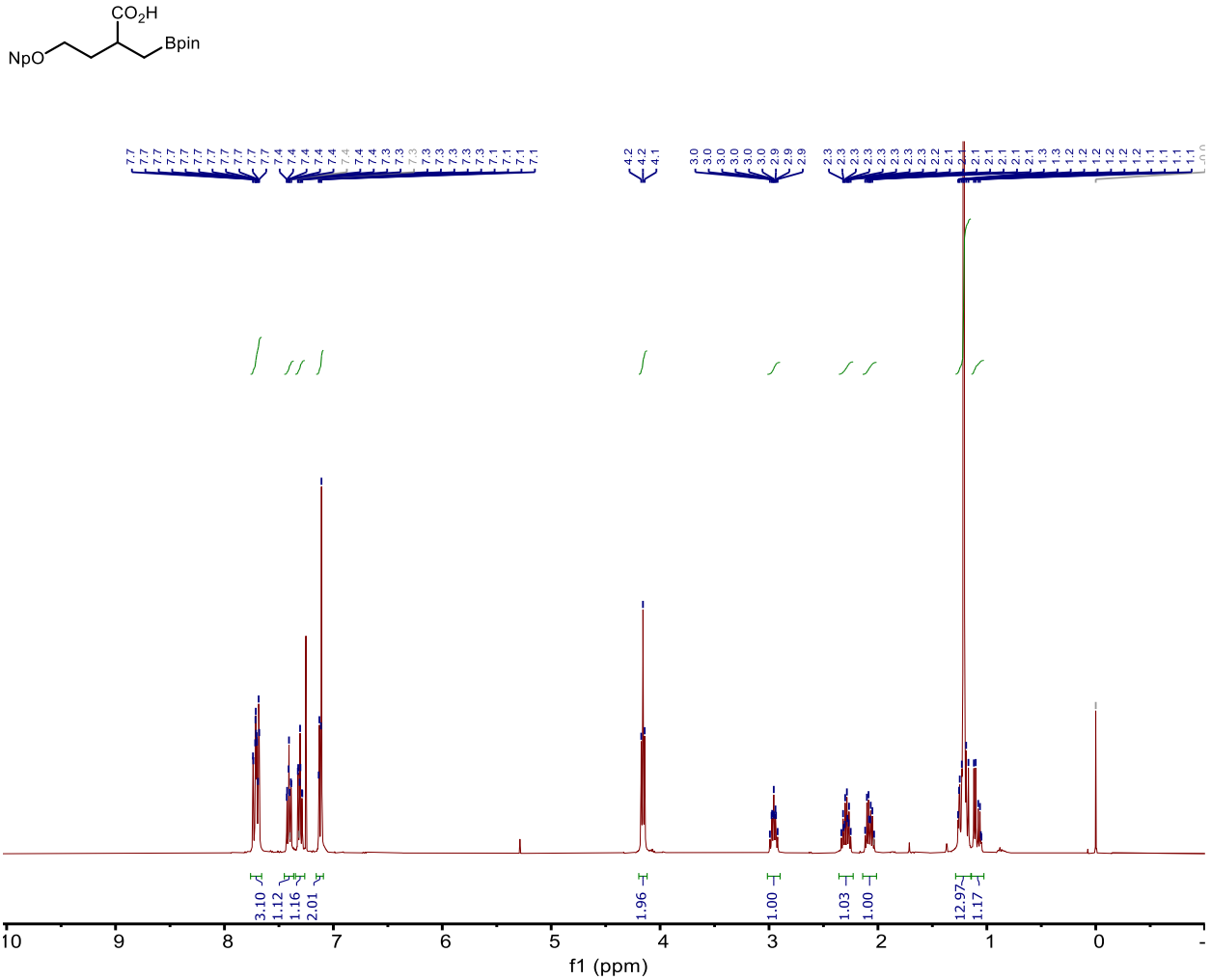

Figure A-85. ^{1}H NMR Spectrum of **2f**.

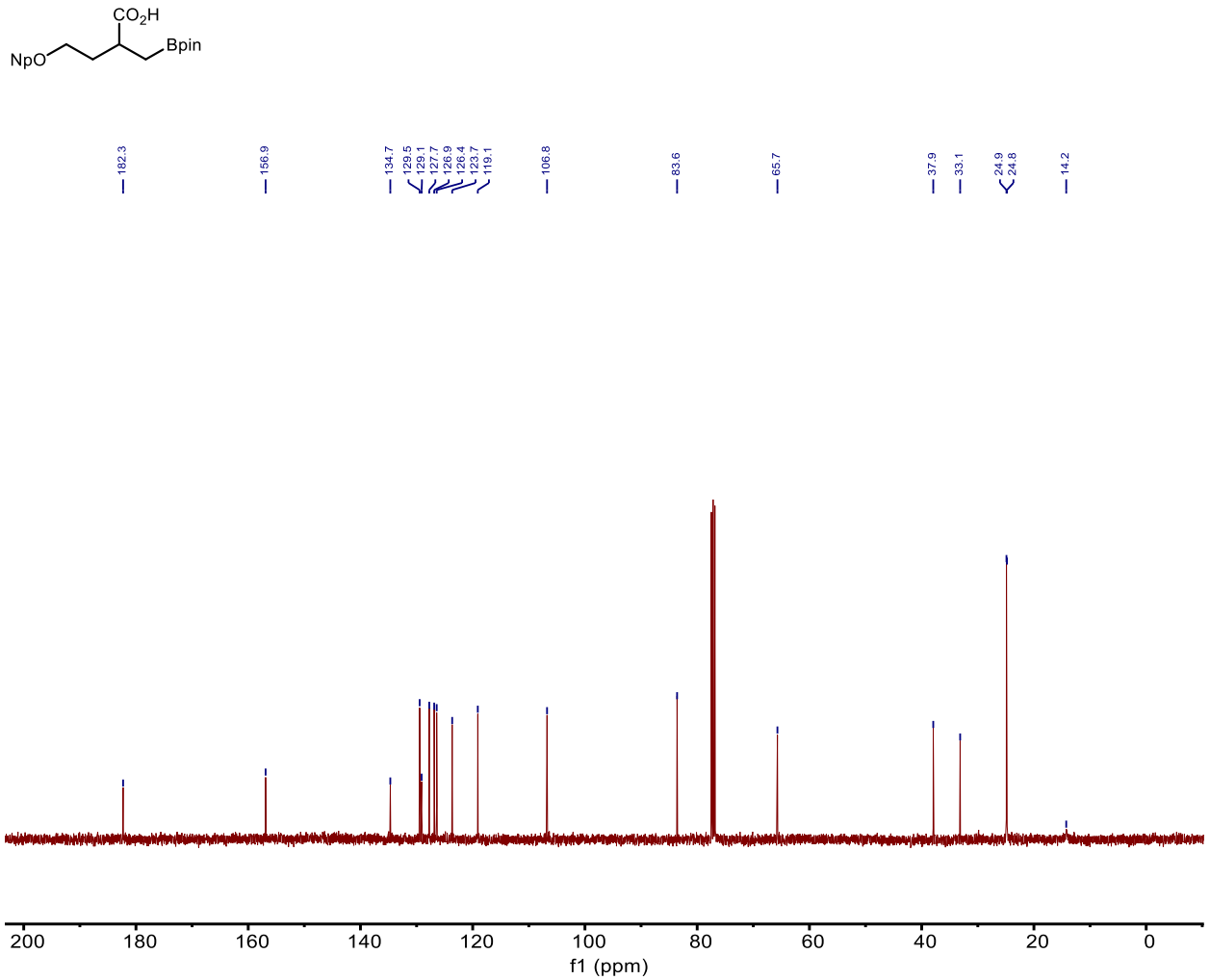

Figure A-86. ^{13}C NMR Spectrum of **2f**.

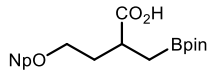

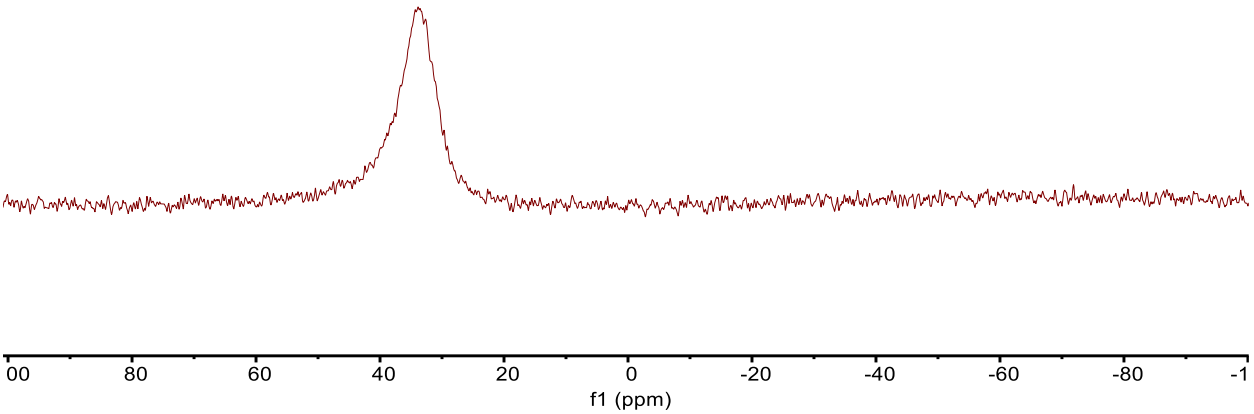

Figure A-87. ^{11}B NMR Spectrum of **2f.**

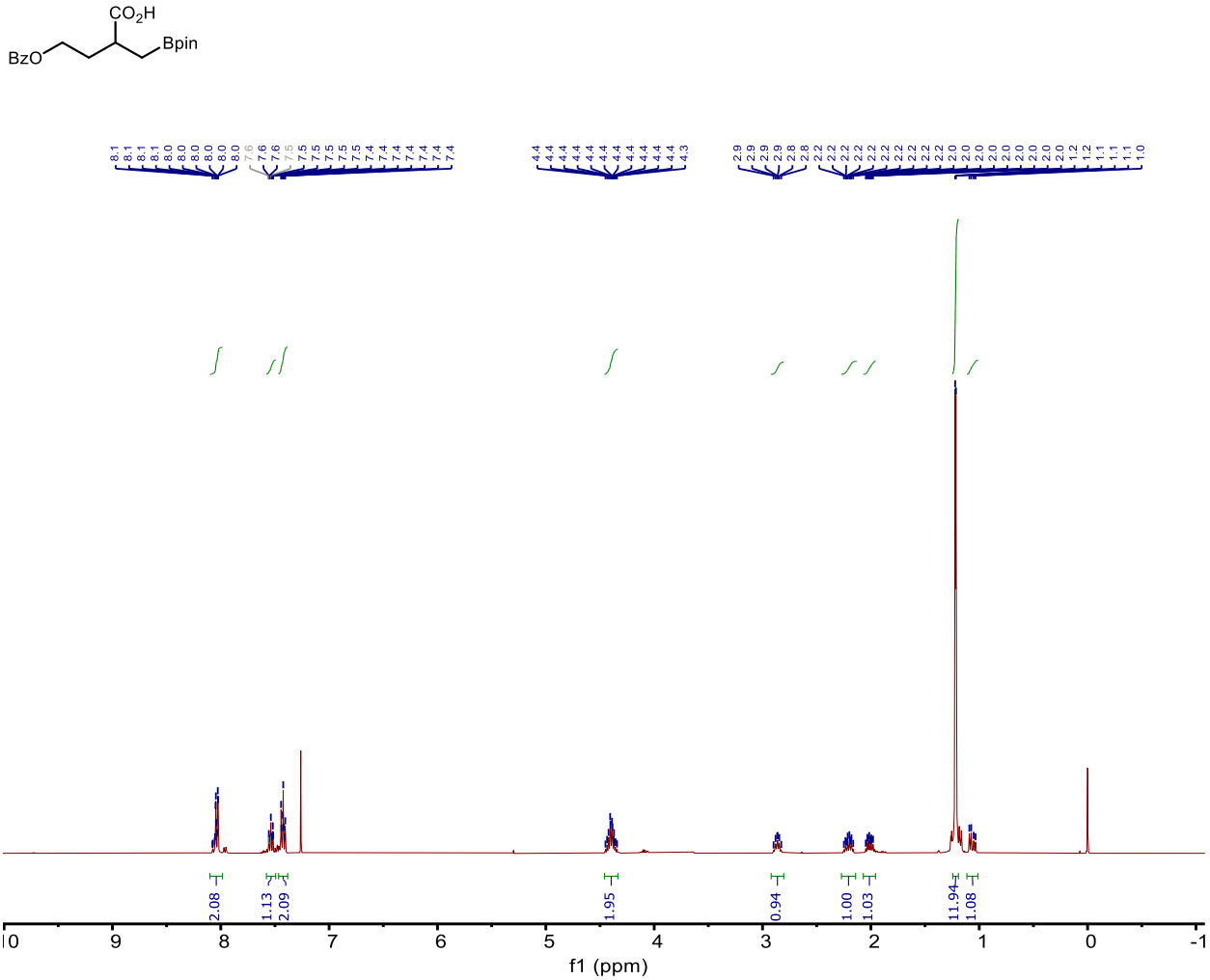

Figure A-88. ^{1}H NMR Spectrum of **2g**.

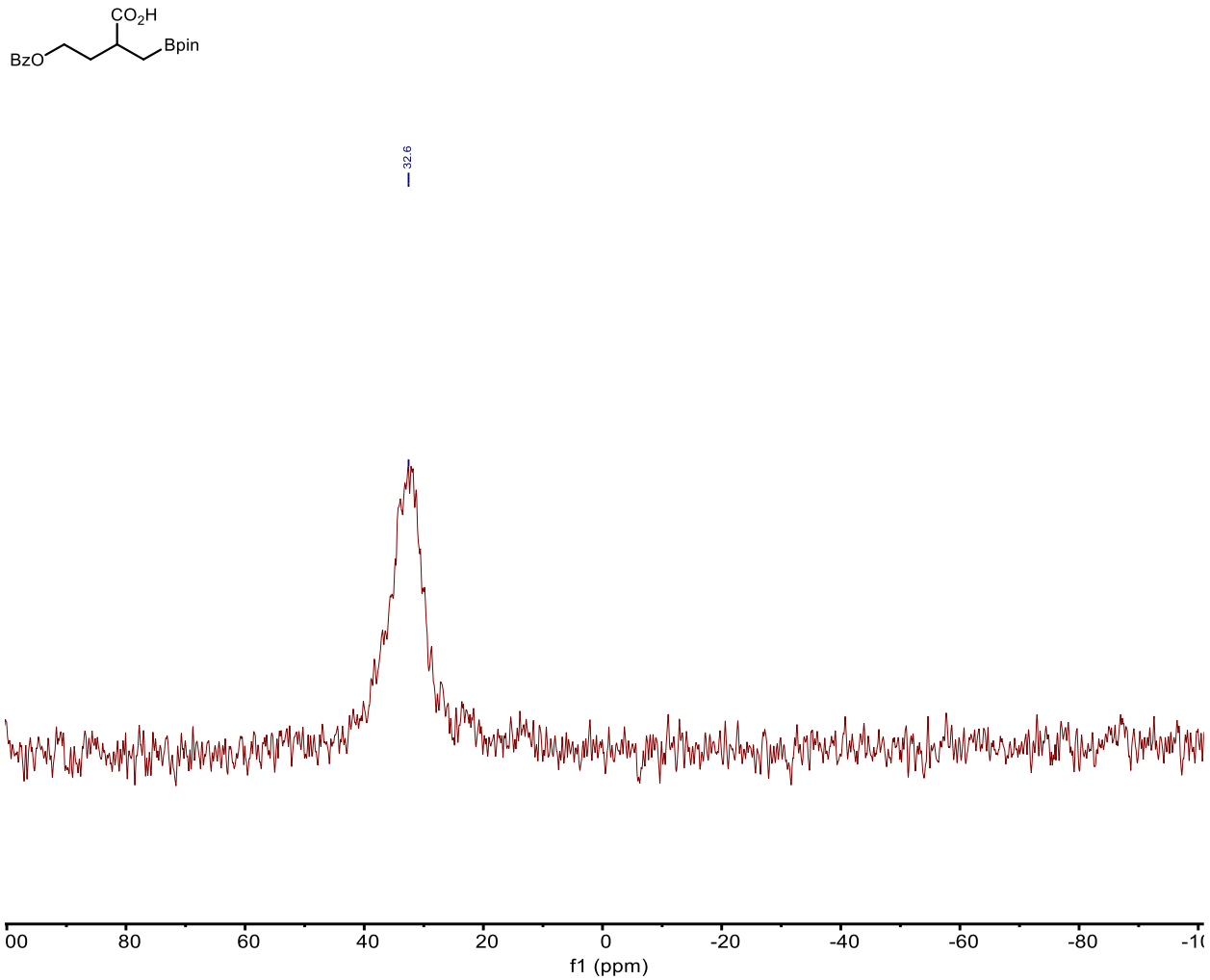

Figure A-89. ^{11}B NMR Spectrum of **2g.**

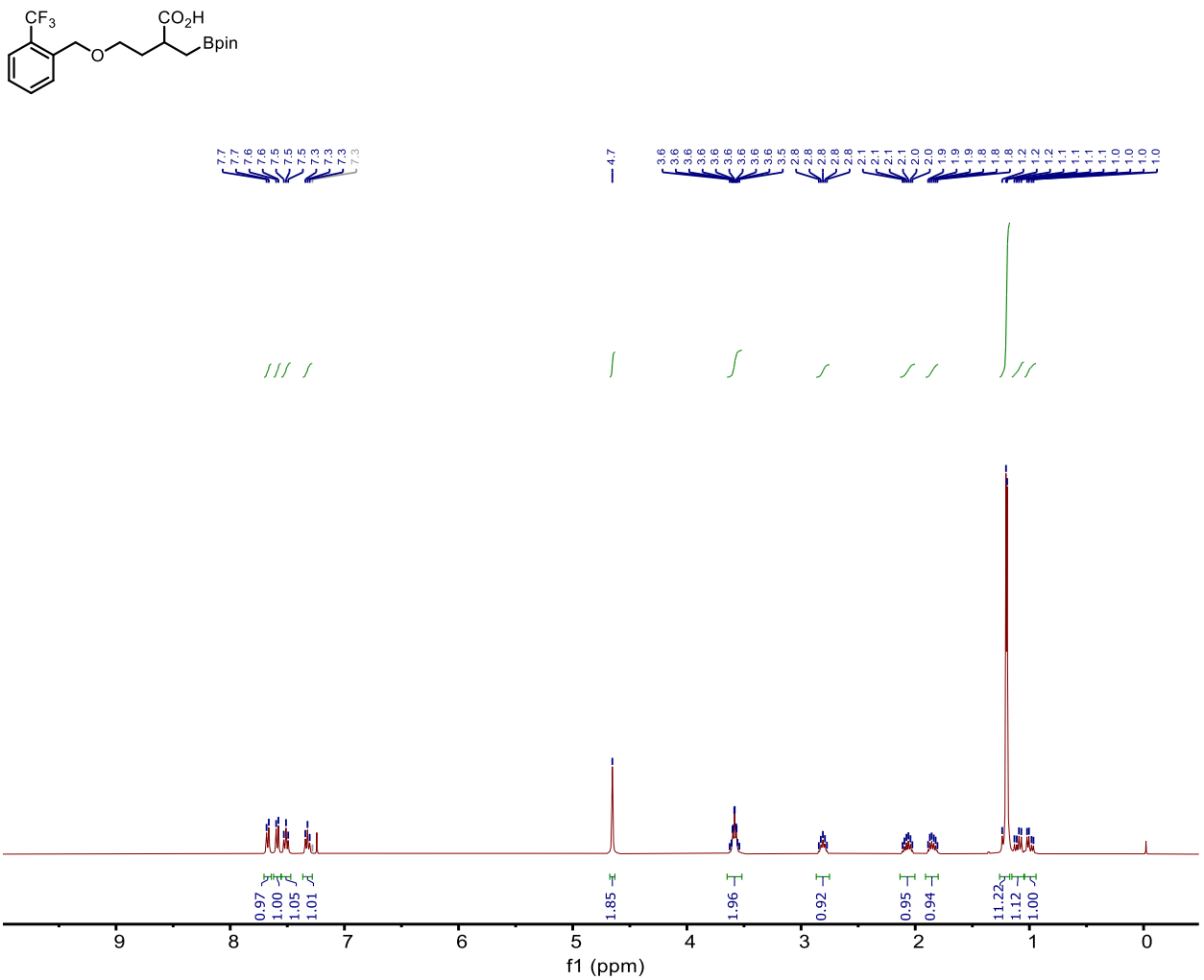

Figure A-90. ^{1}H NMR Spectrum of **2h**.

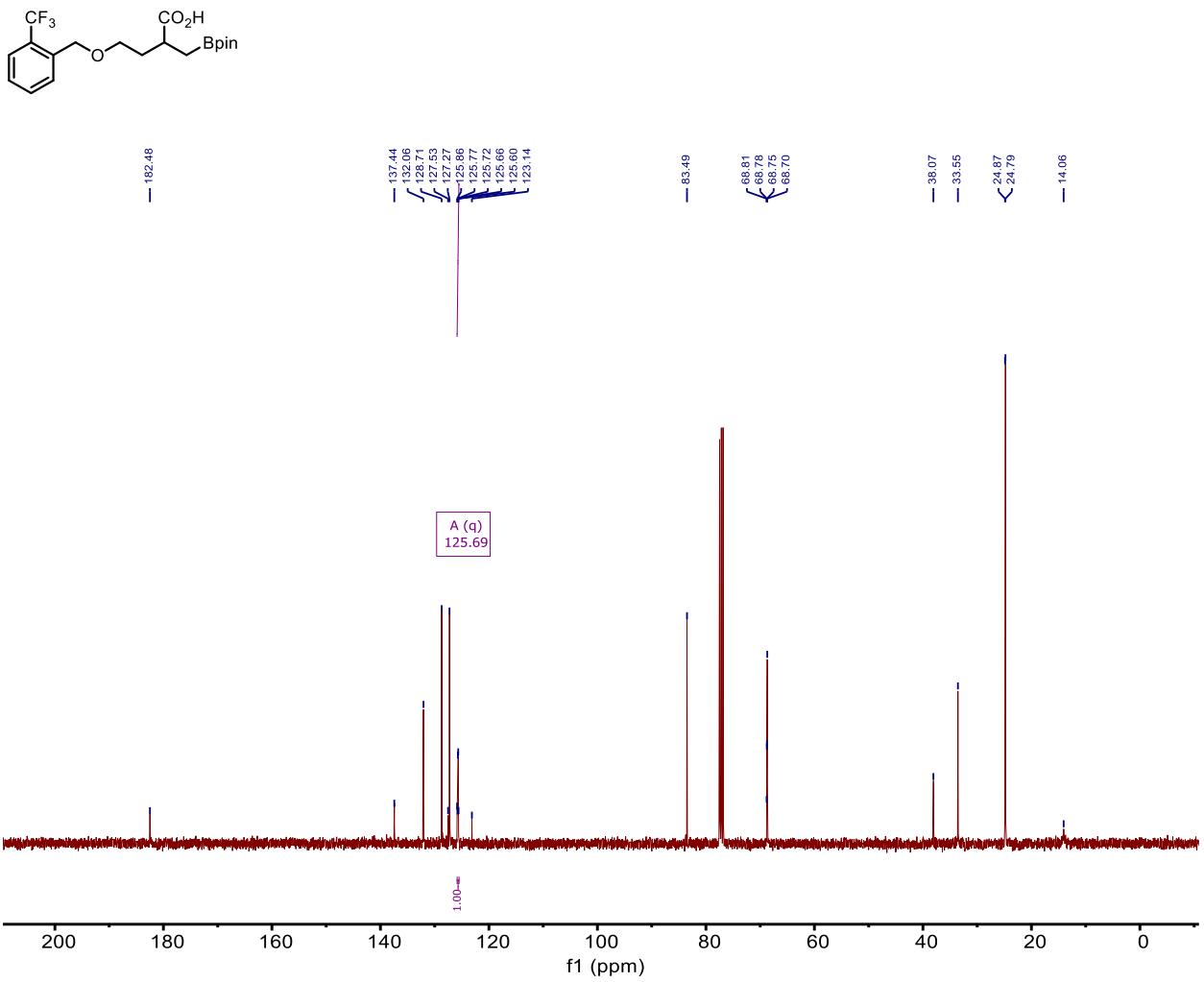

Figure A-91. ^{13}C NMR Spectrum of **2h**.

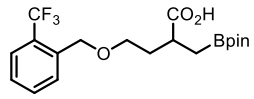

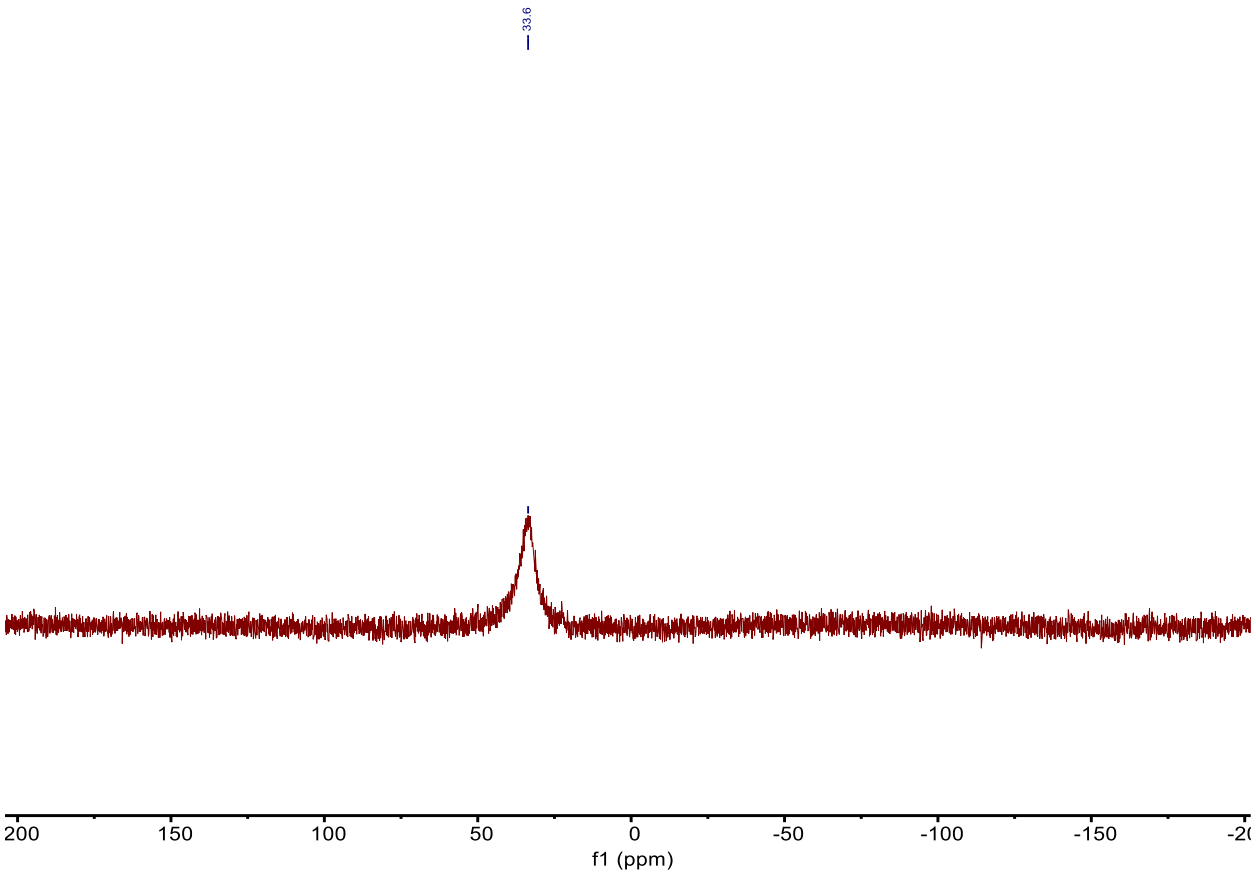

Figure A-92. ^{11}B NMR Spectrum of **2h.**

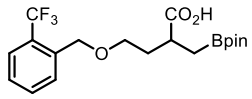

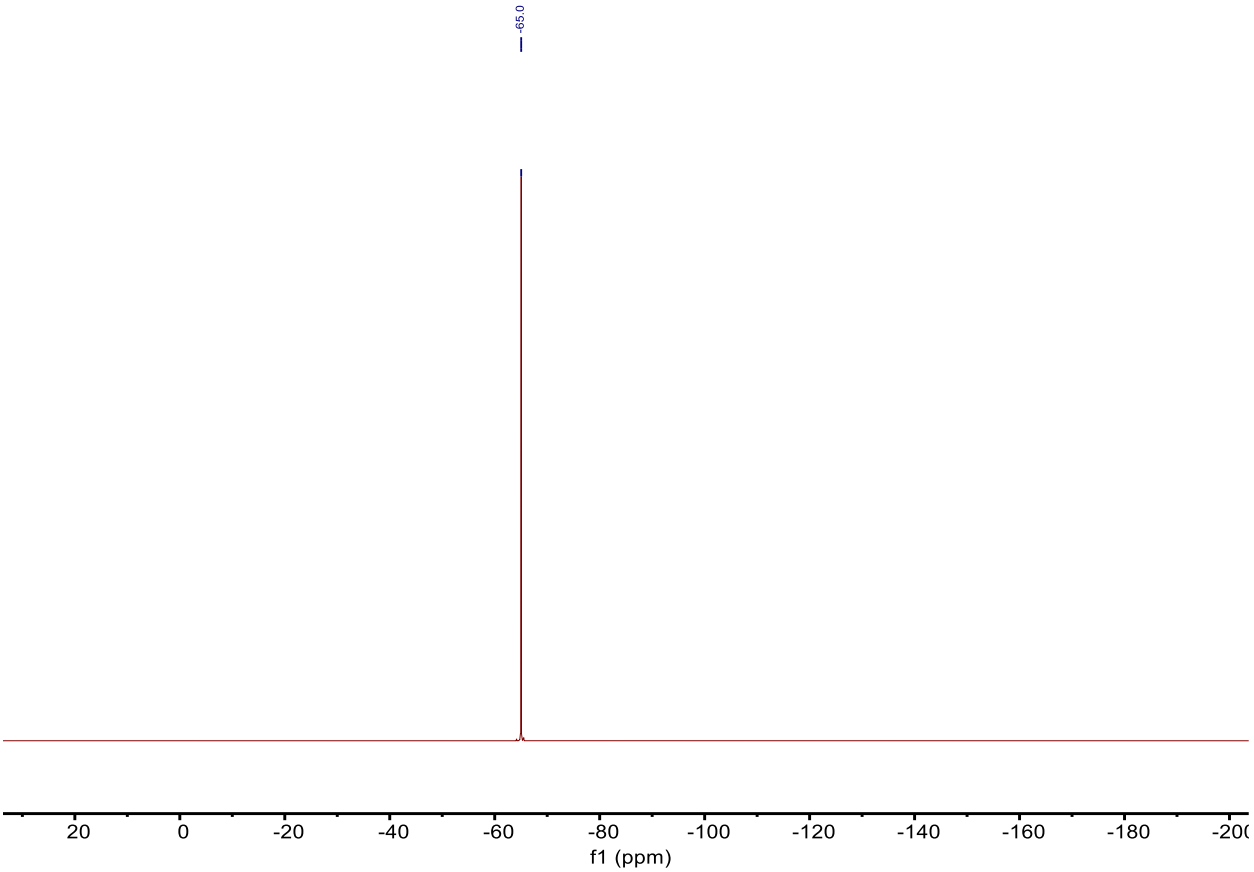

Figure A-93. ^{19}F NMR Spectrum of **2h.**

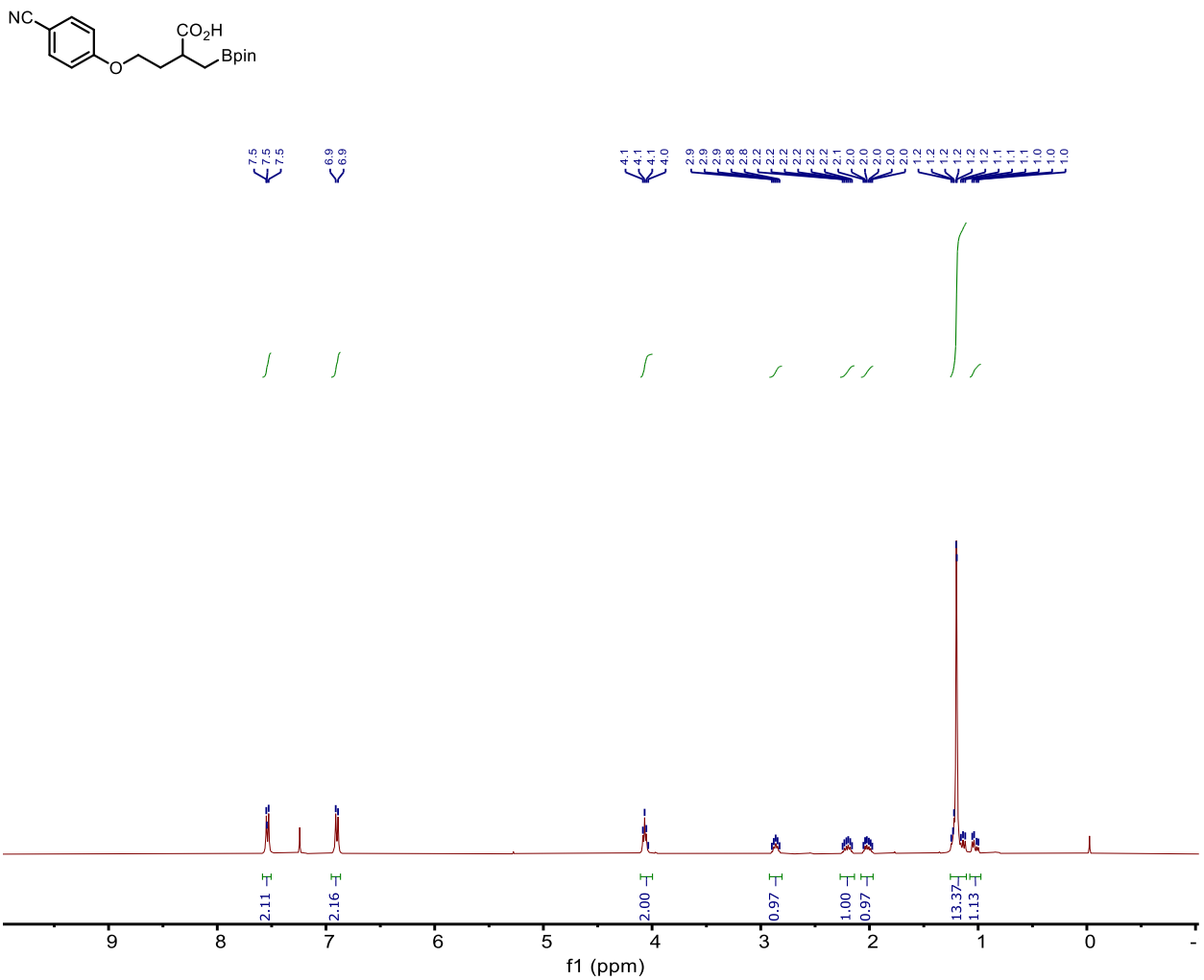

Figure A-95. ^{1}H NMR Spectrum of **2i**.

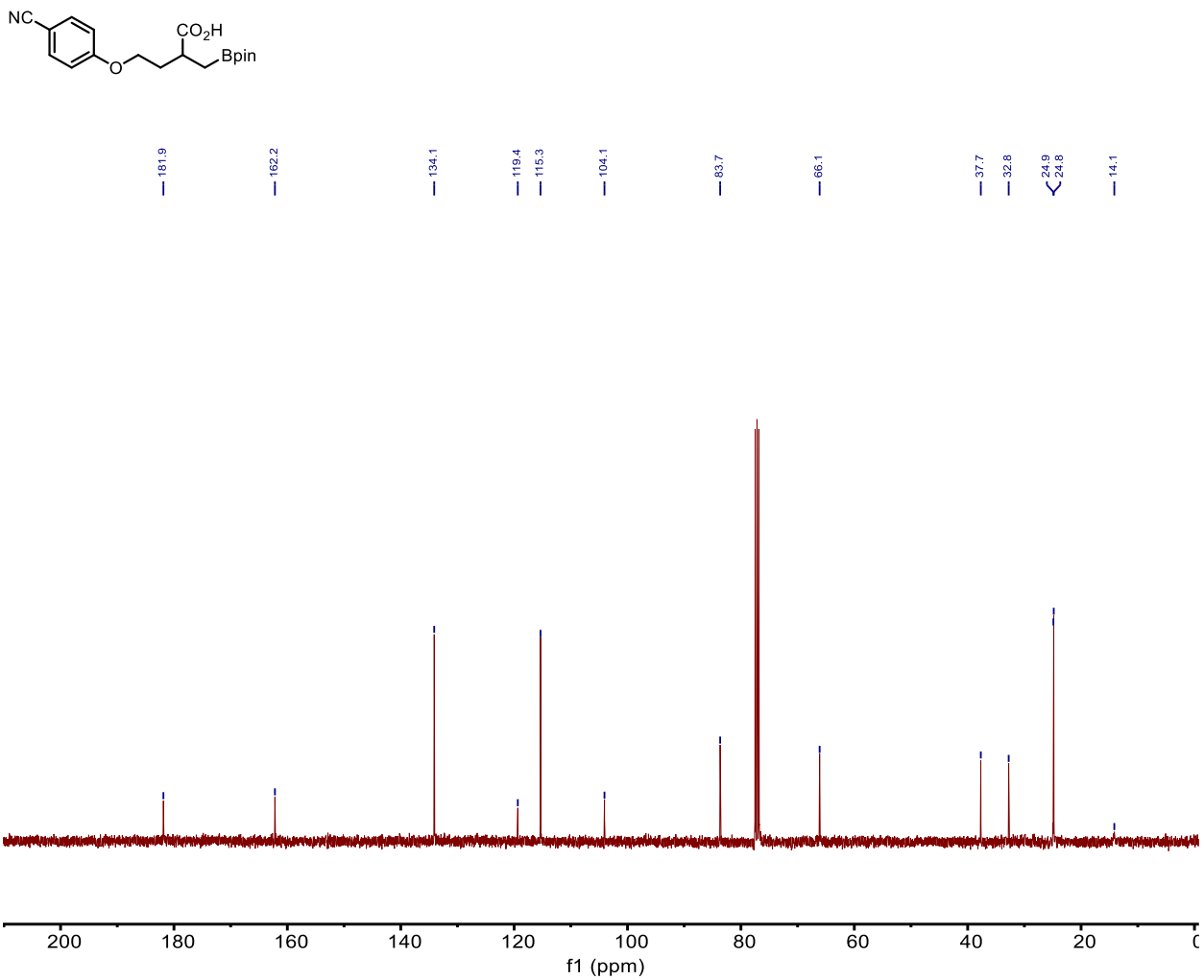

Figure A-96. ^{13}C NMR Spectrum of **2i**.

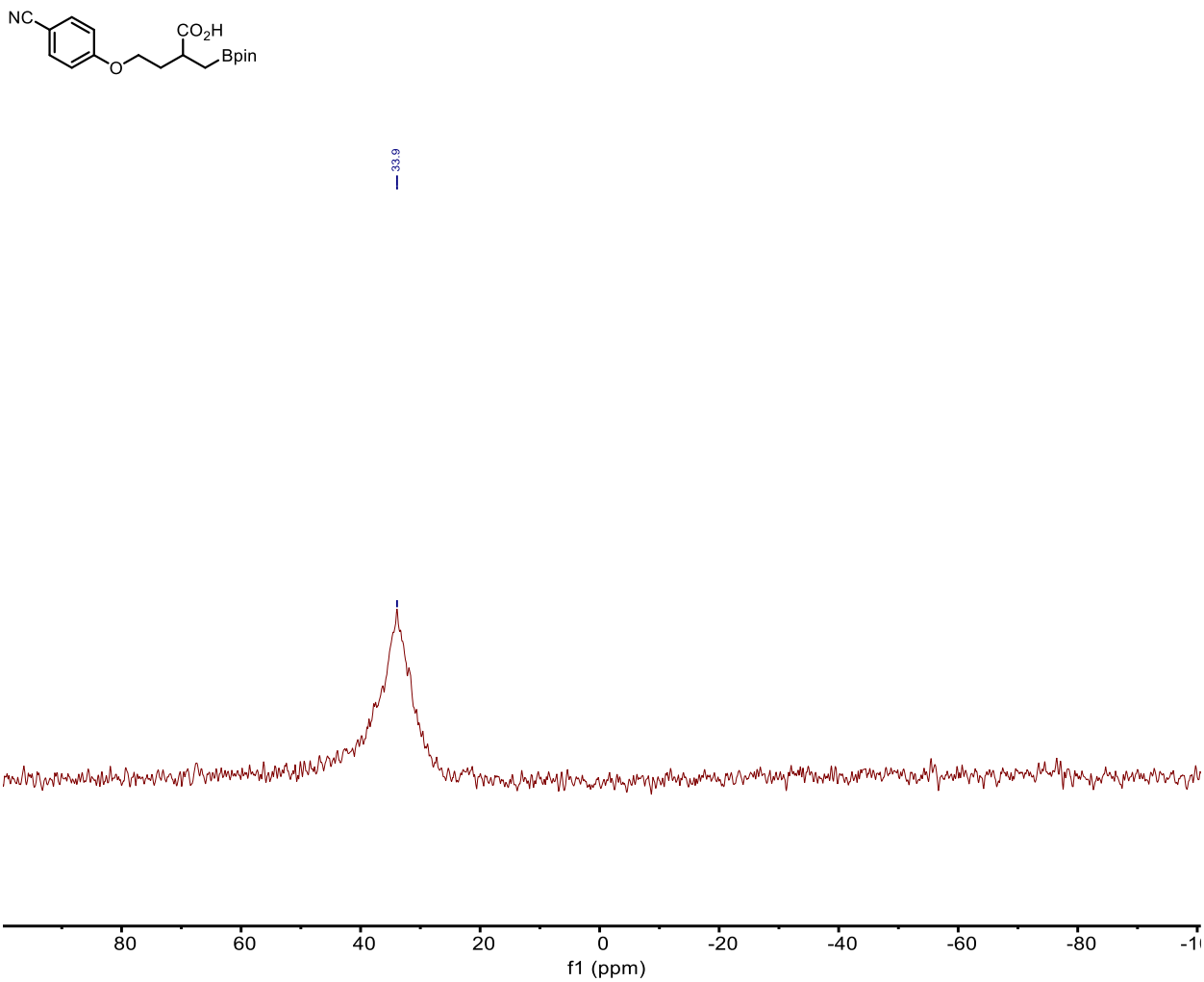

Figure A-97. ^{11}B NMR Spectrum of **2i.**

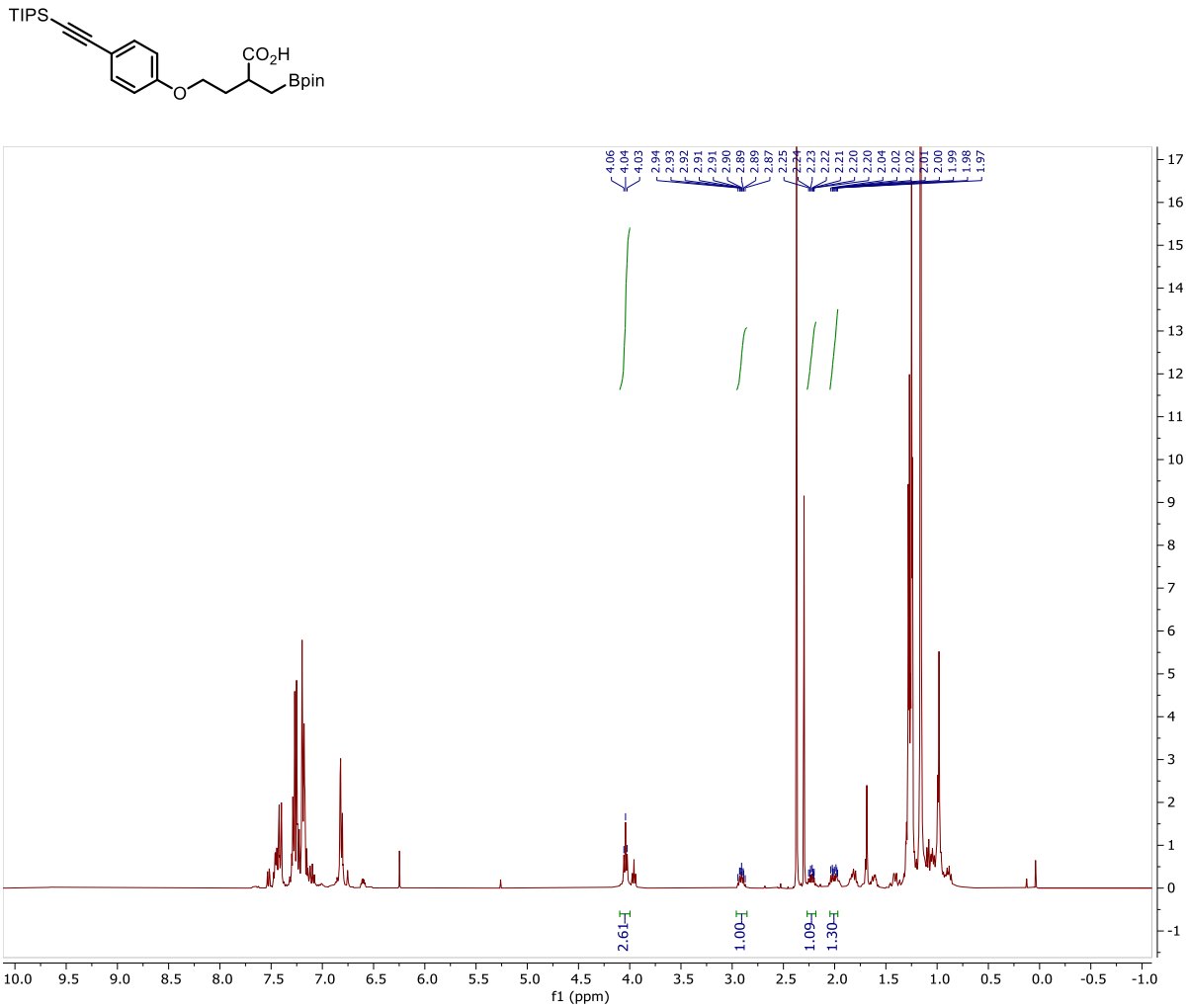

Figure A-98. Crude ^{1}H NMR Spectrum of **2j**.

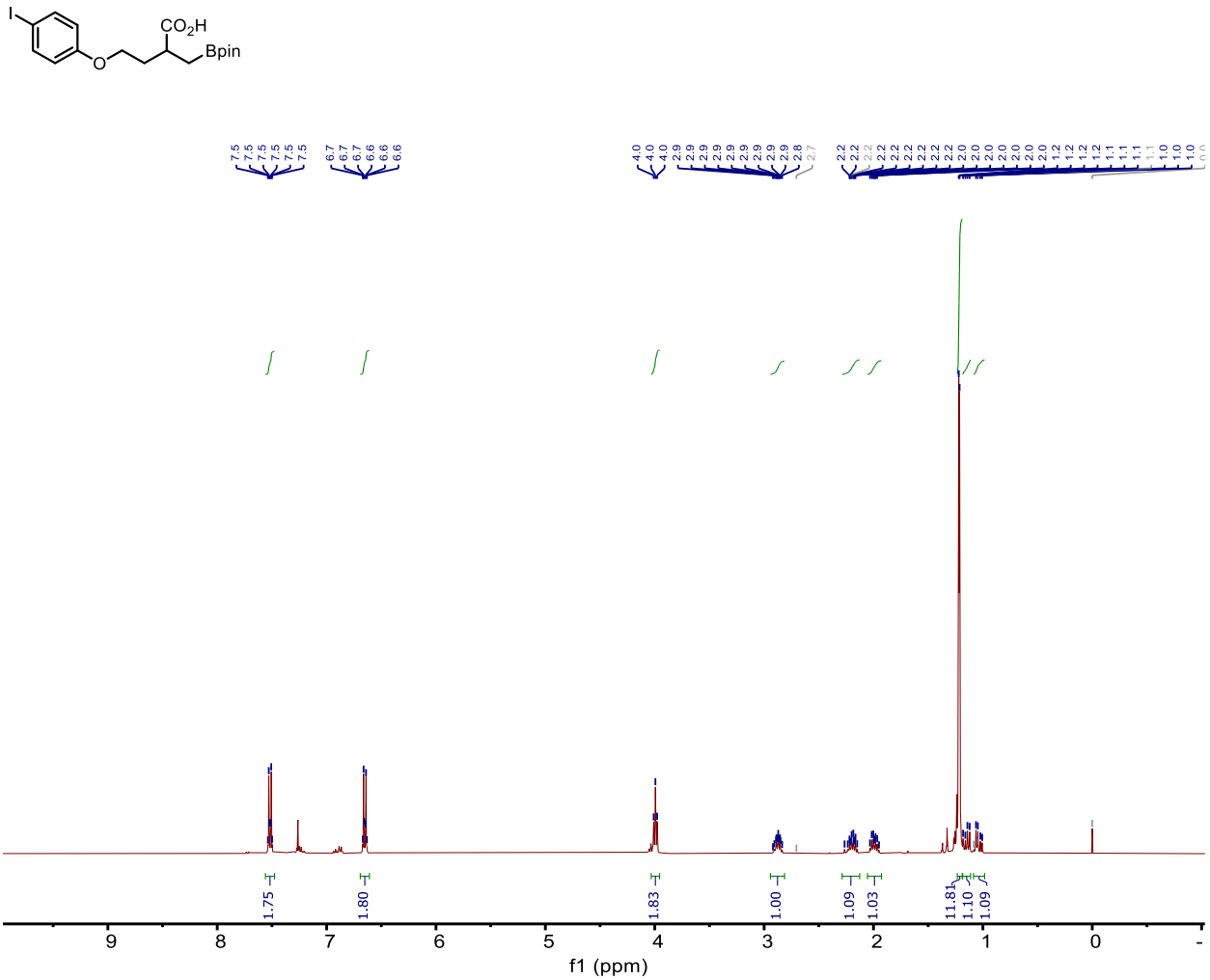

Figure A-99. ^{1}H NMR Spectrum of **2k**.

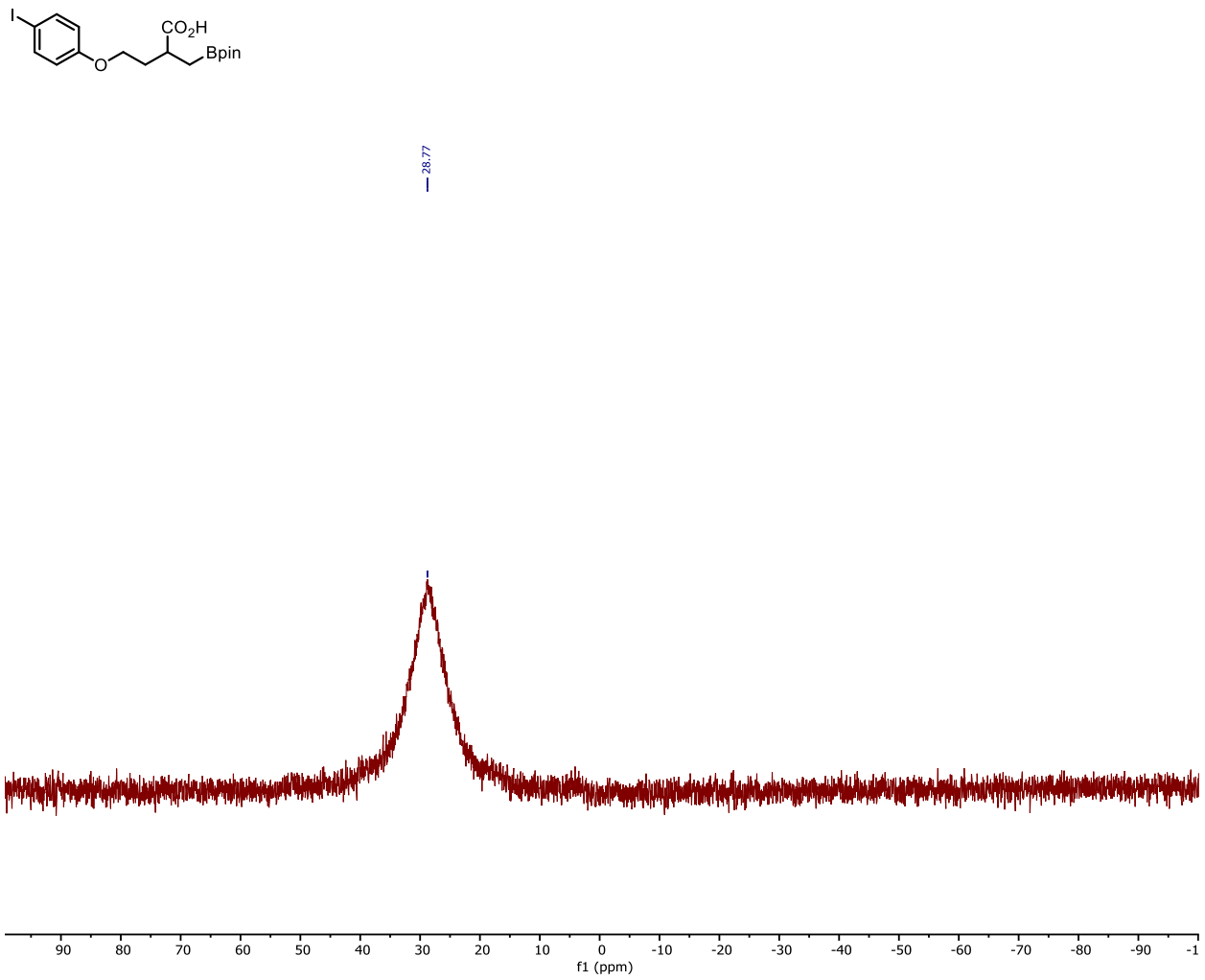

Figure A-100. ^{11}B NMR Spectrum of **2k.**

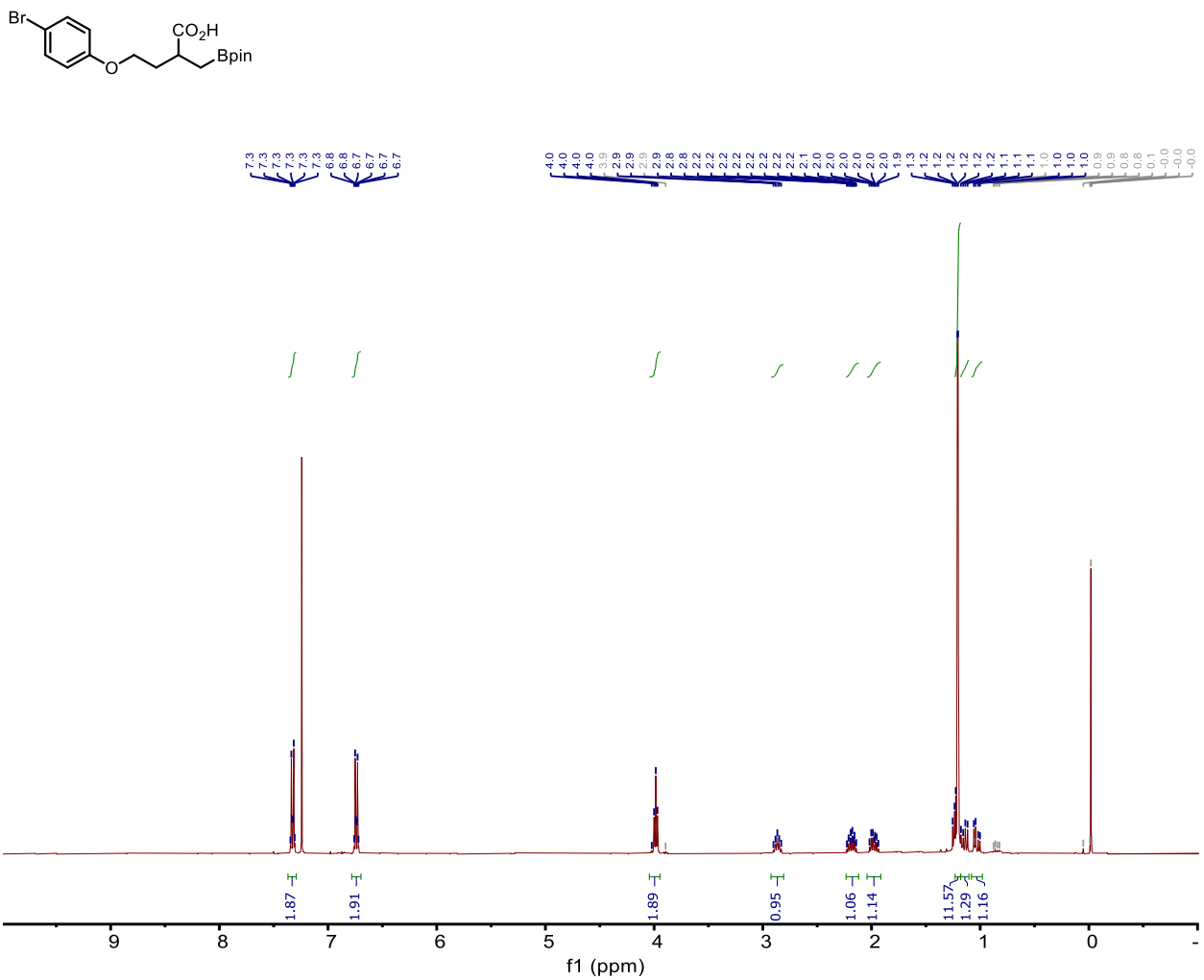

Figure A-101. ^{1}H NMR Spectrum of **2l**.

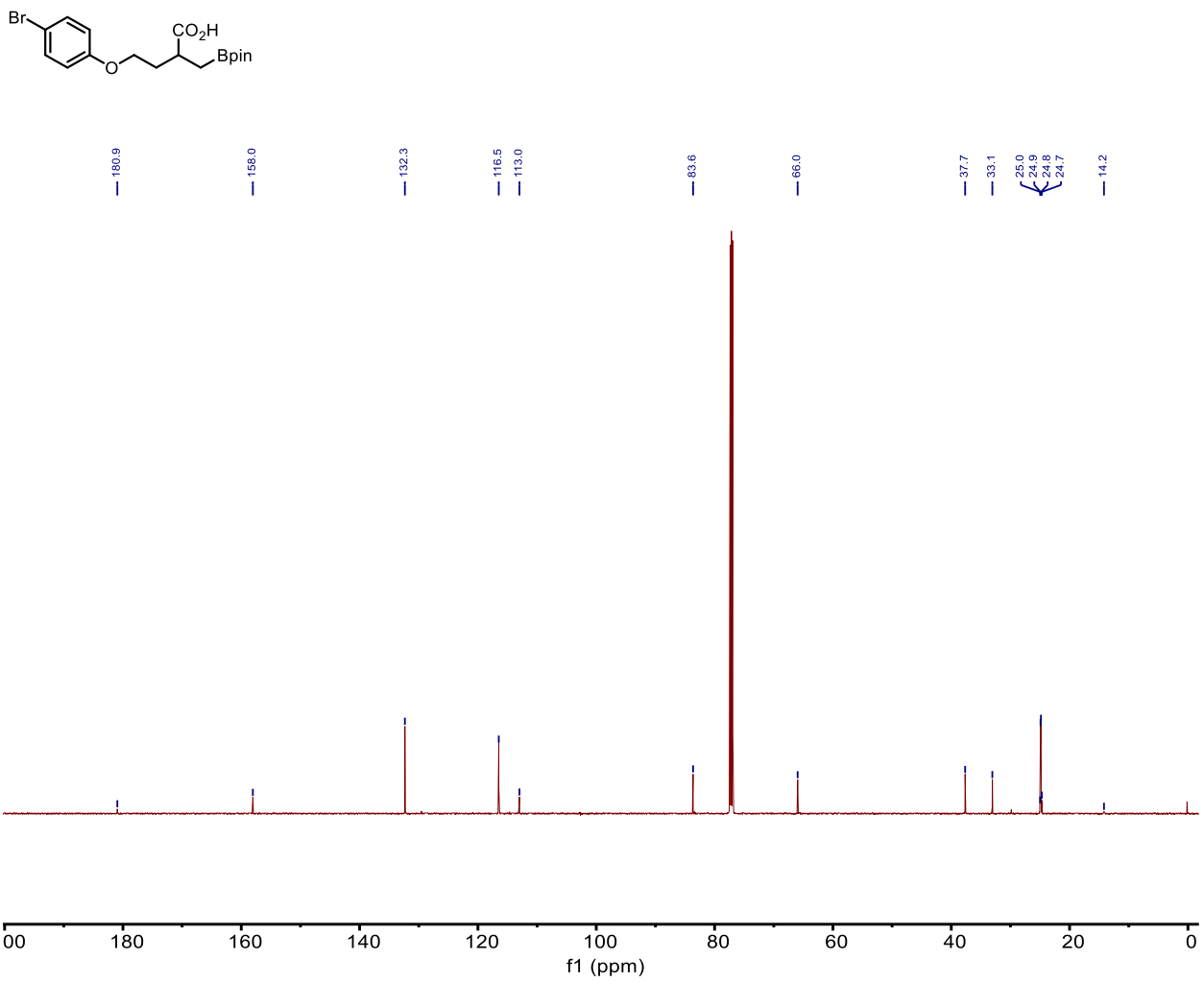

Figure A-102. ^{13}C NMR Spectrum of **2l**.

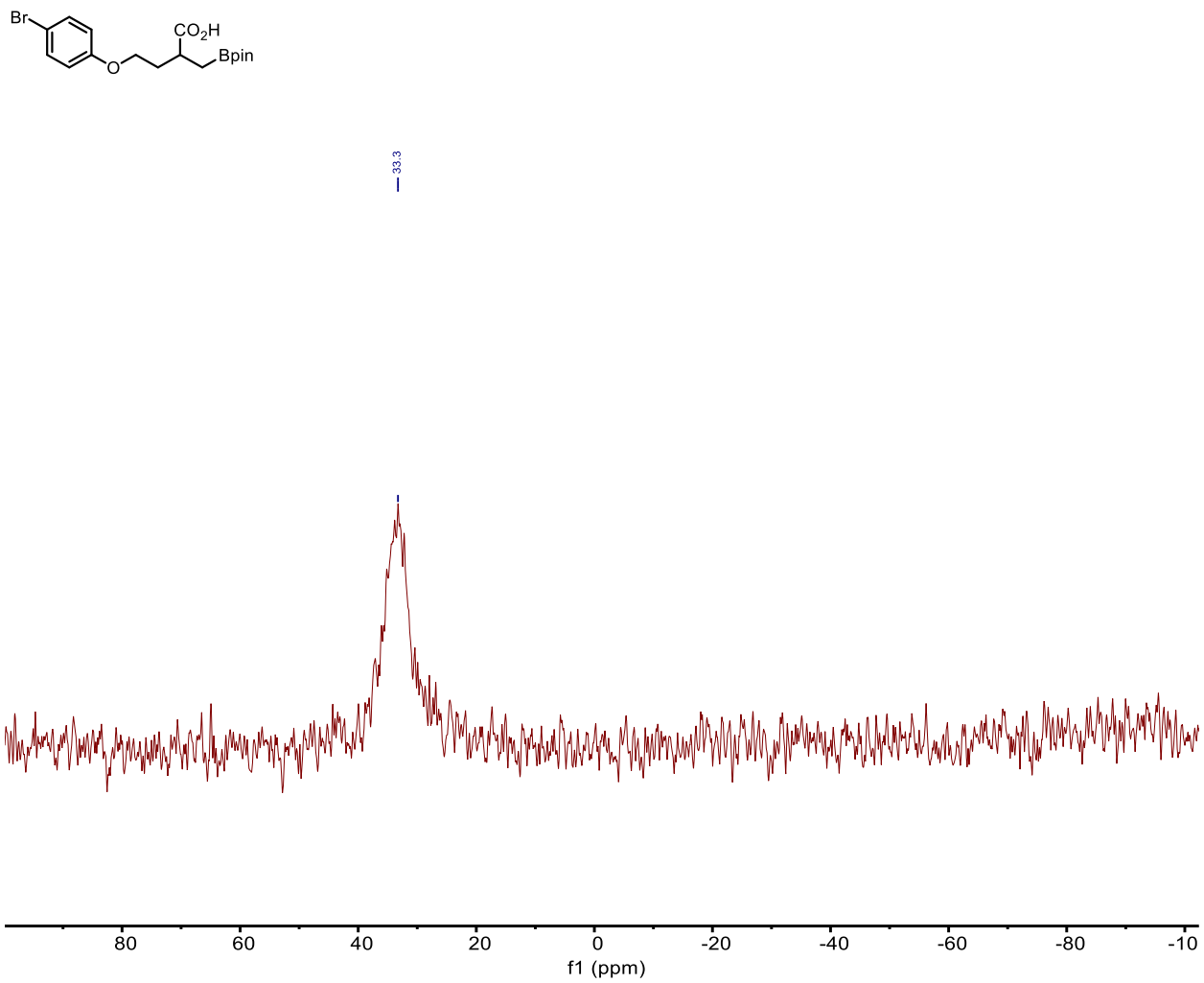

Figure A-103. ^{11}B NMR Spectrum of **2l.**

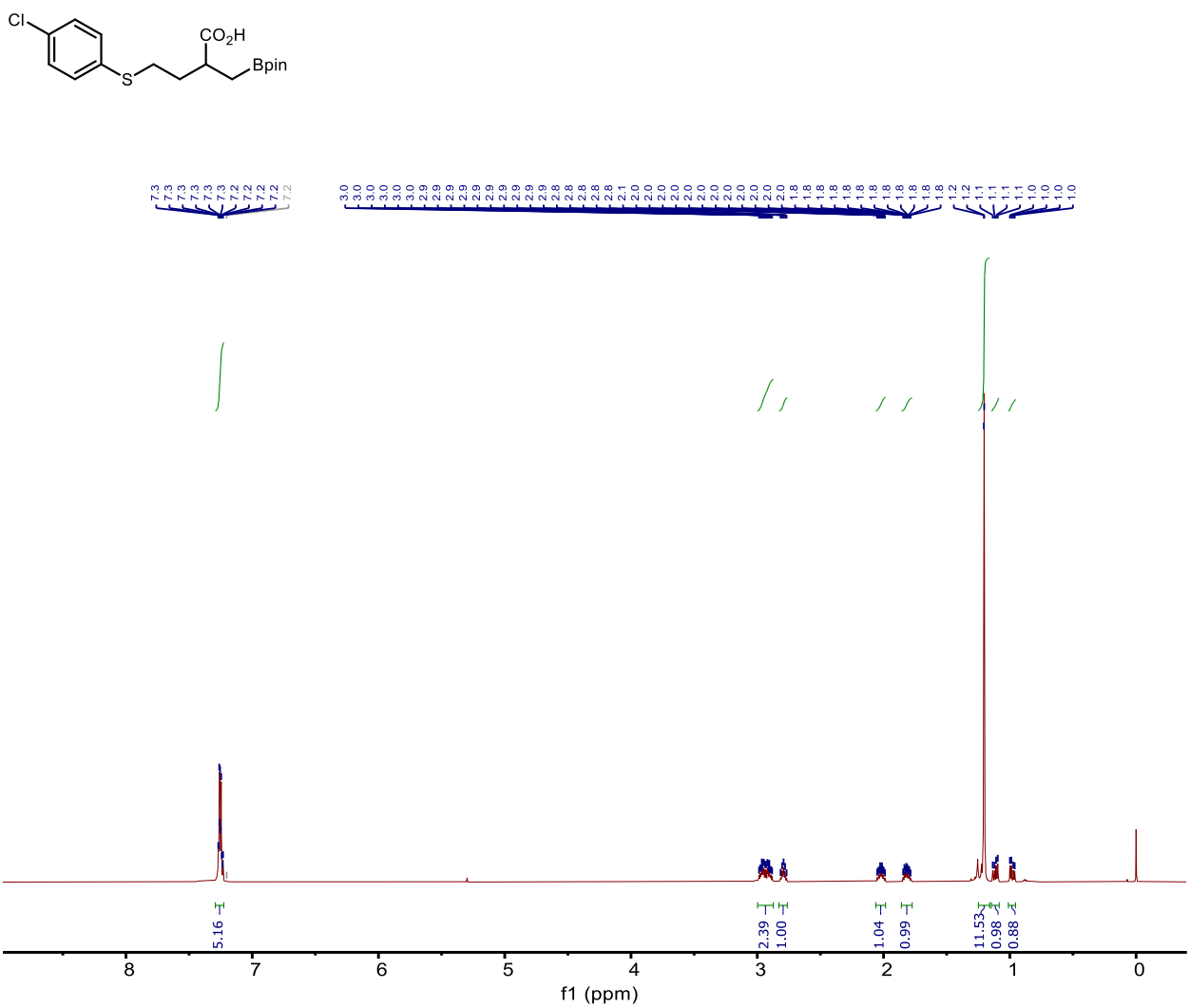

Figure A-104. ^{1}H NMR Spectrum of **2m**.

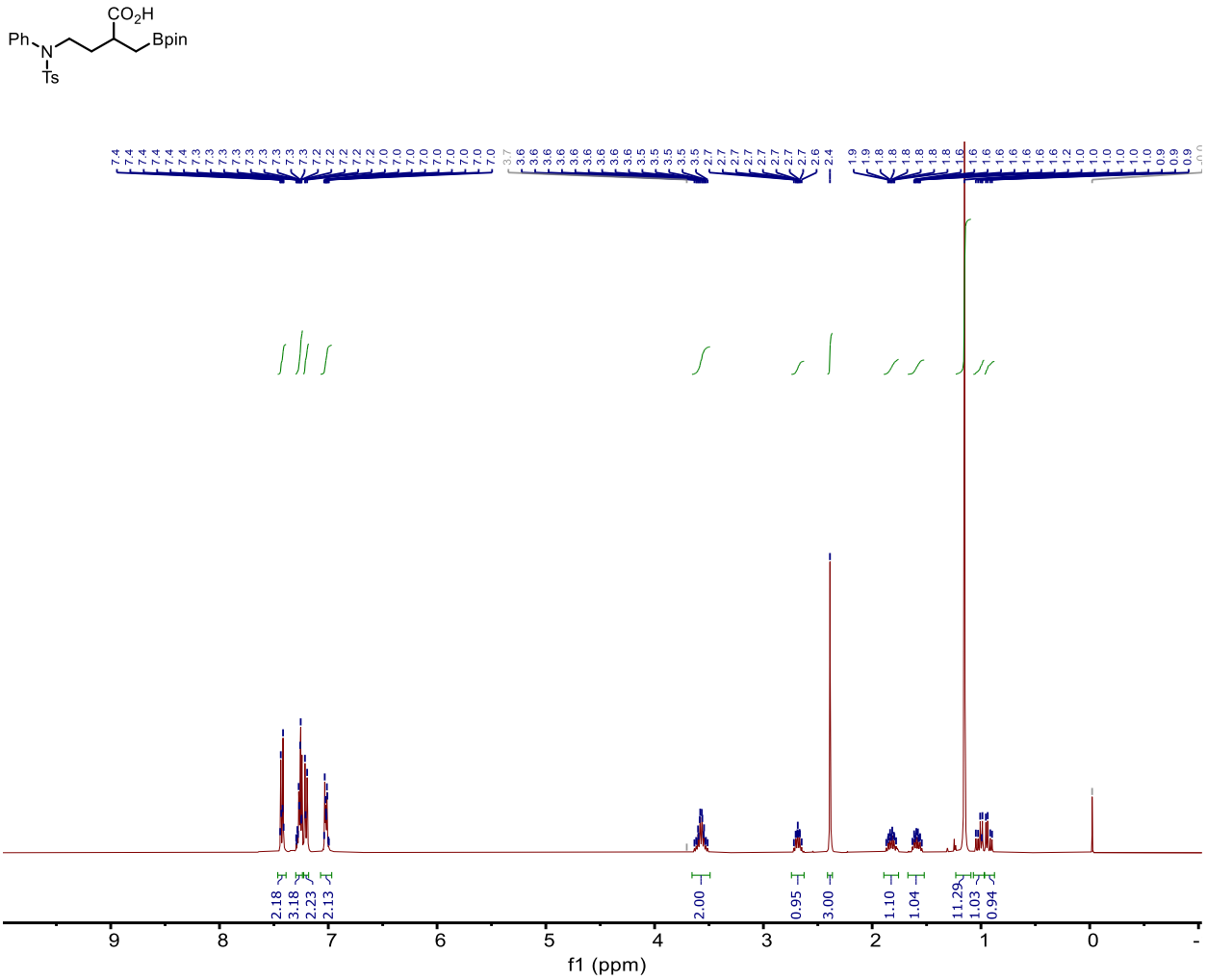

Figure A-105. ^{1}H NMR Spectrum of **2n**.

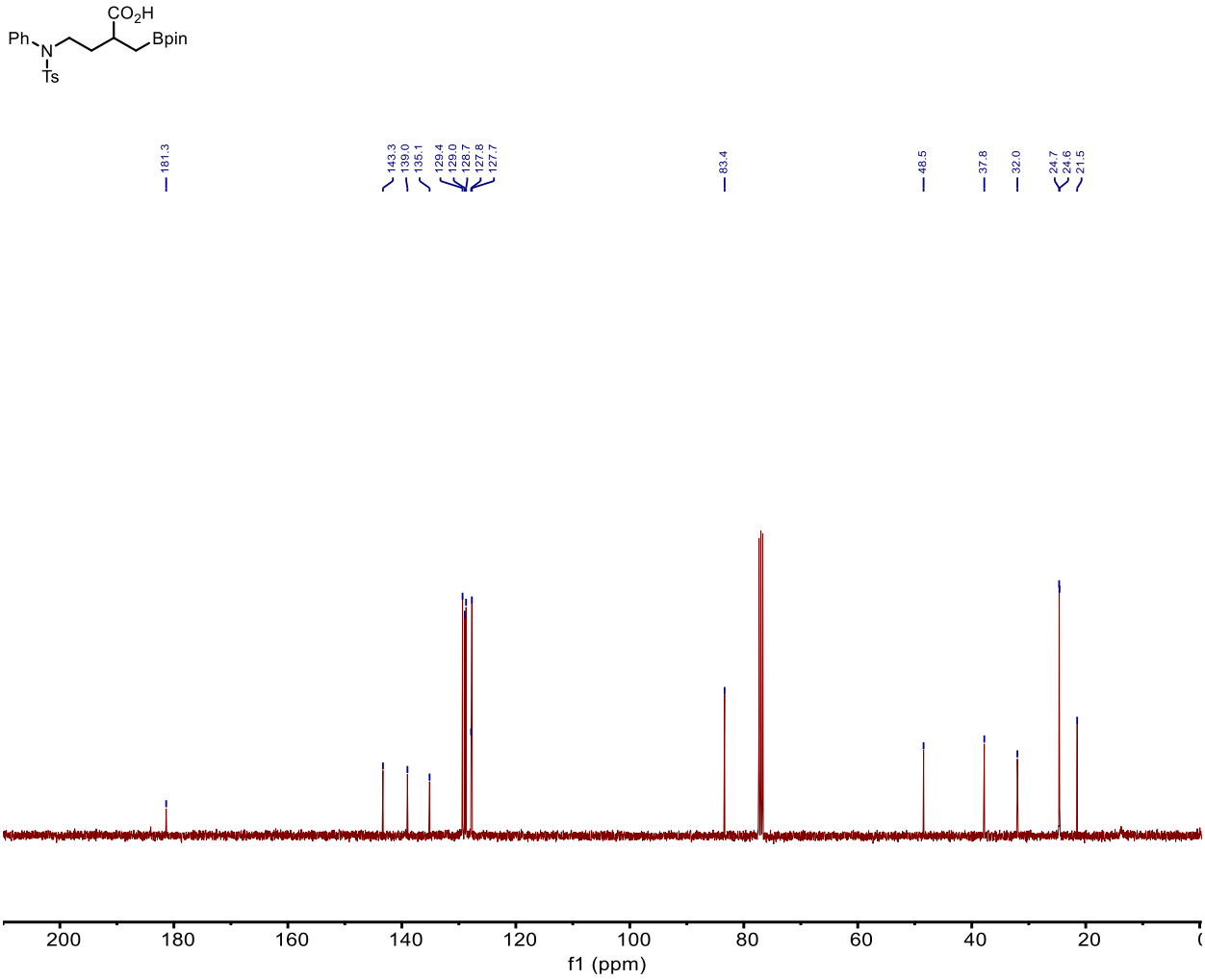

Figure A-106. ^{13}C NMR Spectrum of **2n**.

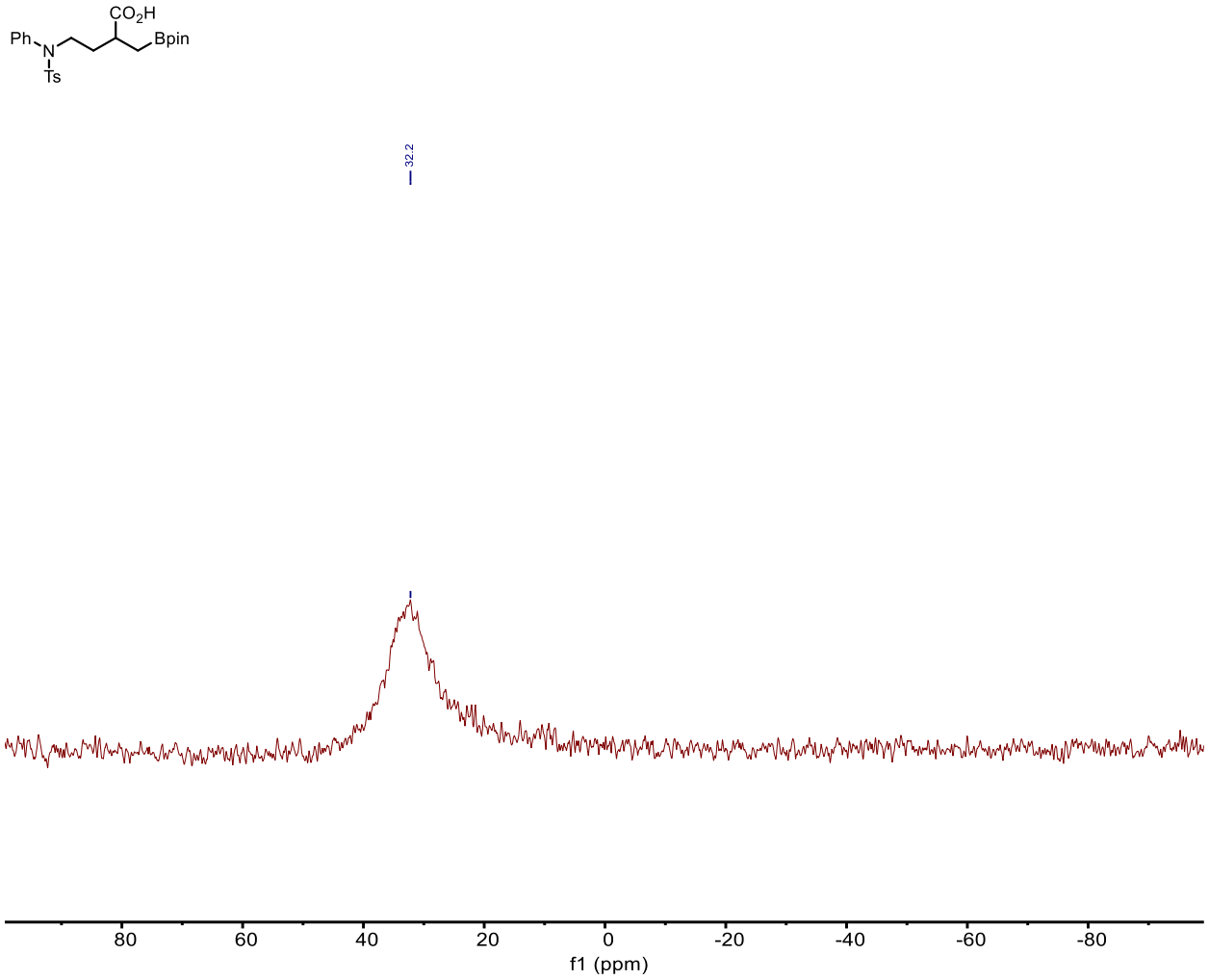

Figure A-107. ^{11}B NMR Spectrum of **2n.**

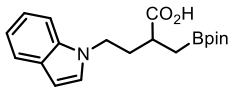

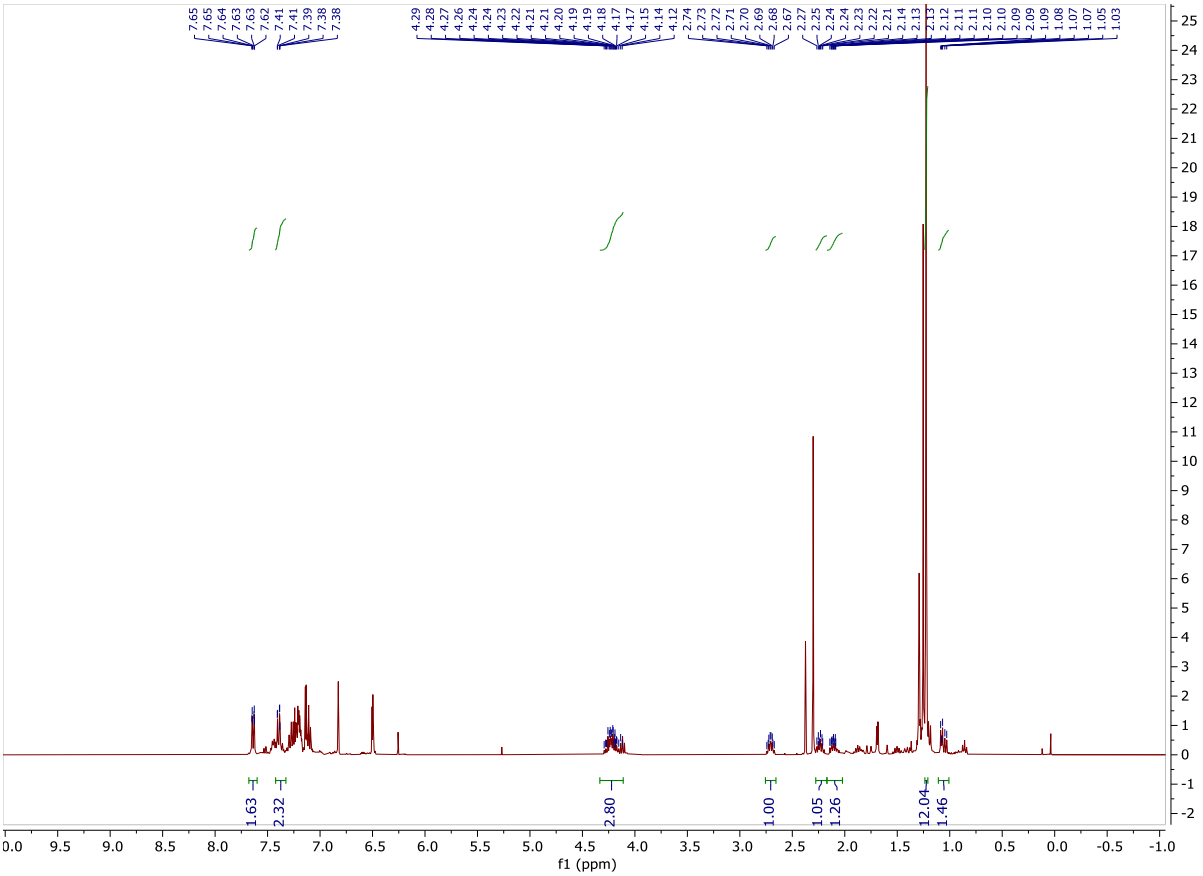

Figure A-108. Crude ^{1}H NMR Spectrum of **2o**.

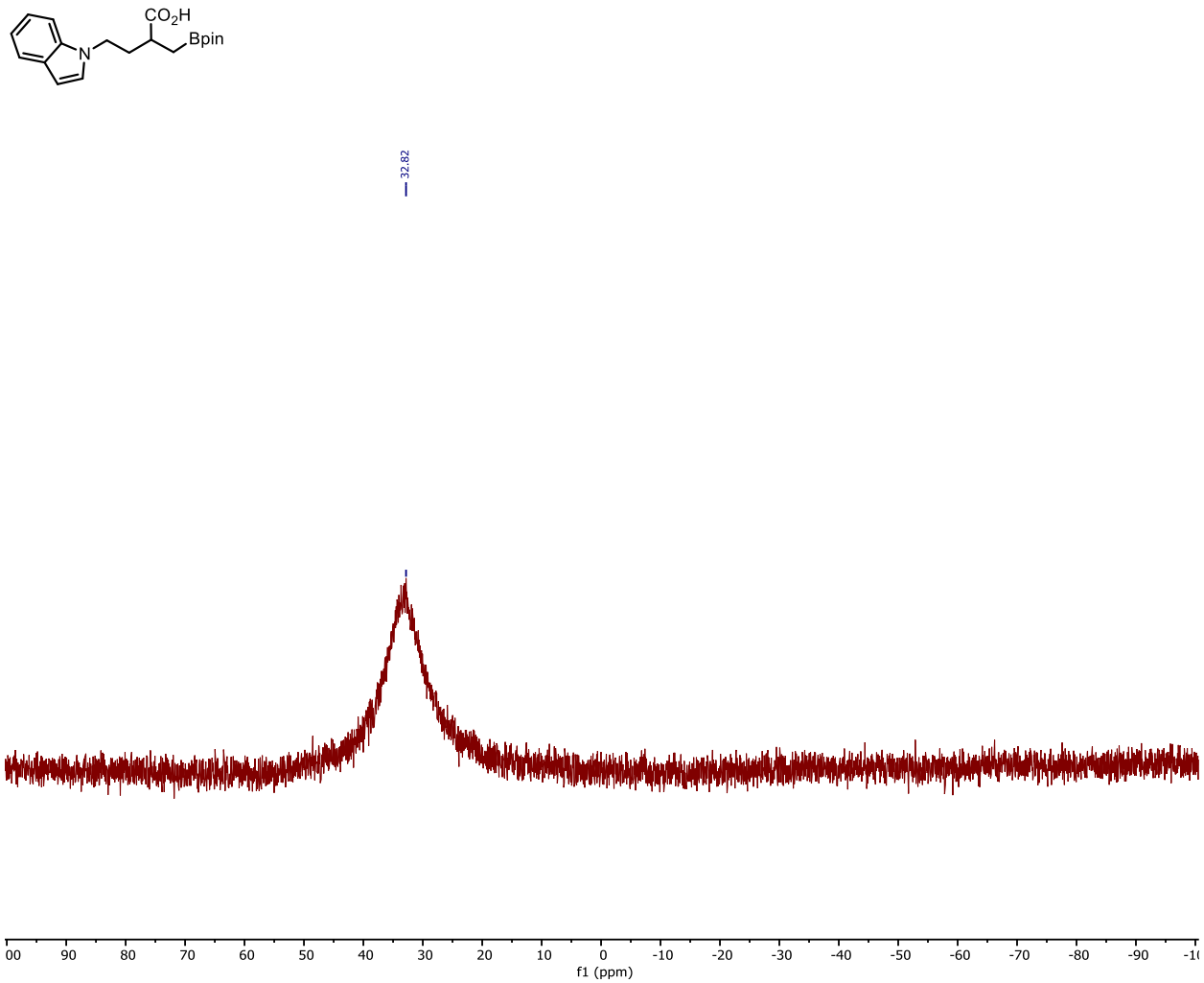

Figure A-109. ^{11}B NMR Spectrum of **2o.**

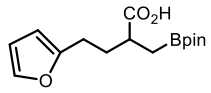

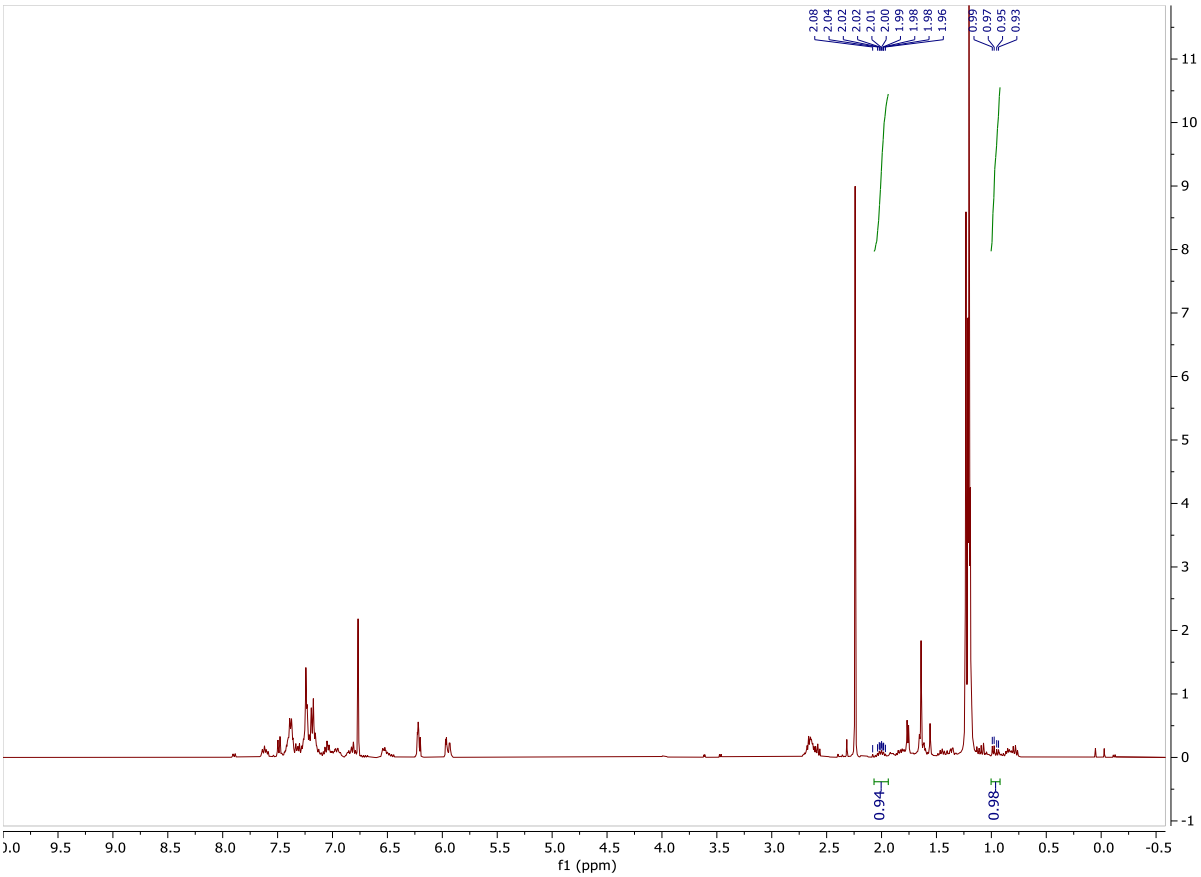

Figure A-110. Crude ^{1}H NMR Spectrum of **2p**.

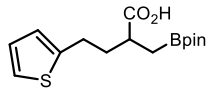

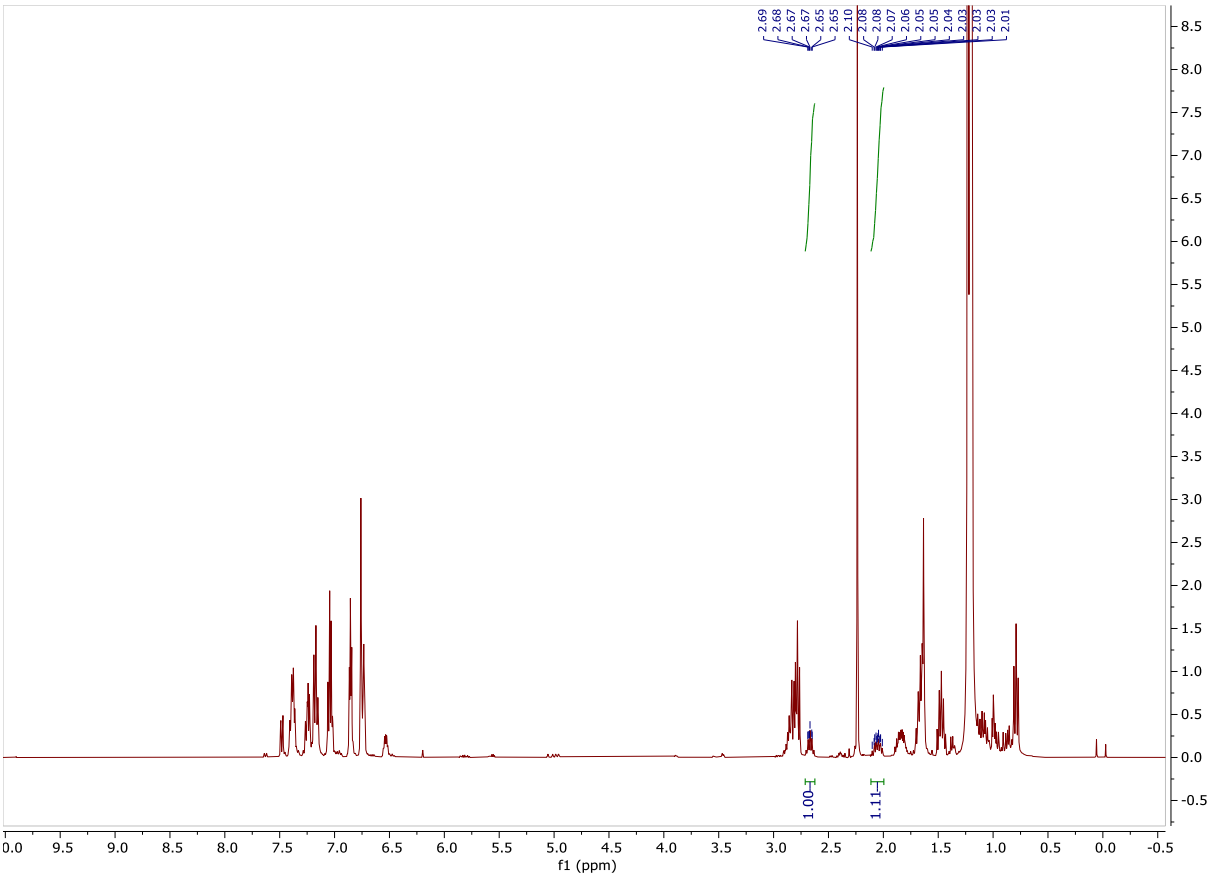

Figure A-110. Crude ^{1}H NMR Spectrum of **2q**.

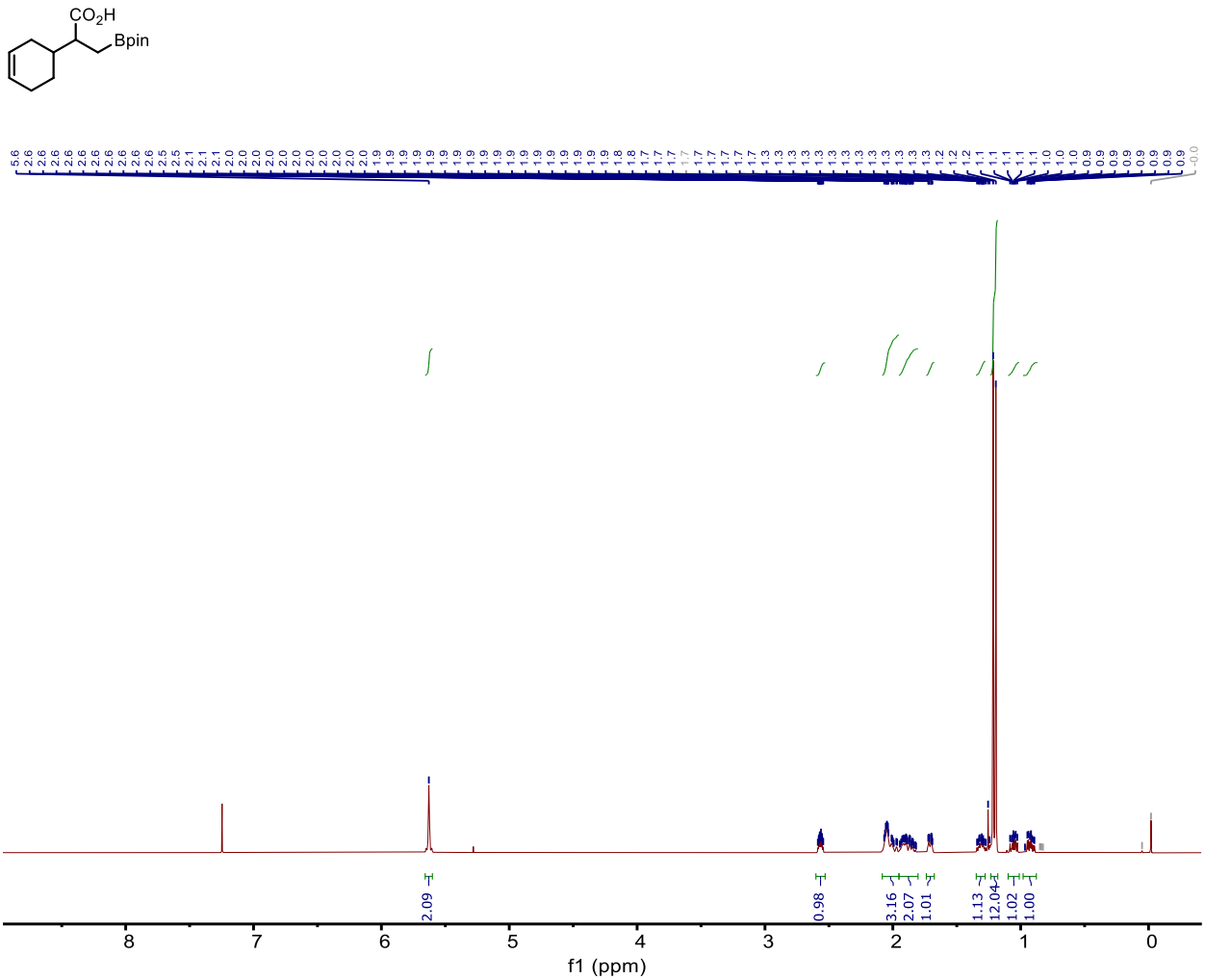

Figure A-111. ^{1}H NMR Spectrum of **2r**.

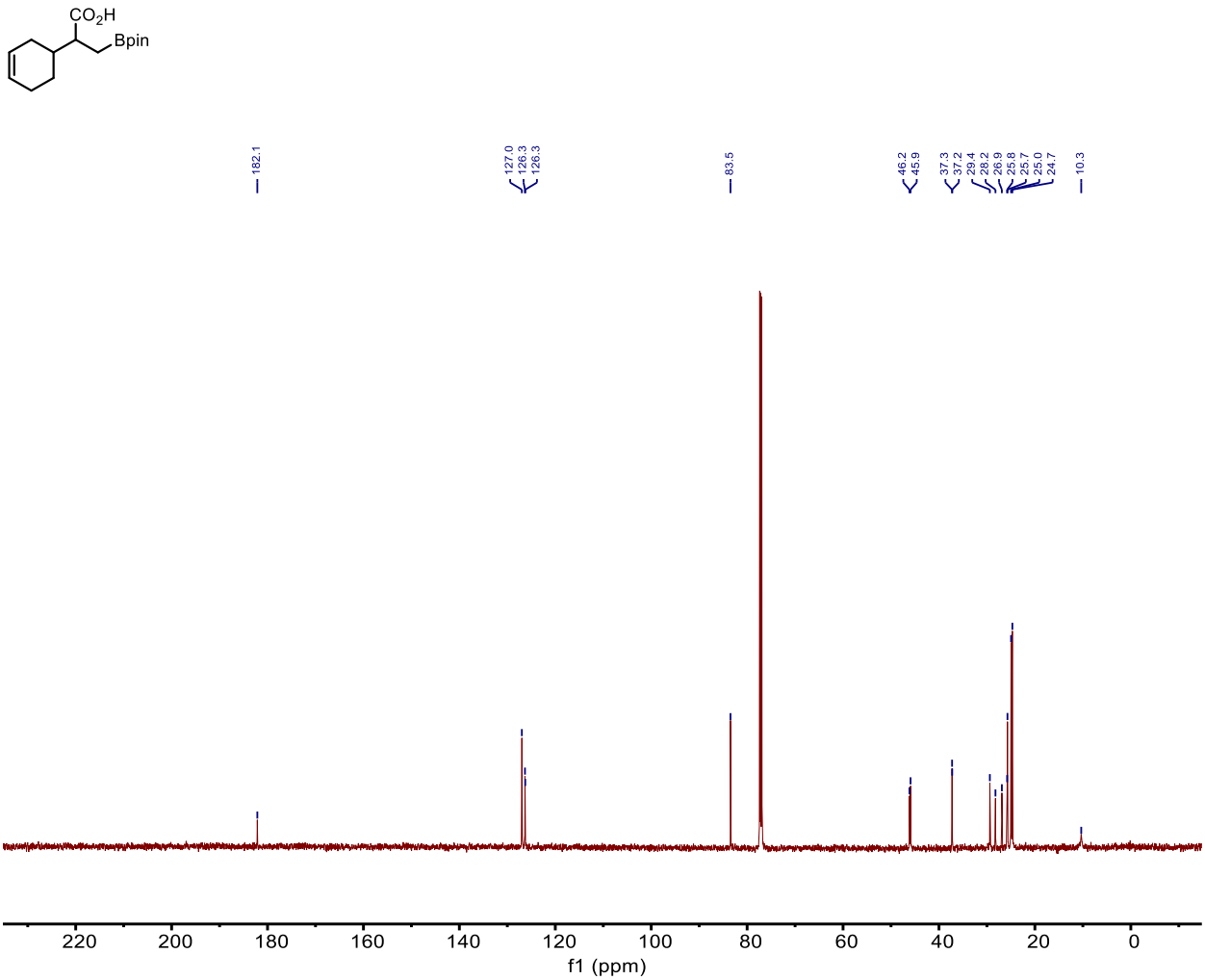

Figure A-112. ^{13}C NMR Spectrum of **2r**.

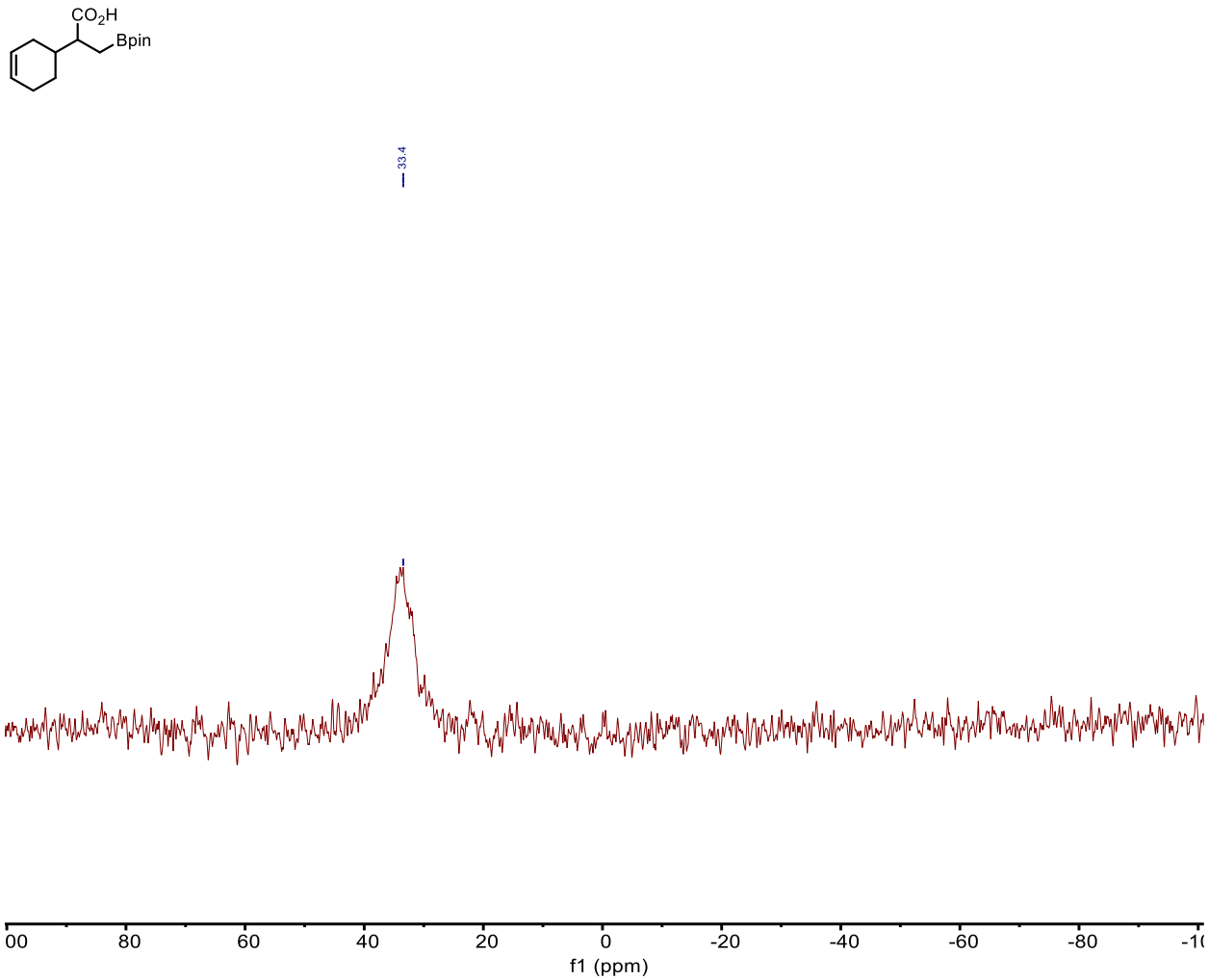

Figure A-113. ^{11}B NMR Spectrum of **2r.**

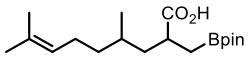

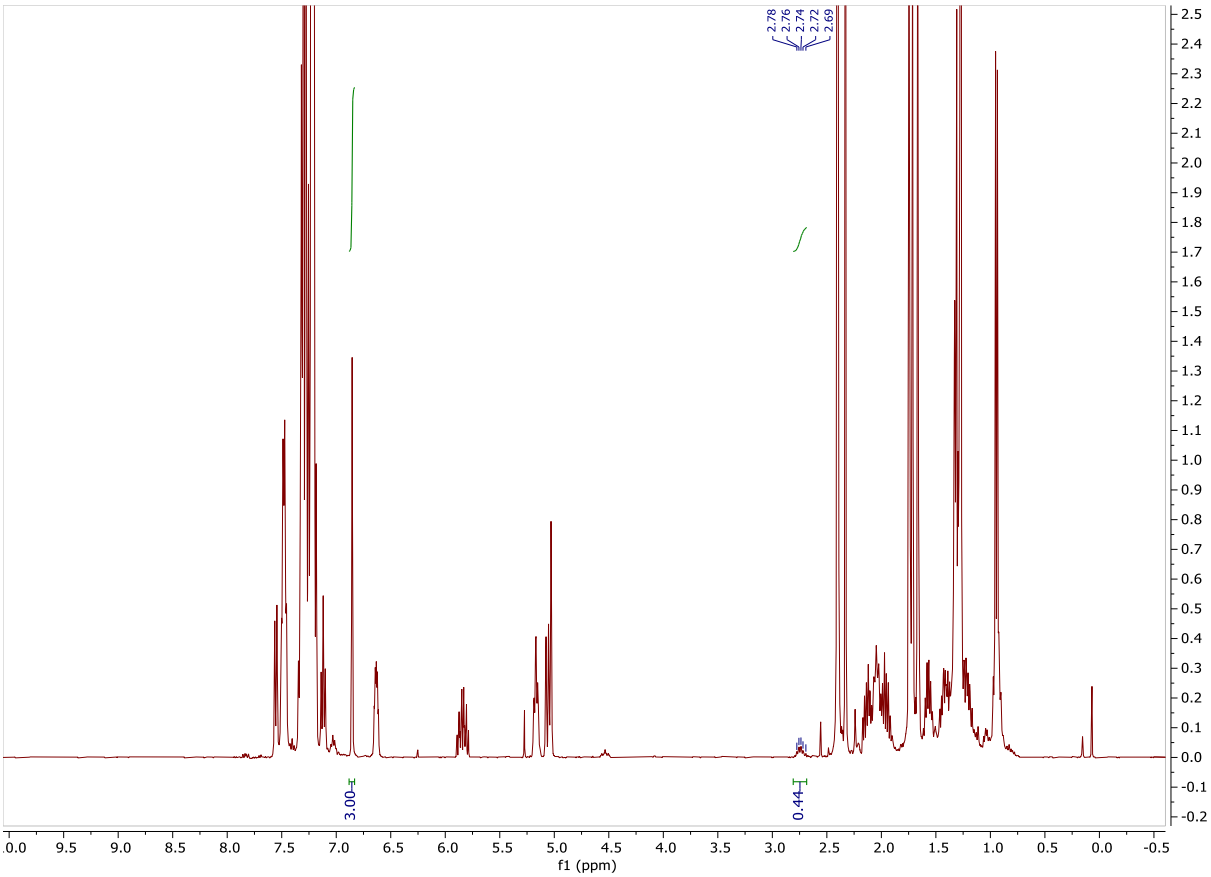

Figure A-114. Crude ^{1}H NMR Spectrum of **2s**.

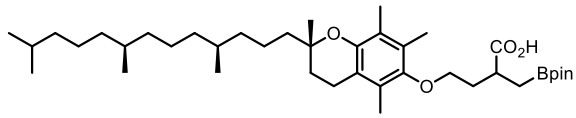

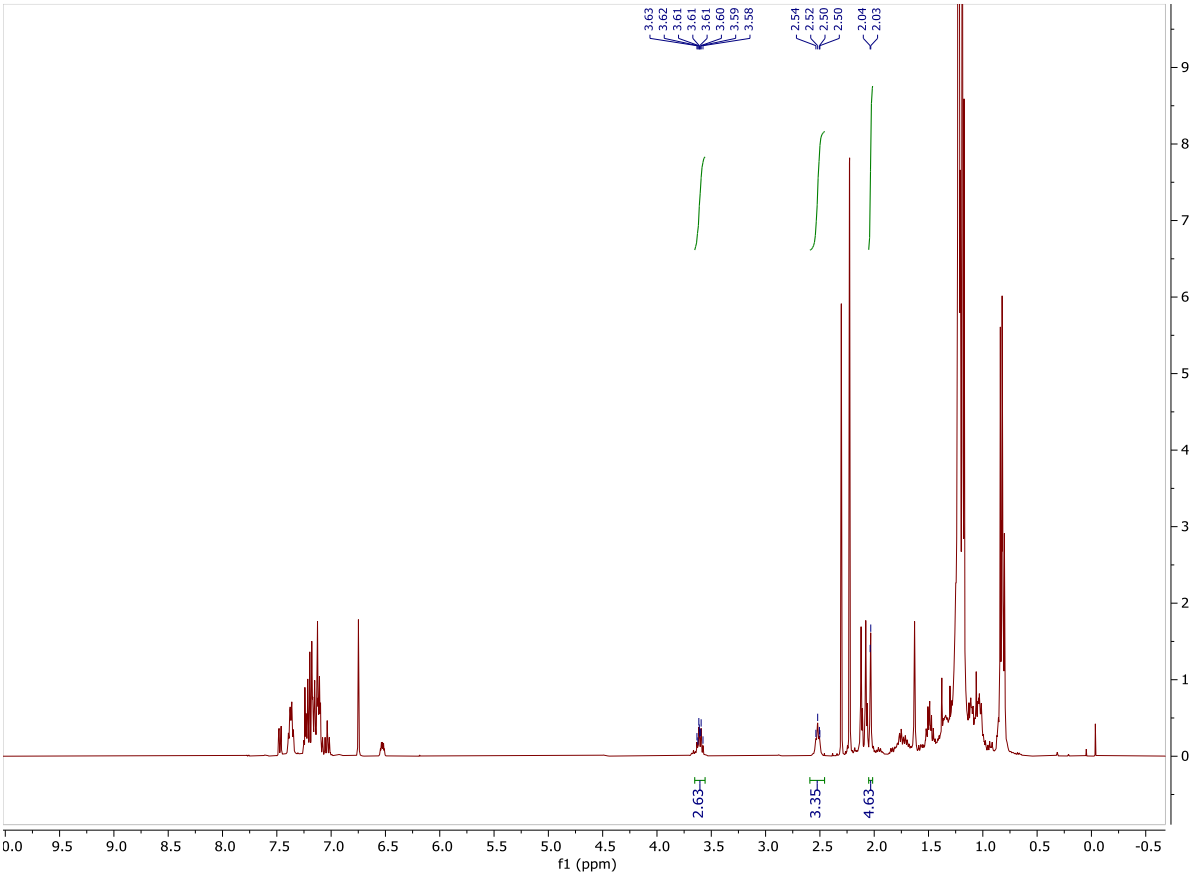

Figure A-115. Crude ^{1}H NMR Spectrum of **2t**.